ATTENTION: The Singapore Copyright Act applies to the use of this document. Nanyang Technological University Library

CHARACTERIZATION AND MODELING OF NEGATIVE BIAS TEMPERATURE INSTABILITY IN P-MOSFETS

YANG JIANBO

School of Electrical and Electronic Engineering

A thesis submitted to Nanyang Technological University

in fulfillment of the requirement for the degree of

Doctor of Philosophy

2010

ATTENTION: The Singapore Copyright Act applies to the use of this document. Nanyang Technological University Library

ACKNOWLEDGMENTS

First and foremost, I would like to express my deepest gratitude to my thesis advisor, Dr. Chen Tupei, for all his generous support and encouragement throughout the entire course of my research at Nanyang Technological University (NTU). His patience and understanding, coupled with his research and teaching experience, have contributed immensely to the enlargement of my knowledge and research ability. Without his dedicated guidance and contribution of time and energy, this research work would never reach fruition.

I would also like to extent my warmest gratitude to Prof. Pey Kin Leong from NTU, Dr. Lap Chan and Dr. Ng Chee Mang from Chartered Semiconductor Manufacturing for granting me the Chartered-NTU graduate research scholarship and for their support and suggestions throughout my research at both NTU and Chartered. I am further indebted to Dr. Tan Shyue Seng for his continuous technical support and to Gong Ying for her generous sharing of the knowledge about TCAD process simulation.

Furthermore, I am very grateful to all my colleagues and friends at the Measurements Lab and Chartered-NTU Lab and to the fellow students in the Chartered Special Project group.

Last but not least, I would like to express my deepest gratitude to my parents, my beloved friend, Wei Quiyan, and all my other family members and good friends, for their love, support and encouragement during all these years.

ATTENTION: The Singapore Copyright Act applies to the use of this document. Nanyang Technological University Library

Specially dedicated to

my parents

& my fiancée - Wei Qiuyan

ATTENTION: The Singapore Copyright Act applies to the use of this document. Nanyang Technological University Library

SUMMARY

It has been the intent of this work to investigate negative bias temperature instability (NBTI) in *p*-MOSFETS with ultra-thin nitrided gate oxides experimentally and theoretically. A systematic study on NBTI has been carried out and the understanding of NBTI mechanism is further enhanced. Firstly, a simple NBTI characterization technique of measuring a single-point saturation drain current has been proposed to minimize the unfavorable NBTI recovery during measurement. With this method, the measurement time can be largely reduced. This method gives a closer-to-real threshold voltage shift and thus yields a more reliable power-law factor. Subsequently, since NBTI has become a key device reliability challenge for advanced CMOS technology nodes, an NBTI in-line test methodology has been developed to monitor NBTI during the device development phase. Moreover, NBTI recovery is experimentally examined, and a combined empirical model for NBTI recovery within the modulated measurement time frame has been proposed to describe the entire process of NBTI recovery in a wide time range.

A comprehensive study on the modeling of NBTI has been conducted. An analytical reaction-diffusion (R-D) model within the framework of the standard R-D model has been developed. This model can well describe NBTI in a wide time scale covering the three regimes of reaction, transition and diffusion. A power-law factor of ~1 is experimentally observed for the nitrided gate oxide, which shows clear evidence of the existence of the reaction-limited regime for NBTI. The analytical R-D model

ATTENTION: The Singapore Copyright Act applies to the use of this document. Nanyang Technological University Library

has been extended to include the cases of other possible hydrogen-related diffusion species, such as hydrogen ion H^+ and hydrogen molecule H_2. Besides, an analytical geometry-dependent R-D model has been established for two- or three-dimensional diffusion. It has been experimentally observed that NBTI degradation increases when the channel-length or channel-width decreases. The increase of NBTI with decreasing channel-length is mainly attributed to the enhancement of NBTI reaction by the increase of mechanical stress as a result of the channel-length reduction, which is supported by process simulation and first-principles calculation, while the increase of NBTI with decreasing channel-width can be explained in terms of the evolution of hydrogen diffusion towards a two- or three-dimensional diffusion with the reduction of channel-width.

Nitrogen-worsen NBTI in *p*-MOSFETs has been systematically studied. It is experimentally shown that both interfacial nitrogen concentration and nitrogen depth profile play important roles in the nitrogen-worsen NBTI. Based on the analytical R-D model, by incorporating the dispersive nature of hydrogen diffusion, an analytical reaction-dispersive-diffusion (R-DD) model has been developed and the influence of hydrogen dispersive diffusion on NBTI has also been examined. It is further verified that the analytical R-DD model can well explain NBTI including its dependence on stress time, temperature and interfacial nitrogen concentration, and its power-law behavior. Furthermore, first-principles calculation has been carried out to examine the effect of nitrogen as either a reaction site at the interface or an adjacent atom near the interface. Lower NBTI reaction energies due to incorporation

ATTENTION: The Singapore Copyright Act applies to the use of this document. Nanyang Technological University Library

of nitrogen suggest that nitrogen is a more effective trapping center than oxygen and thus worsens NBTI. The role of nitrogen on NBTI is also investigated in terms of its influence on the electro-negativity and atomic charge distribution of nitrogen, oxygen and silicon atoms at the interface.

NBTI in 65nm- or 45nm-node *p*-MOSFETs with ultrathin gate dielectrics has been extensively investigated, and in particular, the impact of process technologies on NBTI has been examined. Stress proximity technique (SPT) is found to improve NBTI significantly. First-principles calculation is carried out to examine the effect of strain on NBTI, and it is found that larger strain leads to higher NBTI degradation. Process simulation shows that although compressive stress along the channel direction is enhanced by SPT, vertical tensile stress is greatly reduced by SPT, which is believed to be responsible for the improvement of NBTI. On the other hand, laser spike annealing (LSA) worsens NBTI degradation, which could be attributed to damage induced by high-temperature laser annealing at the interface or in the gate oxide. Moreover, it is observed that NBTI degradation in high-performance devices with ultrathin nitrided gate oxide can be quite pronounced even at or slightly above the operating voltage.

ATTENTION: The Singapore Copyright Act applies to the use of this document. Nanyang Technological University Library

TABLE OF CONTENTS

ACKNOWLEDGMENTS I

SUMMARY IV

TABLE OF CONTENTS VII

LIST OF FIGURES X

LIST OF TABLES XIII

NOMENCLATURES XIV

CHAPTER 1 INTRODUCTION 1

1.1 History of Metal-Oxide-Semiconductor Devices 1

1.2 MOS Device Scaling – Moore's Law 2

1.3 Gate Dielectric Scaling and Oxide Reliability 3

1.4 Motivation 5

1.5 Objectives and Scope of Research 7

1.6 Major Contributions of the Thesis 8

1.7 Organization of the Thesis 9

CHAPTER 2 LITERATURE REVIEW 12

2.1 Substrate/Gate-Dielectric Interface 12

2.1.1 Fabrication Techniques of Silicon Oxide and Oxynitride 13

2.1.2 Charges in the Si-SiO_2 System 15

2.2 Review on NBTI in p-MOSFETs: An Overview 18

2.2.1 History of NBTI 19

2.2.2 New Era of NBTI Since 1999 23

2.3 NBTI Phenomenon and Process Dependence 24

2.3.1 NBTI Observations in MOS Devices 24

2.3.2 Hydrogen, Deuterium and Water 27

2.3.3 Boron 29

2.3.4 Fluorine 31

2.3.5 Nitrogen 32

2.3.6 Other Remarks 33

2.4 NBTI Theories and Models 33

2.4.1 Reaction-Diffusion/Drift Model 33

2.4.2 Statistical Mechanics Model 37

2.4.3 Disorder-Controlled-Kinetics Model 39

ATTENTION: The Singapore Copyright Act applies to the use of this document. Nanyang Technological University Library

2.4.4 Reaction-Limited Model 41
2.4.5 Hole-Trapping Model 44
2.4.6 Deep-Level Hole-Trapping Model 45
2.4.7 Models for NBTI Recovery 45

2.5 NBTI Characterization Techniques 46
2.5.1 Threshold Voltage Measurement 46
2.5.2 Interface Trap Generation Measurement 47
2.5.3 Fast Characterization Techniques 49

2.6 Summary 52

CHAPTER 3 CHARACTERIZATION OF NBTI AND NBTI RECOVERY 53

3.1 Introduction 53

3.2 Single-Point Saturation Drain Current Measurement 55
3.2.1 BTI Issues in MOS Devices 55
3.2.2 NBTI Recovery during Measurement 57
3.2.3 Single-Point Drain Current Method 58

3.3 NBTI In-line Test Methodology 65
3.3.1 NBTI Model for Process Qualification and NBTI Specifications 66
3.3.2 Proposed NBTI In-line Test Framework 68
3.3.3 NBTI In-line Test Validation: Results and Discussion 73

3.4 Characterization of NBTI Recovery 74
3.4.1 NBTI Recovery within Modulated Measurement Time Frame 75
3.4.2 Empirical Model for NBTI Recovery 79
3.4.3 Effect of Measurement Time Delay on NBTI 83

3.5 Summary 85

CHAPTER 4 MODELING OF NBTI IN P-MOSFETS 86

4.1 Introduction 86

4.2 Analytical Reaction-Diffusion Model for NBTI 88
4.2.1 Analytical Reaction-Diffusion Model 88
4.2.2 Evidence of Reaction-Limited Regime 94
4.2.3 Nitrogen Effect on NBTI 98

4.3 Extended Analytical Reaction-Diffusion Model for NBTI 105
4.3.1 Ionic Hydrogen 105
4.3.2 Molecular Hydrogen 108

4.4 Geometry-Dependent Reaction-Diffusion Model for NBTI 112
4.4.1 Geometry-Dependent Reaction-Diffusion Model 112
4.4.2 Strain Effect on NBTI in p-MOSFETs with Small Dimensions 117
4.4.3 Geometry Dependence of NBTI in p-MOSFETs with Small Dimensions 119

4.5 Summary 124

ATTENTION: The Singapore Copyright Act applies to the use of this document. Nanyang Technological University Library

CHAPTER 5 NITROGEN-WORSEN NBTI IN P-MOSFETS....... 126

5.1 Introduction......127

5.2 Effect of Nitrided Oxide on NBTI 128

5.2.1 Experimental 128

5.2.2 Results and Discussion...... 129

5.3 Physical Modeling of NBTI......133

5.3.1 Analytical Reaction-Dispersive-Diffusion Model for NBTI...... 133

5.3.2 Influence of Dispersive Hydrogen Diffusion in Nitrides Gate Oxide on NBTI138

5.4 Atomic Modeling of NBTI......142

5.4.1 Atomic Modeling of Nitrogen Effect on NBTI...... 143

5.4.2 Nitrogen Effect on Atomic Charge Distribution 147

5.5 Summary 149

CHAPTER 6 IMPACT OF PROCESS TECHNOLOGIES ON NBTI 150

6.1 Introduction......150

6.2 Impact of Stress Proximity Technique on NBTI 151

6.2.1 Experimental 154

6.2.2 Impact of SPT on NBTI: Experimental Results...... 154

6.2.3 Impact of Interfacial Strain on NBTI: First-principles Calculation 157

6.2.4 Impact of SPT on Stress Transfer: Process Simulation...... 160

6.2.5 Improvement of NBTI by SPT...... 167

6.3 Impact of Laser Spike Annealing on NBTI......172

6.3.1 Experimental 172

6.3.2 Results & Discussion 173

6.4 Characterization of NBTI in High-performance p-MOEFETs with Ultrathin Gate Dielectrics......177

6.4.1 Experimental 178

6.4.2 Results and Discussion...... 178

6.5 Summary 181

CHAPTER 7 CONCLUSION AND RECOMMENDATIONS....... 182

7.1 Conclusion 182

7.1.1 Characterization of NBTI and NBTI Recovery 182

7.1.2 Modeling and Geometry Dependence of NBTI...... 184

7.1.3 Nitrogen Effects on NBTI and Modeling of Nitrogen-worsen NBTI...... 185

7.1.4 Impacts of Advanced Process Technologies on NBTI 186

7.2 Recommendations 186

7.2.1 Physical Modeling of NBTI Recovery and Dynamic NBTI...... 186

7.2.2 Identification of Hydrogen-related Diffusion Species 187

7.2.3 NBTI for High-K Gate Dielectrics...... 188

ATTENTION: The Singapore Copyright Act applies to the use of this document. Nanyang Technological University Library

List of Publications 189

BIBLIOGRAPHY 191

ATTENTION: The Singapore Copyright Act applies to the use of this document. Nanyang Technological University Library

LIST OF FIGURES

Figure 2.1: *Different techniques of incorporating nitrogen into SiO_2, after [42]*....... 14

Figure 2.2: *Charges and their locations in thermally oxidized silicon, after [52].* 16

Figure 2.3: *Bias conditions of a typical CMOS inverter during circuit operation. GND stands for the "Low" state, while V_{dd} corresponds to the "High" state.* 18

Figure 2.4: *The time development of surface states under stress at 10^6 V/cm at 250°C and 300 °C. A best fit log(time) line is shown for each set of points. After [57].*... 21

Figure 2.5: *Two dimensional sketch of thermally oxidized silicon showing possible origins of charges. After [58].* 21

Figure 2.6: *The increase of the oxide charge measured as the shift of the C-V curve at midband, plotted against the relative surface-trap density at midband. The same relationship is observed after NBS at both 125 ℃, -55 V (5.8 MV/cm) and 25 ℃, -65 V (6.8 MV/cm) and indicates that there is roughly one surface trap per oxide charge. After [61].* 22

Figure 2.7: *(a) V_{th} change and G_m degradation vs. stress time for n- and p-MOSFETs, after [31]. (b) % change in I_d vs. stress time for two drain biases, showing that I_{dsat} degradation is more than I_{dlin} degradation, after [32].* 25

Figure 2.8: *(a) The effect of PMA on ΔV_{th}. D_2 PMA suppresses NBTI. (b) The effect of oxidation on ΔV_{th}. Wet oxidation enhances NBTI. After [34]*................. 28

Figure 2.9: *BT stress time dependence of (a) ΔV_{th} and (b) ΔN_{it} for p-MOSFET's with and without boron penetration. After [67].* 30

Figure 2.10: *NBTI shift as a function of time for wafers with and without added fluorine. Implanted fluorine dose was $5x10^{15}$ cm^{-2}. After [100].*............ 31

Figure 2.11: *V_{th} shift due to NBTI for pure and nitrided oxide. A large V_{th} shift was observed for nitrided oxide. After [34].* 32

Figure 2.12: *Five regimes of time dependent interface-trap generation as obtained from the general solution of the reaction-diffusion equations during NBTI stress. After [133]*.. 35

Figure 2.13: *Evolution of theoretical degradation rate (filled symbols) with respect to stress time, with a disorder-induced variation of dissociation energies for a given temperature, as defined by Eq. (2. 29). After [145]*.................. 43

Figure 3.1: *Comparison of BTI degradation in either n-MOSFETs or p-MOSFETs, in terms of threshold voltage shift (ΔV_{th}) as a function of the stress time. The gate stress voltage (V_{gstr}) is -3.0 V for NBTI and 3.0 V for PBTI, and the stress temperature (T_{str}) is 125 °C.*.. 56

Figure 3.2: *ΔV_{th} recovery as a function of the post-NBTI relaxation time (t_{rec}). The NBTI stress is carried out at V_{gstr} = -3.0 V and T_{str} = 125 °C for 1000*

ATTENTION: The Singapore Copyright Act applies to the use of this document. Nanyang Technological University Library

seconds, and NBTI recovery occurs at V_{gstr} = 0 V. 57

Figure 3.3: *Dependence of saturation drain current (I_d) on drain voltage (V_d) for both fresh and stressed devices. The drain current (I_d) is found to be proportional to (1 – 0.33V_d) for both devices, showing that λ (=0.33) is independent of NBTI stress.* 59

Figure 3.4: *(a) The saturation drain current (I_d) versus (V_g-V_{th}) for both fresh and stressed devices. A linear regression of the experimental data of log|I_d| versus log|V_g-V_{th}| yields the value of θ and θ (=1.5) is found to be independent of NBTI stress. (b) Hole mobility (μ) versus V_g for both fresh and stressed devices. Relative mobility degradation ($\Delta\mu/\mu$) in % at different Vg is also shown.* 60

Figure 3.5: *Comparison between the ΔV_{th} calculated with Eq. (3.3) and the ΔV_{th} measured with the conventional method for a set of fresh (i.e., without any NBTI stress) devices whose threshold voltage randomly varies within a small range (20 mV).* 63

Figure 3.6: *Comparison of NBTI-induced ΔV_{th} between the conventional method and our proposed method.* 65

Figure 3.7: *A proposed NBTI in-line test, where DUT stands for device under test, T_{str} is stress temperature, V_{gstr} is stress gate voltage, t_s is stress time, ΔV_{th} is shift in the threshold voltage, and ΔI_{dsat} is shift in the saturation drain current.* 69

Figure 3.8: *Comparison of NBTI in-line test results in terms of ΔV_{th} extracted by 1st OTF method ("Method 2") and %ΔI_{dsat} measured by single-point I_{dsat} method ("Method 3") for different processes: (a) No SPT vs. SPT; and (b) Spike only vs. LSA.* 74

Figure 3.9: *A general measurement time frame $t_{[i]}$ at ith cycle (i = 1, 2, 3…) with the period of $t_{p\text{-}i}$, for the dynamic NBTI or NBTI recovery.* 76

Figure 3.10: *Comparison of NBTI recovery in the identical devices with different measurement time intervals. The device is pre-stressed with negative gate bias (V_{gstr} = -2.2V) at the elevated temperature (T_{str} = 125°C) for 1000s, and the NBTI stress is purposely removed so as to monitor the NBTI recovery.* 77

Figure 3.11: *Re-plot of Fig. 3.10 for NBTI recovery within the modulated measurement time frame by taking the measurement time (t_m) into account.* 78

Figure 3.12: *Modeling of NBTI recovery with (a) the existing empirical model [37, 111] (i.e. Eq. (3.7)); and (b) the proposed empirical model (i.e. Eq. (3.8)). The devices are stressed under V_{gstr} = -2.2V at T_{str} = 125°C for 1, 10, 100, and 1000s, respectively.* 81

Figure 3.13: *Correlation of m in Eq. (3.8) and β in Eq. (3.7) with ΔV_{th0}.* 82

Figure 3.14: *Plots of the functions βt_r^n, $(1 - \alpha t_r^{-m})$, $(\beta t_r^n + \alpha t_r^{-m})$ and data points until 10000s. Here β = 0.15, n = 0.25, α = 0.94 and m = 0.14. The empirical*

ATTENTION: The Singapore Copyright Act applies to the use of this document. Nanyang Technological University Library

models are valid only when βt_r^n or $(1 - \alpha t_r^{-m})$ is smaller than 1. When $(\beta t_r^n + \alpha t_r^{-m}) \sim 1$, both models are valid. 82

Figure 3.15: *The effect of measurement time delay on NBTI. The pre-factor A and power-law factor n can be extracted and summarized in Table 3.1.* 84

Figure 3.16: *Plot of A and n as a function of the measurement time delay (t_d).* 84

Figure 4.1: *(a) Interface trap generation (ΔN_{it}) calculated with the analytical R-D model (Eq. (4.6)), the R-regime model (Eq. (4.7)), and the D-regime model (Eq. (4.8)). (b) Comparison between the analytical R-D model and the numerical solution. The parameters used in the calculations are $N_o = 1.5\times10^{14}$ cm^{-2}, $k_F=1\times10^{-2}$ /s, $k_R=1\times10^{-18}$ cm^2/s, $D_H = 1\times10^{-16}$ cm^2/s.* 92

Figure 4.2: *The measured and simulated interface trap generation ΔN_{it} as a function of stress time t for nitrided oxides with the interfacial nitrogen concentrations of 3, 8 and 15 at. %. The NBTI stress measurement is carried out at V_{gstr} = -2.2 V and T_{str} = 125 °C. The values of the parameters used in the simulated ΔN_{it} based on the analytical R-D model are given in Table 4.1.* 97

Figure 4.3: *The plot of the fitting parameters: (a) A, $\sqrt{A/B}$, (b) B, D_H, and (c) t_{tr}, t_c, as a function of the interfacial nitrogen concentration N at. %. The values of these parameters used in the plot are given in Table 4.1.* 100

Figure 4.4: *Interface trap generation as a function of time (a) for different pre-factor A and (b) for different diffusion coefficient D_H of H species, as simulated by our proposed unified R-D model for increasing nitrogen concentration, with reference parameters A = $1.4\text{x}10^{12}$ cm^{-2}/s, $k_R=1\text{x}10^{-18}$ cm^2/s, $D_H = 6.1\text{x}10^{-17}$ cm^2/s* 101

Figure 4.5: *Plots of the stress profiles along the channel direction for short-channel (L = 50 nm) and long-channel (L = 1000 nm) devices, as a function of distance x.* 118

Figure 4.6: *NBTI reaction energy change (ΔE_R) and Si-H bonding energy change (ΔE_B) as a function of bond angle change ($\Delta\theta_B$). In the first-principle calculations, ΔE_R is caused by the change in the bond angle ∠Si-N-Si of the nitride oxide, while ΔE_B is purely due to the change in the bond angle in the Si_3-Si-H structure at the interface.* 119

Figure 4.7: *(a) NBTI degradation ΔV_{th} as a function of device channel length for p-MOSFETs with channel width of 2000 nm; (b) the extracted pre-factor A and power-law factor n as a function of device channel length. Te sample size for each device is 4 and the lines are for guiding the eyes only.* 121

Figure 4.8: *(a) Typical NBTI degradation ΔV_{th} as a function of stress time t for p-MOSFETs with short channel length of 60 nm, and with wide and narrow channel width of 5000 nm and 200 nm, respectively; (b) ΔV_{th} as a function of device channel width; (b) the extracted pre-factor A and*

ATTENTION: The Singapore Copyright Act applies to the use of this document. Nanyang Technological University Library

power-law factor n as a function of device channel width. The samples size is 4 and the lines are for guiding the eyes only. 123

Figure 5.1: *Threshold voltage shift* ΔV_{th} *as a function of stress time t in the diffusion-limited regime for nitrided gate oxides at the stress condition: (a)* V_{gstr} = -2.2 V *and* T_{str} = 125 °C *and (b)* V_{gstr} = -2.2 V *and* T_{str} = 25 °C. 130

Figure 5.2: *Arrhenius plots of the pre-factor A for different nitrided gate oxide samples. The activation energies* (E_a) *obtained from the Arrhenius plots are also summarized in Table 5.1. The NBTI stress is carried out at* V_{gstr} = -2.2 V *for 1000s.* 131

Figure 5.3: E_a *extracted from Arrhenius plots of A and* ΔV_{th} *for stress time t = 1, 10, 100, and 1000 s for different samples: sample 1 is RTNO sample with N concentration of 3.7 at. %, and samples 2, 3 and 4 are DPNO samples with N concentration of 3.0, 8.0 and 15.0 at. %, respectively. The NBTI stress is carried out at* V_{gstr} = -2.2 V. 132

Figure 5.4: *Interface trap generation* ΔN_{it} *as a function of NBTI stress time.* ΔN_{it} *is calculated with the reaction-limited regime (R-regime) model (i.e. Eq. (5.3)), diffusion-limited regime (D-regime) model (i.e. Eq. (5.4)), and analytical R-DD model (i.e. Eq. (5.2)), respectively. n is the power-law factor,* β ($0<\beta\leq 1$) *is the dispersion parameter, and* ν *is the characteristic frequency.* 135

Figure 5.5: *Linear plot of power-law factor n as a function of kT to extract the characteristic energy scale* E_0 *for different nitrided gate oxides samples.* 135

Figure 5.6: *The activation energy* E_a *extracted from the Arrhenius plots using either* $A'(= A/\nu^{(\beta-1)/4})$ *or* $\Delta V_{th}'$ $(= \Delta V_{th}/[\nu^{(\beta-1)/4} t^{\beta/4}])$. *The NBTI stress is carried out at* V_{gstr} = -2.2 V *for 1000 seconds.* 138

Figure 5.7: *Simulations to the experimental result of the stress time dependence of interface trap generation* ΔN_{it}. *The NBTI stress was carried out at the voltage* V_{gstr} = -2.2V *and the temperature* T_{str} = 25°C. *The simulation was carried out with either the analytical R-D model [9] or the analytical R-DD model (i.e., Eq.(1)).* 139

Figure 5.8: *Dependence of the power-law factor n on the stress temperature* T_{str}. ...140

Figure 5.9: *Influence of the interfacial nitrogen concentration on the power-law factor n in terms of the dependence of n on the characteristic energy scale* E_0. 141

Figure 5.10: *Arrhenius plots of pre-factor A. The lines are for guiding the eyes only.* 142

Figure 5.11: *Relative reaction energy* ΔE_R *as a function of the number of adjacent nitrogen atoms for three possible types of trapping centers at the interface, namely, vacancy defect, oxygen and nitrogen.* 147

Figure 5.12: *Comparison of the atomic charge for the bridging oxygen or nitrogen*

ATTENTION: The Singapore Copyright Act applies to the use of this document. Nanyang Technological University Library

atom in Si-O-Si or Si_2-N-Si system, respectively, by using three different approaches: (1) Mulliken atomic charge analysis [224], (2) Chirlian-Francll interface cluster model [225], and (3) natural population analysis [226]...148

Figure 6.1: *Schematic diagram of CMOS fabrication process flow with SPT.*..........152

Figure 6.2: *SEM cross sections of devices with and without SPT. After [198].*.........152

Figure 6.3: *Comparison of device performance between p-MOSFETs with and without SPT. About 19% I_{on} improvement is achieved by SPT process.* 153

Figure 6.4: *Comparison of NBTI degradation between the samples with and without SPT. (a) The threshold voltage shift (ΔV_{th}) is measured as a funtion of stress time (t) at gate stress voltage (V_{gstr}) of -2.3 V and stress temperature (T_{str}) of 125 °C; (b) ΔV_{th} is measured as a funtion of T_{str} at V_{gstr} = -2.3 V for stress time of 100 s; and (c) ΔV_{th} is measured as a funtion of V_{gstr} at T_{str} = 125 °C for stress time of 100 s. The relative NBTI improvement by SPT is shown in (b) and (c). The lines are for guiding eyes only.* 156

Figure 6.5: *Comparison of NBTI degradation between the samples with and without SPT and the relative NBTI improvement by SPT as a function of channel length. The stress voltage is -2.3 V, stress temperature is 125 °C, and stress time is 100 s.*...157

Figure 6.6: *(a) Change in Si-H bonding-energy (ΔE_B) as a function of change in bond angle ($\Delta\theta_B$); and (b) change in NBTI reaction energy (ΔE_R) as a function of $\Delta\theta_B$. The values of Si-H bonding-energy and NBTI reaction energy corresponding to the bond angle in equilibrium (i.e., $\Delta\theta_B = 0$) are taken as references. In (a), the bond angle is either ∠Si-Si-H or ∠Si-Si-Si in the Si_3-Si-H structure at interface; and in (b) the bond angle is ∠Si-O-Si and ∠Si-N-Si for pure oxide and nitrided oxide, respectively.*....................159

Figure 6.7: *Definitions of the directions for device simulation.*...............................161

Figure 6.8: *Stress distributions in p-MOSFETs with and without SPT along the longitudinal (X), transverse (Y) and vertical (Z) directions. The dimension of each device stress map is about 0.4μm x 0.4μm, and the channel length is 50nm.*..163

Figure 6.9: *Simulated stress profiles in p-MOSFETs with and without SPT at the interface along the longitudinal (a), transverse (b), and vertical (c) directions as a function of distance x in the channel direction. The results are directly extracted from the device stress maps in Fig. 6.8.* 165

Figure 6.10: *Simulated stress profiles in p-MOSFETs with and without SPT along the longitudinal direction as a function of distance x for the three different positions: at the interface, in the oxide (denoted by the gray color lines), and in the channel.*..166

Figure 6.11: *Sum of the bond angle changes in magnitude as a function of the strain induced in either vertical or longitudinal direction. Poisson's ratio used*

ATTENTION: The Singapore Copyright Act applies to the use of this document. Nanyang Technological University Library

in the calculation is 0.28 for both directions. 168

Figure 6.12: *Electrical performance comparisons of p-MOSFETs with laser spike annealing (denoted as "LSA") and spike-RTA process (denoted as "Spike"). About 5% I_{on} improvement is achieved by LSA.* 173

Figure 6.13: *Typical I_d-V_g and I_d-V_d sweep curves for p-MOSFETs with LSA process, before and after the NBTI stress of 1000 s.* 174

Figure 6.14: *Comparison of NBTI degradation between the samples with spike-RTA and LSA process. The threshold voltage shift (ΔV_{th}) (a), the shift in saturation drain current (ΔI_{dsat}) and the shift in linear drain current (ΔI_{dlin}) (b) are measured as a funtion of stress time (t) at gate stress voltage (V_{gstr}) of -2.3 V and stress temperature (T_{str}) of 125 °C.* 175

Figure 6.15: *The extrapolated device lifetime for both the samples with spike-RTA and LSA process.* 176

Figure 6.16: *NBTI degradation in high-preformance p-MOSFETs with ultra-thin nitrided gate oxide. The threshold voltage shift (ΔV_{th}) are measured as a funtion of stress time (t): (a) at gate stress voltage V_{gstr} = -1.5V for different stress temperatures T_{str}; and (b) at T_{str} = 125 °C for different V_{gstr}.* 179

Figure 6.17: *The threshold voltage shift (ΔV_{th}) in high-performance p-MOSFETs as a funtion of V_{gstr} at T_{str} = 125 °C for stress time of 1, 10, 100, 1000s.* 180

Figure 6.18: *The extrapolated device lifetime of high-performance p-MOSFETs at T_{str} = 125 °C and different V_{gstr}. The lines are for guiding the eyes only.*.....180

ATTENTION: The Singapore Copyright Act applies to the use of this document. Nanyang Technological University Library

LIST OF TABLES

Table 3.1: *A summary on proposed measurement methods for NBTI in-line test with detailed procedures: single-point I_{dlin} method and 1st on-the-fly (OTF) method [40, 152] for ΔV_{th} extraction, and single-point I_{dsat} method [182] for ΔI_{dsat} extraction.* 72

Table 3.2: *The parameters extracted from Fig. 3.15 based on $\Delta V_{th} = At^n$* 84

Table 4.1: *Values of fitting parameters used in the modeling shown in Fig. 4.2. The calculated characteristic transition time (t_{tr}) and critical time (t_c) are also included.* 96

Table 5.1: *Major process conditions for the nitrided gate oxide samples.* 129

Table 5.2: *Summary of the extracted A values for all test samples at V_{gstr} = -2.2 V and T_{str} = 25, 75 and 125 °C. The activation energy E_a obtained from Fig. 5.2 is included.* 131

Table 5.3: *Summary of the extracted n value for all test samples at V_{gstr} = -2.2 V and T_{str} = 25, 75 and 125 °C. The characteristic energy scale E_0 obtained from Fig. 5.5 is included.* 131

Table 5.4: *Summary of E_a (in eV) obtained from the Arrhenius plots of ΔV_{th} for stress time t = 1, 10, 100, and 1000s. The NBTI stress is carried out at V_{gstr} = -2.2 V.* 133

Table 5.5: *Summary of activation energies E_a (eV) obtained from Arrhenius plots of $A'(= A/v^{(\beta-1)/4})$ or $\Delta V_{th}'$ $(= \Delta V_{th}/[\ v^{(\beta-1)/4} t^{\beta/4}])$ at V_{gstr} = -2.2 V for various stress time t.* 138

Table 6.1: *A summary of the extracted stress values at the location (x = 0) for devices with and without SPT along the longitudinal, transverse and vertical directions, at three different positions: at the interface, in the oxide and in the channel.* 162

Table 6.2: *A summary of the extracted stress values at the interface for devices with and without SPT along the longitudinal, transverse and vertical directions, at three different temperatures.* 170

ATTENTION: The Singapore Copyright Act applies to the use of this document. Nanyang Technological University Library

NOMENCLATURES

1-D	One-Dimensional
2-D	Two-Dimensional
3-D	Three-Dimensional
AC	Alternating Current
ALD	Atomic Layer Deposition
BTI	Bias Temperature Instability
CMOS	Complimentary Metal-Oxide-Semiconductor
C-V	Capacitance-Voltage
CP	Charge Pumping
CVD	Chemical Vapor Deposition
DC	Direct Current
DCIV	Direct-Current Current-Voltage
DLHT	Deep-Level Hole-Trapping
DOS	Density-Of-State
DPN	Decoupled Plasma Nitridation
DSL	Dual Stress Liner
DUT	Device Under Test
EOT	Equivalent Oxide Thickness
GCD	Gate-Controlled-Diode
GND	Ground
G-R	Generation-Recombination

ATTENTION: The Singapore Copyright Act applies to the use of this document. Nanyang Technological University Library

HCI	Hot Carrier Injection
HDP	High-Density Plasma
IC	Integrated Circuits
ITRS	International Technology Roadmap for Semiconductors
I-V	Current-Voltage
JVD	Jet Vapor Deposition
LA	Laser Annealing
LSA	Laser Spike Annealing
MNOS	Metal-Nitride-Oxide-Semiconductor
MOS	Metal-Oxide-Semiconductor
MOSFET	Metal-Oxide-Semiconductor Field-Effect-Transistor
NBTI	Negative Bias Temperature Instability
OTF	On-the-Fly
PBTI	Positive Bias Temperature Instability
PDF	Probability Density Function
PECVD	Plasma-Enhanced Chemical Vapor Deposition
PMA	Post Metal Annealing
PNA	Post Nitridation Annealing
R-D	Reaction-Diffusion
R-DD	Reaction-Dispersive-Diffusion
RTA	Rapid Thermal Annealing
RTN	Rapid Thermal Nitridation
RTO	Rapid Thermal Oxidation

ATTENTION: The Singapore Copyright Act applies to the use of this document. Nanyang Technological University Library

SA	Spike Annealing
S/D	Source/Drain
SMT	Stress Memorization Technique
SRH	Shockley-Read-Hall
SPT	Stress Proximity Technique
TCAD	Technology Computer-Aided Design
UFS	Ultra-Fast Switching
ULSI	Ultra-Large-Scale-Integration

ATTENTION: The Singapore Copyright Act applies to the use of this document. Nanyang Technological University Library

CHAPTER 1 INTRODUCTION

This thesis is a presentation of research work done at the Nanyang Technological University. In this work, negative bias temperature instability (NBTI) in *p*-channel metal-oxide-semiconductor field-effect-transistors (*p*-MOSFETs) with ultra-thin gate oxide has been studied and explored. This chapter introduces the background, motivation, objectives and major contributions of this work. Details of this study are presented in the following chapters.

1.1 History of Metal-Oxide-Semiconductor Devices

The first bipolar transistor was built at Bell Labs in 1947 [1, 2], mainly based on the concept of surface field-effect transistor, the predecessor of modern MOSFETs, which was first proposed in late 1920s by Lilienfeld [3, 4] and Heil [5] separately. Since then, especially after the realization of metal-oxide-semiconductor (MOS) gate stacks within the thermal SiO_2-Si framework, the silicon science and technology has progressed explosively. However, today's ultra-large-scale-integration (ULSI) system is still mainly built upon the low-power high-density MOS structure, such as the metal-oxide-semiconductor field effect transistors (MOSFETs), which was first proposed in 1960 [6], and the complementary MOSFETs (CMOS) in 1963 [7]. The integrated circuits (IC) was first invented as early as in 1959 [8], and the rapid development of IC has accelerated the silicon technology to be mature and constantly undergo the down-scaling towards smaller dimensions, better device performance and

ATTENTION: The Singapore Copyright Act applies to the use of this document. Nanyang Technological University Library

higher packing density. Over the last four decades, the modern CMOS technology has emerged as the most prevailing technology for today's ULSI applications.

1.2 MOS Device Scaling – Moore's Law

The famous Moore's law [9, 10] describes a long-term trend in the history and development of computing hardware, and it states that: the number of transistors that can be placed inexpensively on an integrated circuit has increased exponentially, doubling approximately every two years. It has continued for almost half a century and is expected to continue for another decade at least or even much longer. Indeed, Moore's law has become the main driving force of technological and social change in the late 20th and early 21st centuries.

To follow the Moore's law, a set of scaling rules has been well established over the decades to achieve smaller dimension, higher density, faster speed, less power dissipation and lower cost per circuit. According to the scaling rules as in Ref. [10], for every three years, the device dimension is reduced by a factor of 0.707, the chip size is increased by a factor of 1.5, and the total number of transistors in a chip is increased by a factor of 4. Down-scaling in device dimension, particularly in the transistor gate length, induces a higher transistor current, which enables the device to switch faster and thus leads to faster computations for the chip. In addition, transistor size becomes smaller and hence more transistors can be integrated into a single chip. Consequently, the complexity and functionality of ICs is also increased while the manufacturing cost per chip is still kept low.

ATTENTION: The Singapore Copyright Act applies to the use of this document. Nanyang Technological University Library

To achieve the target that is predicted by Moore's law, MOS device scaling needs to be further developed, and the down-scaling involves all aspects of the advanced silicon technology, including lithography, etching, thin film deposition, ion implantation, diffusion, gate length/width, gate dielectric thickness, power supply voltage, threshold voltage, short-channel effects, high-field effects, dopant density fluctuation, interconnect, novel device structures, circuit design and device reliability [11-13]. Device scaling was traditionally limited by the development of new lithography tools, masks and photoresist materials, and the critical-dimension etch processes. Nevertheless, in the past few years, it has become clear that: despite the advances in these crucial technologies and other innovations to produce smaller feature sizes down to nanometer-scale, the front end technologies cannot keep pace, and thus the device performance has to be compromised. Indeed, the crux of this problem comes from the fact that the traditional gate dielectric film has been pushed to its fundamental limit. As a result, continuous device down-scaling requires a modification of the existing materials or an introduction of other new materials.

1.3 Gate Dielectric Scaling and Oxide Reliability

The gate stack, as the heart of MOS devices, is most critical to the success of the CMOS technology. As early as the 1960s, the thermally-grown silicon dioxide (SiO_2) has been used as the gate dielectric for the MOSFETs [14], and extensive research and development over the past four decades have shown that SiO_2 exhibits superior interfacial properties and can provide an excellent passivation for the silicon surface against contamination. This is mainly due to the fact that SiO_2 has many unique and outstanding properties in nature. Most importantly, SiO_2 is native to silicon, and thus

ATTENTION: The Singapore Copyright Act applies to the use of this document. Nanyang Technological University Library

forms an interface with low defect density (~10^{10} $eV^{-1}cm^{-2}$, after H_2 passivation). SiO_2 also possesses excellent thermal and chemical stability, which enable high-temperature processing. Besides, SiO_2 has very high resistivity (~10^{15} Ω cm), excellent dielectric strength (~1×10^7 V/cm), and a large band gap (~9 eV). All these properties make SiO_2 the best candidate for the gate dielectrics in the gate stack, which indeed has triggered the revolutions of microelectronics for decades.

However, according to the ITRS roadmap 2007 [15], reduction of equivalent gate oxide thickness (EOT) has emerged as the most critical and difficult challenge for further down-scaling, which is constantly required for continuous improvement of device performance. EOT for pure oxide is now approaching its fundamental material limits. Nevertheless, the ultra-thin gate oxide or nitrided oxide still remains a hot research topic for 65nm or 45nm technology nodes. Regarding the employment of ultra-thin gate oxide, some issues need to be solved, such as the direct tunneling, quantum mechanical effect, boron penetration, gate poly-silicon depletion, and oxide reliability. Among them, the gate oxide reliability has been one most critical issue and might become a possible showstopper for further down-scaling, since gate oxide degradation or breakdown can lead to malfunctions or immediate failure of advanced ULSI devices and circuits [16-25]. Gate oxide breakdown is partially attributed to the increasing oxide field ξ_{ox} due to a less-aggressive scaling of the supply voltage [16, 20]. In addition, the charge-to-breakdown decreases significantly as the oxide thickness shrinks. Therefore, under constant voltage stress, oxide breakdown becomes easier [21, 22].

Besides oxide breakdown, there are two other main oxide degradation mechanisms: namely, hot-carrier injection (HCI) [26-30], particularly in *n*-channel

ATTENTION: The Singapore Copyright Act applies to the use of this document. Nanyang Technological University Library

MOSFETs, which used to limit the lifetime of CMOS circuits for 0.35μm technology node and above, and negative bias temperature instability (NBTI) [31], particularly in *p*-channel MOSFETs. With all these concerns mentioned above, the reliability of ultra-thin gate dielectrics has become one major limiting factor for future ULSI development.

1.4 Motivation

In recent years, NBTI has been widely recognized as one major device reliability issue, especially for high performance *p*-MOSFETs with ultrathin gate oxide, and it would become the showstopper for further down-scaling of gate-dielectric [31-33]. When the device is stressed with a negative gate bias at an elevated temperature, NBTI could lead to a significant increase of the threshold voltage (ΔV_{th}) in *p*-MOSFET by as much as 20~50 mV over a period of time, depending on the operating condition of the chip. As a consequence, the device becomes more difficult to turn on, the drive current decreases and thus the circuit speed is largely reduced. With the aggressive down-scaling of the gate oxide thickness into the direct-tunneling regime, when the oxide thickness becomes less than 3.5 nm, instead of HCI-induced degradation in *n*-MOSFETs, NBTI degradation in *p*-MOSFETs starts to limit the lifetime of CMOS circuits [31, 32]. Moreover, the nature of dielectric degradation in ultra-thin oxides could be quite different from that in thicker oxides. Therefore, as the gate dielectric thickness shrinks to sub-2nm, which is only several-atomic-layers thick, gate dielectric reliability issues such as NBTI in *p*-MOSFETs need to be re-examined.

For 0.13μm technology node and beyond, instead of pure SiO_2, nitrided oxide or

ATTENTION: The Singapore Copyright Act applies to the use of this document. Nanyang Technological University Library

oxynitride (SiO_xN_y) has been widely used as the insulating gate dielectric, because the incorporation of nitrogen overcomes the problem of boron-penetration, provides a relatively-higher dielectric constant *k* value, preserves the good interface quality, and reduces HCI degradation effectively in *n*-MOSFETs. However, it has been intensively reported that incorporation of nitrogen into the gate oxide worsens NBTI degradation quite significantly [34-38]. The role of nitrogen in NBTI has to be further investigated experimentally, and the underlying mechanism of the nitrogen-worsen NBTI also needs to be studied and revealed, through physical and atomistic modeling. Moreover, the characterization of NBTI becomes quite critical since NBTI recovery is universally observed upon the removal of stress [32, 39-41], which occurs in the reality and might be encountered quite frequently during electrical measurement as well.

Moreover, in the semiconductor manufacturing industry, as driven by Moore's Law [9, 10], device down-scaling will at least continue in another decade or longer. Concurrently, in order to further boost device performance, various advanced or novel process technologies, such as stress engineering and material innovations, will be developed and implemented in the real chip fabrication. The impact of these new processes or techniques on NBTI degradation and other related reliability issues ought to be addressed immediately during development. Therefore, some sort of in-line test methodology on NBTI would be quite beneficial, and the study of the process-dependent NBTI also becomes quite necessary and useful for further process development and optimization.

ATTENTION: The Singapore Copyright Act applies to the use of this document. Nanyang Technological University Library

1.5 Objectives and Scope of Research

The main objectives of this thesis are to investigate NBTI degradation in *p*-MOSFETs and to study the underlying mechanism of NBTI through physical and atomistic modeling, process simulation and device characterization. The scope of the research and approach is as follows:

1. Electrical characterization of BTI degradation in MOSFETs by using different measurement methods, including conventional Current-Voltage (*I*-*V*) method, single-point saturation/linear drain current method, On-the-Fly (OTF) method, Direct-Current Current-Voltage (DCIV) method, and Charge Pumping (CP) method.
2. Experimental investigation of NBTI and NBTI recovery in *p*-MOSFETs.
3. Development of a simple and fast NBTI measurement method, based on the measurement of single-point saturation drain current.
4. Development of an in-line test methodology for NBTI.
5. Physical modeling of NBTI in *p*-MOSFETs, mainly based on the classical reaction-diffusion (RD) model by incorporating the dispersive nature of hydrogen diffusion.
6. Characterization and modeling of nitrogen-worsen NBTI degradation, and a thorough examination of the underlying mechanism.
7. Modeling and characterization of geometry-dependent NBTI in *p*-MOSFETs with various device channel dimensions.
8. Experimental investigation and modeling of the impact of process technologies on NBTI in *p*-MOSFETs for 65nm/45nm technology nodes.

ATTENTION: The Singapore Copyright Act applies to the use of this document. Nanyang Technological University Library

1.6 Major Contributions of the Thesis

In this thesis, characterization and modeling of NBTI degradation in *p*-MOSFETs with ultra-thin gate dielectric have been investigated and studied in detail. The major contributions of this thesis are listed as follows:

1. A simple NBTI characterization method has been developed to minimize the immediate recovery effect during measurement, and an NBTI in-line test methodology has been proposed to examine NBTI degradation during the development phase.
2. NBTI recovery phenomenon in *p*-MOSFETs has been investigated experimentally, and a combined empirical model of NBTI recovery has been proposed so as to describe the entire process of NBTI recovery in a wide time range.
3. An analytical reaction-diffusion (R-D) model has been proposed to describe NBTI in *p*-MOSFETs in a wide time scale covering the three regimes of reaction, transition and diffusion, and the analytical R-D model has also been extended to include other possible hydrogen diffusing species.
4. Based on an analytical geometry-dependent R-D model, the geometry dependence of NBTI has been investigated experimentally and studied thoroughly in terms of the strain effect and hydrogen diffusion in devices with smaller dimensions.
5. The nitrogen-worsen NBTI degradation in *p*-MOSFETs has been well explained by an analytical reaction-dispersive-diffusion (R-DD) model that incorporates the dispersive nature of hydrogen diffusion, in terms of the dependence of NBTI on stress time, stress temperature and interfacial nitrogen concentration, and the power-law behavior as well, and first-principles calculation has been carried out to examine the influence of nitrogen on NBTI, in terms of the NBTI reaction energy,

ATTENTION: The Singapore Copyright Act applies to the use of this document. Nanyang Technological University Library

electro-negativity and atomic charge distribution of nitrogen, oxygen and silicon atoms at the interface.

6. Impact of various advanced process technologies, such as the stress proximity technique (SPT) and laser spike annealing (LSA), on NBTI in 65nm or 45nm low-power *p*-MOSFETs has been investigated. NBTI in high-performance devices with ultrathin nitrided gate oxide has also been studied.

1.7 Organization of the Thesis

This thesis mainly focuses on the study of NBTI in *p*-MOSFETs with ultra-thin gate dielectric, and it is organized as follows:

CHAPTER 1 provides an introduction on the history and development of MOS devices, MOS device scaling and gate dielectric scaling, and the oxide reliability is briefly reviewed, particularly on the NBTI issue in *p*-MOSFETs. The motivation, objectives and major contributions of this thesis are also presented in this chapter.

CHAPTER 2 reviews some fabrication techniques of silicon oxide and oxynitride and some basic theory on the gate oxide interface as well. An overview on NBTI in *p*-MOSFETs is given, including a brief history and some latest highlights, and it is followed by a compact review on the material/process-dependence of NBTI. The physical models for NBTI, in terms of interface trap generation/re-passivation, positive oxide trap generation, hole trapping/de-trapping and deep-level hole-trapping, and some models for NBTI recovery, are summarized. Lastly, some conventional and fast NBTI characterization techniques are briefly reviewed.

ATTENTION: The Singapore Copyright Act applies to the use of this document. Nanyang Technological University Library

CHAPTER 3 focuses on the characterization of NBTI and NBTI recovery. A simple NBTI characterization technique of measuring a single-point saturation drain current is developed to minimize the unwanted NBTI recovery during measurement. An NBTI in-line test methodology is proposed here to monitor NBTI degradation during process development, aiming for process comparison and optimization in an advanced technology node. NBTI recovery is also examined and a combined empirical model for NBTI recovery is used to describe the entire process of NBTI recovery in a wide time range.

CHAPTER 4 gives a comprehensive study on the modeling of NBTI degradation. Based on the classical reaction-diffusion model, an analytical reaction-diffusion (RD) model is developed to describe NBTI degradation in *p*-MOSFETs in a wide time scale covering the three regimes of reaction, transition and diffusion. This analytical R-D model for NBTI is then extended to become a more general model that includes other possible hydrogen-related diffusing species, such as the positively-charged hydrogen ion H^+ and hydrogen molecule H_2. Lastly, an analytical geometry-dependent R-D model is derived, and the geometry dependence of NBTI is evidenced and studied, in terms of the strain effect and the influence of hydrogen diffusion at edges and corners for devices with smaller dimensions.

CHAPTER 5 presents a systematic study on nitrogen-worsen NBTI. NBTI degradation for the nitrided gate oxides can be well described by an analytical reaction-dispersive-diffusion (R-DD) model in diffusion-limited regime, and it is found that both the interfacial nitrogen concentration and the nitrogen profile in the nitrided oxides play important roles in the nitrogen-worsen NBTI. The influence of hydrogen dispersive diffusion on NBTI is examined and the R-DD model can well

ATTENTION: The Singapore Copyright Act applies to the use of this document. Nanyang Technological University Library

explain the dependence of NBTI on stress time, temperature and interfacial nitrogen concentration, and its power-law behavior as well. Lastly, first-principles calculation is carried out to examine the effect of nitrogen as either a reaction site or adjacent atom(s) at the interface, in terms of the NBTI reaction energy, electro-negativity and atomic charge distribution of nitrogen, oxygen and silicon atoms at the interface.

CHAPTER 6 mainly investigates the impact of various advanced process technologies, such as stress proximity technique and laser spike annealing, on NBTI degradation in *p*-MOSFETs. NBTI degradation in high-performance devices with ultrathin gate dielectrics is also examined.

CHAPTER 7 summarizes the work that has been done in this thesis, and lastly, the recommendations for future research are presented.

ATTENTION: The Singapore Copyright Act applies to the use of this document. Nanyang Technological University Library

CHAPTER 2 LITERATURE REVIEW

This chapter starts with a brief review on the basic theory of the Si-SiO_2 interface. An overview of negative bias temperature instability (NBTI) in *p*-channel metal-oxide-semiconductor field-effect-transistors (*p*-MOSFETs) is presented, followed by a brief summary on the process dependence of NBTI. Moreover, various NBTI models and models for NBTI recovery, in terms of interface trap generation/re-passivation, positive oxide trap and hole trapping/de-trapping, are summarized. Lastly, some conventional and fast NBTI characterization techniques are briefly reviewed.

2.1 Substrate/Gate-Dielectric Interface

The substrate/gate-dielectric interface, as the main part of the gate stack, is one of the most important systems in the MOS device, and hence high-quality gate dielectric layers are always highly desired in order to meet the stringent requirement of CMOS technology development. The silicon dioxide (SiO_2) was used as the gate dielectric for the MOS device as early as the 1960s [14], and from then on, the SiO_2-based dielectric system has been widely adapted in CMOS technology. The basic structure of thermally-grown amorphous SiO_2 is tetrahedral. The silicon ion is surrounded by four oxygen ions which act as bridges linking with other silicon ions to form various phases of SiO_2.

ATTENTION: The Singapore Copyright Act applies to the use of this document. Nanyang Technological University Library

2.1.1 Fabrication Techniques of Silicon Oxide and Oxynitride

The ultra-thin gate dielectric can be fabricated by thermal growth, deposition or implantation. The fabrication process may directly influence the quality of the gate dielectric and eventually affect the characteristics of CMOS-based ICs. The detailed fabrication techniques of SiO_2 are listed in the followings:

- **Thermal growth**

  The conventional and simplest method to fabricate SiO_2 is to grow it thermally by exposing Si to O_2 at a high temperature. In fact, all commercial SiO_2 gate dielectrics are grown by thermal oxidation, using O_2 or H_2O as oxidant species. However, the thermal method incurs a high thermal budget. Therefore, for the growth of ultrathin gate dielectrics in advanced CMOS technology, rapid thermal processing is used after the thermal growth to control the thermal budget.

- **Chemical deposition**

  Chemical deposition is used when a low thermal budget is desired. This technique does not involve the reaction with Si substrate. Instead, the SiO_2 layer is purely deposited by chemical vapor deposition (CVD). However, this method is not suitable for growing ultrathin gate oxide, mainly due to its poor uniformity and quality as well.

- **Physical deposition**

  There are two types of physical deposition techniques, namely, ion implantation and high-density plasma. Ion implantation is usually followed by thermal anneal or oxidation treatment, while high-density plasma is mainly for nitridation. Both techniques can well control thickness, composition and structure of the deposited dielectric to a certain degree. The physical deposition techniques are quite distinct

ATTENTION: The Singapore Copyright Act applies to the use of this document. Nanyang Technological University Library

from plasma- or ion-induced chemical deposition. The dielectric layer is grown by the incorporation of energetic species and the subsequent reaction of these species with the substrate. As a consequence, these techniques might induce large damage to the substrate.

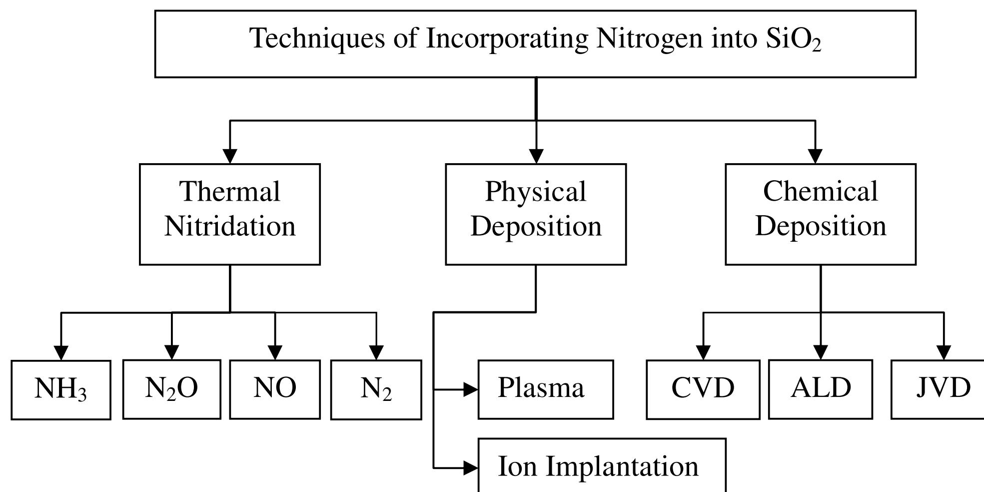

Figure 2.1: *Different techniques of incorporating nitrogen into SiO_2, after [42].*

As the development of advanced CMOS technology continues, Si-O-N or oxynitride (SiO_xN_y) is widely adapted as the gate dielectric to replace pure SiO_2. Incorporation of nitrogen into the gate oxide can suppress boron penetration [43, 44], preserve a good interface quality, and hence reduce gate leakage and enhance the resistance to hot-carrier aging and dielectric degradation [45, 46]. Besides, Si_3N_4 has a higher dielectric constant, and thus SiO_xN_y film with the same EOT as that of pure SiO_2 film will be physically thicker. Similarly, nitrogen can be incorporated into SiO_2 by three different methods, namely thermal nitridation, physical deposition and chemical deposition, which are summarized in Fig. 2.1. Although thermal nitridation is usually carried out at very high temperature, it can only induce a relatively low nitrogen concentration in the film on the order of 10^{15} N/cm^2 [42]. To achieve a higher

ATTENTION: The Singapore Copyright Act applies to the use of this document. Nanyang Technological University Library

nitrogen concentration in oxide film with a lower thermal budget, other deposition methods, such as chemical vapor deposition (CVD) [47], jet vapor deposition (JVD) [48], atomic layer deposition (ALD) [49], or nitridation by nitrogen plasma generated by the impact of low-energy electrons [50], can be used. However, these low-temperature deposition methods normally result in non-equilibrium films, which are thermodynamically unstable, and thus subsequent thermal annealing treatment is often required to minimize defects and improve film quality [51].

2.1.2 Charges in the Si-SiO_2 System

As the heart of MOSFETs, the MOS capacitor is the most fundamental structure for understanding the Si-SiO_2 system. The MOS capacitor has been well studied because it is directly related to most planar devices and ICs.

An ideal MOS capacitor, with the assumptions of zero work-function difference, ideal metal/poly-Si gate, flawless bulk substrate, perfect gate dielectric and defect-free interface, is the foundation to understand the practical MOS diode and to explore the physics of semiconductor devices and circuits. When an ideal MOS capacitor is biased with an external voltage, three surface conditions may exist according to the change of the surface potential ψ_s, namely accumulation, depletion and inversion, which correspond to $\psi_s<0$, $\psi_B>\psi_s>0$ and $\psi_s>\psi_B$ for the p-type substrate, respectively, where ψ_B is defined as the potential difference between the Fermi level (E_F) and the intrinsic Fermi level (E_i).

ATTENTION: The Singapore Copyright Act applies to the use of this document. Nanyang Technological University Library

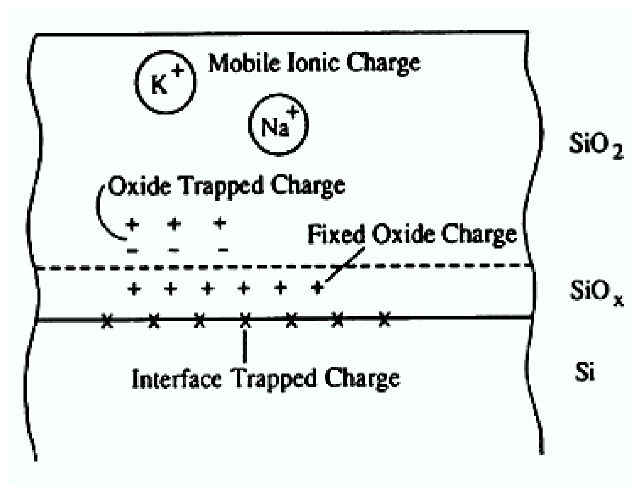

Figure 2.2: *Charges and their locations in thermally oxidized silicon, after [52].*

For a practical MOS capacitor, work-function difference between the metal and semiconductor would bend the energy band upwards or downwards. Meanwhile, interface traps and oxide charges may also largely affect the MOS characteristics. External influences, such as temperature, ionizing radiation, hot-carrier injection and voltage stress, have strong impact on interface trap and oxide charge generation. In real application, interface traps and oxide charges might be responsible for the failure of MOS devices. Fig. 2.2 shows the classifications of these charges in the Si-SiO_2 system. They are briefly introduced as follows [52, 53]:

(1) Fixed oxide charge (Q_f, N_f)

The fixed oxide charge is positive, mainly due to structural defects in the oxide layer less than 25Å from the Si-SiO_2 interface. The fixed oxide charge is immobile under an applied electrical field and not affected by the oxide thickness or by the type and concentration of dopant in the silicon. It is usually believed that excess silicon atoms and/or the loss of electrons from excess oxygen atoms near the Si/SiO_2 interface is the origin of the fixed oxide charges.

ATTENTION: The Singapore Copyright Act applies to the use of this document. Nanyang Technological University Library

(2) Mobile oxide charge (Q_m, N_m)

The mobile oxide charge primarily refers to alkali ions such as Na^+, Li^+, K^+ and possibly H^+. The development of CMOS technology was ever delayed due to the mobile charges in the early days, but they are no longer a critical concern in the state-of-art CMOS technology nowadays.

(3) Interface trapped charge (Q_{it}, N_{it}, D_{it})

The interface states, also known as the interface traps, have energy states in the silicon band-gap and can result in charges trapped at the Si-SiO_2 interface. Interface trapped charges are mainly caused by oxidation-induced structural defects, metal impurity and other defects from radiation or similar bond-breaking process. For a thermally-grown SiO_2, most of the interface trapped charges can be neutralized by forming-gas anneal. There are two types of interface traps, namely donor-like trap and acceptor-like trap. The interface states can be charged or discharged, depending on the surface potential. The acceptor-like interface trap is neutral when the Fermi level (E_F) is below the state and it will become negatively charged if E_F is above the state, while the donor-like interface trap is neutral when E_F is above the state and it will become positively charged if E_F is below the state.

(4) Oxide trapped charge (Q_{ot}, N_{ot})

The oxide trapped charge may be positive or negative, due to holes or electrons trapped in the oxide by ionizing radiation, avalanche injection, tunneling and hot-carrier injection during device operation. These oxide traps are associated with defects in SiO_2, and most of them can be eliminated by the subsequent anneal, although neutral traps may still remain and are distributed through the oxide layer.

ATTENTION: The Singapore Copyright Act applies to the use of this document. Nanyang Technological University Library

2.2 Review on NBTI in p-MOSFETs: An Overview

Negative bias temperature instability (NBTI) occurs particularly in *p*-channel metal-oxide-semiconductor field-effect-transistor (*p*-MOSFET) when the device is stressed with a negative gate bias at an elevated temperature for a certain period of time. As a result, it leads to an instability of device performance in terms of the increase of threshold voltage and the decrease of drain current, trans-conductance and hole mobility. More specifically, NBTI degradation originates from the generation of interface traps and oxide traps in device under NBTI stress. In real IC, e.g. a typical CMOS inverter as shown in Fig. 2.3, when the input is at GND (Low), the output is High, and correspondingly, the top *p*-MOSFET is under a negative gate bias with respect to the substrate. Similarly, when the input is at High, the output is Low and the bottom top *n*-MOSFET is under a positive gate bias. Therefore, NBTI in *p*-MOSFET occurs very commonly during real IC operation.

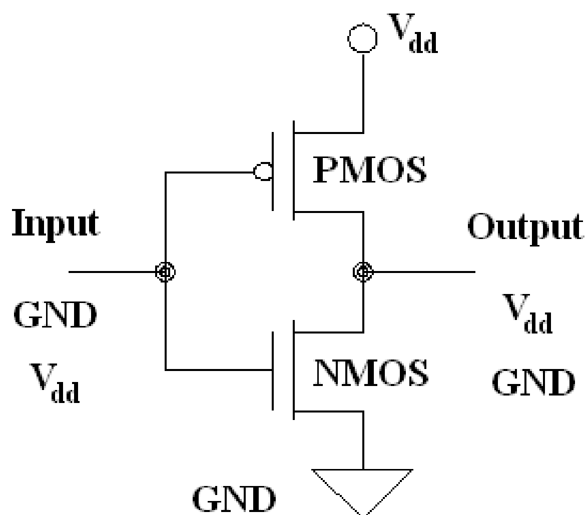

Figure 2.3: *Bias conditions of a typical CMOS inverter during circuit operation. GND stands for the "Low" state, while V_{dd} corresponds to the "High" state.*

ATTENTION: The Singapore Copyright Act applies to the use of this document. Nanyang Technological University Library

2.2.1 History of NBTI

NBTI can be traced back to the very early days of MOS device development, first observed by Miura and Matukura in 1965 [54], and also reported by Goetzberger *et al.* in 1966 [55] and Deal *et al.* in 1967 [56]. All these studies were carried out based on MOS structure with Al electrode and thermally-grown SiO_2 on Si substrate, and device degradation was monitored by the accumulated electron density N_{FB} (obtained from the flat-band voltage V_{FB} of device *C-V* characteristics) [54], the flat-band voltage V_{FB} [55, 57], the surface-state charge/density Q_{ss}/N_{ss} [56-58] and the fast surface-state density N_{st} [56, 58]. By assuming that the distribution and the density of surface-states were unchanged, Minra and Matukura attributed the increase in the flat-band voltage V_{FB} under negative bias temperature stress as an indication of the generation of accumulated electrons N_{FB} in the SiO_2 near the interface, and N_{FB} was originated from oxygen vacancy ions resulting from the electrochemical reaction of SiO_2 under a strong electric field [54]. Similarly, Goetzberger *et al.* observed the phenomenon of negative V_{FB} shift in the Al-SiO_2-Si MOS structure under a negative bias, and the change in V_{FB} was larger for a more negative bias. It was explained by either the injection of carriers from substrate into traps deeper in the oxide or the space charge limited emission of positive ions from the substrate, but the former possible explanation was invalidated by the absence of time dependence [55]. However, in their later study [57], the logarithmic time-dependence of the increase in surface-state density was observed, which is shown in Fig. 2.4. It could be explained on the basis of either a charge model [59] that involves the tunneling of carriers from the silicon to the oxide or a chemical model that alters the chemical bonds to form

ATTENTION: The Singapore Copyright Act applies to the use of this document. Nanyang Technological University Library

defects. The defects could effectively trap electrons or holes, which was further illustrated by Breed in his work [60]. Moreover, an essentially linear dependence of surface state density on the stress voltage was observed and there was no threshold for this effect. Indeed, the data extracted from [57] and re-plotted in Fig. 2.4 can better fit the power-law time-dependence, and it yields an exponent factor of ~0.29 at 250°C. In Deal's early work [56], besides initial surface state charges Q_{ss}, fast surface-state density N_{st} was also observed from the device *C-V* characteristics and it is linearly correlated to the initial Q_{ss} value. Moreover, the results for different oxide thicknesses implied that the effect was proportional to the applied electric field rather than the applied voltage, and interestingly, this stress-induced Q_{ss} could be partially recovered towards the original value by applying a subsequent positive bias or by shorting the field plate to the silicon at a higher temperature. A comprehensive summary on the charges in thermal SiO_2 was given in Deal's later work [58], in which the understanding and possible origins of the fixed surface state charge Q_{ss}, fast surface-state density N_{st} and oxide trapped charge Q_{ot} under negative bias temperature stress were presented. As can be seen in Fig. 2.5, in the transition region, there were two kinds of fast states $N_{st'}$ - dangling silicon bond unpassivated with hydrogen and $N_{st''}$ - dangling silicon bond due to a missing oxygen atom, which was at that stage believed to be the source of Q_{ss} but in later development was solved or improved by advanced techniques as mentioned in previous section 2.1.1. If a negative electric field is applied across the oxide, with the assistance of high temperature anneal or ionizing radiation, various kinds of silicon-oxygen bonds at/near the interface and in the oxide could be broken, which in turn leads to N_{st}, Q_{ss}, and N_{ot}. It was reported that N_{st} could be minimized by hydrogen anneal, which was nowadays widely adapted in

ATTENTION: The Singapore Copyright Act applies to the use of this document. Nanyang Technological University Library

advanced silicon technology as the most common process of forming gas anneal to improve oxide interface by passivating the dangling silicon bonds at the interface.

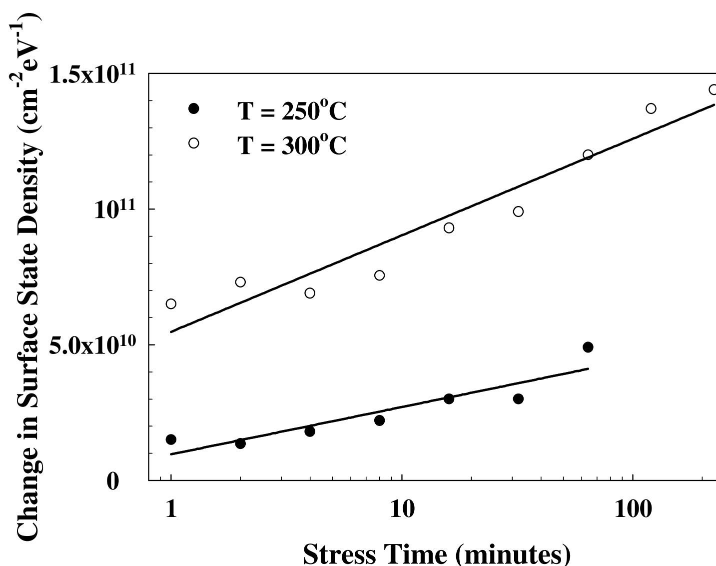

Figure 2.4: *The time development of surface states under stress at 10^6 V/cm at 250°C and 300 °C. A best fit log(time) line is shown for each set of points. After [57].*

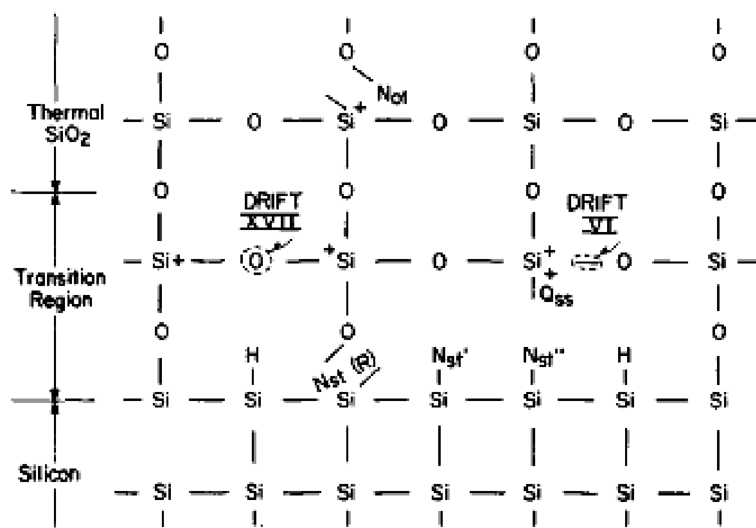

Figure 2.5: *Two dimensional sketch of thermally oxidized silicon showing possible origins of charges. After [58].*

ATTENTION: The Singapore Copyright Act applies to the use of this document. Nanyang Technological University Library

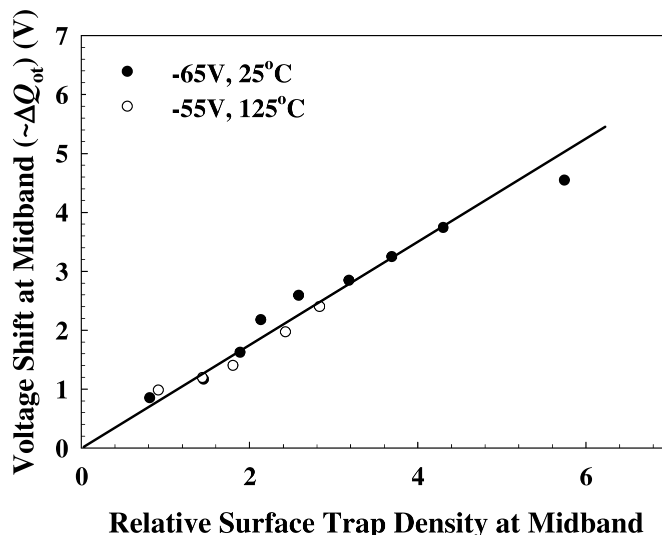

Figure 2.6: *The increase of the oxide charge measured as the shift of the C-V curve at midband, plotted against the relative surface-trap density at midband. The same relationship is observed after NBS at both 125 ℃, -55 V (5.8 MV/cm) and 25 ℃, -65 V (6.8 MV/cm) and indicates that there is roughly one surface trap per oxide charge. After [61].*

In 1977, Jeppson and Svensson [61] observed NBT-stress induced degradation in the Metal-Nitride-Oxide-Semiconductor (MNOS) transistor in terms of a negative shift in the threshold voltage window and a decrease in the retention time, and further confirmed that interface trapped charges N_{it} and oxide trapped charges N_{ot} were equally generated, as shown in Fig. 2.6. Besides, a power-law time-dependence of the interface trap generation with an exponent factor of 1/4 was extensively observed at low electric field, and it could be well explained by a diffusion-controlled electrochemical reaction occurring at the interface with hydrogen-terminated silicon bonds (Si-H) acting as precursors of this reaction [61]. The one-to-one correlation between NBTI-induced N_{it} and N_{ot} was further confirmed by many researchers

ATTENTION: The Singapore Copyright Act applies to the use of this document. Nanyang Technological University Library

[62-65], while the power-law time-dependence of NBTI was extensively observed and the power-law factor n was reported in range of 0.20~0.30 [62-67]. The diffusion-controlled electrochemical reaction model was also well-known as the reaction-diffusion (R-D) model, and it was further unified and generalized for both the charged and neutral diffusing species by Ogawa and Shiono in 1995 [68]. On the other hand, Blat *et al.* proposed their NBTI model, mainly based on a first-order electrochemical reaction that involved hydrogen-terminated trivalent silicon atoms, neutral water-related species and holes at the surface. The reaction would result in a trivalent silicon at the interface and a positively-charged water-related species in the oxide when the device is under the NBTI stress [64].

2.2.2 New Era of NBTI Since 1999

With aggressive down-scaling of gate oxide thickness into the direct-tunneling regime, when the oxide thickness is reduced to be less than 3.5nm, instead of the hot carrier degradation, NBTI degradation starts to limit the device lifetime. It was first predicted by Kimusuka *et al.* in 1999 [31]. Indeed, as the gate dielectric migrated to the nitrided oxides, the nitrogen content in the oxide was found to worsen NBTI significantly, and it made NBTI as one of the most critical device reliability issues shortly after the nitrided oxide became industry standard for the advanced CMOS technology [34, 35, 69-74]. Since then, research on NBTI has progressed very fast. NBTI was examined in all aspects, including its material/process-dependence, time-dependence, temperature-dependence and voltage/field-dependence. Theoretical work, in terms of physical models and atomic models, was carried out to understand NBTI mechanism and explain the origin of interface traps N_{it} and/or oxide charges N_{ot}

ATTENTION: The Singapore Copyright Act applies to the use of this document. Nanyang Technological University Library

and various dependences of NBTI as well. In particular, the effect of nitrogen on NBTI was extensively studied. Moreover, the frequency-dependence of NBTI and its impact on actual device lifetime in real application were also examined. On the other hand, in order to minimize the undesirable measurement-induced NBTI recovery, various fast or ultra-fast characterization techniques are developed to facilitate NBTI research on ultra-thin gate oxide, nitrided oxide and other conventional or novel high-k dielectrics. All these NBTI-related topics mentioned above will be briefly reviewed in the following sections separately.

2.3 NBTI Phenomenon and Process Dependence

NBTI is quite sensitive to process conditions, and a comprehensive review on this topic can be found in Ref. [33]. Some key points and an updated review on NBTI observations as well as its process-dependence will be presented in this section.

2.3.1 NBTI Observations in MOS Devices

In early research, NBTI mainly refers to the generation of positive interface traps N_{it} and oxide charges N_{ot} in the MOS structure under a negative gate bias at an elevated temperature. For state-of-art *p*-channel MOSFETs, the net contribution of N_{it} and N_{ot} to the threshold voltage shift ΔV_{th} will be:

$$\Delta V_{th} = \frac{q\left(\Delta N_{it} + \Delta N_{ot}\right)}{C_{ox}} \qquad (2.1)$$

where q is the unit electron charge and C_{ox} is the oxide capacitance.

ATTENTION: The Singapore Copyright Act applies to the use of this document. Nanyang Technological University Library

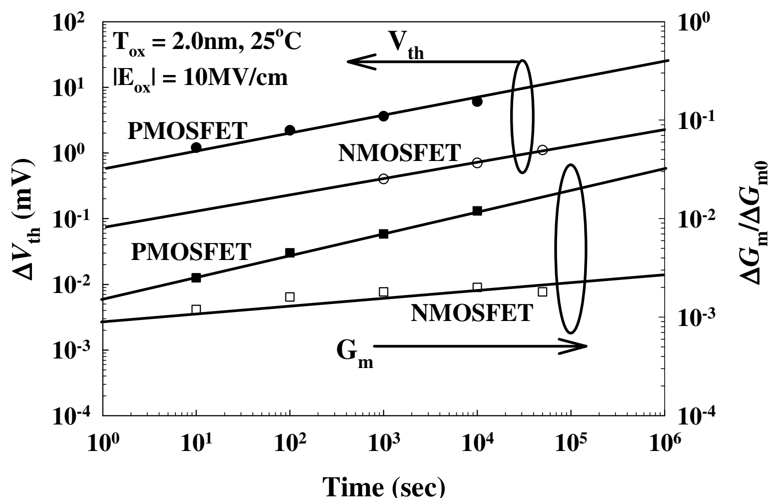

(a)

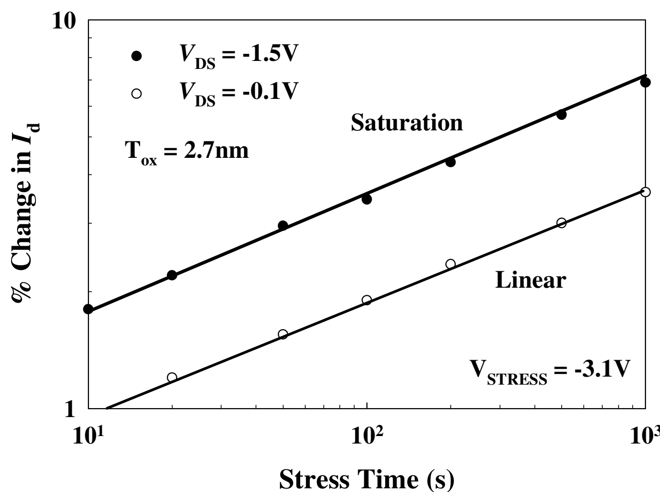

(b)

Figure 2.7: *(a) V_{th} change and G_m degradation vs. stress time for n- and p-MOSFETs, after [31]. (b) % change in I_d vs. stress time for two drain biases, showing that I_{dsat} degradation is more than I_{dlin} degradation, after [32].*

The saturation drain current I_{dsat}, linear drain current I_{dlin} and trans-conductance G_{m} for the *p*-MOSFET are generally given by Eqs. (2.2-2.4) respectively:

ATTENTION: The Singapore Copyright Act applies to the use of this document. Nanyang Technological University Library

$$I_{dsat} = \frac{u_{eff} C_{ox} W}{2L} \left(V_g - V_{th}\right)^2 \tag{2.2}$$

$$I_{dlin} = \frac{u_{eff} C_{ox} W}{L} \left[\left(V_g - V_{th}\right) V_{ds} - \frac{V_{ds}^2}{2} \right] \tag{2.3}$$

$$G_m = \frac{2 I_{dsat}}{\left(V_g - V_{th}\right)} \tag{2.4}$$

where W is the device channel width, L is the device channel length, μ_{eff} is the effective hole mobility, C_{ox} is the oxide capacitance, V_{g} is the gate bias and V_{ds} is the drain bias with the source and body at ground.

Therefore, changes in the threshold voltage V_{th} and/or in hole mobility μ_{eff} could lead to a degradation in I_{dsat}, I_{dlin} and G_{m}. NBTI-induced ΔV_{th} is shown in Eq. (2.1) and degradation of hole mobility may come from interface trap generation that leads to additional surface scatterings at the interface. As can be seen in Fig. 2.7(a), both ΔV_{th} and ΔG_{m} were observed for MOS devices subjected to NBTI stress, and it was clearly shown that BTI degradation in *p*-MOSFETs was much larger than that in *n*-MOSFETs. In Fig. 2.7(b), I_{d} degradations were observed for two different drain biases and it was clearly shown that I_{dsat} degradation was much more than I_{dlin} degradation.

Moreover, the projected device lifetime [34, 75-80] is widely used to monitor NBTI degradation, and mismatch of V_{th} and β [81, 82], noise characteristics [83, 84] and delay degradation and/or frequency shift in ring oscillator [32, 85-88] may also be used to examine the impact of NBTI on the circuit performance.

ATTENTION: The Singapore Copyright Act applies to the use of this document. Nanyang Technological University Library

2.3.2 Hydrogen, Deuterium and Water

Hydrogen is believed to play a critical role in NBTI because it is widely accepted to be the main species that passivates silicon dangling bonds at the interface due to mismatch of silicon and silicon dioxide during forming gas anneal or other processes. The hydrogen-terminated Si-H bond acts as a precursor of NBTI reaction, and it will break under NBTI stress to form interface trap. Hydrogen incorporation would lead to the formation of Si-H and O-H at the interface and in the oxide as well, and the concentration of Si-H and O-H could be quite high in the range of 10^{18}~10^{20}cm^{-3} for both dry and wet oxides [89]. The distribution of hydrogen in the oxide is non-uniform and a substantial pileup can be observed near the interface [89, 90]. Moreover, hydrogen can exist in various forms, such as atomic H, molecular H_2, proton H^+, or as a part of hydroxyl OH, hydronium H_3O^+ and hydroxide ions OH^-.

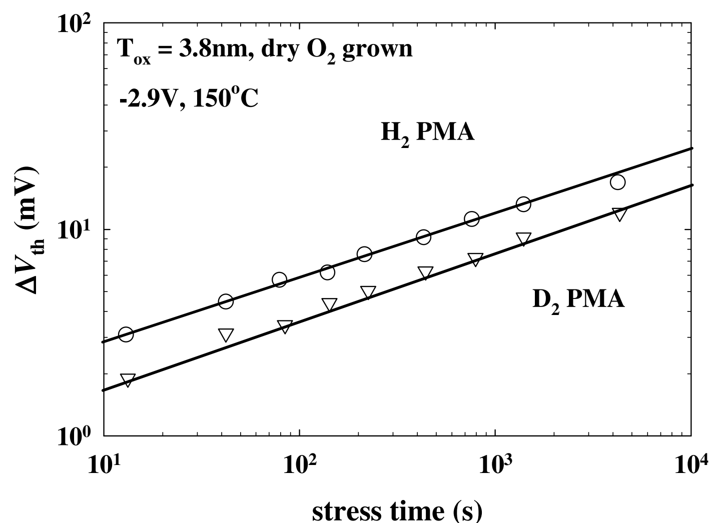

(a)

ATTENTION: The Singapore Copyright Act applies to the use of this document. Nanyang Technological University Library

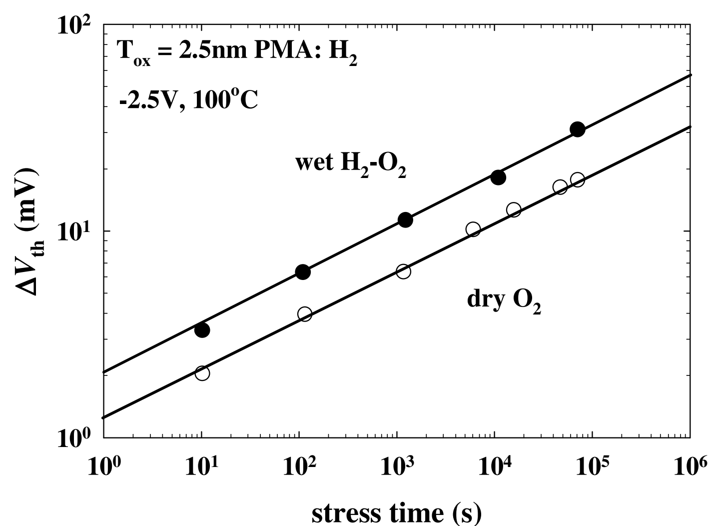

(b)

Figure 2.8: *(a) The effect of PMA on ΔV_{th}. D_2 PMA suppresses NBTI. (b) The effect of oxidation on ΔV_{th}. Wet oxidation enhances NBTI. After [34].*

Deuterium, a stable isotope of hydrogen with heavier mass, has been shown to reduce NBTI [34, 69]. Fig. 2.8(a) depicts the effect of H_2 and D_2 post metal annealing (PMA) on NBTI-induced ΔV_{th}. It was clearly shown that deuterium PMA suppressed NBTI. Recent studies on HfO_2 [91-93] or nitrided oxide [94-96] also confirmed the improvement of NBTI by deuterium, although Mitani and Satake [96] found no isotope effect in the p+-gate *p*-MOSFETs.

Water in the oxide worsens NBTI. Water or moisture can be easily incorporated through various processes, such as etching, cleaning and oxidation. For instance, oxides can be grown in different environments. Dry oxide is grown in O_2, damp oxide is grown by exposing the dry oxide to post metal annealing at 450 °C, and wet oxide is grown in the presence of water vapor. Blat *et al.* [64] carried out NBTI experiments for the dry, damp and wet oxides and observed N_{it} and N_{ot} generation in damp and wet

ATTENTION: The Singapore Copyright Act applies to the use of this document. Nanyang Technological University Library

oxides but not in dry oxide, Based on this, they proposed a model as mentioned previously that both water-related species and hole should be present near the interface so as to enable NBTI reaction. Helms *et al.* [65] also confirmed this, but they proposed that H_2O was most likely as the de-passivating reactant for the formation of dangling Si bonds at the interface while H appeared to be less likely as the attacking reactant. Later, Kimuzuka *et al.* [34] found that, as compared to the dry O_2 grown oxide, the wet H_2-O_2 grown oxide induces more NBTI degradation, which was clearly shown in Fig. 2.8(b) and further confirmed that water worsen NBTI. Although the process is well controlled for advanced CMOS technology, extra-care must be taken to minimize the presence of water during manufacturing process.

2.3.3 Boron

Boron was found to worsen NBTI by Yamamoto *et al.* [67]. It is believed that boron can diffuse into the gate oxide from the boron-doped gate. Figure 2.9(b) shows that boron penetration could suppress the NBTI-induced interface trap generation, which was mainly attributed to the formation of Si-F bonds from the BF_2-based boron implantation [97]. However, as can be seen in Fig. 2.9(a), the overall ΔV_{th} degradation is worse for the sample with boron penetration, mainly because of much larger positive oxide charge generation due to more boron-initiated defects in the oxides. Moreover, a significant device lifetime improvement was observed if boron penetration was suppressed [67, 98]. Later, Ang *et al.* [71] found that the NBTI mechanism was insensitive to the boron penetration. On the other hand, Makabe *et al.* [99] observed an opposite effect and concluded that NBTI could be suppressed by boron penetration when boron was incorporated with higher annealing temperature,

ATTENTION: The Singapore Copyright Act applies to the use of this document. Nanyang Technological University Library

which could be due to smaller electron current at the electrode and less oxide traps as well. Therefore, more studies are needed to elucidate the role of boron in NBTI.

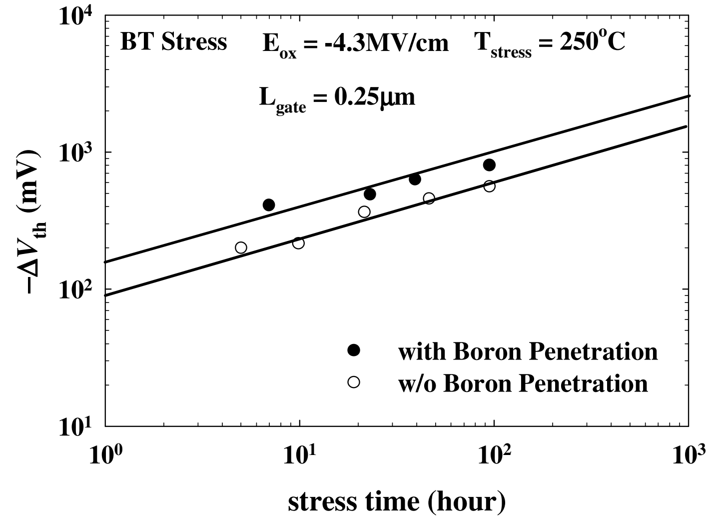

(a)

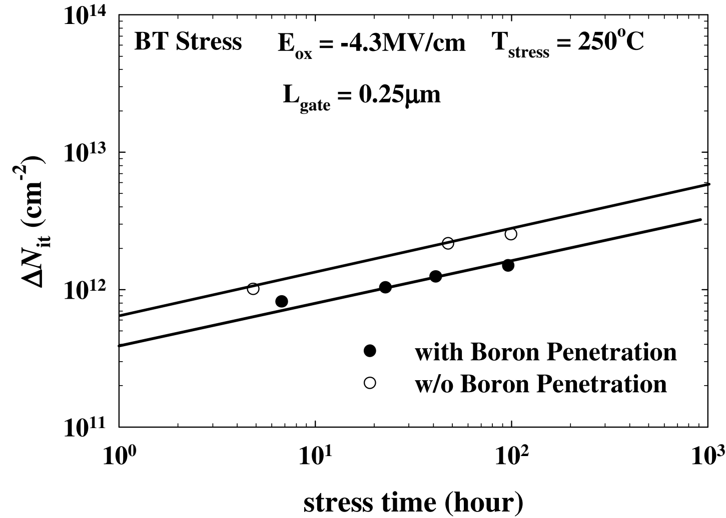

(b)

Figure 2.9: *BT stress time dependence of (a)* ΔV_{th} *and (b)* ΔN_{it} *for p-MOSFET's with and without boron penetration. After [67].*

ATTENTION: The Singapore Copyright Act applies to the use of this document. Nanyang Technological University Library

2.3.4 Fluorine

Fluorine is known to have many beneficial effects on the MOS device. Fluorine improves dielectric integrity and thus reduces HCI and NBTI. Hook *et al.* [100] reported that fluorine could reduce NBTI. As shown in Fig. 2.10, the reduction of NBTI increases as the implanted fluorine dose increases. This fluorine-improved NBTI phenomenon was observed and further confirmed by many other researchers [35, 97, 101-103]. The improvement of NBTI by fluorine is mainly attributed to the formation of stronger Si-F bonds at the interface, which increases the resistance against NBTI degradation. However, fluorine may enhance boron penetration [103] and induce higher junction leakage as well, both of which are not favorable for device performance. Besides, Fleetwood *et al.* [104] also found that fluorine could worsen NBTI in some cases, depending on the concentration and profile of fluorine species in the near-interfacial SiO2.

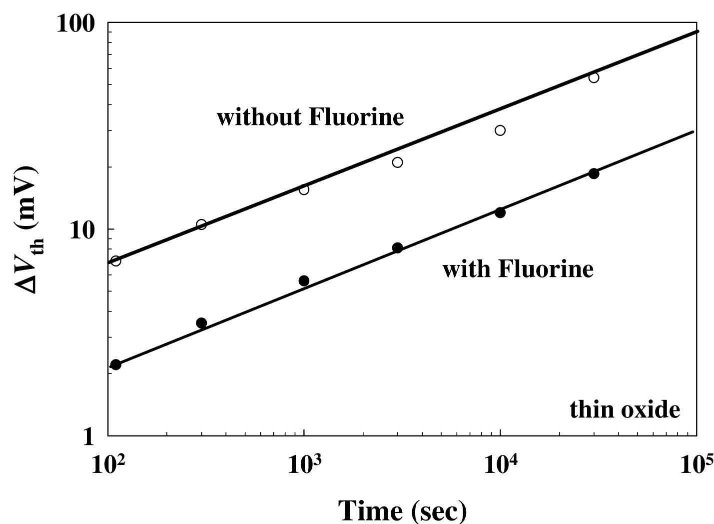

Figure 2.10: *NBTI shift as a function of time for wafers with and without added fluorine. Implanted fluorine dose was $5x10^{15}$ cm^{-2}. After [100].*

ATTENTION: The Singapore Copyright Act applies to the use of this document. Nanyang Technological University Library

2.3.5 Nitrogen

The incorporation of nitrogen into the gate oxide overcomes the problem of boron penetration in *p*-MOSFETs, provides a relatively-higher dielectric constant, preserves a good interface quality, and also reduces HCI degradation effectively in *n*-MOSFETs. However, nitrogen was extensively reported to worsen NBTI degradation [34-37, 71, 74, 105-111]. This well-known nitrogen-worsen NBTI was evidently shown in Fig. 2.11, which compared the NBTI-induced threshold voltage shift (ΔV_{th}) between the pure and nitrided oxides. When the gate oxide is further down-scaled, higher amount of nitrogen is required to suppress boron penetration and it must be weighed against the enhancement on NBTI by optimizing the nitridation process. However, the effect of nitrogen was only experimentally observed, and thus more in-depth studies on the underlying mechanism and the modeling of this nitrogen-worsen NBTI are quite critical for us to fully understand the role of nitrogen in NBTI.

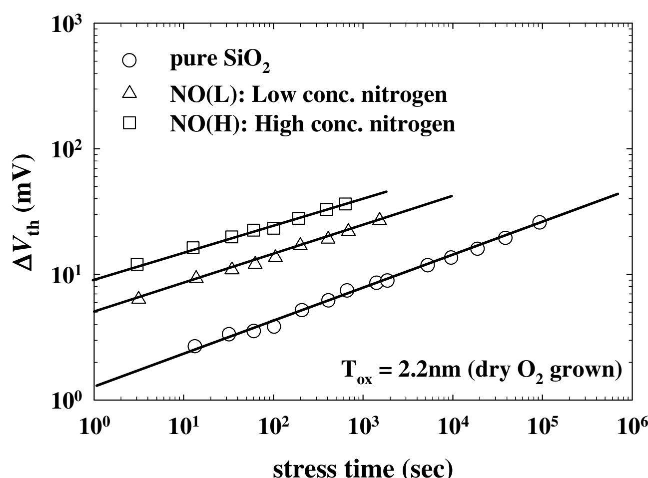

Figure 2.11: *V_{th} shift due to NBTI for pure and nitrided oxide. A large V_{th} shift was observed for nitrided oxide. After [34].*

ATTENTION: The Singapore Copyright Act applies to the use of this document. Nanyang Technological University Library

2.3.6 Other Remarks

Besides the effects of hydrogen, boron, fluorine and nitrogen, NBTI might also be largely affected by other materials or processes, such as the interconnect [112-115], stress/strain [107, 116-119], plasma-induced oxide damage [120-122], high-k gate dielectrics [91, 123-130], etc. Moreover, because only NBTI in *p*-MOSFETs was observed to be quite significant for thin oxide and nitrided oxide, it seemed that holes were required [64] for NBTI. Various physical or atomic models [36, 110, 131] have qualitatively shown the role of holes in NBTI, although there is still no direct evidence that clearly shows the role of holes in NBTI reaction. Besides, various dependences of NBTI, such as the time-dependence, temperature-dependence and stress voltage/field-dependence, can be commonly observed and these in turn require certain theoretical treatment of NBTI so as to reveal the underlying NBTI mechanism.

2.4 NBTI Theories and Models

In this section, various NBTI models are reviewed, and they are mainly based on the generation of NBTI-induced interface traps ΔN_{it} and oxide trapped charge ΔN_{ot}.

2.4.1 Reaction-Diffusion/Drift Model

This reaction-diffusion/drift (R-D) model is mainly based on an electrochemical reaction at the interface and a subsequent diffusion or drift process, and it is described

ATTENTION: The Singapore Copyright Act applies to the use of this document. Nanyang Technological University Library

as follows by Jeppson and Svensson [61]:

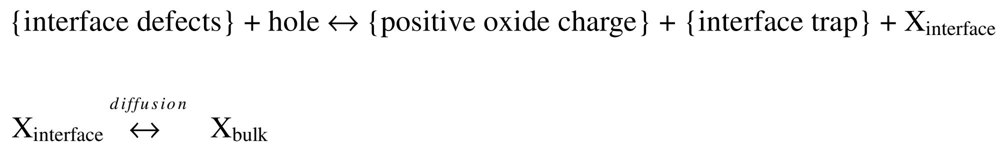

$$\{\text{interface defects}\} + \text{hole} \leftrightarrow \{\text{positive oxide charge}\} + \{\text{interface trap}\} + X_{\text{interface}}$$

$$X_{\text{interface}} \overset{diffusion}{\leftrightarrow} X_{\text{bulk}}$$

where X represents the diffusion species. In this R-D model, it is assumed that the interface contains a large number of defect precursors (i.e. Si-H bonds), which are electrically inactive but would become electrically active upon BTI stress. In addition, another assumption is that the oxide thickness is relatively large so that the effect of poly-interface is not taken into account. A general power-law time-dependence of the BTI-induced interface traps N_{it} with an exponent factor of 1/4 can be obtained, if we also assume that N_{it} generation is far from saturation, the diffusion species is neutral and the net reaction is diffusion-limited.

This R-D model was further generalized for both charged and neutral species by Ogawa and Shiono [68] and then unified by Alam and Mahapatra [132, 133] to become a comprehensive model for NBTI which includes five regimes of time-dependent interface trap (N_{it}) generation, as shown in Fig. 2.12: N_{it} is initially reaction-limited with a linear time-dependence and it is followed by a short quasi-equilibrium phase with a constant N_{it} generation; in the third phase, when more hydrogen-related species are generated and diffuse away from the interface, the process becomes diffusion-limited and a general power-law time-dependence with an exponent factor (n) of 1/4 is resulted for the neutral H species; in the fourth phase, the poly-interface plays a role and it will affect the time-dependence of N_{it}; and finally, N_{it} generation would saturate. The detailed NBTI mechanism and formulations of this generalized R-D model for NBTI are discussed as follows.

ATTENTION: The Singapore Copyright Act applies to the use of this document. Nanyang Technological University Library

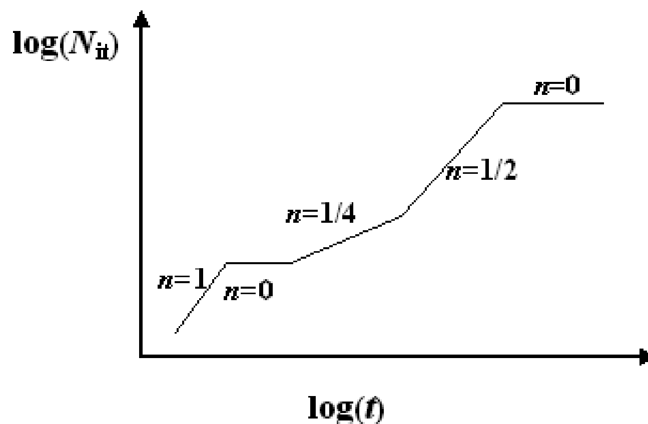

Figure 2.12: *Five regimes of time dependent interface-trap generation as obtained from the general solution of the reaction-diffusion equations during NBTI stress. After [133].*

When *p*-MOSEFETs are negatively-biased at the gate, holes in the inversion layer interact with hydrogen-terminated trivalent Si defect precursors (Si_3≡Si-H) at the interface. This interaction would lead to dissociation of Si-H bonds and thus cause the generation of interface traps. Initially, N_{it} generation is limited by the dissociation of Si-H bonds at the interface. Later, the diffusion of H-related species becomes the limiting factor for N_{it} generation. Mathematically, this R-D model can be described by the following two equations [68]:

$$\frac{dN_{it}}{dt} = k_F\left(N_O - N_{it}\right) - k_R N_H\left(0\right) N_{it} \tag{2.5}$$

$$\frac{dN_H}{dt} = D_H \frac{d^2 N_H}{dx^2} \pm \mu_H \xi_{ox} \frac{dN_H}{dx} = D_H\left(\frac{d^2 N_H}{dx^2} \pm \frac{q}{kT}\xi_{ox}\frac{dN_H}{dx}\right) \tag{2.6}$$

where N_o is the initial density of Si-H bonds at the interface, k_F is the forward reaction rate, k_R is the reverse reaction rate, N_H is the concentration of H-related diffusing

ATTENTION: The Singapore Copyright Act applies to the use of this document. Nanyang Technological University Library

species (where $N_H(0)$ corresponds to N_H concentration exactly at the interface), ξ_{ox} is the electric field, D_H and μ_H are the diffusion coefficient and effective mobility of the diffusing H-related species, respectively, and they obey the Einstein's relation:

$$\frac{\mu_H}{D_H} = \frac{q}{kT} \tag{2.7}$$

where q, k, T are the unit electronic charge, Boltzmann's constant and the absolute temperature, respectively. Besides, another useful relation is the conservation of the hydrogen-related diffusing species as described by Eq. (2.8), which indicates that each released hydrogen species would leave behind one interface trap.

$$N_{it}(t) = \int_{x=0}^{x(t)} N_H(x,t)dx \tag{2.8}$$

where $x(t)$ is the diffusing/drift front. For a positively-charged H-related species (H^+), the drift profile is approximated to be rectangular with a drift front of distance ($\mu_H \xi_{ox}$) from the Si/SiO_2 interface, while for a neutral H-related species (H or H_2), the diffusion profile is approximated to be triangular for simplicity, and "tip" of the diffusing front is expressed as $\sqrt{D_H t}$. In addition, the conversion between H and H_2 is governed by mass action, i.e. $N_H(0)^2/ N_{H2}(0)$ = Constant. Thereafter, N_{it} can be obtained by solving Eqs. (2.5-2.8) for various kinds of species H^+, H and H_2, and the results are shown below in Eqs. (2.9-2.11) [133, 134], respectively:

$$N_{it}(t) = \sqrt{\frac{k_F N_O}{k_R}} \left(\mu_H \xi_{ox} t\right)^{1/2} \qquad \text{for } H^+ \tag{2.9}$$

$$N_{it}(t) = \sqrt{\frac{k_F N_O}{2k_R}} \left(D_H t\right)^{1/4} \qquad \text{for H} \tag{2.10}$$

ATTENTION: The Singapore Copyright Act applies to the use of this document. Nanyang Technological University Library

$$N_{it}(t) \propto \left[\frac{k_F N_O}{2k_R}\right]^{2/3} (D_H t)^{1/6} \qquad \text{for } H_2 \qquad (2.11)$$

Moreover, the saturation characteristics of NBTI, due to either the reflection at the ploy-oxide boundary or the depletion of Si-H bonds, can be well-predicted by this R-D model as well, and more details can be found in Ref. [134]. Besides, NBTI recovery can also be modeled with this approach, as in Ref. [132].

2.4.2 Statistical Mechanics Model

The statistical mechanics model, proposed by Zafar *et al.* [127, 135, 136], is also mainly based on the dissociation of Si-H bonds at the interface. Three key assumptions are made here. Firstly, NBTI is a thermally-driven process, and it implies that both bonded and interstitial hydrogen atoms are in thermal equilibrium. Secondly, once the interstitial hydrogen H_i is formed, it converts into proton H^+ under a negative stress bias. Lastly, transport of H^+ in the oxide is assumed to be dispersive, i.e., $D_H = D_{H0}(\nu t)^{\beta-1}$, where t is the time, D_{H0} is the diffusion constant, β is the dispersion parameter with its value decreasing from 1 to 0 depending on the degree of dispersion (β = 0 being most dispersive), and ν is the characteristic frequency. Furthermore, it also obeys the general diffusion/drift law, i.e., Eq. (2.6). Because of H^+ as drift species, the first term on the right-hand side of Eq. (2.6) can be eliminated and it yields:

$$\frac{dN_{it}}{dt} = H^+ \frac{q\xi_{ox}}{kT} D_H \qquad (2.12)$$

Based on statistical mechanics, the density of interstitial hydrogen H_i in thermal equilibrium can be expressed as [136, 137]:

ATTENTION: The Singapore Copyright Act applies to the use of this document. Nanyang Technological University Library

$$H_i = N_{\text{int}}\left(\frac{N_0}{N_{it}} - 1\right)\exp\left(\frac{-E_H}{kT}\right) \tag{2.13}$$

where N_{int} is the total density of interstitial sites at the interface, N_0 is the total density of Si-H bonds at the interface and E_H is the average energy required to break a Si-H bond into H_i. Since $H_i \sim H^+$, Eq. (2.13) can be substituted into Eq. (2.12) and it yields:

$$\frac{dN_{it}}{dt} = N_{\text{int}}\left(\frac{N_0}{N_{it}} - 1\right)\frac{q\xi_{ox}}{kT}D_{H0}\left(\nu t\right)^{\beta-1}\exp\left(\frac{-E_H}{kT}\right) \tag{2.14}$$

Eq. (2.14) can be integrated and it gives:

$$N_{it} - N_0 \ln\frac{N_0}{N_0 - N_{it}} = -R\left(\nu t\right)^{\beta} \tag{2.15}$$

where $R = \dfrac{D_{H0}}{\beta\nu}\dfrac{q\xi_{ox}}{kT}N_{\text{int}}\exp\left(\dfrac{-E_H}{kT}\right)$

When the time t is short, Eq. (2.15) gives:

$$N_{it}\left(t\right) = R\left(\nu t\right)^{\beta} \tag{2.16}$$

When the time t is long, by assuming $N_{it} \ll N_0$, Eq. (2.15) becomes a stretched exponential function of time t and N_{it} can be obtained:

$$N_{it}\left(t\right) = N_0\left[1 - \exp\left(\frac{-R\left(\nu t\right)^{\beta}}{N_0}\right)\right] = N_0\left\{1 - \exp\left[-\left(\frac{t}{\tau}\right)^{\beta}\right]\right\} \tag{2.17}$$

where τ is the saturation time, given by $\nu^{-1}\left[\dfrac{N_{\text{int}}D_{H0}q\xi_{ox}}{N_0\beta\nu kT}\exp\left(\dfrac{-E_H}{kT}\right)\right]^{-1/\beta}$

ATTENTION: The Singapore Copyright Act applies to the use of this document. Nanyang Technological University Library

2.4.3 Disorder-Controlled-Kinetics Model

The disorder-controlled-kinetic model for NBTI is proposed by Kaczer *et al.* [138-140]. The model extends the classical R-D model by assuming dispersive particle kinetics in the gate oxide. This disorder modifies the properties of hydrogen transport towards and from the Si/SiO_2 interface and it in turn influences the properties of the entire NBTI process. In this model, disorder is assumed to arise from the energy distribution *g*(E) of the deep-localized hydrogen states in the oxide bulk, which results in a wide distribution of hydrogen hopping time. Therefore, diffusion in the R-D model, i.e., Eq. (2.6), is replaced by Eq. (2.18), which describes dispersive diffusion of hydrogen in the amorphous dielectric [141, 142]:

$$N_H - D_H \tau(t) \frac{d^2 N_H}{dx^2} = 0 \tag{2.18}$$

where the function τ(t) is determined by Eq. (2.19):

$$\tau(t) = \frac{N_C}{\nu} \left[\int_{kT\ln(\nu t)}^{\infty} g(E)\, dE \right]^{-1} \tag{2.19}$$

where N_C is the density of the shallow hydrogen hopping sites and ν is the attempt-to-jump frequency of hydrogen. Furthermore, for an exponential hydrogen density-of-state (DOS) distribution, *g*(E) is given by Eq. (2.20):

$$g(E) = \frac{N_T}{E_0} \exp\left(-\frac{E}{E_0} \right) \tag{2.20}$$

ATTENTION: The Singapore Copyright Act applies to the use of this document. Nanyang Technological University Library

where N_T is the total density of the localized states and E_0 is the characteristic width of the DOS distribution. By substituting Eq. (2.20) into Eq. (2.19), the function τ(t) becomes an algebraic function of time *t*, as shown in Eq. (2.21):

$$\tau(t) = \nu^{-1} \frac{N_C}{N_T} (\nu t)^{\beta} \tag{2.21}$$

where β is the dispersion parameter, which is determined by temperature *T* and E_0:

$$\beta = \frac{kT}{E_0} \tag{2.22}$$

However, the dispersive transport regime is possible if and only if E_0 is much larger than *kT*, i.e., β<1. When β is approaching 1, the dispersive characteristic of hydrogen transport is near its thermal equilibrium. On the other hand, Eq. (2.18) can be readily solved with the boundary condition ($N_H(x, t) \sim 0$ at $x \sim \infty$), and it yields:

$$N_H(x,t) = N_H(0,t) \exp\left[-\frac{x}{\sqrt{D_H \tau(t)}}\right] \tag{2.23}$$

By substituting Eq. (2.23) into (2.8), a relation between N_{it} and $N_H(0, t)$ at the interface can be obtained:

$$N_{it}(t) = N_H(0,t) \sqrt{D_H \tau(t)} \tag{2.24}$$

Similarly, with Eq. (2.24), the reaction equation (or the generation-recombination equation) Eq. (2.5) can be solved in the diffusion-limited regime, based on similar assumptions, and N_{it} can be shown to have a similar power-law time-dependence but the power-law exponent factor is β/4, as shown in Eq. (2.25):

ATTENTION: The Singapore Copyright Act applies to the use of this document. Nanyang Technological University Library

$$N_{it}\left(t\right)=\left(\frac{k_F N_O}{k_R}\right)^{\frac{1}{2}}\left(\frac{D_H}{\nu}\frac{N_C}{N_T}\right)^{\frac{1}{4}}\left(\nu t\right)^{\frac{\beta}{4}} \quad (2.25)$$

The disorder-controlled kinetic model can also be extended to describe NBTI recovery and it has the asymptotic form, as shown in Eq. (2.26) [139]:

$$N_{it}\left(\zeta\right)=\frac{1-\zeta^{\beta/2}}{1-\zeta^{\beta}}N_{it}\left(0\right) \quad (2.26)$$

where $\zeta = t/t_{\mathrm{stress}}$ is the dimensionless recovery time and $N_{\mathrm{it}}(0)$ is the interface trap density at the beginning of NBTI recovery. The solution behaves logarithmically over several decades when $\zeta = 1$, while it is approximately a power-law for small and large ζ. A generalized disorder-controlled-kinetics model was recently summarized and more details could be found in Ref. [143].

2.4.4 Reaction-Limited Model

Huard *et al.* [144-146] proposed a reaction-limited model for the generation of interface traps, which was also mainly based on the dissociation of Si-H bonds at the interface. The process is described by a first-order reaction with the reaction rate R:

$$R\left(t,\tau\right)=1-\exp\left(-t/\tau\right) \quad (2.27)$$

where τ is the time constant of the reaction. When time is shorter than the time constant, i.e., $t < \tau$, the reaction rate exhibits a linear relationship with time at a constant defect generation rate of $1/\tau$. Indeed, τ is supposed to be directly related to the dissociation energy of the Si-H bond (E_{d}), which is defined here as the energy that

ATTENTION: The Singapore Copyright Act applies to the use of this document. Nanyang Technological University Library

is required to break the bond or the migration barrier that the H atom has to pass over in order for it to be released.

The dissociation energy E_d is not constant but is expected to have a statistical distribution continuum of the dissociation energies [147, 148]. It can be described by a broadened Fermi derivative distribution $g(E_d, \sigma)$ due to disorder-induced variations:

$$g(E_d, \sigma) = \frac{1}{\sigma} \frac{\exp\left(\frac{E_{dm} - E_d}{\sigma}\right)}{\left[1 + \exp\left(\frac{E_{dm} - E_d}{\sigma}\right)\right]^2} \tag{2.28}$$

where E_{dm} is the median dissociation energy and σ is the spread of the distribution with an experimental value of about 0.1eV.

In this approach, according to first-order reaction, every single Si-H bond could be broken, but each of them has a specific time constant depending on its own dissociation energy. As a result, bonds with lower E_d would be broken relatively fast, while those bonds with higher E_d would dissociate more slowly. The overall degradation rate is a combination of all single bond dissociation rates as governed by the equation for first-order reaction, which has been analytically derived by Haggag *et al.* in their work [149], and it results in an expression for N_{it} generation:

$$\frac{\Delta N_{it}}{N_{it\max}}(t) = \int_0^\infty g(E_d, \sigma) R(t, \tau(E_d)) dE_d \propto \frac{1}{1 + \left(\frac{t}{\tau}\right)^{-\alpha}} \tag{2.29}$$

where $\tau = \tau_0 \exp(E_d(E_{ox})/kT)$ and $\alpha = kT/\sigma$ for $\tau_{min} < t < \tau$, T is the bond temperature and τ_{min} is the time constant of the weakest defect.

ATTENTION: The Singapore Copyright Act applies to the use of this document. Nanyang Technological University Library

The evolution of N_{it} generation with respect to stress time, as described by Eq. (2.29), is shown in Fig. 2.13. For very short time ($t < \tau_{min}$), the degradation is linear, with a slope that is directly linked to the defect generation rate of the weakest bond(s). For longer stress time, more bonds participate in the degradation reaction, and it yields a power-law time-dependence. This is followed by saturation when fewer bonds are left to dissociate.

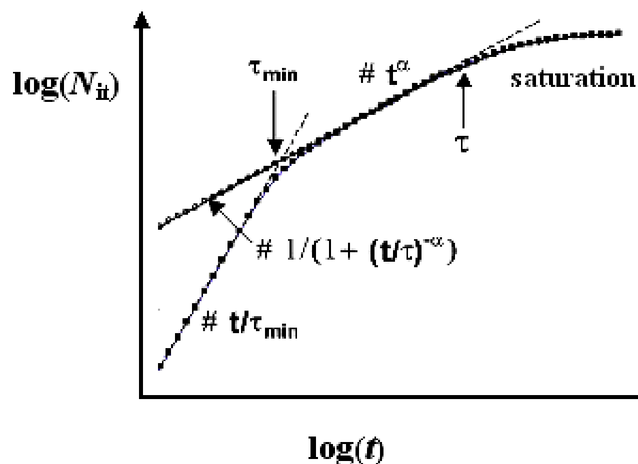

Figure 2.13: *Evolution of theoretical degradation rate (filled symbols) with respect to stress time, with a disorder-induced variation of dissociation energies for a given temperature, as defined by Eq. (2. 29). After [145].*

Beside interface traps, Huard *et al.* also emphasized a second possible component for NBTI degradation - the oxide traps (N_{ot}). N_{ot} generation is largely attributed to hole-trapping in the oxide, which acts as the recoverable part [146, 150], and NBTI recovery is believed to be mainly due to hole de-trapping [151-153]. In next a few sections, the models for oxide traps and NBTI recovery are briefly reviewed.

ATTENTION: The Singapore Copyright Act applies to the use of this document. Nanyang Technological University Library

2.4.5 Hole-Trapping Model

Yang *et al.* [80, 154, 155] investigated the dynamic NBTI systematically and distinguished two different components for NBTI degradation – the slow component that is largely attributed to interface traps N_{it} generation and passivation, and the fast component that is mainly due to trapping and de-trapping of hole traps N_{ot} in the gate oxide. The fast component can be modeled by Eqs. (2.30-2.31), as shown below, which describe the trapping and de-trapping of pre-existing hole traps N_{ot} in the gate oxide [156]:

$$\frac{dp}{dt}=\frac{1}{\tau_C}\left(N_{ot}-p\right)-\frac{1}{\tau_{E1}}p \tag{2.30}$$

$$\frac{dp}{dt}=-\frac{1}{\tau_{E2}}p \tag{2.31}$$

where p is the hole concentration, N_{ot} is the trap concentration, and τ_{C} and τ_{E} are the trapping and de-trapping time constant, respectively.

Based on this hole-trapping model, with well-designed frequency-dependent dynamic NBTI experiments by using fast I_{d}-V_{g} measurements [157, 158] at both rising and falling edges, the spectrum of the trap concentration PDF (probability density function) over the trapping and de-trapping time constants τ_{C} and τ_{E} deployed in Eqs. (2.30-31) can be shown and the continuous distribution of PDF can be used to explain the power-law time-dependence of NBTI. More details on the physical origins of these slow and fast components for NBTI can be found in Ref. [159].

ATTENTION: The Singapore Copyright Act applies to the use of this document. Nanyang Technological University Library

2.4.6 Deep-Level Hole-Trapping Model

Ang and Pey [160] provided clear evidence for two distinct components of positive oxide traps under NBTI stress. The slow component is commonly associated with interface trap generation and it can be fully recovered under pulsed gate condition regardless of the stress voltage. On the other hand, the fast component can only be partially recovered and it might be linked to the rapid hole trapping at the interface. As a result, two distinct mechanisms for NBTI degradation were observed from temperature dependence of NBTI for nitrided oxide, and the new mechanism could be closely related to the spontaneous trapping of the positive oxide traps at nitrogen-related precursor sites near the interface [161]. NBTI partial recovery phenomenon was well explained by a deep-level hole-trapping (DLHT) model, and with the model, some fraction of the oxide traps were believed to be pinned by the interface conduction-band offset and remained there even if a positive voltage was applied during recovery phase [122, 162]. A consistent deep-level hole-trapping model for NBTI was recently summarized by Ang *et al.* in Ref. [163].

2.4.7 Models for NBTI Recovery

As discussed in previous sections, NBTI recovery was reported and explained within the frameworks of reaction-diffusion model [132], disorder-controlled-kinetics model [139], hole-trapping model [80, 154, 155] and deep-level hole-trapping model [161, 162, 164-166], and it was also widely observed by other researchers [40, 77, 79, 152, 167-170]. NBTI recovery could be closely associated with re-passivation of interface traps and hole de-trapping of oxide traps. Indeed, in the real application, the

ATTENTION: The Singapore Copyright Act applies to the use of this document. Nanyang Technological University Library

devices are operating under AC condition, which corresponds to a stress phase followed by a spontaneous recovery phase. Therefore, measurement for static NBTI would largely overestimate the degradation and thus underestimate the device lifetime. The universal NBTI recovery phenomenon brings another great challenge for NBTI characterization techniques, and the measurement time has to be minimized so as to suppress the unfavorable recovery effect during NBTI characterization.

2.5 NBTI Characterization Techniques

In this section, some conventional NBTI characterization techniques to measure threshold voltage shift ΔV_{th} and interface trap generation ΔN_{it} are introduced first, and it is followed by a brief review on various fast NBTI characterization techniques.

2.5.1 Threshold Voltage Measurement

There are two conventional methods to measure the threshold voltage V_{th}, namely, the constant current method and maximum G_m (trans-conductance) method.

a. Constant current method

The constant current method is quite straightforward and thus widely employed in industry. It requires only one single I_d-V_g measurement. V_{th} is defined as the gate voltage corresponding to a user-specified constant current I_{ref}, and I_{ref} is normalized by the channel width-to-length (W/L) ratio. The main drawback of this method is that the measured V_{th} is lack of physical meaning since I_{ref} is chosen arbitrarily. However,

ATTENTION: The Singapore Copyright Act applies to the use of this document. Nanyang Technological University Library

it offers a relatively accurate comparison when device reliability is concerned.

b. maximum G_m method

The maximum G_m method is most commonly used by researchers to extract V_{th}. The method is based on the linear-region drain-current equation at a small drain bias, referring to Eq. (2.3) in section 2.3.1, and V_{th} is the value linearly extrapolated to the gate-voltage axis from the maximum G_m point of the I_d-V_g curve.

2.5.2 Interface Trap Generation Measurement

There are several techniques to measure interface trap generation N_{it}, such as the gate-controlled-diode (GCD) method, charge pumping (CP) method and direct current current-voltage (DCIV) method.

a. Gate-Controlled-Diode (GCD) method

MOSFETs with the source/drain floating or with the source connected to drain can be considered a typical Gate-Controlled-Diode (GCD) structure [171]. For such a structure, with the drain and substrate reverse-biased, when the gate voltage is swept from the accumulation to inversion, depending on the applied gate voltage, the drain current may consist of one or more of the following three components: the current that is generated within the depletion region of the metallurgical junction, the current that is generated within the depletion region of the field-induced junction, and the current that corresponds to surface generation via interface traps. The former two junction-reverse currents are mainly due to Shockley-Read-Hall (SRH) generation via the generation-recombination (G-R) centers in the depletion regions of the

ATTENTION: The Singapore Copyright Act applies to the use of this document. Nanyang Technological University Library

metallurgical or field-induced junctions or at the SiO_2/Si interface. However, when the MOS device is subjected to an electrical stress, interface trap generation or charge trapping in the gate oxide could alter the characteristics of the GCD. By measuring the reverse drain current under the accumulation, depletion and inversion conditions with the GCD setup for a fresh and stressed device, stress-induced interface trap generation can be obtained accordingly. However, for an ultra-thin gate oxide, this method might not be applicable because of high leakage current.

b. Charge Pumping (CP) method

The charge pumping technique, first proposed by Brugler and Jespers in 1969 [172], is widely used to extract interface trap generation N_{it} due to its convenience and good detection limit[173-176]. With source/drain grounded or reverse-biased, the MOS device is applied with a periodic triangular, sinusoidal, bi-level (square, trapezoidal) or tri-level gate voltage, where in real application a square-pulse-wave at high frequency is commonly used, and the gate pulse top and base are well selected such that it corresponds to a full cycle from the accumulation to strong inversion. Due to the asymmetry of capture and emission processes during gate pulse cycling, at inversion, the interface traps are mostly filled by the capture of channel minority carriers, while at accumulation, they are emptied by the capture of majority carriers that are supplied by the substrate. As a result, there is a net DC recombination current I_{CP} at the substrate terminal over one period, and the charge pumping current I_{CP} has a linear relationship with the gate area, N_{it} and pulse frequency. This CP technique can be applied to a small geometry by increasing the pulse frequency and several modes of bi-level charge pumping measurement can be used. Moreover, we can also vary the gate pulse swing with a fixed base gate voltage, or sweep the base gate voltage from

ATTENTION: The Singapore Copyright Act applies to the use of this document. Nanyang Technological University Library

accumulation to inversion with a fixed gate pulse swing, or experiment with the rise time and the fall time, to optimize this CP technique [173]. The spatial profile of interface trapped charges can also be obtained by this technique [177, 178].

c. Direct-Current Current Voltage (DCIV) method

The Direct-Current Current-Voltage (DCIV) method is also quite accurate for measuring the interface trap density. It was first demonstrated by Neugroschel *et al.* by using a novel BiMOST (BJT-MOST transistor) [179-181]. In this method, the gate-controlled parasitic bipolar junction transistor structure in a MOSFET is used to monitor the change of oxide trapped charges and interface trap density. The method measures the dc base (i.e. well) and collector (i.e. substrate) currents versus the gate voltage, which is thus known as DCIV method. The source and drain are connected together and forward biased, and the gate voltage is applied and swept accordingly to change the Si surface from inversion to accumulation. At the same time, the substrate current I_B is monitored. When the Si surface changes from inversion to accumulation, carrier recombination via interface traps occurs, and a peak substrate current I_B is resulted when the electron-hole recombination rate reaches its maximum.

2.5.3 Fast Characterization Techniques

To minimize unwanted NBTI recovery during measurement, various fast characterization techniques are proposed, such as the single-point drain-current measurement, on-the-fly (OTF) measurement, pulsed I_d-V_g measurement, ultra-fast switching (UFS) measurement and OTF interface trap measurement. Here only a brief review is given for each measurement method. The detailed setup and procedures can

ATTENTION: The Singapore Copyright Act applies to the use of this document. Nanyang Technological University Library

be found from the reference given at the beginning of each section.

a. Single-point drain-current measurement

This single-point drain-current method [182] is quite simple and straightforward. It measures a single drain current I_d and then uses the drain current degradation ΔI_d to extract the threshold voltage shift ΔV_{th} with certain correlation based on derivation of the drain current equation. More details are to be illustrated in Chapter 3.

b. On-the-fly (OTF) measurement

This method was first proposed by Rangan *et al.* [40] by measuring the linear drain current I_{dlin} with constant V_d = 50 mV. Then based on the measured linear drain shift ΔI_{dlin}, by differentiating the linear drain current equation i.e. Eq. (2.3) with respect to V_{th}, the threshold voltage shift ΔV_{th} can be extracted according to Eq. (2.32) with the assumption that mobility degradation is negligible at the stress voltage that is much higher than V_{th} [152]:

$$\frac{\Delta I_{dlin}}{I_{dlin0}} = \frac{\Delta u_{eff}}{u_{eff}} - \frac{\Delta V_{th}}{V_g - V_{th0}} \qquad (2.32)$$

where I_{dlin0} is I_{dlin} at time = 0 s and V_{th0} is the threshold voltage of the fresh device.

The OTF measurement was later modified by Denais *et al.* [183-186] with a small bipolar pulse superimposed on the DC gate stress voltage. Correspondingly, the constant small V_d = 50 mV is changed to a pulse that is synchronized with the bipolar pulse at gate when each measurement is taken. Oscillation of the drain current in response to the bipolar pulse is used to calculate the evolution of trans-conductance, and hence the effect of mobility degradation in Eq. (2.32) can be included. However,

ATTENTION: The Singapore Copyright Act applies to the use of this document. Nanyang Technological University Library

this OTF technique has a "time-zero" issue. The first data point after the initiation of stress requires a certain amount of time that varies from instrument to instrument. As a result, the initial data points might be contaminated by the "time-zero" I_{dlin} value.

c. Pulsed I_d-V_g measurement

The pulsed I_d-V_g measurement was first developed by Kerber et al. [157]. The pulse is generated to bias or stress the device under test, and the oscilloscope is used to monitor the drain current. *I*-*V* characteristics at the pulse rising and falling edges are used to reconstruct the I_d-V_g curves of the device and thus the threshold voltage shift ΔV_{th} can be extracted. Shen *et al.* [158] modified this technique by using the operational amplifier, which further reduced measurement time to 1μs or lower.

d. Ultra-fast switching (UFS) measurement

The UFS measurement was recently developed by Du *et al.* [187]. It combines the advantages of the single-point drain-current measurement and pulsed OTF measurement. The measurement time is largely reduced and can be well-controlled as well, and there is no "time-zero" issue since the linear drain current is measured at a lower gate voltage. However, this technique might require a similar correlation as shown in Eq. (2.32) to extract the threshold voltage shift ΔV_{th}. Moreover, the UFS technique could be improved by taking into account the effect of source/drain series resistance and vertical-field-induced mobility reduction [188].

e. OTF interface trap measurement

Recently, an OTF interface trap measurement was proposed by Liu *et al.* [189]. It simply combines the pulsed OTF measurement and CP measurement to monitor

ATTENTION: The Singapore Copyright Act applies to the use of this document. Nanyang Technological University Library

interface trap generation during the NBTI stress and recovery phases. In the stress phase, the gate stress voltage is always on, and during I_{cp} measurement, the CP pulses are applied. The pulse rising and falling rates are the same for the stress and recovery phases. As compared with the conventional CP method, the OTF interface trap method could reduce the interruption time by a factor of 10^{-2} to 10^{-3}.

2.6 Summary

In summary, NBTI in *p*-MOSFETs is briefly reviewed. Firstly, some fabrication techniques for nitrided oxide are introduced, and it is followed by the basic theory on the Si-SiO_2 interface. The history of NBTI is presented with some early studies on this topic, and NBTI in *p*-MOSFETs is emphasized for the modern MOS device. The dependences of NBTI on various process conditions are discussed, among which the nitrogen-worsen NBTI will be further studied. Theory on NBTI, in particular, the existing physical models for NBTI and NBTI recovery, in terms of interface trap generation/re-passivation, positive oxide trap and hole trapping/de-trapping, are reviewed thoroughly. Among all these models, the reaction-diffusion model will be further investigated in our work. Lastly, a summary of various conventional and fast characterization techniques for measuring threshold voltage and interface traps is given.

ATTENTION: The Singapore Copyright Act applies to the use of this document. Nanyang Technological University Library

CHAPTER 3 CHARACTERIZATION OF NBTI AND NBTI RECOVERY

Negative bias temperature instability (NBTI) in *p*-MOSFETs is significantly underestimated by using conventional characterization techniques due to severe NBTI recovery during measurement. In this chapter, a simple characterization method based on single-point measurement of saturation drain current is first proposed to minimize the unwanted NBTI recovery during measurement. Since NBTI degradation in *p*-MOSFETs has become one of the most critical device reliability issues for sub-90nm technology node, an NBTI in-line test methodology is developed to monitor NBTI degradation during the development phase, aiming for process comparison and optimization. Moreover, NBTI recovery is studied and a combined empirical model is proposed to describe NBTI recovery within a modulated measurement time frame. The effect of measurement time delay on NBTI is also examined.

3.1 Introduction

NBTI is a degradation mechanism mainly caused by the breaking of hydrogen-terminated silicon bond (Si-H) at the interface when the device is stressed with a negative gate bias at an elevated temperature for a considerable time period [64]. It could lead to a significant increase in the magnitude of threshold voltage (V_{th}) and decrease in saturation drain current (I_{dsat}). In spite of intensive studies in recent

ATTENTION: The Singapore Copyright Act applies to the use of this document. Nanyang Technological University Library

years, physical and chemical characteristics of NBTI are still not fully understood, and reliable and accurate characterization of NBTI is complicated by the lack of a standard measurement procedure. Ershov *et al.* have reported that NBTI recovery is quite significant upon removal of the stress voltage [39]. It is also found that the relaxation duration after stress interruption would affect the apparent device lifetime quite significantly [190]. NBTI degradation is commonly measured or characterized by some conventional techniques such as threshold voltage (ΔV_{th}) measurement, direct-current current-voltage (DCIV) measurement [179-181], charge pumping (CP) measurement [172-176], mid-gap voltage (ΔV_{MG}) measurement [109, 110, 191, 192], etc. With all these measurements, data collection time is sufficiently long such that NBTI recovery during measurement is quite significant. In this case, NBTI degradation is largely underestimated, which in turn leads to a false picture of NBTI degradation. In order to obtain a more realistic picture of NBTI, measurement-induced NBTI recovery needs to be minimized.

In this chapter, instead of measuring threshold voltage shift (ΔV_{th}) based on typical *I-V* transfer characteristics (denoted as "conventional method"), single-point saturation drain current (I_{dsat}) is directly measured to reduce the measurement time. With this method, NBTI recovery during measurement is minimized and thus a more realistic ΔV_{th} is obtained. An NBTI in-line test methodology is proposed for sub-90nm technology nodes to monitor NBTI degradation in devices during the development phase, aiming for process comparison, optimization and qualification. Three different characterization methods are proposed here, among which the right choice of the most appropriate method mainly depends on customer requirements, test conventions and NBTI specifications. Lastly, NBTI recovery and the effect of measurement time delay on NBTI are studied.

ATTENTION: The Singapore Copyright Act applies to the use of this document. Nanyang Technological University Library

3.2 Single-Point Saturation Drain Current Measurement

In this section, a simple and straightforward characterization method based on single-point measurement of saturation drain current (I_{dsat}) is proposed to minimize the unwanted NBTI recovery during measurement [182]. This method is accurate as is proven by a carefully-designed experiment. With this method, the measurement time is reduced to tens of milliseconds. This method gives a closer-to-real threshold voltage shift and thus yields a more reliable power-law factor. Obviously, accurate information of these parameters is critical for the understanding of underlying NBTI mechanism and hence depicts a more realistic NBTI picture.

3.2.1 BTI Issues in MOS Devices

The device used here was fabricated by a commercial 0.13 μm CMOS process. The equivalent gate oxide thickness (EOT) is about 27.3 Å. The channel length and width are 0.13 μm and 10 μm, respectively. The nominal operating voltage (V_{dd}) is -1.5 V. The gate stress voltage (V_{gstr}) is -3.0 V for NBTI and 3.0 V for PBTI, and the stress temperature (T_{str}) is 125 °C. The threshold voltage shift (ΔV_{th}) is measured with conventional *I-V* sweep method. In this work, unless otherwise mentioned, all the electrical parameters to represent BTI degradation in MOSFETs, such as threshold voltage shift (ΔV_{th}), degradation in linear or saturation drain current (ΔI_{dlin} or ΔI_{dsat}), degradation in mobility ($\Delta \mu$), etc., are expressed by absolute values, i.e., in magnitude. More specifically, for NBTI in *p*-MOSFETs, ΔV_{th} means the increase in $|V_{th}|$, while ΔI_{dlin}, ΔI_{dsat} and $\Delta \mu$ indicate the decrease in $|I_{dlin}|$, $|I_{dsat}|$ and $|\mu_{eff}|$, respectively.

ATTENTION: The Singapore Copyright Act applies to the use of this document. Nanyang Technological University Library

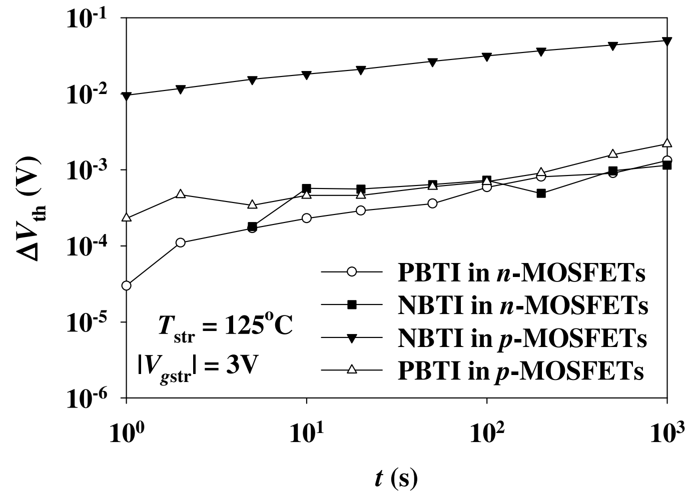

Figure 3.1: *Comparison of BTI degradation in either n-MOSFETs or p-MOSFETs, in terms of threshold voltage shift (ΔV_{th}) as a function of the stress time. The gate stress voltage (V_{gstr}) is -3.0 V for NBTI and 3.0 V for PBTI, and the stress temperature (T_{str}) is 125 °C.*

Figure 3.1 shows the comparison of bias temperature instability (BTI) (i.e., both NBTI and PBTI) in either *n*-MOSFETs or *p*-MOSFETs and it clearly shows that ΔV_{th} is the largest for NBTI in *p*-MOSFETs. In other words, among the four possible BTI issues, NBTI in *p*-MOSFETs is the most critical one. The reasons are explained as follows. BTI degradation is believed to be mainly involving of holes, which interact with Si-H bonds at the interface and cause device degradation. As a result, PBTI, which mainly induces electrons, is expected to be less severe than NBTI in both *p*-MOSFETs and *n*-MOSFETs. Moreover, under NBTI stress, donor-like interface state is generated, and it acts as a charged state in *p*-MOSFETs during device operation, which causes device degradation. However, NBTI-induced donor-like interface state is neutral in *n*-MOSFETs during device operation and hence it yields less or no degradation. In fact, holes are inversion carriers in *p*-MOSFETs during

ATTENTION: The Singapore Copyright Act applies to the use of this document. Nanyang Technological University Library

device operation, while holes only present as accumulation carriers in *n*-MOSFETs, which rarely occurs during circuit operation. Therefore, NBTI in *p*-MOSFETs, rather than NBTI in *n*-MOSFETs, will become a real problem during actual circuit operation. As a result, in real application of integrated circuits (IC), NBTI in *p*-MOSFETs would degrade the circuit most, and thus cause IC malfunction or even failure under certain unfavorable circumstances for a period of time.

3.2.2 NBTI Recovery during Measurement

Moreover, NBTI recovery occurs immediately after the NBTI stress is relaxed, which could be either due to a measurement interruption or purposely for a designed characterization of dynamic NBTI.

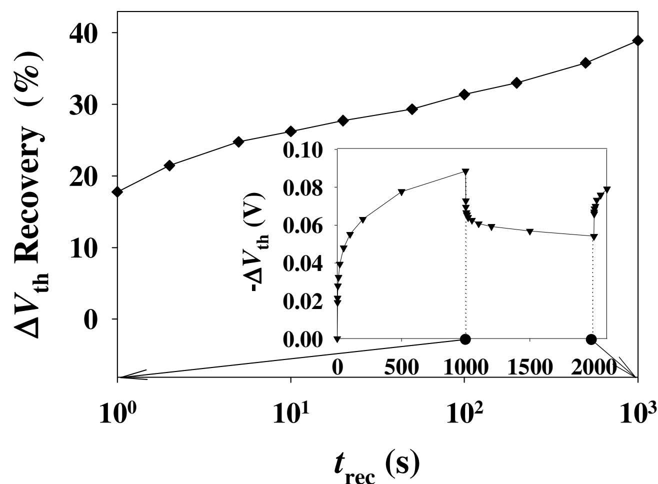

Figure 3.2: ΔV_{th} *recovery as a function of the post-NBTI relaxation time* (t_{rec}). *The NBTI stress is carried out at* V_{gstr} = -3.0 V *and* T_{str} = 125 °C *for 1000 seconds, and NBTI recovery occurs at* V_{gstr} = 0 V.

ATTENTION: The Singapore Copyright Act applies to the use of this document. Nanyang Technological University Library

Figure 3.2 shows NBTI recovery as a function of post-NBTI relaxation time, where ΔV_{th} recovery is defined as:

$$\Delta V_{th} \text{ Recovery} = \frac{\Delta V_{th}(t_{rec}=0) - \Delta V_{th}(t_{rec})}{\Delta V_{th}(t_{rec}=0)} \times 100\% \tag{3.1}$$

where t_{rec} is the duration of post-NBTI relaxation time. As shown in Fig. 3. 2, for only one second of stress relaxation, as much as 18% of threshold voltage degradation (ΔV_{th}) is recovered, and for a longer time of stress relaxation, more than 40% recovery in ΔV_{th} is observed. Obviously, ignoring NBTI recovery during NBTI measurement would lead to a much distorted picture of NBTI degradation.

3.2.3 Single-Point Drain Current Method

One straightforward solution for this issue is to minimize the measurement time (t_{m}) while sufficient information of NBTI degradation can still be obtained. Therefore, a simple and fast method is proposed here to measure a single-point saturation drain current (I_{dsat}) directly such that the measurement time can be reduced to tens of milliseconds, which is intrinsically limited by the measurement tool being used. The average total measurement duration of our proposed method including transient stages, measurement and data collection, is monitored to be less than one second, but each measurement of conventional I_{d}-V_{g} or I_{d}-V_{d} curve (denoted as "conventional method") will take at least 6 seconds. As a result, to monitor both V_{th} and I_{dsat} by using the conventional method, the total measurement time would be about 15 seconds, which is highly undesirable.

ATTENTION: The Singapore Copyright Act applies to the use of this document. Nanyang Technological University Library

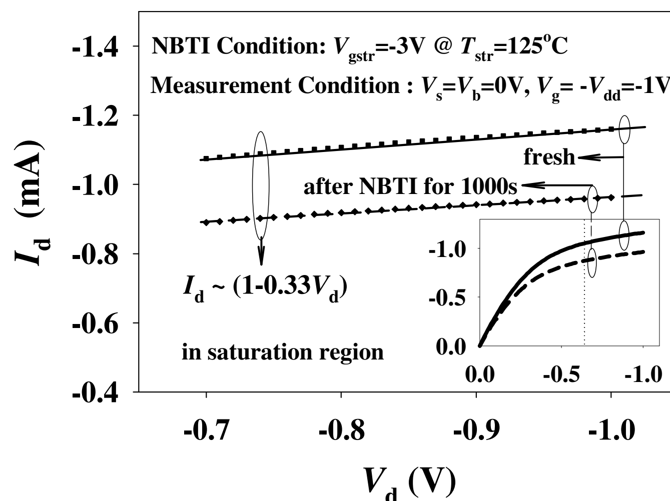

Figure 3.3: *Dependence of saturation drain current (I_d) on drain voltage (V_d) for both fresh and stressed devices. The drain current (I_d) is found to be proportional to (1 – 0.33V_d) for both devices, showing that λ (=0.33) is independent of NBTI stress.*

Figure 3.3 shows typical I_d-V_d curves for both fresh and NBTI-stressed devices. A reduction in saturation drain current (I_{dsat}) can be clearly observed. Since only I_{dsat} is monitored in our method, it is important to establish a reliable relationship between ΔI_{dsat} and ΔV_{th}. With short-channel effect taken into account, saturation drain current (I_{dsat}) can be mathematically expressed as [32, 193]:

$$I_{dsat} = -\frac{u_{eff} C_{ox} W}{2L} \left(V_g - V_{th}\right)^{\theta} \left(1 + \lambda V_d\right) \ , \quad V_d \geq V_{dsat} \approx V_g - V_{th} \qquad (3.2)$$

where W is channel width, L is channel length, μ_{eff} is effective hole mobility, C_{ox} is gate dielectric capacitance, V_g is gate voltage, V_d is drain voltage, λ is channel-length modulation parameter, and θ is a scattering parameter within a range of $1 < \theta \leq 2$. For an ideal case of a long channel device, θ is equal to 2, while for a short channel device, θ is smaller than 2.

ATTENTION: The Singapore Copyright Act applies to the use of this document. Nanyang Technological University Library

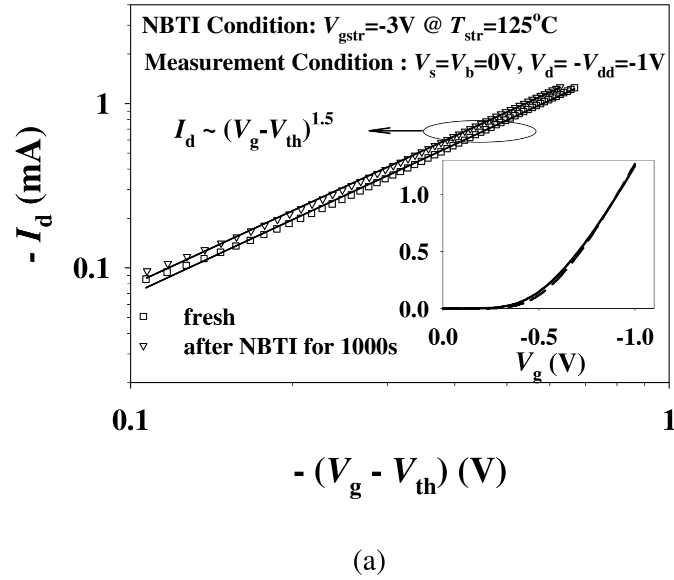

(a)

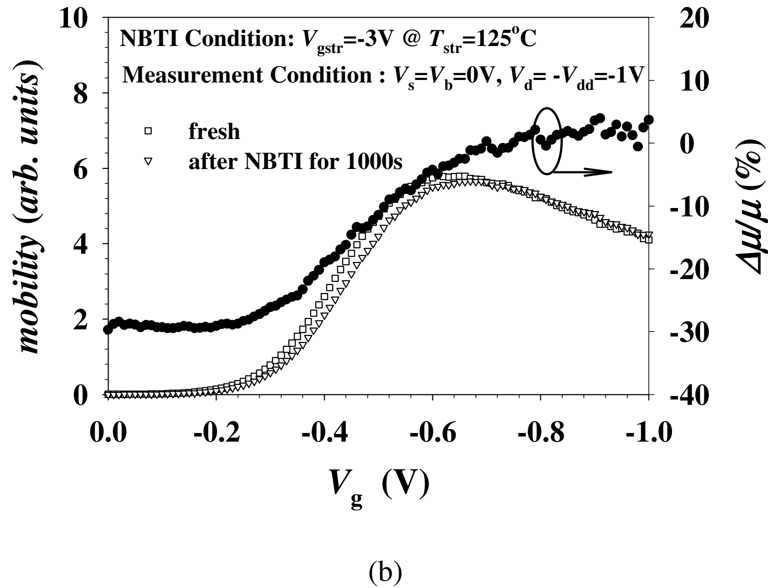

(b)

Figure 3.4: *(a) The saturation drain current (I_d) versus (V_g-V_{th}) for both fresh and stressed devices. A linear regression of the experimental data of log|I_d| versus log|V_g-V_{th}| yields the value of θ and θ (=1.5) is found to be independent of NBTI stress. (b) Hole mobility (μ) versus V_g for both fresh and stressed devices. Relative mobility degradation (Δμ/μ) in % at different Vg is also shown.*

ATTENTION: The Singapore Copyright Act applies to the use of this document. Nanyang Technological University Library

By neglecting relatively small mobility degradation at relatively high field [32], which is true for the case of I_{dsat} measurement at relatively large gate voltage of about V_{dd}, and by differentiating Eq. (3.2) on both sides and rearranging, we can obtain the relationship between ΔI_{dsat} and ΔV_{th}, as shown in Eq. (3.3):

$$\frac{\Delta I_{dsat}}{I_{dsat}} = \theta \frac{(-\Delta V_{th})}{(V_g - V_{th})} \tag{3.3}$$

Therefore, once ΔI_{dsat} is measured in the saturation region, NBTI degradation ΔV_{th} can be easily calculated by using Eq. (3.3). In other words, the magnitude of NBTI-induced ΔI_{dsat} can be used directly to determine NBTI-induced ΔV_{th}.

Before applying the above approach to investigate NBTI degradation, it is necessary to understand the independence of parameters λ and θ, and to determine the θ value as well. Eq. (3.2) predicts that I_{dsat} is proportional to $(1 + \lambda V_d)$, and this is confirmed by linear fitting of the experimental data of I_{dsat} versus V_d as shown in Fig. 3.3. The slope yields the value of λ. For the fresh and NBTI-stressed devices, both λ values obtained are about 0.33, indicating that λ is independent of NBTI. On the other hand, as shown in Fig. 3.4(a), $\log|I_{dsat}|$ is found to be a well-fit linear function of $\log|V_g - V_{th}|$ for $V_g - V_{th} > 0.1$V, and a linear fitting of the experimental results yields the value of θ. The θ values obtained are about 1.5 for both fresh and NBTI-stressed devices, indicating that θ is also independent of NBTI degradation.

Regarding the assumption of neglecting mobility degradation during the derivation of Eq. (3.3), according to Krishnan *et al.* in their work [32], mobility degradation is observed to be smaller at higher field, and in Fig. 3.4(b), instead of plotting mobility versus electrical field, we plotted hole mobility and relative mobility

ATTENTION: The Singapore Copyright Act applies to the use of this document. Nanyang Technological University Library

degradation ($\Delta\mu/\mu$) as a function of V_g since I_{dsat} is measured under same gate bias of -1.0 V rather than under same electrical field. As can be seen in Fig. 3.4(b), relative mobility degradation is quite significant at small $|V_g|$ and decreases as $|V_g|$ increases; moreover, relative mobility degradation is quite small when V_g is equal or smaller than -0.8 V. Indeed, I_{dsat} measurement used here is carried out at V_g of -1.0 V. Therefore, the assumption of neglecting mobility degradation in the derivation of Eq. (3.3) is validated, and Eq. (3.3) can be used to determine ΔV_{th} based on the measured ΔI_{dsat} at V_g of -1.0 V.

Before further investigation on Eq. (3.3), the choice of V_g = -1.0 V is also briefly discussed as follows. There are two main reasons to set V_g = -1.0 V. Firstly, it is found from the experiments that about 0.3% of I_{dsat} degradation is induced by V_g = -1.5 V after 1 second at 125ºC. In other words, with V_g = -1.5 V, a degraded I_{dsat} reference is obtained from the first measurement of I_{dsat} for the fresh device, which is highly undesirable. However, with V_g = -1.0 V, there is no obvious I_{dsat} difference observed after 1 second or longer time at 125ºC. Secondly, magnitude of V_g cannot be too low either, because a low V_g induces significant mobility degradation, as shown in Fig. 3.4(b), or may also cause possible severe NBTI recovery during measurement.

Moreover, an experiment has been carefully designed to verify the accuracy of ΔV_{th} as determined by Eq. (3.3). A set of identical fresh devices are used. The threshold voltage of these devices randomly varies in a very small range (~20 mV). The threshold voltage variation is used to simulate NBTI-induced ΔV_{th}. Both V_{th} and I_{dsat} of the devices are measured. The device with the smallest magnitude of V_{th} is taken as the reference, and thus there is a difference in V_{th} and I_{dsat} (i.e., ΔV_{th} and ΔI_{dsat}, respectively) between the reference device and other devices. Note that ΔV_{th} here is

ATTENTION: The Singapore Copyright Act applies to the use of this document. Nanyang Technological University Library

denoted as "measured ΔV_{th}" as it is directly obtained from measurement. On the other hand, for a given ΔI_{dsat}, its corresponding ΔV_{th} is calculated by using Eq. (3.3). The correctness and accuracy of Eq. (3.3) can be demonstrated by the comparison between "measured ΔV_{th}" and "calculated ΔV_{th}". As can be seen in Fig. 3.5, the plot clearly shows that the "calculated ΔV_{th}" is proportional to the "measured ΔV_{th}" with a slope of about 1.0.

In other words, from Fig. 3.5, it is also indirectly verified that there is no significant change in hole mobility at V_g = -1.0 V, otherwise Eq. (3.3) is not correct and thus ΔV_{th} calculated with Eq. (3.3) would not be equal to the measured ΔV_{th}. This agrees well with previous result that hole mobility is not much degraded at relatively high V_g of -1.0 V. Therefore, we could conclude that ΔV_{th} determined by using Eq. (3.3) is reliable and accurate.

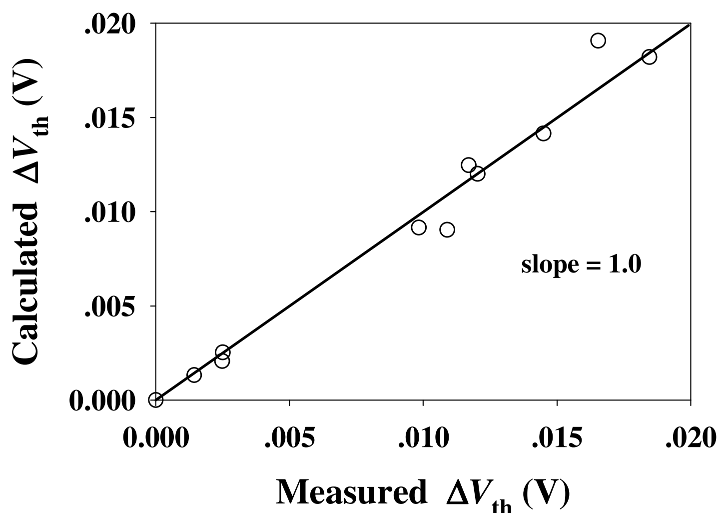

Figure 3.5: *Comparison between the ΔV_{th} calculated with Eq. (3.3) and the ΔV_{th} measured with the conventional method for a set of fresh (i.e., without any NBTI stress) devices whose threshold voltage randomly varies within a small range (20 mV).*

ATTENTION: The Singapore Copyright Act applies to the use of this document. Nanyang Technological University Library

Once the value of θ is obtained with the procedure described above, Eq. (3.3) can be used to extract the NBTI-induced ΔV_{th} based on the measurement of NBTI-induced ΔI_{dsat}. For example, Figure 3.6 shows calculated ΔV_{th} as a function of NBTI stress time, where ΔV_{th} is obtained with this proposed method. For comparison purpose, ΔV_{th} obtained by the conventional method is also included in the figure. As can be clearly seen in Fig. 3.6, ΔV_{th} obtained with our proposed method is significantly larger than that with the conventional method. The difference in ΔV_{th} between these two methods is purely due to NBTI recovery during measurement. Since the measurement duration of conventional method is much longer than that of our method, ΔV_{th} recovery of the former is expected to be much more significant than that of the latter. As a result, ΔV_{th} obtained with the conventional method is significantly smaller than that with our proposed method.

Therefore, it is confirmed that NBTI degradation is largely underestimated with the conventional method, while our proposed method yields a ΔV_{th} much closer to its real value. ΔV_{th} obtained from both methods exhibits a power-law dependence on the NBTI stress time (t), namely $|\Delta V_{th}| = At^n$, where A and n are two parameters independent of stress time. While the n factor from the conventional method is 0.23, the n factor from our method is about 0.18. The n factor has been used to explain the NBTI mechanism [68, 109]. In particular, n = 1/4 has been used to argue that NBTI is due to diffusion-limited electrochemical reactions that involves the neutral hydrogen diffusing species [109]. Therefore, the result here raises a serious concern that a possible distorted picture of NBTI may have been frequently presented in the literature. For examples, n has been reported to be 1/4 [36, 71], 1/5 [63], or other values [194-196]. Obviously, NBTI recovery during measurement could also be used to explain the discrepancy in the n factor. For our proposed method, it yields a

ATTENTION: The Singapore Copyright Act applies to the use of this document. Nanyang Technological University Library

closer-to-real NBTI-induced ΔV_{th}, and hence it can be used to re-examine the true behaviors of NBTI degradation. However, it has to be pointed out that our proposed method cannot totally eliminate the recovery, since it still takes tens of millisecond with which the recovery could still be considerable. Moreover, it is also reported that that ΔV_{th} may increase with sensing V_g [197], and thus the enhanced ΔV_{th} in Fig. 3.6 by our proposed method could partially contribute to higher sensing V_g of -1.0 V.

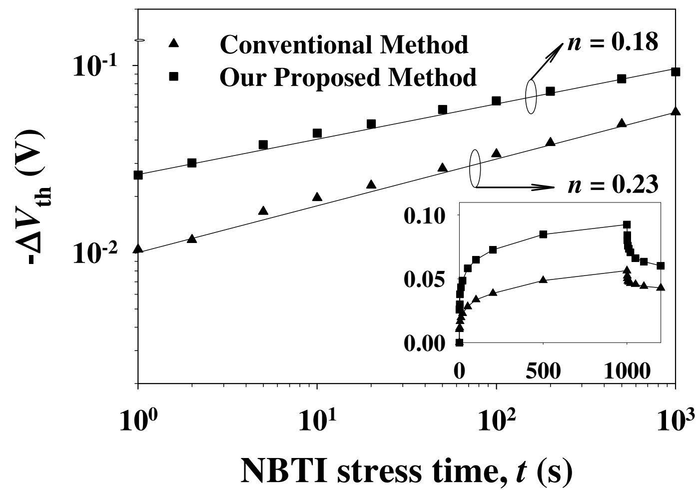

Figure 3.6: *Comparison of NBTI-induced ΔV_{th} between the conventional method and our proposed method.*

3.3 NBTI In-line Test Methodology

As the gate oxide thickness continues to shrink down to less than 20Å for sub-90nm low-power devices or even as thin as 11Å for high-performance devices, NBTI in *p*-MOSFETs has indeed become most critical for further device scaling and future technology development. Typically, for advanced CMOS technology nodes,

ATTENTION: The Singapore Copyright Act applies to the use of this document. Nanyang Technological University Library

various new process technologies or novel techniques are developed to boost device performance, and some of them, if qualified, are to be incorporated into the baseline process for mass production. Therefore, to evaluate a new process, a quick NBTI in-line test becomes quite necessary and useful, with which we can examine the impact of new process technologies on NBTI during the development phase rather than wait until the device is done but found to fail in the NBTI off-line qualification test in the worst case scenario. Moreover, if well benchmarked, NBTI in-line test can become an alternative tool for process qualification and the NBTI results from the in-line test can also be used for the purpose of process optimization as well.

3.3.1 NBTI Model for Process Qualification and NBTI Specifications

Before the introduction of NBTI in-line test methodology, the most commonly-used empirical NBTI model in industry for process qualification is presented here, as shown in Eq. (3.4):

$$\Delta V_{th} = A_0 \exp\left(-E_a / kT\right)\left(V_g / t_{ox}\right)^m t_{eq}^n \qquad (3.4)$$

where ΔV_{th} is the threshold voltage shift, E_a is the activation energy, t_{ox} is the gate oxide thickness, V_g is the gate voltage, t_{eq} is the equivalent DC stress time, T is the junction temperature, k is Boltzmann's constant, A_0 is a constant, and m is the stress acceleration factor and n is the power-law factor. The values of A_0, m and n can be obtained experimentally. In certain circumstances, instead of using the power-law dependence of the gate voltage over the oxide thickness, i.e. the term $(V_g/t_{ox})^m$ in Eq. (3.4), an exponential-law dependence of E_{ox}, i.e. $\exp(E_{ox})$, might be used, where E_{ox} is

ATTENTION: The Singapore Copyright Act applies to the use of this document. Nanyang Technological University Library

the electric field across the gate oxide.

In semiconductor manufacturing, device specifications, such as threshold voltage, drive current, leakage current, sheet resistance, time delay, etc., must be set first, either by the customer or by the manufacturer aiming for a competitive edge in the market. This also applies to NBTI qualification, since NBTI has become one of the most critical reliability issues for sub-90nm technology nodes.

In practice, the most commonly-used criteria for device failure due to NBTI could be either 10% reduction in the saturation drain current (I_{dsat}) (denoted as "ΔI_{dsat} criterion" in following discussion) or threshold voltage shift (ΔV_{th}) when ΔV_{th} increases up to 5% of the nominal operating voltage (V_{dd}) (denoted as "ΔV_{th} criterion" in following discussion). ΔI_{dsat} criterion is quite straightforward but it might introduce some complications into the qualification because I_{dsat} itself is a function of various factors, such as the threshold voltage and the bias conditions, which might have a direct impact on the NBTI results, particularly for devices with different V_{th} under different stress biases. However, the main advantage of this criterion is that I_{dsat} can be measured directly and thus ΔI_{dsat} obtained is most reliable. Besides, in certain aspect, ΔI_{dsat} also includes mobility degradation due to NBTI stress, which might be negligible but definitely not accounted by the threshold voltage shift ΔV_{th}. ΔV_{th} criterion is simple and most-commonly used in both research and industry to examine NBTI degradation. The shift of entire *I-V* curve after NBTI stress can almost be completely characterized by ΔV_{th} such that the delay impact of the device or circuit could be calculated and monitored. Nevertheless, there are some concerns regarding the extraction methods of V_{th}. The widely-used constant current method gives consistent ΔV_{th}, but criteria of the constant current might have an impact on the NBTI

ATTENTION: The Singapore Copyright Act applies to the use of this document. Nanyang Technological University Library

results, especially for devices with different dimensions. On the other hand, the maximum G_m method is quite straightforward but may not yield consistent ΔV_{th}, especially for the devices with smaller dimensions, mainly due to the fluctuations of maximum G_m point under the NBTI stress. In short, neither ΔI_{dsat} criterion nor ΔV_{th} criterion is perfect, and there is a trade-off between them. Therefore, in our proposed NBTI in-line test methodology, different approaches are used.

3.3.2 Proposed NBTI In-line Test Framework

As mentioned previously, NBTI in-line test could be quite necessary and useful for the evaluation of new process technologies, and NBTI in-line test methodology mainly aims for the "feed-forward" of NBTI performance in devices during development phase, through analyzing the impact of various process technologies on NBTI, predicting the device lifetimes and qualitatively comparing NBTI degradation among different splits or between the old and new processes. Figure 3.7 shows a proposed NBTI in-line test. The device under test, i.e., DUT, goes through NBTI in-line test, and NBTI results, in terms of ΔV_{th} or ΔI_{dsat} or both, can be either directly measured or indirectly extracted. Based on ΔV_{th} and/or ΔI_{dsat}, the device lifetime can be estimated with a proper NBTI model, as shown in Eq. (3.4). Meanwhile, the control chart can be plotted and it would directly feedback to the on-going process. This loop iterates until the process is finally done. Moreover, with off-line NBTI full test, the empirical NBTI model can be refined. Based on the refined NBTI model, more accurate device lifetime can be extracted and thus benchmarked with the previous results from NBTI in-line test.

ATTENTION: The Singapore Copyright Act applies to the use of this document. Nanyang Technological University Library

In particular, for NBTI in-line test, there are three main tasks before it can be implemented. Firstly, specify NBTI in-line test conditions (T_{str}, V_{gstr} and t_s) for DUT. Secondly, use a proper measurement method to measure and/or extract NBTI degradation in terms of ΔV_{th} or ΔI_{dsat} or both. Lastly, choose or formulate a proper NBTI model to predict the device lifetime.

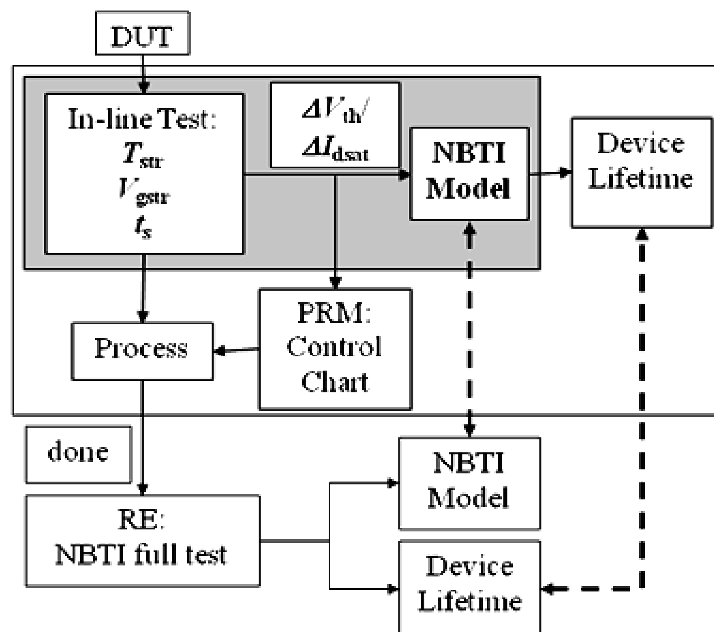

Figure 3.7: *A proposed NBTI in-line test, where DUT stands for device under test, T_{str} is stress temperature, V_{gstr} is stress gate voltage, t_s is stress time, ΔV_{th} is shift in the threshold voltage, and ΔI_{dsat} is shift in the saturation drain current.*

For stress conditions, there are some constrains due to nature of the in-line test, which ought to be simple, fast and dynamic. As we know, temperature measurement requires some extra equipment, such as heater and cooler, and thus it complicates the test procedure. More importantly, temperature rising, stabilizing and cooling process usually take relatively long time (in minutes or hours), thus NBTI in-line test at high temperature is neither practical nor appropriate. As a result, stress temperature (T_{str})

ATTENTION: The Singapore Copyright Act applies to the use of this document. Nanyang Technological University Library

has to be fixed at room temperature or at 25 °C. In-line test must also be very fast. As a result, stress time () has to be as short as possible, for example, 10s or even less. With T_{str} and t_s fixed, only stress voltage (V_{gstr}) can be used to accelerate NBTI degradation. V_{gstr} should be high enough to accelerate NBTI and make it observable, but not too high because large V_{gstr} will cause gate oxide breakdown. The rule of thumb on choosing V_{gstr} is to use the upper limit of V_{gstr} as specified in previous NBTI qualification report for same technology node. Moreover, stress condition, i.e., T_{str} = 25 °C, t_s = 10 s and V_{gstr} = -2.3 V for 65nm- or 45nm-node low-power devices, must be undergoing test round first for several times before the actual implementation of NBTI in-line test, mainly to confirm that NBTI degradation under this stress condition is observable and the result is consistent as well.

Besides the setting of stress conditions specified, measurement methods are also critical for the success of NBTI in-line test. As mentioned previously, there are two possible specifications for device failure due to NBTI degradation, in terms of ΔV_{th} and $\%\Delta I_{dsat}$, respectively. As a result, two categories of NBTI measurement methods are proposed, as summarized in Table 3.1, in which detailed procedures and the formula for extraction of either ΔV_{th} or ΔI_{dsat} are also presented. Each method has its own advantages and limitations. Single-point I_{dlin} and I_{dsat} methods (i.e. Method 1 and 3) are relatively fast such that NBTI recovery is minimized, and 1st on-the-fly (OTF) method (i.e. Method 2) has simplest setup with no stress interruption during measurement. Although the results by single-point I_{dlin} method can be directly used to compare with the simulated results as predicted by empirical NBTI model, ΔV_{th} is estimated by assuming that sub-threshold swing is not much affected by NBTI stress, and it needs further verification by measuring *I-V* curves before and after NBTI stress. 1st OTF method gives good NBTI results because the stress is not interrupted during

ATTENTION: The Singapore Copyright Act applies to the use of this document. Nanyang Technological University Library

measurement. However, as reviewed in section 2.5.3, Chapter 2, OTF method has a time-zero problem and it directly affects the accuracy of extracted ΔV_{th} and its consistency as well. Single-point I_{dsat} method is one of the most promising methods, because it gives most reliable results with measured I_{dsat} and also minimizes NBTI recovery during measurement. Moreover, based on the method proposed in previous section 3.2, ΔV_{th} can also be extracted accordingly. However, as discussed previously, ΔI_{dsat} criterion has its own limitation, and thus single-point I_{dsat} method should not be set as the only method for NBTI in-line test.

On the other hand, as reviewed in section 2.5, Chapter 2, there are some other NBTI characterization methods. They are not included here, either due to time constrain of the in-line test, such as conventional *I-V* sweep method (which may also induce severe recovery during measurement), or due to complication of the experimental set-up that makes them unsuitable for in-line test, such as pulsed OTF method [183-186], pulsed I_d-V_g method [157] and ultra-fast switching (UFS) method [187].

Method 1: single-point I_{dlin} method to extract ΔV_{th}					
	V_g	V_d	V_s	V_b	before test: define $V_{g1}<V_{th0}$ in subthreshold range
1	0~V_{th0}	-0.05	GND	GND	sweep V_g in subthreshold range to get I_{dlin} @ $V_g = V_{g1}$, V_d = -0.05V & $V_s = V_b$ = GND, and subthreshold swing SS
2	V_{gstr}	GND	GND	GND	hold for time t_s
3	V_{g1}	-0.05	GND	GND	measure I_{dlin1} @ $V_g = V_{g1}$, V_d = -0.05V & V_s = V_b = GND
	V_{th} degradation can be extracted: ΔV_{th} = SS*lg(I_{dlin}/ I_{dlin1})				

ATTENTION: The Singapore Copyright Act applies to the use of this document. Nanyang Technological University Library

Method 2: 1st on-the-fly (OTF) method to extract ΔV_{th}					
	V_g	V_d	V_s	V_b	before test: get the V_{th0} of the fresh device
1	V_{gstr}	-0.05	GND	GND	measure I_{dlin} @ $V_g = V_{gstr}$, V_d = -0.05V & $V_s = V_b$ = GND
2	V_{gstr}	-0.05	GND	GND	hold for t_s, and measure I_{dlin1} @ $V_g = V_{gstr}$, V_d=-0.05V & $V_s = V_b$ = GND
	V_{th} degradation can be extracted: $\Delta V_{th} =(V_{gstr} - V_{th0})*(I_{dlin} - I_{dlin1})/ I_{dlin}$				

Method 3: single-point I_{dsat} method to extract ΔI_{dsat}					
	V_g	V_d	V_s	V_b	
1	V_{dd}	V_{dd}	GND	GND	measure I_{dsat} @ $V_g = V_d = V_{dd}$ & $V_s = V_b$ = GND
2	V_{gstr}	GND	GND	GND	hold for time t_s
3	V_{dd}	V_{dd}	GND	GND	measure I_{dsat1} @ $V_g = V_d = V_{dd}$ & $V_s = V_b$ = GND
	I_{dsat} degradation can be calculated: $\% \Delta I_{dsat} = (I_{dsat} - I_{dsat1})/ I_{dsat} *100\%$				

Table 3.1: *A summary on proposed measurement methods for NBTI in-line test with detailed procedures: single-point I_{dlin} method and 1st on-the-fly (OTF) method [40, 152] for ΔV_{th} extraction, and single-point I_{dsat} method [182] for ΔI_{dsat} extraction.*

Lastly, regarding the NBTI model, the rule of thumb is to use most updated empirical NBTI model. If available, NBTI physical model can also be adapted to predict the impact of process technologies on NBTI. NBTI in-line test is not designed to fully replace final NBTI off-line test. Instead, it is mainly used as a quick check for new processes during development. Device lifetime obtained from NBTI in-line test might deviate from the actual one, mainly due to stringent stress conditions at room temperature and high stress gate bias for a short stress time. Stress condition for in-line test is not commonly used for extraction of the model parameters. As a result, only the trend as predicted by NBTI in-line test, when comparing among splits or

ATTENTION: The Singapore Copyright Act applies to the use of this document. Nanyang Technological University Library

between old and new processes, would be valuable. In the next section, some NBTI in-line test results between old and new processes are shown to validate NBTI in-line test methodology.

3.3.3 NBTI In-line Test Validation: Results and Discussion

For advanced technology nodes, various kinds of new processes or techniques, such as stress proximity technique (SPT) [198, 199] and laser spike annealing (LSA) [200-202], are developed to boost device performance. The *p*-MOSFETs used here are fabricated with 65nm or 45nm baseline process with integrated stress memorization technique (SMT) [203, 204] and dual stress liner (DSL) [198, 199, 205, 206] process. Proximity of compressive stress liner is enhanced by spacer removal before DSL deposition and it is known as SPT process. Spike annealing or LSA is carried out after salicidation, mainly to effectively activate dopant in source/drain region. NBTI in-line test is conducted and the results are shown in Fig. 3.8. Both ΔV_{th} extracted by 1$^{\mathrm{st}}$ OTF method and $\%\Delta I_{\mathrm{dsat}}$ measured by single-point I_{dsat} method give the same trend. By comparing the results, the impact of new process on NBTI can be observed. Figure 3.8(a) clearly shows that SPT induces much smaller NBTI degradation and thus improve NBTI immunity quite significantly. From Fig. 3.8(b), as compared with spike-only process, LSA process worsens NBTI degradation in certain way. However, these preliminary results obtained from NBTI in-line test are not adequate to draw final conclusions on the impact of SPT and LSA on NBTI. Systematical NBTI off-line test under normal stress conditions must be carried out to confirm the trend by NBTI in-line test, and these will be covered with more details in Chapter 6.

ATTENTION: The Singapore Copyright Act applies to the use of this document. Nanyang Technological University Library

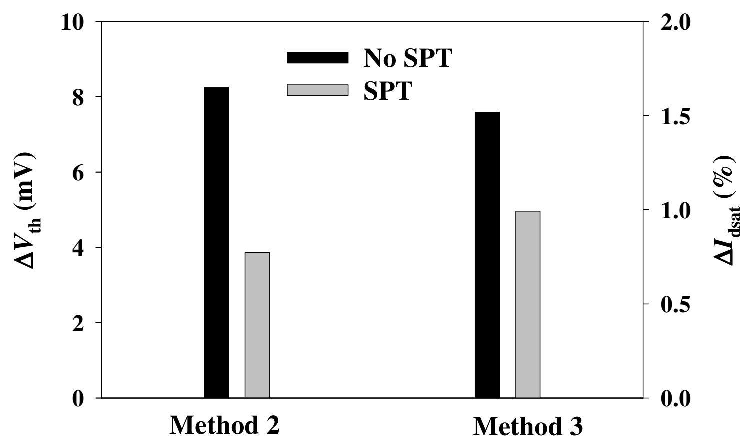

(a)

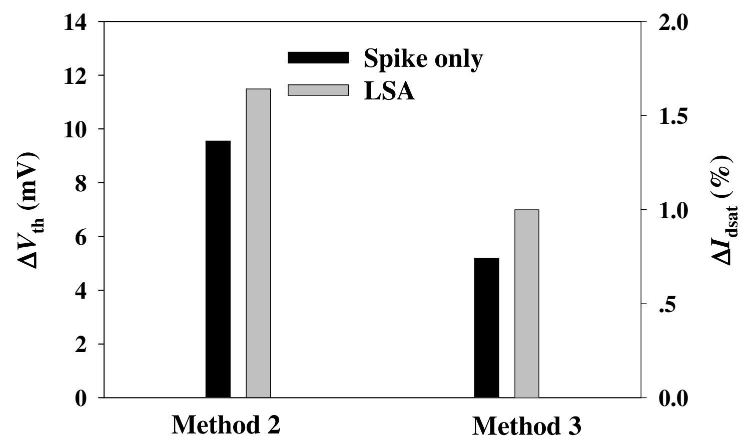

(b)

Figure 3.8: *Comparison of NBTI in-line test results in terms of* ΔV_{th} *extracted by* 1st *OTF method ("Method 2") and* $\%\Delta I_{dsat}$ *measured by single-point* I_{dsat} *method ("Method 3") for different processes: (a) No SPT vs. SPT; and (b) Spike only vs. LSA.*

3.4 Characterization of NBTI Recovery

NBTI in *p*-MOSFETs gets recovered immediately when the NBTI stress is removed, and hence electrical measurement tends to underestimate NBTI degradation

ATTENTION: The Singapore Copyright Act applies to the use of this document. Nanyang Technological University Library

due to its unavoidable measurement time. The measurement-induced additional NBTI recovery must be taken into account, especially during electrical measurement of NBTI recovery, because it would directly affect the measurement time frames. In this section, NBTI recovery is observed to be highly reproducible under same conditions and hence it is used to extract the critical measurement time by using different measurement time intervals for the characterization of NBTI recovery. Thereafter, within a modulated measurement time frame, a combined empirical model for NBTI recovery [207] is proposed to describe the entire process of NBTI recovery in a wide time range. Lastly, the effect of measurement time delay on NBTI is examined.

3.4.1 NBTI Recovery within Modulated Measurement Time Frame

Intuitively, a general NBTI measurement time frame $t_{[i]}$ at i^{th} cycle (i = 1, 2, 3 …) with the period of $t_{p\text{-}i}$, can be described by Eq. (3.5), and also graphically represented in Fig. 3.9:

$$t_{[i]} = [t_{[s]\text{-}i}, t_{[r]\text{-}i}] = \{\text{stress, recovery}\} \qquad (3.5)$$

where $t_{[s]\text{-}i} = [t_{1\text{-}i}, t_{2\text{-}i}, t_{3\text{-}i}, \ldots, t_{k\text{-}i}]$ and $t_{[r]\text{-}i} = [t_{k+1\text{-}i}, t_{k+2\text{-}i}, t_{k+3\text{-}i}, \ldots]$ are the time vectors for NBTI stress and recovery phases, respectively. More specifically, at i^{th} cycle, measurements are taken at the time $t_{j\text{-}i}$ (j = 1, 2 … k, k+1 …), and the stress is removed at time $t_{k\text{-}i}$, while the NBTI stress is resumed at the next (i+1) cycle, i.e., $t_{[i+1]}= t_{[i]}+ t_{p\text{-}i}$. For a normal case of the measurement time frame with a high symmetry, $t_{p\text{-}i}$ is a constant value, i.e. $t_{p\text{-}i} = t_p$, and hence any $t_{[i+1]}$ can then be extracted from $t_{[1]}$ with $t_{[i+1]}= t_{[1]}+ it_p$, and by assuming that the stress time duration is equal to the recovery time duration, i.e. $t_k = 0.5t_p$, $t_{[k\text{-}i]+j}$ is simply the summation of

ATTENTION: The Singapore Copyright Act applies to the use of this document. Nanyang Technological University Library

$t_{[k-i]}$ and t_j, i.e. $t_{[k-i]+j} = t_j + 0.5t_p$ for j=1, 2 … k. The measurement time frame for static NBTI can be obtained by setting i=1, i.e., $t_{[s]-1}$ only, while for static NBTI with recovery phase, $t_{[r]-1}$ is added, i.e., $[t_{[s]-1}, t_{[r]-1}]$.

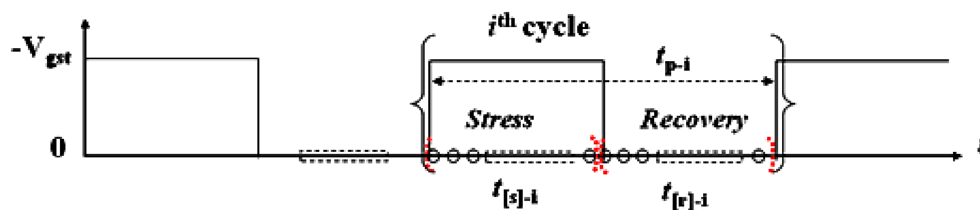

Figure 3.9: *A general measurement time frame $t_{[i]}$ at i^{th} cycle (i = 1, 2, 3…) with the period of t_{p-i}, for the dynamic NBTI or NBTI recovery.*

Instead of examining the measurement effect on NBTI, here we investigate the measurement effect on NBTI recovery. It is typically observed that, under the same stress and recovery conditions, the experiments for NBTI and NBTI recovery are highly reproducible, and the reproducibility of NBTI recovery in turn suggests that an empirical model for NBTI recovery should be possible and useful. However, as can be seen from Fig. 3.10, with all other conditions kept the same, NBTI recovery changes with measurement time interval, where the measurement time interval is defined as either the smallest repeatable time duration for two adjacent measurements or the average time duration. The measurement time interval is an indication of compactness of measurement time frame.

Figure 3.10 clearly shows that a smaller measurement time interval yields a faster NBTI recovery, which implies that the measurement time interval has a large impact on NBTI recovery. However, this phenomenon does not imply that there are different NBTI recovery mechanisms for different measurement time intervals. Instead, it can be attributed to the measurement time interval itself only. During the

ATTENTION: The Singapore Copyright Act applies to the use of this document. Nanyang Technological University Library

NBTI stress phase, measurement causes unwanted recovery, but once the stress is resumed, if the measurement time is minimized, the experimental NBTI results would not be largely affected. In contrast, during the NBTI recovery phase, measurement-induced recovery is accumulated. As a result, when the measurement time interval is very compact, even if the measurement time (t_m) is minimized, this accumulated recovery effect could still lead to a much distorted picture of NBTI recovery, especially in the early stage of NBTI recovery.

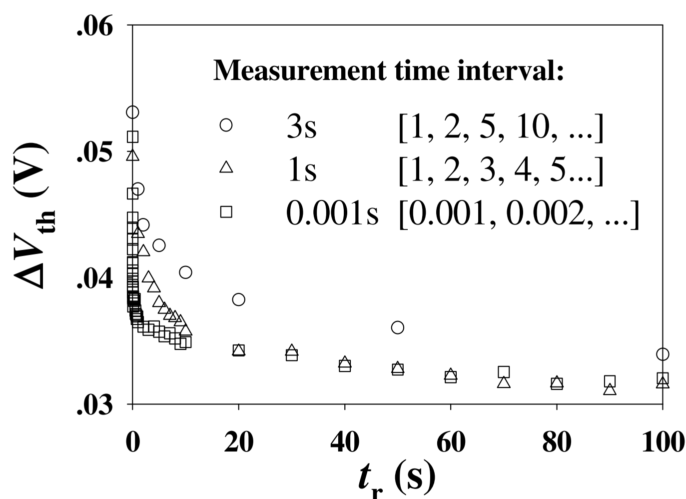

Figure 3.10: *Comparison of NBTI recovery in the identical devices with different measurement time intervals. The device is pre-stressed with negative gate bias (V_{gstr} = -2.2V) at the elevated temperature (T_{str} = 125°C) for 1000s, and the NBTI stress is purposely removed so as to monitor the NBTI recovery.*

This problem can be solved by two approaches. One is to use a big measurement time interval (which should be much larger than t_m) such that the accumulated recovery is comparably small and thus can be ignored. The other is to take t_m into account. To study NBTI recovery, we cannot skip the early stage because it might

ATTENTION: The Singapore Copyright Act applies to the use of this document. Nanyang Technological University Library

provide clues on the underlying mechanism. Therefore, the second approach is more useful and thus is discussed as follows.

The second approach is based on the modulated measurement time frame. In this approach, typical t_m must be obtained first. The value of t_m can be manually calculated by measuring the time duration for many repeated measurements and taking the average time, or it can be extracted from the experiments. Thereafter, the unwanted measurement-induced effect on NBTI recovery can be eliminated by modulating the measurement time frame with t_m, and the modulated time vector for the NBTI recovery phase, i.e. $t_{[r]}$', is described by

$$t_{[r]}' = [t_{k+1}', t_{k+2}', t_{k+3}', \ldots] = t_{[r]} + t_{[m]} \qquad (3.6)$$

where $t_{k+j}' = t_{k+j} + jt_m$ (j = 1, 2, 3 …), and the measurement time vector $t_{[m]}$ is defined as $t_{[m]} = [1, 2, 3, \ldots, n] \times t_m$, where n = length($t_{[r]}$).

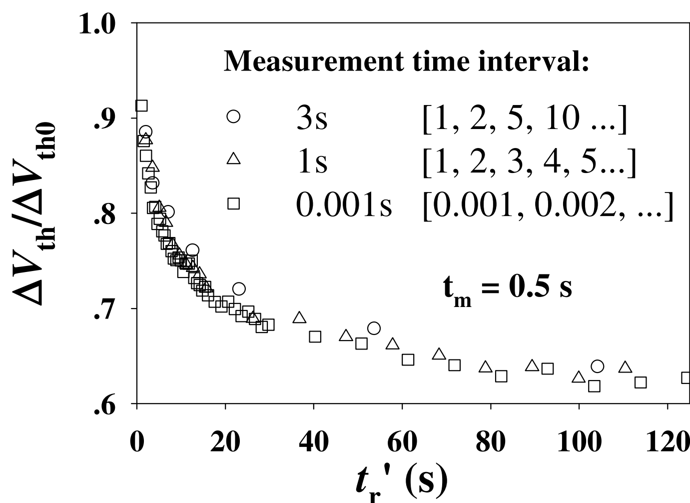

Figure 3.11: *Re-plot of Fig. 3.10 for NBTI recovery within the modulated measurement time frame by taking the measurement time (t_m) into account.*

ATTENTION: The Singapore Copyright Act applies to the use of this document. Nanyang Technological University Library

As shown in Fig. 3.10, NBTI recovery without taking the accumulated measurement-induced recovery into account is different for different measurement time intervals. In contrast, as can be seen in Fig. 3.11, NBTI recovery obtained via the above modulated measurement time frame is highly repeatable for different measurement time intervals. This highlights the validity of the approach and the importance of the influence of the accumulated recovery. In addition, the value of t_{m} can be obtained from the approach. For example, the value of t_{m} extracted from Fig. 3.11 is about 0.5s for the single-point measurement method, being consistent with the average measurement time (t_{m}<1s) manually obtained.

3.4.2 Empirical Model for NBTI Recovery

On the other hand, NBTI recovery obtained with the above approach can be well described by the following empirical model [37, 111]:

$$\Delta V_{th0} - \Delta V_{th} = \Delta V_{th0} \beta t_r^n \tag{3.7}$$

where ΔV_{th0} corresponds to the initial ΔV_{th} at the exact moment when NBTI stress is removed, t_{r} is the recovery time, n is the power-law factor which is a constant (~0.25) [37, 111], and β is a fitting parameter.

In order to test the above empirical model, four identical p-MOSFETs are stressed for 1s, 10s, 100s and 1000s respectively, and the recovery for each device is monitored. In this case, only ΔV_{th0} is different among the devices. The experimental NBTI recovery of the four devices obtained within the modulated measurement time frame are shown in Fig. 3.12(a). As can be seen in the figure, the experimental

ATTENTION: The Singapore Copyright Act applies to the use of this document. Nanyang Technological University Library

results are well fitted by Eq. (3.7), and the power-law factor n obtained from the fitting is a constant with the value of ~0.25 being consistent with the previous studies [37, 111]. On the other hand, the β value obtained from the fitting exhibits a linear relation with ΔV_{th0}, as shown in Fig. 3.13. However, according to Eq. (3.7), $(\Delta V_{th0}-\Delta V_{th})/\Delta V_{th0}$, i.e., βt_r^n, becomes more than 1 for a sufficiently long time, which results in zero or even negative ΔV_{th}. This means that NBTI degradation is fully recovered or over recovered. Such situations are not reasonable because no full recovery or over recovery has been observed. Actually this empirical model is valid only for a relatively short recovery time. Recently, Kaczer *et al.* [208] proposed a universal recovery model which seems to fit the recovery data very well more than 6 orders of magnitude in time, where the data starts at ms or below. Nevertheless, the logarithmic-law model [208-210] also encounters the same problem of possible full or over recovery with sufficiently long recovery time.

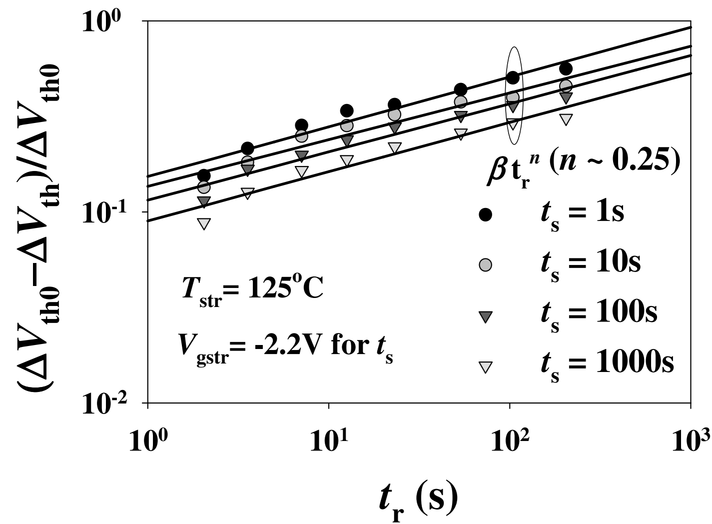

(a)

ATTENTION: The Singapore Copyright Act applies to the use of this document. Nanyang Technological University Library

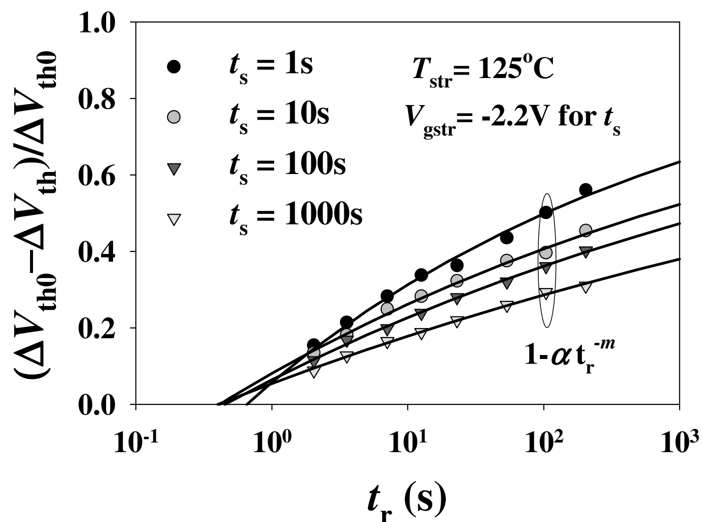

(b)

Figure 3.12: *Modeling of NBTI recovery with (a) the existing empirical model [37, 111] (i.e. Eq. (3.7)); and (b) the proposed empirical model (i.e. Eq. (3.8)). The devices are stressed under* V_{gstr} *= -2.2V at* T_{str} *= 125°C for 1, 10, 100, and 1000s, respectively.*

To overcome the limitation of existing empirical models for a long recovery time, another empirical model is proposed as below

$$\Delta V_{th0} - \Delta V_{th} = \Delta V_{th0} - \Delta V_{th0}\alpha t_r^{-m} \qquad (3.8)$$

where α and m are two fitting parameters. The experimental data shown in Fig. 3.12(a) is re-plotted in Fig. 3.12(b) according to Eq. (3.8). As shown in Fig. 3.12(b), the new model can also well describe the experimental results. It is found that α is slightly less than unit 1, whereas m has a strong correlation with ΔV_{th0} as shown in Fig. 3.13. This model can describe the recovery behavior for a long recovery time. However, it fails for a small time scale as Eq. (3.8) shows that a negative value of $(\Delta V_{th0}-\Delta V_{th})/\Delta V_{th0}$ could be reached when t_r is very small.

ATTENTION: The Singapore Copyright Act applies to the use of this document. Nanyang Technological University Library

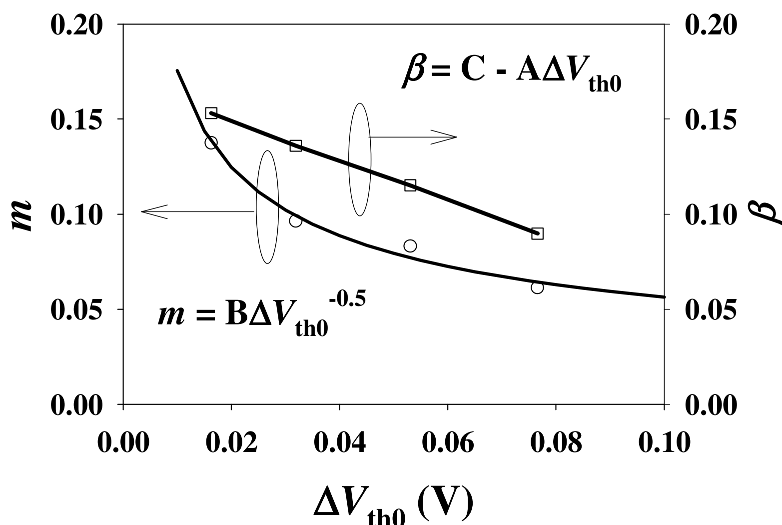

Figure 3.13: *Correlation of m in Eq. (3.8) and β in Eq. (3.7) with* ΔV_{th0}.

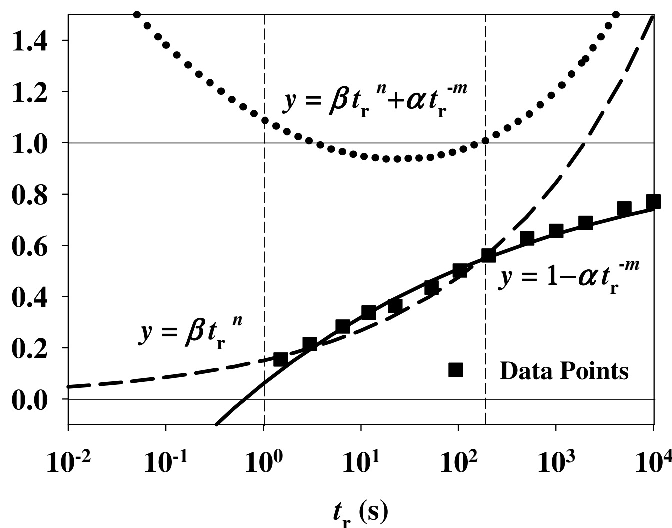

Figure 3.14: *Plots of the functions* βt_r^n, $(1 - \alpha t_r^{-m})$, $(\beta t_r^n + \alpha t_r^{-m})$ *and data points until 10000s. Here* $\beta = 0.15$, $n = 0.25$, $\alpha = 0.94$ *and* $m = 0.14$. *The empirical models are valid only when* βt_r^n *or* $(1 - \alpha t_r^{-m})$ *is smaller than 1. When* $(\beta t_r^n + \alpha t_r^{-m})$ *~1, both models are valid.*

ATTENTION: The Singapore Copyright Act applies to the use of this document. Nanyang Technological University Library

Obviously, Eq. (3.7) is valid only for $\beta t_r^n < 1$ while Eq. (3.8) is valid only for $(1 - \alpha t_r^{-m}) > 0$. In addition, ideally, $(\beta t_r^n + \alpha t_r^{-m})$ should be equal to 1. To determine the time scales in which the models are valid, βt_r^n, $(1 - \alpha t_r^{-m})$ and $(\beta t_r^n + \alpha t_r^{-m})$ as a function of t_r are presented in Fig. 3.14. As can be found from this figure, Eq. (3.7) is only valid until ~200 s, while Eq. (3.8) is valid from 0.5 s onwards and can fit the data points reasonably well until 10000 s. However, as shown in Fig. 3.14, $(\beta t_r^n + \alpha t_r^{-m})$ in the time range of [1, 200] is approximately equal to 1, which indicates that both models can be used to describe NBTI recovery in the time range of [1, 200]. Therefore, with the complementarities of these two models, the entire process of NBTI recovery in a wide time range can be empirically described.

3.4.3 Effect of Measurement Time Delay on NBTI

Lastly, the effect of measurement time delay (t_d) on NBTI is experimentally examined. As can be seen in Fig. 3.15, as the measurement time delay (t_d) increases, the NBTI-induced ΔV_{th} decreases, which indicates that ΔV_{th} is more significantly underestimated for longer measurement time delay. Based on the general power-law time dependence of NBTI, i.e., $\Delta V_{th} = At^n$, the pre-factor A and power-law factor n can be extracted accordingly, which are summarized in Table 3.2 and plotted in Fig. 3.16. As can be seen from the figure, when t_d gets longer, the pre-factor A becomes smaller, whereas the power-law factor n tends to be larger, which is quite consistent with the results obtained by Ershov *et al.* [39]. However, as shown in Fig. 3.16, both the pre-factor A and power-law factor n can be well approximated to be linear with $\log(t_m)$, and thus the actual A and n (at t_d = 0s) is not back-traceable.

ATTENTION: The Singapore Copyright Act applies to the use of this document. Nanyang Technological University Library

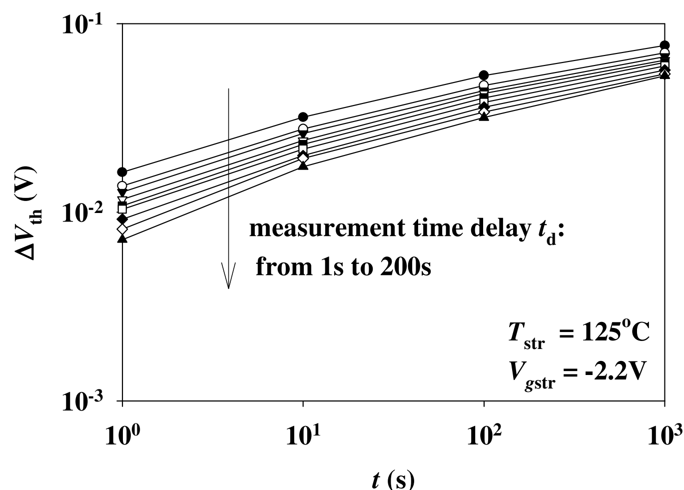

Figure 3.15: *The effect of measurement time delay on NBTI. The pre-factor A and power-law factor n can be extracted and summarized in Table 3.1.*

t_d(s)	1	2	5	10	20	50	100	200
n	0.2346	0.2381	0.2464	0.2527	0.2529	0.2626	0.2717	0.2865
A	0.0149	0.0138	0.0126	0.0117	0.0112	0.0100	0.0091	0.0080

Table 3.2: *The parameters extracted from Fig. 3.15 based on* $\Delta V_{th} = At^n$

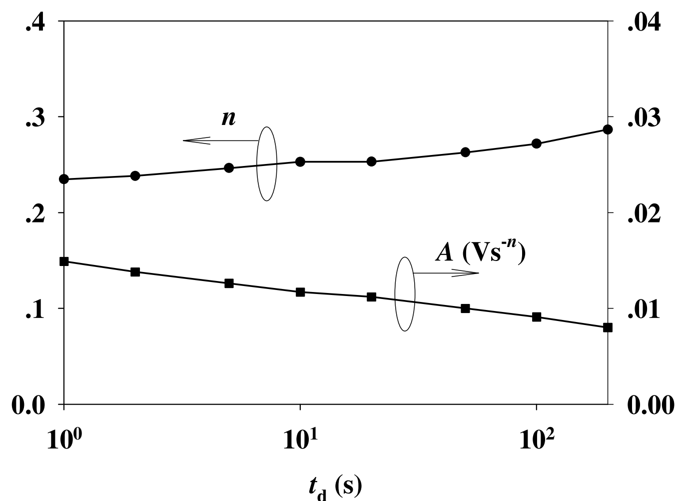

Figure 3.16: *Plot of A and n as a function of the measurement time delay (t_d).*

ATTENTION: The Singapore Copyright Act applies to the use of this document. Nanyang Technological University Library

3.5 Summary

In summary, a simple characterization technique based on ingle-point measurement of saturation drain current has been proposed to minimize the unwanted NBTI recovery effect during the electrical measurement of NBTI. An NBTI in-line test methodology is developed here to monitor NBTI degradation in devices during the development phase, aiming for process comparison and optimization in advanced CMOS technology nodes. NBTI recovery is experimentally investigated and within the modulated measurement time frame, a combined empirical model for NBTI recovery has been proposed in our work to describe the entire process of NBTI recovery in a wide time range. Lastly, the effect of measurement time delay on NBTI is examined.

ATTENTION: The Singapore Copyright Act applies to the use of this document. Nanyang Technological University Library

CHAPTER 4 MODELING OF NBTI IN P-MOSFETS

In this chapter, an analytical reaction-diffusion (R-D) model within the framework of the standard R-D model is proposed to describe the negative bias temperature instability (NBTI) process in a wide time scale covering the three regimes of reaction, transition and diffusion. A power-law factor of ~1 is experimentally observed for nitrided gate oxide and it shows clear evidence of the existence of the reaction-limited regime for NBTI. The model is also used to examine the nitrogen effect on NBTI. The analytical R-D model is extended to include cases of other possible H-related diffusing species, such as the positively-charged hydrogen ion H^+ and hydrogen molecule H_2. Lastly, an analytical geometry-dependent R-D model is obtained for two- and three-dimensional hydrogen diffusion. The geometry dependence of NBTI is investigated experimentally and it can also be well explained in terms of strain and hydrogen diffusion in devices with small dimensions.

4.1 Introduction

As reviewed in section 2.4, Chapter 2, various mechanisms have been proposed to explain NBTI degradation, among which one of the most accepted models is commonly known as the reaction-diffusion (R-D) model. The R-D model was first proposed by Jeppson and Svensson in 1977 [61] and mathematically-generalized by Ogawa and Shiono in 1995 [68]. Subsequently, it was further unified by Alam *et al.* [132, 133]. The R-D model states that: interface trap generation is initially

ATTENTION: The Singapore Copyright Act applies to the use of this document. Nanyang Technological University Library

reaction-limited and exhibits a linear dependence with respect to the stress time; and as time goes on, with the released hydrogen species diffusing away from the interface, the process becomes diffusion-limited and a general power-law time-dependence with the exponent factor of 1/4 is obtained for neutral H diffusing species [68, 132, 133].

Nevertheless, so far, the reaction-limited regime has not been experimentally verified yet, nor the time-independent transition regime [132, 133]. Moreover, it has also been intensively reported that incorporation of nitrogen into the gate oxide (i.e. oxynitride) worsens NBTI [34-38], and NBTI degradation is also strongly dependent on the nitrogen depth profile [74, 108]. However, the impact of nitrogen in the reaction-limited regime has not been reported yet.

In this chapter, an analytical R-D model [211] is first proposed to describe the entire process of NBTI degradation. Direct experimental evidence has been observed to prove the existence of the reaction-limited regime with a power-law factor of ~1. A smooth transition from the reaction-limited regime to the diffusion-limited regime is experimentally observed and theoretically simulated. By examining the dependence of NBTI on the initial Si-H density, the reaction energy and the diffusion coefficient of the H-related species, the analytical R-D model can well explain the nitrogen effect on NBTI. The analytical R-D model is also extended to include other possible H-related diffusing species, such as positively-charged hydrogen ion H^+ and hydrogen molecule H_2. Lastly, an analytical geometry-dependent R-D model is developed, and the geometry dependence of NBTI is examined in terms of strain and hydrogen diffusion in devices with small dimensions.

ATTENTION: The Singapore Copyright Act applies to the use of this document. Nanyang Technological University Library

4.2 Analytical Reaction-Diffusion Model for NBTI

4.2.1 Analytical Reaction-Diffusion Model

The detailed NBTI mechanism and formulations of generalized R-D model are described as follows. When *p*-MOSFETs are negatively-biased, holes in the inversion layer interact with hydrogen-terminated trivalent Si bonds (Si-H), with an initial defect density N_o, at the interface, and this interaction leads to the dissociation of Si-H bonds, which in turn leads to the generation of interface traps (N_{it}). Initially, N_{it} generation is limited by the dissociation of Si-H bonds at the interface (with the forward reaction rate k_F and reverse reaction rate k_R). As the time goes on, diffusion of H-related species becomes the limiting factor for N_{it} generation. Mathematically, the generalized R-D model can be described by the following two equations [68]:

$$\frac{dN_{it}}{dt} = k_F\left(N_O - N_{it}\right) - k_R N_H\left(0\right) N_{it} \tag{4.1}$$

$$\frac{dN_H}{dt} = D_H \frac{d^2 N_H}{dx^2} \pm \mu_H \xi_{ox} \frac{dN_H}{dx} = D_H\left(\frac{d^2 N_H}{dx^2} \pm \frac{q}{kT}\xi_{ox}\frac{dN_H}{dx}\right) \tag{4.2}$$

where N_H is the diffusing hydrogen concentration, $N_H(0)$ corresponds to the diffusing hydrogen concentration N_H at the interface, D_H and μ_H are the diffusion coefficient and the effective mobility of the H-related diffusing species, respectively and they obey Einstein's relation $\mu_H / D_H = q / kT$, where q, k, T are the unit electronic charge, Boltzmann's constant and temperature, respectively.

For neutral H-related diffusing species, the electric field ξ_{ox} on the right-hand side

ATTENTION: The Singapore Copyright Act applies to the use of this document. Nanyang Technological University Library

of Eq. (4.2) takes no effect and thus can be neglected for simplicity. Besides, another useful relation is the conservation of H-related diffusing species which indicates that each released species leaves behind one interface trap, and it is described by Eq. (4.3):

$$N_{it}(t) = \int_{x=0}^{x(t)} N_H(x,t)dx \tag{4.3}$$

where $x(t)$ is the tip of diffusing front and approximated as $\sqrt{D_H t}$ with a triangular diffusion profile for neutral H-related diffusing species [132, 133]. Hence, based on Eq. (4.3), by assuming one-sided diffusion towards the gate oxide, interface trap generation $N_{it}(t)$ can obtained, as shown in Eq. (4.4):

$$N_{it}(t) = \int_{x=0}^{x(t)=\sqrt{D_H t}} N_H(x,t)dx = \frac{1}{2} N_H(0)\sqrt{D_H t} \tag{4.4}$$

or $$N_H(0) = \frac{N_{it}(t)}{\frac{1}{2}\sqrt{D_H t}} \tag{4.4'}$$

An analytical R-D model is proposed here, mainly to unify both the reaction-limited and diffusion-limited regimes. In the following discussion, we make the assumption of $N_{it} << N_o$, i.e., N_{it} is much smaller than N_o. We also assume $t < t_c$, where $t_c = t_{ox}^2/(4D_H)$, t_c is the critical time and t_{ox} is the gate oxide thickness, mainly to satisfy the condition $t_{ox} > \sqrt{4D_H t}$. In other words, a relatively thick oxide is considered here. As a result, only the diffusion inside the gate dielectric is considered while the effect of poly-Si gate (either reflecting or absorbing) on N_H is not included. In contrast to the assumption that the net trap generation is so slow that it is negligible (i.e. $\frac{dN_{it}}{dt} \sim 0$) in comparison to the large flux on the right-hand side of Eq. (4.1) [132,

ATTENTION: The Singapore Copyright Act applies to the use of this document. Nanyang Technological University Library

133], here we assume that both N_{it} generation due to the forward reaction and N_{it} re-passivation due to the reverse reaction are linear functions of time such that $\frac{dN_{it}}{dt} \sim \frac{N_{it}}{t}$. Eq. (4.2) describes the diffusion process, and by substituting Eq. (4.4) into Eq. (4.1) and rearranging, it yields:

$$N_{it}^{2}(t)+\frac{1}{t\dfrac{k_R}{\frac{1}{2}\sqrt{D_H t}}}N_{it}(t)-\frac{k_F N_O}{\dfrac{k_R}{\frac{1}{2}\sqrt{D_H t}}}=0 \qquad (4.5)$$

or $$N_{it}^{2}(t)+\frac{1}{B\sqrt{t}}N_{it}(t)-\frac{A\sqrt{t}}{B}=0 \qquad (4.5)'$$

where $A=k_F N_O$ and $B=k_R\Big/\left(\frac{1}{2}\sqrt{D_H}\right)$.

By solving Eq. (4.5), N_{it} can be obtained as shown in Eq. (4.6):

$$N_{it}(t)=\frac{2At}{\left(1+\sqrt{1+4ABt^{3/2}}\right)}=\frac{2k_F N_O t}{1+\sqrt{1+4k_F N_O\dfrac{k_R}{\left(\frac{1}{2}\sqrt{D_H}\right)}t^{3/2}}} \qquad (4.6)$$

Certainly, two distinguished regimes can be observed from Eq. (4.6):

the reaction-limited regime (denoted as “R-regime”)

$$N_{it}(t)=At=k_F N_O t \qquad \text{(when } 4ABt^{3/2} \ll 1) \qquad (4.7)$$

and the diffusion-limited regime (denoted as “D-regime”)

$$N_{it}(t)=\sqrt{\frac{A}{B}}t^{1/4}=\sqrt{\frac{k_F N_O}{2k_R}}\left(D_H t\right)^{1/4} \qquad \text{(when } 4ABt^{3/2} \gg 1) \qquad (4.8)$$

ATTENTION: The Singapore Copyright Act applies to the use of this document. Nanyang Technological University Library

In the reaction-limited regime, Eq. (4.7) clearly shows that N_{it} generation increases linearly with the time, which is also suggested by Alam, *et al.* [132, 133]. In the diffusion-limited regime, Eq. (4.8) is also consistent with the widely-observed $t^{1/4}$ time-dependence as given in prior studies [61, 68]. Indeed, the reaction-limited regime is purely accounted by the pre-factor A, while the diffusion-limited regime involves both A and B and is accounted by a pre-factor $\sqrt{A/B}$. The simulated data is shown in Fig. 4.1(a), which clearly indicates that Eq. (4.6) is accurately accounting for both the reaction-limited and diffusion-limited regimes. In other words, the analytical R-D model (Eq. (4.6)) can well unify both the R-regime model (Eq. (4.7)) and the D-regime model (Eq. (4.8)).

To verify the analytical R-D model, a numerical-solution approach was employed to solve the basic set of Eqs. (4.1-3) without assuming that N_{it} has a linear time-dependence on the left side of Eq. (4.1). As shown in Fig. 4.1(b), the numerical solution is very close to the analytical R-D model based on Eq. (4.6). Although ΔN_{it} calculated by the numerical solution is slightly larger than that by the analytical R-D model in the transition regime (i.e. the regime between the reaction-limited and diffusion-limited regimes), they match perfectly in both the reaction-limited and diffusion-limited regimes. This indicates that the analytical R-D model is not just accurate in both the reaction-limited and diffusion-limited regimes but also quite adequate in the transition regime. More importantly, instead of a flat transition [132, 133], the transition regime in our analytical R-D model is of a smooth shape where a power-law factor n of the range [0.25, 1] is possible. This can be used as a possible explanation for the recent finding of 0.5 power-law factor at the initial phase of NBTI [74] by attributing it purely to a transition regime.

ATTENTION: The Singapore Copyright Act applies to the use of this document. Nanyang Technological University Library

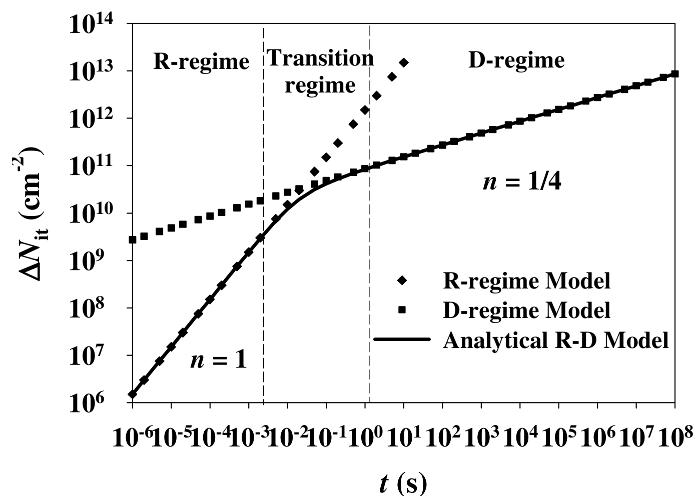

(a)

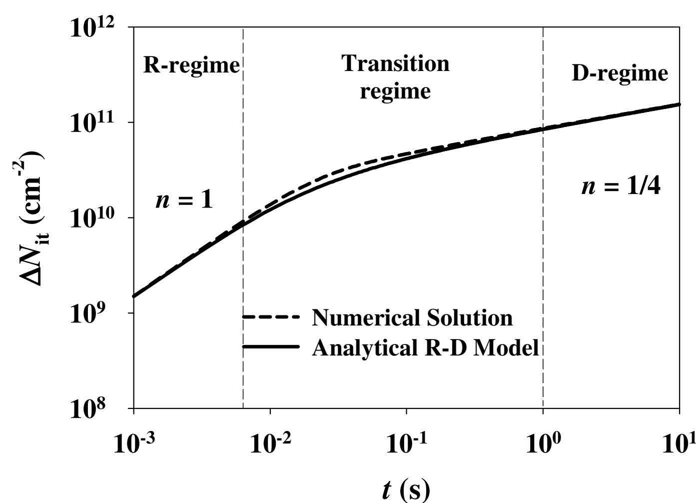

(b)

Figure 4.1: *(a) Interface trap generation (ΔN_{it}) calculated with the analytical R-D model (Eq. (4.6)), the R-regime model (Eq. (4.7)), and the D-regime model (Eq. (4.8)). (b) Comparison between the analytical R-D model and the numerical solution. The parameters used in the calculations are $N_o = 1.5\times10^{14}$ cm^{-2}, $k_F=1\times10^{-2}$ /s, $k_R=1\times10^{-18}$ cm^2/s, $D_H = 1\times10^{-16}$ cm^2/s.*

ATTENTION: The Singapore Copyright Act applies to the use of this document. Nanyang Technological University Library

The transition regime can be described by a characteristic transition time t_{tr}, as shown in Eq. (4.9), which is defined as the intersection of the R-regime model (Eq. (4.7)) and the D-regime model (Eq. (4.8)):

$$t_{tr} = (AB)^{-2/3} = \left(k_F N_O \frac{k_R}{\frac{1}{2}\sqrt{D_H}} \right)^{-2/3} \tag{4.9}$$

There are some interesting observations that are related to the transition point corresponding to interface trap generation N_{it} at the transition time, i.e. $N_{it}(t_{tr})$. As shown in Eq. (4.10), the linear coefficient of $N_{it}(t)$ at the transition point is obtained to be a value of 0.362A, which has a linear dependence on the pre-factor A:

$$\left.\frac{dN_{it}(t)}{dt}\right|_{t=t_{tr}=(AB)^{-2/3}} = \frac{2A\left(1+\sqrt{1+4ABt^{3/2}}\right) - 2At\frac{1}{2}\frac{1}{\sqrt{1+4ABt^{3/2}}}4AB\frac{3}{2}t^{1/2}}{\left(1+\sqrt{1+4ABt^{3/2}}\right)^2}$$

$$= \frac{2\left(1+\sqrt{5}\right) - \frac{6}{\sqrt{5}}}{\left(1+\sqrt{5}\right)^2} A = 0.362A \tag{4.10}$$

Similarly, based on Eq. (4.6), the instantaneous power-law factor at the transition point can also be derived, which is a constant of 0.585, as shown in Eq. (4.11):

$$\left.\frac{d\ln\left(N_{it}(t)\right)}{d\ln(t)}\right|_{t=t_{tr}=(AB)^{-2/3}} = \left.\frac{dy}{dx}\right|_{x=\ln(t_{tr})=-\frac{2}{3}\ln(AB)}$$

ATTENTION: The Singapore Copyright Act applies to the use of this document. Nanyang Technological University Library

$$= 1 - \frac{1}{\left(1+\sqrt{1+4ABe^{\frac{3}{2}x}}\right)} \frac{1}{2} \frac{1}{\sqrt{1+4ABe^{\frac{3}{2}x}}} 4AB\frac{3}{2}e^{\frac{3}{2}x} \Bigg|_{x=\ln(t_{tr})=-\frac{2}{3}\ln(AB)}$$

$$= 1 - \frac{3}{\sqrt{5}\left(1+\sqrt{5}\right)} = 0.585 \tag{4.11}$$

where $x = \ln(t)$ or $t = e^x$ and

$$y = \ln\left(N_{it}(t)\right) = \ln(2At) - \ln\left(1+\sqrt{1+4ABt^{3/2}}\right) = \ln(2A) + x - \ln\left(1+\sqrt{1+4ABe^{\frac{3}{2}x}}\right)$$

Significance of Eq. (4.10) and Eq. (4.11) is discussed as follows. If the experiment is well planned, Eq. (4.11) can be directly used to identify the transition point, and thus at the transition point, Eq. (4.10) can be used as an alternative way to extract the pre-factor *A*, which could be quite useful if the reaction-limited regime is not clearly indicated in the plot.

4.2.2 Evidence of Reaction-Limited Regime

To further verify the analytical R-D model, NBTI experiment on *p*-MOSFETs with interfacial nitrogen concentrations of 3, 8, and 15 at. % was carried out. The nitrided gate oxide was prepared using remote plasma nitridation technique to minimize excessive nitrogen diffusion. The thickness (t_{ox}) of the nitrided oxides is about 18 Å. The channel width and length are 20 μm and 0.15 μm, respectively. The NBTI stress measurement was carried out with a negative gate bias (V_{gstr} = -2.2 V) at

ATTENTION: The Singapore Copyright Act applies to the use of this document. Nanyang Technological University Library

elevated temperature (T_{str} =125°C). To minimize measurement-induced recovery, single-point measurement of saturation current [182] with the measurement delay of about 0.5 s was adapted here to extract the threshold voltage shift ΔV_{th}, and direct-current current-voltage (DCIV) [36, 179-181] measurement was also conducted to determine interface trap generation ΔN_{it}.

Figure 4.2 shows the comparison between the simulated (based on the analytical R-D model) and measured NBTI for nitrided gate oxides with three different nitrogen concentrations. Values of the fitting parameters used in the model are given in Table 4.1, and also plotted as a function of interfacial nitrogen concentrations in Fig. 4.3. An excellent agreement between the simulated and measured data is shown in Fig. 4.2. The results clearly show that interface trap generation ΔN_{it} at the initial stage exhibits a power-law time-dependence with the exponent factor n of ~1 for all nitrogen concentrations. In other words, ΔN_{it} is a linear function with respect to the stress time when the time is relatively short, which is a direct evidence of the reaction-limited regime at the initial NBTI degradation according to the R-D model. Since the measurement is not free of delay, one may argue that NBTI recovery might occur during the measurement and thus affect the experimental results and time exponent as well, especially in the reaction-limited regime, because the measurement time interval is relatively smaller than the measurement time delay. This issue is further discussed as follows. As discussed in previous section 3.4.3, Chapter 3, the measurement time delay affects the time exponent n and a larger exponent is resulted from more recovery. More specifically, from Table 3.2, time delay of 100 s will gives n of ~0.27, which is about 0.02 larger than that from time delay of 10 s (~0.25) and 0.035 larger than that from time delay of 1 s (~0.235). Therefore, the observation of exponent of ~1 could not be solely due to possible recovery during measurement, and thus we claimed that

ATTENTION: The Singapore Copyright Act applies to the use of this document. Nanyang Technological University Library

a reaction-limited regime was observed. Moreover, the experimental results could be well explained by the analytical R-D model.

For the nitrided oxides used in this study, the characteristic transition time can be calculated by Eq. (4.9) and the values shown in Table 4.1 are in the range of 2×10^{-2} to 3×10^{-2}s, depending on nitrogen concentrations. Figure 4.2 clearly shows the evidence of the transition regime in the time range of 10^{-2} to 10^{-1}s for all three nitrided oxide samples. For a longer stress time, a power-law time-dependence with n ~ 1/4 can be obtained, which indicates that NBTI is dominated by the diffusion process. In other words, NBTI enters into the commonly-observed diffusion-limited regime. Therefore, it is very clear that the analytical R-D model can well describe the experimental NBTI results for the nitrided oxide samples with different interfacial nitrogen concentrations, and this model covers all the three regimes of reaction, transition and diffusion.

N at. %	A	$(A/B)^{1/2}$	B	D_H (cm^2/s)	t_{tr} (s)	t_c (s)
3	$1.39\text{x}10^{12}$	$7.38\text{x}10^{10}$	$2.55\text{ x}10^{-10}$	$6.14\text{ x}10^{-17}$	$2.00\text{ x}10^{-2}$	132
8	$1.96\text{ x}10^{12}$	$1.32\text{ x}10^{11}$	$1.12\text{ x}10^{-10}$	$3.16\text{ x}10^{-16}$	$2.74\text{ x}10^{-2}$	25.6
15	$2.67\text{ x}10^{12}$	$1.96\text{ x}10^{11}$	$6.95\text{ x}10^{-11}$	$8.28\text{ x}10^{-16}$	$3.07\text{ x}10^{-2}$	9.78

Table 4.1: *Values of fitting parameters used in the modeling shown in Fig. 4.2. The calculated characteristic transition time (t_{tr}) and critical time (t_c) are also included.*

Moreover, from Fig. 4.2, the experimental result re-confirms the prediction of our analytical R-D model that a smooth transition takes place after the reaction-limited regime rather than a flat transition regime as described in ref. [133]. A flat transition regime has been attributed to cancellation of the forward (generation) and reverse (re-passivation) reactions of Eq. (4.1), which results in net-zero generation of N_{it}, with

ATTENTION: The Singapore Copyright Act applies to the use of this document. Nanyang Technological University Library

the assumption that all hydrogen released from the reaction-limited regime is still at the interface. In other words, a flat transition regime indicates zero diffusion of the hydrogen-related species under certain condition. However, based on the result in Fig 4.2, a smooth transition region provides the evidence that the control of N_{it} generation or re-passivation is indeed a competing process between the reaction-limited and diffusion-limited regimes. It clearly shows that N_{it} generation is slowed down due to large fluxes on the right hand side of Eq. (4.1) which results in re-passivation of interface traps. Therefore, N_{it} generation is controlled by both the rate of Si-H bond dissociation and rate of released hydrogen species that diffuses away from the interface. After the transition point, N_{it} generation starts to be gradually dominated by the diffusion process as described by Eq. (4.8).

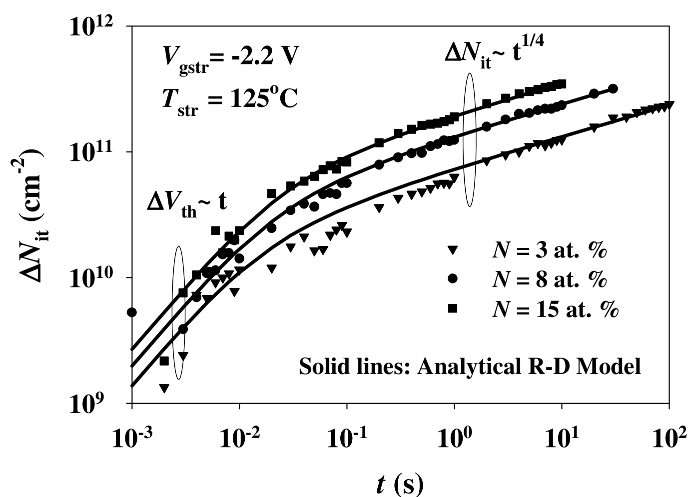

Figure 4.2: *The measured and simulated interface trap generation ΔN_{it} as a function of stress time t for nitrided oxides with the interfacial nitrogen concentrations of 3, 8 and 15 at. %. The NBTI stress measurement is carried out at V_{gstr} = -2.2 V and T_{str} = 125 °C. The values of the parameters used in the simulated ΔN_{it} based on the analytical R-D model are given in Table 4.1.*

ATTENTION: The Singapore Copyright Act applies to the use of this document. Nanyang Technological University Library

4.2.3 Nitrogen Effect on NBTI

The analytical R-D model can also provide a new insight into the effect of nitrogen on NBTI. Figure 4.2 clearly shows that NBTI degradation is worse in both the reaction-limited and diffusion-limited regimes for the nitrided gate oxide with higher interfacial nitrogen concentration. Moreover, as can be seen in Fig. 4.3(a), the parameter A (i.e. $k_F N_o$) increases with the nitrogen concentration, indicating that the incorporation of nitrogen into the gate oxide can increase the initial neutral defect density N_o and/or increase the forward reaction rate k_F. The initial neutral defect density N_o has been observed to increase with nitrogen concentration [107]. The incorporation of nitrogen also reduces the reaction energy of either H-trapping [110, 212] or hole-trapping [131, 213] process and hence enhances the forward reaction of Si-H dissociation. In Fig. 4.4(a), with an increasing A (i.e. due to the nitrogen effect), interface trap generation increases for all three regimes (i.e. the reaction, transition and diffusion regimes).

However, the previous results in Fig. 4.2 have shown that as the nitrogen concentration increases, the increase in N_{it} generation is observed to be much larger in the diffusion-limited regime than that in the reaction-limited regime. In other words, the nitrogen-worsen N_{it} generation is more significant in the diffusion-limited regime than that in the reaction-limited regime. Additional NBTI degradation in the diffusion-limited regime can be attributed to the enhanced diffusion of neutral H-related species in nitrided oxide, which might be partially due to the lower activation energy at nitrided oxide with higher nitrogen concentration [35, 109, 212].

ATTENTION: The Singapore Copyright Act applies to the use of this document. Nanyang Technological University Library

This effect is indeed further confirmed by a larger diffusion coefficient D_H value for the sample with a higher interfacial nitrogen concentration, as observed in Fig. 4.3(b). Furthermore, Figure 4.4(b) also clearly shows that an increase in the diffusion coefficient D_H leads to a large increase in interface trap generation ΔN_{it} in the diffusion-limited regime, and this effect is quite insignificant in the reaction-limited regime. In other words, with the incorporation of nitrogen and an increasing nitrogen concentration, both the pre-factor A and the diffusion coefficient D_H increases, and this combined effect leads to a significant increase in the pre-factor $\sqrt{A/B}$, which in turn largely worsens NBTI degradation in the diffusion-limited regime.

Moreover, as shown in Fig. 4.3(c), as the interfacial nitrogen concentration increases, the characteristic transition time (t_{tr}) slightly increases, while the critical time (t_c) shows a significant decrease (in log scale) for the nitrided oxide with higher nitrogen concentration.

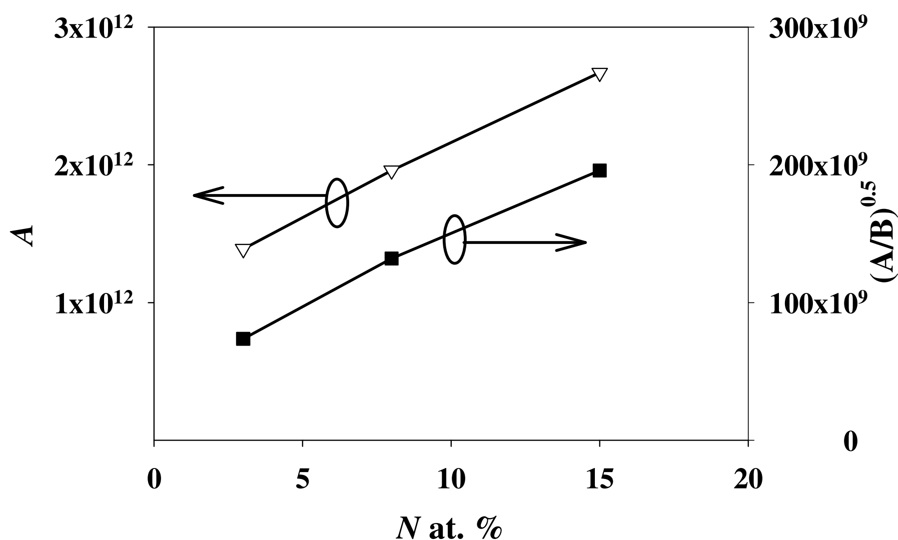

(a)

ATTENTION: The Singapore Copyright Act applies to the use of this document. Nanyang Technological University Library

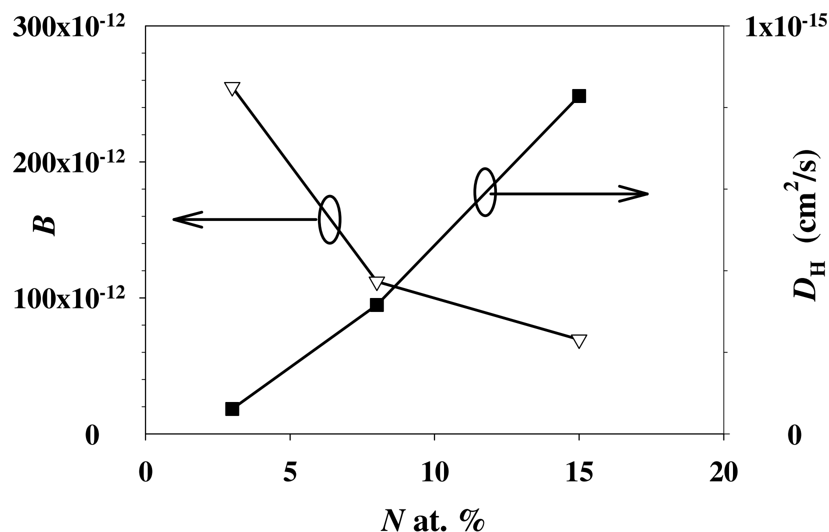

(b)

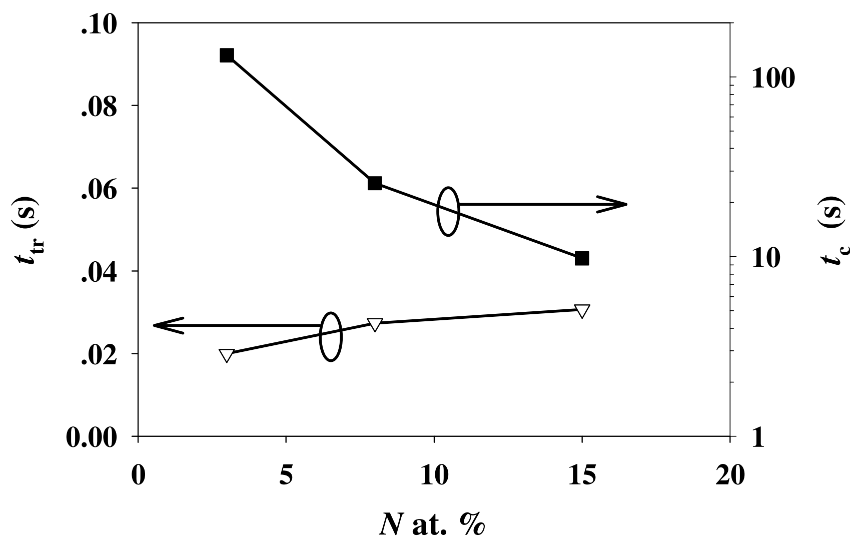

(c)

Figure 4.3: *The plot of the fitting parameters: (a) A,* $\sqrt{A/B}$*, (b) B,* D_H*, and (c)* t_{tr}*,* t_c*, as a function of the interfacial nitrogen concentration N at. %. The values of these parameters used in the plot are given in Table 4.1.*

ATTENTION: The Singapore Copyright Act applies to the use of this document. Nanyang Technological University Library

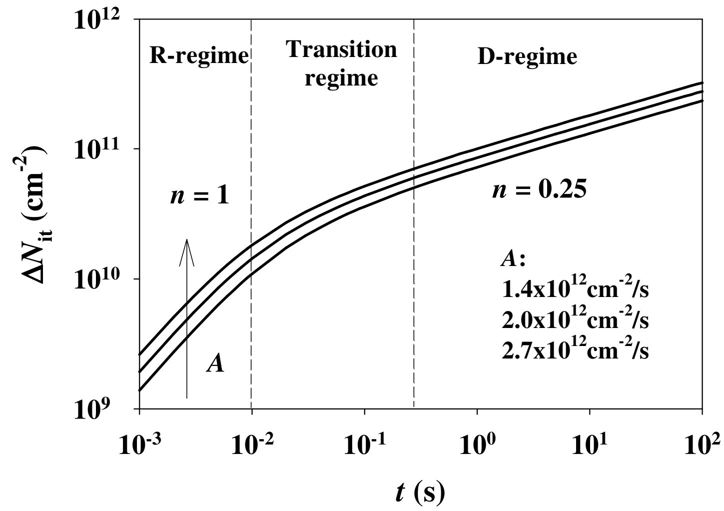

(a)

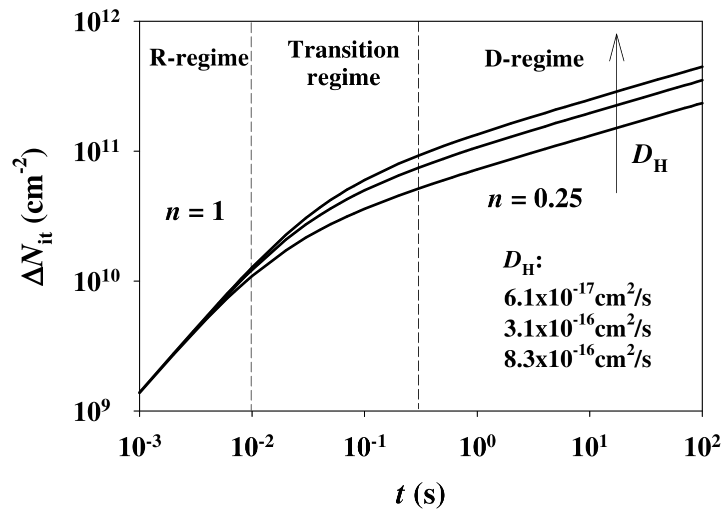

(b)

Figure 4.4: *Interface trap generation as a function of time (a) for different pre-factor A and (b) for different diffusion coefficient D_H of H species, as simulated by our proposed unified R-D model for increasing nitrogen concentration, with reference parameters A = $1.4x10^{12}$ cm^{-2}/s, k_R=$1x10^{-18}$ cm^2/s, D_H = $6.1x10^{-17}$ cm^2/s*

ATTENTION: The Singapore Copyright Act applies to the use of this document. Nanyang Technological University Library

Before further discussion on extended analytical R-D model(s) in next section, there are some critical issues on the analytical R-D model to clarify. Firstly, why are the R-D model and its variation (to be discussed subsequently and in Chapter 5 as well) chosen? It is mainly because the R-D model, in particular, the proposed analytical R-D model, can be used to well explain NBTI experimental results and the effect of nitrogen on NBTI, which has been extensively discussed above. Other NBTI models may also be used, but they are not well enough to explain what we observed here, in terms of time dependence of NBTI and the effect of nitrogen on NBTI. However, as reviewed in section 2.4, Chapter 2, other NBTI models have their own advantages. In particular, hole-trapping model can be used to distinguish slow and fast components for NBTI degradation, i.e., interface traps and oxide traps, and deep-level hole-trapping model can well explain NBTI partial recovery by attributing some fraction of oxide traps pinned by the interface conduction-band offset. Moreover, although physical modeling of NBTI in this work is mainly focused on interface traps, it does not imply that oxide traps and/or trapping of holes are not important in NBTI. In fact, the interaction of cold holes with the initial defect at the interface plays a key role in the generation of interface traps. Besides, in the classical R-D model, it has been reported that there is a strong one-to-one correlation between positive oxide charges and interface traps [62-65].

Secondly, regarding the parameter values used in Fig. 4.1 to simulate the analytical R-D model, such as N_o, k_F and k_R, how are these values determined? Indeed, they were mainly quoted from the previous work by Alam [132], and the plot in Fig. 4.1 was just for a demonstration purpose of the analytical R-D model. It has been previously reported that P_{bo} centers at the Si/SiO_2 interface would saturate at the level of ~10^{12} cm^{-2}. However, the value of initial defect density N_o used here is 1.5×10^{14}

ATTENTION: The Singapore Copyright Act applies to the use of this document. Nanyang Technological University Library

cm^{-2}, and it is much larger than the saturated level of P_{bo} centers. However, if needed, this discrepancy can be reconciled by reducing N_o by two orders (at the level of ~10^{12} cm^{-2}) and increasing k_F by two orders (at the level of ~1 s^{-1}) correspondingly. The final plot will still be the same as that in Fig. 4.1. Similarly, the value of D_H also partially depends on the value of k_R. Nevertheless, these parameters can still be used as important indicators for the purpose of comparison, although the absolute values of these parameters are not absolutely accurate.

Thirdly, regarding hydrogen diffusion through a layer as thin as 1.5 nm, i.e. only a few mono-layers of oxide or nitrided oxide, how is it possible? Indeed, the microscopic view of hydrogen diffusion through a layer as thin as 1.5 nm is hard to imagine. Macroscopically, diffusion occurs anywhere as long as there is a concentration gradient, and this certainly implies to hydrogen diffusion. Moreover, as discussed in section 2.3.2, Chapter 2, hydrogen can exist in various forms, such as atomic H, molecular H_2, proton H^+, or as a part of hydroxyl OH, hydronium H_3O^+ and hydroxide ions OH^-. It is believed that the claim of hydrogen acting as either acceptor or donor is mainly based on the view of a hydrogen defect at a fixed position of Fermi level. In our model, the hydrogen-related diffusion species is quite dynamic. It is generated at the interface and diffuses towards the oxide or bulk as well. Most importantly, the experimental results cannot be well explained with the assumption of hydrogen as either an acceptor, H^-, or donor, H^+, although in next section, we will extend the model to include the cases of molecular H_2 and proton H^+ as the diffusion species. One may also question about whether atomic H is stable in oxide or nitrided oxide. Indeed, from the microscopic view, it can be explained as follows. In the oxide, atomic hydrogen, which is slightly positive-charged, might be easily attracted by a negative charge center, i.e. the oxygen atom in the oxide, and thus forms hydroxyl OH

ATTENTION: The Singapore Copyright Act applies to the use of this document. Nanyang Technological University Library

group, which is expected to be more stable than atomic hydrogen. In this case, hydroxyl OH group, similarly as atomic hydrogen, can diffuse away from the interface, and the R-D model is still valid.

Moreover, regarding the critical time that distinguishes the diffusion-limited regime and the unknown regime (where the poly-Si would play a role), it is quite short, as summarized in Table 4.1, although a typical NBTI test time is much longer than 10 s. However, the stress time is not necessarily so short, depending on the value of D_H. On the other hand, the slope for longer time is also examined. It is found that as time goes beyond the critical time, the slope gets slightly smaller than 0.25, which could be partially due to the effect of poly-Si gate, or partially due to the dispersive transport, which are to be discussed in Chapter 5. Moreover, the values of parameters, as discussed above, would also affect the critical time, and hence the analytical R-D model only demonstrates one possible explanation for the underlying NBTI mechanism, mainly based on the experimental results observed and some other assumptions made. In real situation, hydrogen diffuses away from the interface and towards gate oxide and poly-Si gate and thus the R-D model could be further extended to include the hydrogen diffusion in poly-Si. The role of poly-Si could be either reflecting or absorbing, or just as a normal medium for hydrogen diffusion. However, by taking poly-Si into account, the model will become quite complicated and no simple analytical solution could be obtained.

Lastly, regarding hydrogen diffusion in nitrided oxide, since silicon nitride is a well-known barrier to hydrogen diffusion, one would expect that hydrogen diffusion becomes increasingly difficult when the nitrogen concentration in SiO_2 increases, but it is found that a larger value of D_H is obtained for nitrided oxide with a higher

ATTENTION: The Singapore Copyright Act applies to the use of this document. Nanyang Technological University Library

interfacial nitrogen concentration, i.e., hydrogen diffusion is enhanced by nitrogen. It is explained as follows. Although silicon nitride (SiN) is widely used nowadays in industry as the passivation film for IC, the silicon nitride used as a barrier to hydrogen diffusion is usually grown by PECVD. In this work, nitrogen is incorporated by either rapid thermal nitridation or decoupled plasma nitridation. According to Regolini *et. al* in their work [214], the silicon nitride passivation film should be dense enough to encapsulate hydrogen species in IC and thus perform the function of passivation. Benoit *et. al* [215] further studied hydrogen desorption and diffusion in PECVD silicon nitride and they found that, a low density film desorbs a high amount of hydrogen and is permeable to hydrogen, while a high density film is a barrier to hydrogen. In other words, even PECVD silicon nitride layer can be a source of hydrogen or a barrier to hydrogen, depending on the film density. Therefore, it is highly possible that hydrogen diffusion is enhanced by nitrogen.

4.3 Extended Analytical Reaction-Diffusion Model for NBTI

In this section, the analytical R-D model is extended to include cases of other possible hydrogen species, such as the hydrogen ion H^+ and hydrogen molecule H_2.

4.3.1 Ionic Hydrogen

Based on the generalized R-D model [68], the basic set of the reaction equation (Eq. (4.1)), the diffusion/drift equation (Eq. (4.2)) and the conservation equation (Eq. (4.3)) can always be used to describe NBTI degradation mechanism, regardless of the

ATTENTION: The Singapore Copyright Act applies to the use of this document. Nanyang Technological University Library

type or nature of the H-related diffusion species.

If the H-related diffusing species is positively-charged hydrogen ion H^+, the drift portion on the right side of Eq. (4.2) due to the electric field ξ_{ox} will dominate the overall effect and thus the diffusion portion in Eq. (4.2) can be neglected for simplicity. In other words, only the drift process will be considered for H^+ as the diffusing species, and Eq. (4.2) becomes:

$$\frac{dN_H}{dt} = \mu_H \xi_{ox} \frac{dN_H}{dx} \tag{4.12}$$

For the conservation of H-related diffusing species, as described by Eq. (4.3), the tip of drift front $x(t)$ is approximated to be $\mu_H \xi_{ox} t$ with a rectangular profile for H^+ [133]. Hence, based on Eq. (4.3), as H^+ is drifted by the electric field away from the gate oxide, similarly, interface trap generation $N_{it}(t)$ can be expressed approximately as a linear function of $N_H(0)$, as shown in Eq. (4.4):

$$N_{it}(t) = \int_{x=0}^{x(t)=\mu_H \xi_{ox} t} N_H(x,t)dx = N_H(0)\mu_H \xi_{ox} t \tag{4.13}$$

or $$N_H(0) = \frac{N_{it}(t)}{\mu_H \xi_{ox} t} \tag{4.13'}$$

Similarly, we make the general assumption that interface trap generation N_{it} is much smaller than the initial defect density N_o, i.e. $N_{it} << N_o$, and we also assume that both the N_{it} generation due to the forward reaction and the N_{it} re-passivation due to the reverse reaction are linear functions of time such that $\frac{dN_{it}}{dt} \sim \frac{N_{it}}{t}$. Eq. (4.12) describes the drift process, and by substituting Eq. (4.13) into Eq. (4.1) and rearranging the

ATTENTION: The Singapore Copyright Act applies to the use of this document. Nanyang Technological University Library

orders of the new equation, it yields:

$$N_{it}^{2}(t)+\frac{1}{\dfrac{k_R}{\mu_H \xi_{ox}}}N_{it}(t)-\frac{k_F N_O}{\dfrac{k_R}{\mu_H \xi_{ox} t}}=0 \tag{4.14}$$

or $$N_{it}^{2}(t)+\frac{1}{B}N_{it}(t)-\frac{At}{B}=0 \tag{4.14'}$$

where $A=k_F N_O$ and $B=k_R/\mu_H \xi_{ox}$.

By solving Eq. (4.14), interface trap generation N_{it} can be obtained in the case of the hydrogen ion H^+ as the diffusing species, as shown in Eq. (4.15):

$$N_{it}(t)=\frac{2At}{\left(1+\sqrt{1+4ABt}\right)}=\frac{2k_F N_O t}{1+\sqrt{1+4k_F N_O \dfrac{k_R}{\mu_H \xi_{ox}}t}} \tag{4.15}$$

Similarly, two distinguished regimes can be observed from Eq. (4.15):

the reaction-limited regime

$$N_{it}(t)=At=k_F N_O t \qquad \text{(when 4ABt << 1)} \tag{4.16}$$

and the drift-limited regime

$$N_{it}(t)=\sqrt{\frac{A}{B}}(t)^{1/2}=\sqrt{\frac{k_F N_O \mu_H \xi_{ox}}{k_R}}(t)^{1/2} \qquad \text{(when 4ABt >> 1)} \tag{4.17}$$

In the reaction-limited regime, Eq. (4.16) clearly shows a linear time-dependence of N_{it} generation, while in the drift-limited regime, Eq. (4.17) gives a power-law time-dependence with an exponent factor of 1/2, which is also quite consistent with

ATTENTION: The Singapore Copyright Act applies to the use of this document. Nanyang Technological University Library

the prior modeling results [68, 133]. Similarly, in the case of H^+ as the diffusing species, the reaction-limited regime is also accounted by the pre-factor A, while the drift-limited regime involves both A and B and accounted by pre-factor $\sqrt{A/B}$.

4.3.2 Molecular Hydrogen

If the H-related diffusing species is molecular hydrogen H_2, similar to the neutral hydrogen as the diffusing species, the drift portion on the right side of Eq. (4.2) due to electric field can be neglected for simplicity. Diffusion of H_2 dominates the overall effect, and thus Eq. (4.2) becomes:

$$\frac{dN_{H2}}{dt} = D_{H2}\frac{d^2N_{H2}}{dx^2} \tag{4.18}$$

where N_{H2} is the concentration of molecular hydrogen H_2 that diffuses away from the interface, and D_{H2} is the diffusion coefficient of H_2. In addition, the conservation of the H-related diffusing species can also be described by Eq. (4.3) by replacing $N_H(x, t)$ with $1/2N_{H2}(x, t)$, which indicates that each released H-related species leaves behind one interface trap and every two dissociated-hydrogen atoms form one molecular hydrogen H_2. The conservation between H and H_2 at the interface would be given by the law of mass action [134]:

$$\frac{N_{H2}(0)}{N_H^2(0)} = C \tag{4.19}$$

where C is a constant. Similar to the neutral hydrogen as the diffusing species, the tip of diffusion front $x(t)$ of the molecular hydrogen H_2 is also approximated to be

ATTENTION: The Singapore Copyright Act applies to the use of this document. Nanyang Technological University Library

$\sqrt{D_{H2}t}$ with a triangular diffusion profile for the molecular hydrogen H_2 [133, 134]. Hence, based on Eq. (4.3), interface trap generation $N_{it}(t)$ can be expressed approximately as a linear function of $N_{H2}(0)$, as shown in Eq. (4.4):

$$N_{it}(t) = \int_{x=0}^{x(t)=\sqrt{D_{H2}t}} \frac{1}{2} N_{H2}(x,t)dx = \frac{1}{4} N_{H2}(0)\sqrt{D_{H2}t} \tag{4.20}$$

or $$N_{H2}(0) = \frac{N_{it}(t)}{\frac{1}{4}\sqrt{D_{H2}t}} \tag{4.20'}$$

By substituting Eq. (4.20)' into Eq. (4.19), we can obtain the relationship between $N_H(0)$ and $N_{it}(t)$, as shown in Eq. (4.21):

$$N_H(0) = \sqrt{\frac{N_{H2}(0)}{C}} = \sqrt{\frac{4N_{it}(t)}{C\sqrt{D_{H2}t}}} \tag{4.21}$$

Similarly, we make the general assumption that interface trap generation N_{it} is much smaller than the initial defect density N_o, i.e. $N_{it} << N_o$, and we also assume that both the N_{it} generation due to the forward reaction and the N_{it} re-passivation due to the reverse reaction are linear functions of time such that $\frac{dN_{it}}{dt} \sim \frac{N_{it}}{t}$. By substituting Eq. (4.21) into Eq. (4.1), it yields:

$$\frac{N_{it}(t)}{t} = k_F N_O - k_R \sqrt{\frac{4N_{it}(t)}{C\sqrt{D_{H2}t}}} N_{it}(t) \tag{4.22}$$

or $$k_R \sqrt{\frac{4N_{it}(t)}{C\sqrt{D_{H2}t}}} N_{it}(t) = k_F N_O - \frac{N_{it}(t)}{t} \tag{4.22'}$$

ATTENTION: The Singapore Copyright Act applies to the use of this document. Nanyang Technological University Library

By taking a square on each side of Eq. (4.22)', it becomes:

$$\frac{4k_R^2}{C\sqrt{D_{H2}t}}N_{it}^3(t)=\left[k_F N_O-\frac{N_{it}(t)}{t}\right]^2 \tag{4.23}$$

$$\text{or}\quad \frac{B}{\sqrt{t}}N_{it}^3(t)=\left[A-\frac{N_{it}(t)}{t}\right]^2 \tag{4.23'}$$

$$\text{or}\quad \frac{B}{A^2\sqrt{t}}N_{it}^3(t)=\left[1-\frac{N_{it}(t)}{At}\right]^2 \tag{4.23''}$$

where $A=k_F N_O$ and $B=\frac{4k_R^2}{C\sqrt{D_{H2}}}$.

Equation (4.23) can be solved either analytically or numerically, and N_{it} can also be obtained to be as a function of time. Here, we consider the two extreme cases where certain approximations are made to get a much simpler analytical solution.

When the time is very short, i.e. in the reaction-limited regime, the right-side of Eq. (4.23)'' can be ignored and approximated to be zero, such that $N_{it}(t)$ can be obtained as shown in Eq. (4.24):

$$N_{it}(t)=At=k_F N_O t \tag{4.24}$$

In the reaction-limited regime, Eq. (4.24) clearly shows a linear time-dependence of N_{it} generation, and similarly, in the case of H_2 as the diffusing species, the reaction-limited regime is also purely accounted by the pre-factor *A*. By substituting Eq. (4.24) in to Eq. (4.23), the right-side of Eq. (4.23)'' is dimensionless and equal to zero, and thus the left-side of Eq. (4.23)'' must also equal to zero, or as in a

ATTENTION: The Singapore Copyright Act applies to the use of this document. Nanyang Technological University Library

dimensionless scale, much smaller than 1. Therefore, by substituting Eq. (4.24) into the left-side of Eq. (4.23)'', the stress time t must satisfy the following condition:

$$\frac{B}{A^2\sqrt{t}}N_{it}^3(t)=\frac{B}{A^2\sqrt{t}}(At)^3=ABt^{\frac{5}{2}}<<1 \qquad (4.25)$$

When the time is relatively long, i.e. in the diffusion-limited regime, the second term $[N_{it}(t)/(At)]$ on the left-side of Eq. (4.23)'' could be ignored when it is much smaller than 1, such that $N_{it}(t)$ can be obtained as shown in Eq. (4.26):

$$N_{it}(t)=\left(\frac{A^2}{B}\right)^{\frac{1}{3}}t^{1/6}=(C)^{\frac{1}{3}}\left(\frac{k_F N_O}{2k_R}\right)^{\frac{2}{3}}(D_{H2}t)^{1/6} \qquad (4.26)$$

By substituting Eq. (4.26) into the second term $[N_{it}(t)/(At)]$ on the left-side of Eq. (4.23)'', the stress time t must satisfy the following condition:

$$\frac{N_{it}(t)}{At}=\frac{\left(\frac{A^2}{B}\right)^{\frac{1}{3}}t^{1/6}}{At}=\left(\frac{1}{AB}\right)^{\frac{1}{3}}t^{-5/6}<<1 \qquad (4.27)$$

or $$\left(ABt^{\frac{5}{2}}\right)^{\frac{1}{3}}>>1 \qquad (4.27)'$$

Indeed, the time constrains as depicted in Eq. (4.25) and Eq. (4.27)' to separate the two regimes are identical. The characteristic transition time t_{tr}, which is defined as the intersection of the R-regime model (Eq. (4.24)) and the D-regime model (Eq. (4.26)), can also be obtained:

ATTENTION: The Singapore Copyright Act applies to the use of this document. Nanyang Technological University Library

$$t_{tr} = \left(AB\right)^{-2/5} = \left(k_F N_O \frac{4k_R^2}{C\sqrt{D_{H2}}}\right)^{-2/5} \tag{4.28}$$

Lastly, the significance of extended analytical R-D models, as mentioned above, is briefly discussed as follows. The time evolution of NBTI is affected by various factors, such as measurement method, fabricated samples, etc. As discussed in Chapter 3, the measurement time delay would affect the exponent factor in the diffusion-limited regime, and to be discussed in Chapter 5, the time evolution might also affected by the dispersive nature of hydrogen diffusion and it differs among nitrided oxide samples with different nitrogen concentration. Regardless of effect of measurement or fabricated sample or dispersive diffusion, in real situation, the diffusion could involve different kinds of hydrogen species, such as ionic hydrogen or molecular hydrogen, although atomic hydrogen is believed to be more dominant than others. Therefore, although no comparison with experimental results is made here, the extended analytical R-D models could still be quite useful, in particular, power-law factor of smaller than 0.25 in the diffusion-limited regime might be partially attributed to a contribution of possible molecular hydrogen diffusion, and the determination of exact diffusion species could be a good direction for future study of NBTI.

4.4 Geometry-Dependent Reaction-Diffusion Model for NBTI

4.4.1 Geometry-Dependent Reaction-Diffusion Model

The reaction-diffusion (R-D) model, as analyzed in previous sections, is based on

ATTENTION: The Singapore Copyright Act applies to the use of this document. Nanyang Technological University Library

an assumption that the geometry (i.e. channel length and channel width) is much larger than the diffusion/drift length, i.e., diffusion is one-dimensional (1-D). This 1-D diffusion is only valid in the channel region where distribution of NBTI-induced traps is relatively uniform. However, diffusion at the edge is two-dimensional (2-D), while diffusion at the corner is three-dimensional (3-D). Therefore, conservation of the hydrogen-related diffusing species, i.e. Eq. (4.3) in the case of 1-D, is replaced by a more general form as shown in Eq. (4.29):

$$\int N_{it}(t) = \int_V N_H(r,t)dV \tag{4.29}$$

where V stands for a general form of length, area or volume, depending on the degree of dimension, and total N_{it} is the integration of $N_H(r, t)$ over dV.

Similarly, a triangular diffusion profile is assumed for the neutral hydrogen diffusing species [132, 133, 216], and the diffusion front is approximated as the diffusion length $\sqrt{D_H t}$. In other words, $N_H(r, t)$ can be generally expressed as:

$$N_H(r,t) = N_H(0)\left(1 - \frac{r}{\sqrt{D_H t}}\right) \tag{4.30}$$

Moreover, N_{it} is assumed to be generated and distribute evenly at the interface, with thickness of δ for 1-D, area of $\pi\delta^2$ for 2-D or volume of $\frac{4}{3}\pi\delta^3$ for 3-D.

For ideal 1-D diffusion, N_{it} can be obtained by solving the basic set of the reaction equation (Eq. (4.1)), the diffusion/drift equation (Eq. (4.2)) and the conservation equation (Eq. (4.29)) in 1-D:

ATTENTION: The Singapore Copyright Act applies to the use of this document. Nanyang Technological University Library

$$N_{it}\left(t\right)=\frac{2k_F N_O t}{\left(1+\sqrt{1+8k_F N_O \frac{k_R \delta}{\sqrt{D_H}} t^{3/2}}\right)} \qquad (4.31)$$

When the time is relatively long, i.e. in the diffusion-limited regime, Eq. (4.31) can be simplified as shown in Eq. (4.32), and it shows that N_{it} has a power-law time-dependence with an exponent of 1/4:

$$N_{it}\left(t\right)=\sqrt{\frac{k_F N_O}{2k_R \delta}}\left(D_H t\right)^{1/4} \qquad (4.32)$$

For ideal 2-D diffusion from a line source, the diffusion front is assumed to be a circle, i.e., dV in Eq. (4.29) is replaced by ($2\pi r$dr), and thus by integrating r from 0 to $\sqrt{D_H t}$, it gives:

$$\int N_{it}\left(t\right)=\int_0^{\sqrt{D_H t}} N_H\left(0\right)\left(1-\frac{r}{\sqrt{D_H t}}\right)2\pi r dr=\frac{\pi}{3}N_H\left(0\right)\left(D_H t\right) \qquad (4.33)$$

Similarly, by solving the basic set of the reaction equation (Eq. (4.1)), the diffusion/drift equation (Eq. (4.2)) and the conservation equation (Eq. (4.33)), N_{it} for 2-D diffusion can be obtained, as shown in Eq. (4.34):

$$N_{it}\left(t\right)=\frac{2k_F N_O t}{\left(1+\sqrt{1+12k_F N_O \frac{k_R \delta^2}{D_H} t}\right)} \qquad (4.34)$$

When the time is relatively long, i.e. in the diffusion-limited regime, Eq. (4.34) can be simplified as in Eq. (4.35), where N_{it} has a power-law time-dependence with an exponent of 1/2:

ATTENTION: The Singapore Copyright Act applies to the use of this document. Nanyang Technological University Library

$$N_{it}\left(t\right)=\sqrt{\frac{k_F N_O}{3k_R\delta^2}}\left(D_H t\right)^{1/2} \tag{4.35}$$

For ideal 3-D diffusion from a point source, the diffusion front is assumed to be a sphere, i.e., dV in Eq. (4.29) is replaced by ($4\pi r^2$dr), and thus by integrating r from 0 to $\sqrt{D_H t}$, it yields:

$$\int N_{it}\left(t\right)=\int_0^{\sqrt{D_H t}} N_H\left(0\right)\left(1-\frac{r}{\sqrt{D_H t}}\right)4\pi r^2 dr=\frac{\pi}{3}N_H\left(0\right)\left(D_H t\right)^{3/2} \tag{4.36}$$

Similarly, by solving the basic set of the reaction equation (Eq. (4.1)), the diffusion/drift equation (Eq. (4.2)) and the conservation equation (Eq. (4.36)), N_{it} for 3-D diffusion can be obtained, as shown in Eq. (4.34):

$$N_{it}\left(t\right)=\frac{2k_F N_O t}{\left(1+\sqrt{1+16k_F N_O\frac{k_R\delta^3}{\left(D_H\right)^{3/2}}t^{1/2}}\right)} \tag{4.37}$$

When the stress time is relatively long, i.e. in the diffusion-limited regime, Equation (4.37) can be approximated to be Eq. (4.38), where N_{it} has a power-law time-dependence with an exponent of 3/4:

$$N_{it}\left(t\right)=\sqrt{\frac{k_F N_O}{4k_R\delta^3}}\left(D_H t\right)^{3/4} \tag{4.38}$$

The geometry-dependent analytical R-D model for neutral hydrogen diffusing species in 1-D, 2-D and 3-D is summarized here:

ATTENTION: The Singapore Copyright Act applies to the use of this document. Nanyang Technological University Library

$$N_{it}(t)=\begin{cases}\dfrac{2k_F N_O t}{\left(1+\sqrt{1+8k_F N_O k_R \delta D_H^{-1/2} t^{3/2}}\right)} & \text{(1-D)}\\[2ex] \dfrac{2k_F N_O t}{\left(1+\sqrt{1+12k_F N_O k_R \delta^2 D_H^{-1} t}\right)} & \text{(2-D)}\\[2ex] \dfrac{2k_F N_O t}{\left(1+\sqrt{1+16k_F N_O k_R \delta^3 D_H^{-3/2} t^{1/2}}\right)} & \text{(3-D)}\end{cases} \qquad (4.39)$$

And for a sufficiently long time, i.e., in the diffusion-limited regime, a general power-law time-dependence of N_{it} is obtained:

$$N_{it}(t)=At^n \qquad (4.40)$$

where the pre-factor $A=\begin{cases}\sqrt{\dfrac{k_F N_O}{2k_R}}\left(\dfrac{D_H}{\delta^2}\right)^{1/4} & \text{(1-D)}\\[2ex] \sqrt{\dfrac{k_F N_O}{3k_R}}\left(\dfrac{D_H}{\delta^2}\right)^{1/2} & \text{(2-D)}\\[2ex] \sqrt{\dfrac{k_F N_O}{4k_R}}\left(\dfrac{D_H}{\delta^2}\right)^{3/4} & \text{(3-D)}\end{cases}$ and the power-law factor

$n=\begin{cases}1/4 & \text{(1-D)}\\ 1/2 & \text{(2-D)}\\ 3/4 & \text{(3-D)}\end{cases}$, if the term D_H/δ^2 is treated as the effective diffusion coefficient, the result shown above for 1-D diffusion is quite consistent with the one obtained in section 4.2.

Moreover, if a dispersive nature of hydrogen diffusion is taken into account, the power-law factor n for 1-D, 2-D and 3-D diffusion becomes $\beta/4$, $\beta/2$ and $3\beta/4$, respectively, where β is the dispersion parameter and $0<\beta\leq 1$. In another case, if the hydrogen-related diffusing species is molecular hydrogen H_2, the power-law factor n

ATTENTION: The Singapore Copyright Act applies to the use of this document. Nanyang Technological University Library

in the diffusion-limited regime can also be obtained to be 1/6, 1/3 and 1/2 for 1-D, 2-D and 3-D diffusion, respectively. The actual hydrogen diffusion in an MOSFET could be between 1-D and 3-D diffusion, depending on the device geometry. For example, hydrogen diffusion from the interface tends to be 1-D and 3-D diffusion for large device dimensions (i.e. wide channel width and long channel length) and small device dimensions, respectively. In addition, diffusion at edges and corners may play an important role for small dimensions. Therefore, it is clear from the above discussions that the geometry plays an important role in NBTI degradation. In particular, the power-law factor n is largely affected by the geometry effect, in the context of the R-D model.

4.4.2 Strain Effect on NBTI in p-MOSFETs with Small Dimensions

Besides the influence of hydrogen diffusion, the effect of stress/strain in the MOSFET device may also play a role in the geometry dependence of NBTI, as stress/strain can affect the breaking of Si-H bonds and NBTI reaction energy as well. Indeed, strain engineering is widely used to induce strain in the device and thus boost device performance for sub-100nm technology node. Nevertheless, it is found that the deposition of a compressive silicon nitride (SiN) liner, as one of the most effective performance boosters for *p*-MOSFETs, worsens NBTI degradation, and it is mainly attributed to a higher amount of hydrogen that might be incorporated during the SiN deposition and a higher strain energy that is stored in the channel [217].

This can be confirmed by the standard 45nm CMOS process simulation with TCAD tools, and the stress profiles along the channel direction for both short-channel

ATTENTION: The Singapore Copyright Act applies to the use of this document. Nanyang Technological University Library

(L = 50 nm) and long-channel (L = 1000 nm) devices are shown in Fig. 4.5. As can be seen in Fig. 4.5, for the device with a long channel length of 1000 nm, the stress transferred along the channel direction is much smaller than that with a shorter channel length of 50 nm. Besides, the transfer of stress/strain is also more efficient at/near the channel edge.

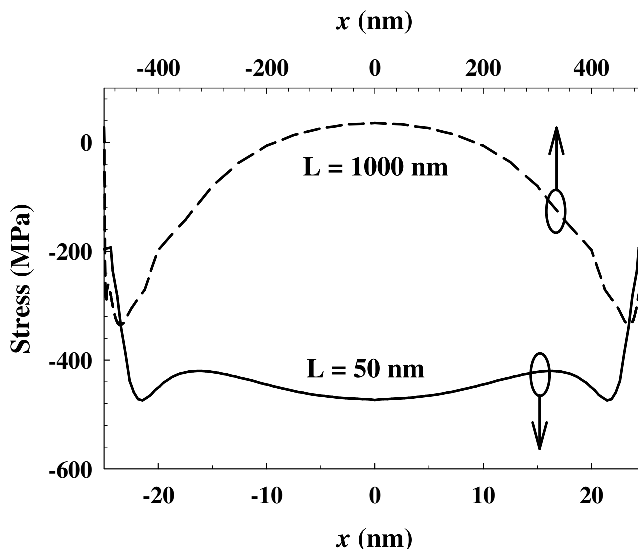

Figure 4.5: *Plots of the stress profiles along the channel direction for short-channel (L = 50 nm) and long-channel (L = 1000 nm) devices, as a function of distance x.*

Moreover, first-principles calculation is carried out to examine the strain effect in terms of the NBTI reaction energy E_R [36, 110, 213, 218]. As shown in Fig. 4.6, a larger bond angle change due to a higher strain can lead to a reduction in the NBTI reaction energy E_R. In other words, a higher strain causes a more favorable NBTI reaction at the interface. Besides, the strain also has an impact on the bonding energy E_B of the NBTI precursor, i.e. the Si-H bond at the interface, and similarly, a more-negative E_B is resulted for a larger bond angle change, which indicates that under a higher strain the Si-H bond is weaker and thus easier to break. Overall, by the

ATTENTION: The Singapore Copyright Act applies to the use of this document. Nanyang Technological University Library

first-principles calculation, it is found that NBTI degradation is worsen by the strain, in terms of the NBTI reaction energy and the bond breaking of the Si-H bonds at the interface, and by correlating the results obtained from TCAD process simulation, a higher NBTI degradation is expected for smaller dimensions.

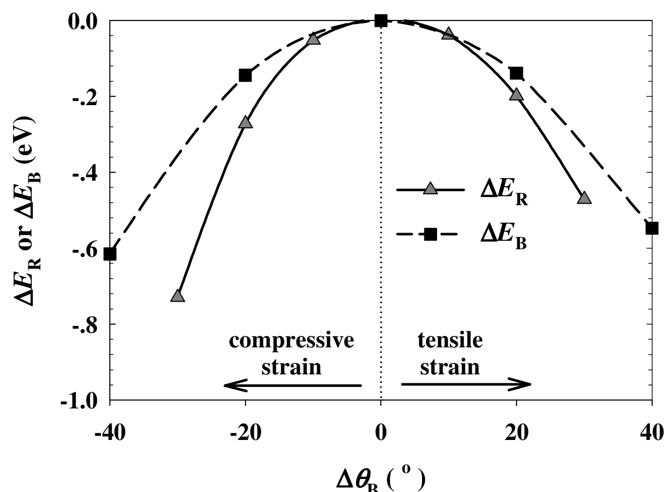

Figure 4.6: *NBTI reaction energy change (ΔE_R) and Si-H bonding energy change (ΔE_B) as a function of bond angle change ($\Delta\theta_B$). In the first-principle calculations, ΔE_R is caused by the change in the bond angle ∠Si-N-Si of the nitride oxide, while ΔE_B is purely due to the change in the bond angle in the Si_3-Si-H structure at the interface.*

4.4.3 Geometry Dependence of NBTI in p-MOSFETs with Small Dimensions

To investigate the geometry dependence of NBTI, firstly, *p*-MOSFETs with nitrided gate oxide of ~17.5 Å and different channel lengths (L) in the range of 48 nm to 1000 nm are stressed at T_{str} = 125 °C and V_{gstr} = -2.0 V for about 100 s. The

ATTENTION: The Singapore Copyright Act applies to the use of this document. Nanyang Technological University Library

single-point saturation drain current (I_{dsat}) measurement [182] is used to extract the threshold voltage shift (ΔV_{th}). Moreover, the conventional *I-V* measurement method and 1st on-the-fly (OTF) measurement method [40, 152] in a short time range are also conducted to re-confirm the trend observed by using the single-point I_{dsat} method.

NBTI degradation results are shown in Fig. 4.7. Figure 4.7(a) clearly shows that ΔV_{th} is higher for the device with shorter channel length, and this enhancement effect for shorter channel length could be attributed to either the edge/corner effect that is illustrated previously in the geometry-dependent R-D model for NBTI or the effect of the process-induced stress/strain that worsens NBTI for smaller dimensions, or both. Moreover, based on the general power-law time-dependence of NBTI that is shown in Eq. (4.40), the pre-factor A and power-law factor n can be extracted accordingly, and the results are shown in Fig. 4.7(b). As can be seen from the figure, the pre-factor A increases as the channel length shrinks, and this can be mainly attributed to an increase in the forward reaction rate k_F due to a lower NBTI reaction energy E_R and/or a lower bonding energy E_B of precursor Si-H bonds at the interface. Figure 4.7(b) also shows that the power law factor n is almost a constant for devices with different channel lengths. Based on the geometry-dependent R-D model, if the edge/corner effect is significant, an increase in the power law factor n should be evidenced. However, the result of a constant power law factor n in Fig. 4.7(b) gives no such evidence, which might be mainly due to a relatively wide channel width of 2000 nm. Therefore, it can be concluded that the channel length dependence of NBTI for the device with wide channel width is mainly attributed to the enhancement of the stress/strain transfer during the process for the device with shorter channel length, which in turn leads to a higher NBTI degradation.

ATTENTION: The Singapore Copyright Act applies to the use of this document. Nanyang Technological University Library

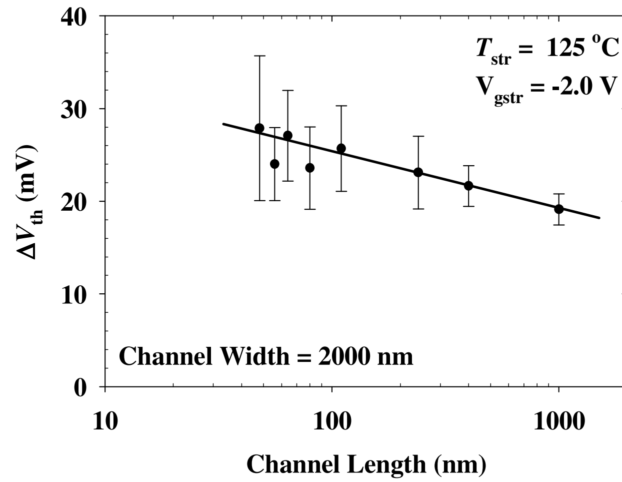

(a)

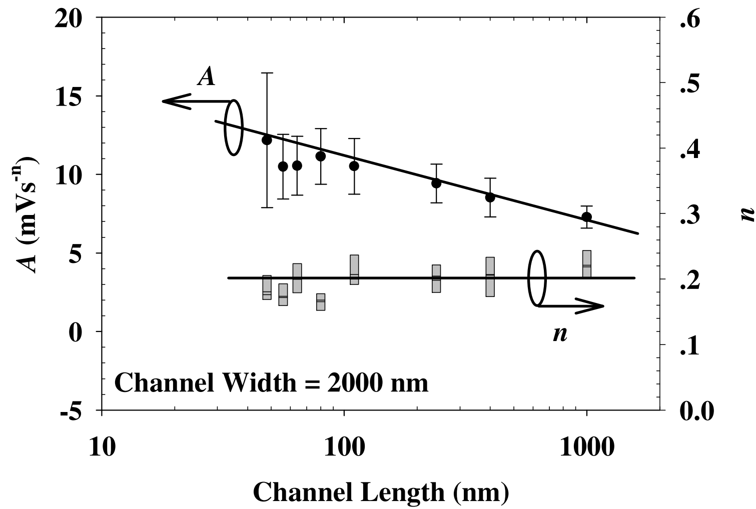

(b)

Figure 4.7: *(a) NBTI degradation* ΔV_{th} *as a function of device channel length for p-MOSFETs with channel width of 2000 nm; (b) the extracted pre-factor A and power-law factor n as a function of device channel length. Te sample size for each device is 4 and the lines are for guiding the eyes only.*

ATTENTION: The Singapore Copyright Act applies to the use of this document. Nanyang Technological University Library

To further investigate the geometry dependence of NBTI, *p*-MOSFETs with short channel lengths (L = 60 nm) and different channel width (W) are examined, and the results are shown in Fig. 4.8. Figure 4.8(a) shows the typical ΔV_{th} curves as a function of stress time for the devices with wide and narrow channel width of 5000 nm and 200 nm, respectively. As can be seen from this figure, as the stress time is more than 1 s, i.e. in the diffusion-limited regime, ΔV_{th} is observed to be higher for the device with narrower channel width. It is further confirmed in Fig. 4.8(b). Similarly, *A* and *n* can be extracted, based on Eq. (4.40), and the results are shown in Fig. 4.8(c). Fig. 4.8(c) clearly shows that channel width has an insignificant impact on the pre-factor *A*, while the power law factor *n* is observed to increase as the channel width decreases below 1000 nm. The larger *n* value highly indicates that the edge/corner effect as depicted by the geometry-dependent R-D model is significant when both channel length and width are comparably small. In other words, when the device dimensions are smaller, 2-D or 3-D hydrogen diffusion at the edge or corner respectively, might start to play an important role, which in turn affects the power-law factor *n*.

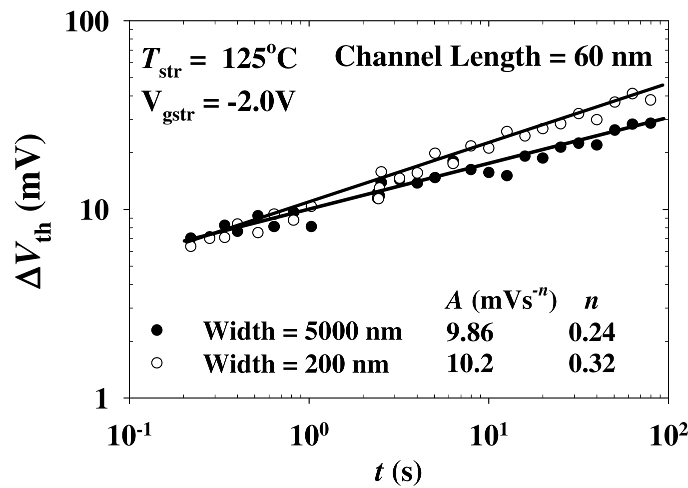

(a)

ATTENTION: The Singapore Copyright Act applies to the use of this document. Nanyang Technological University Library

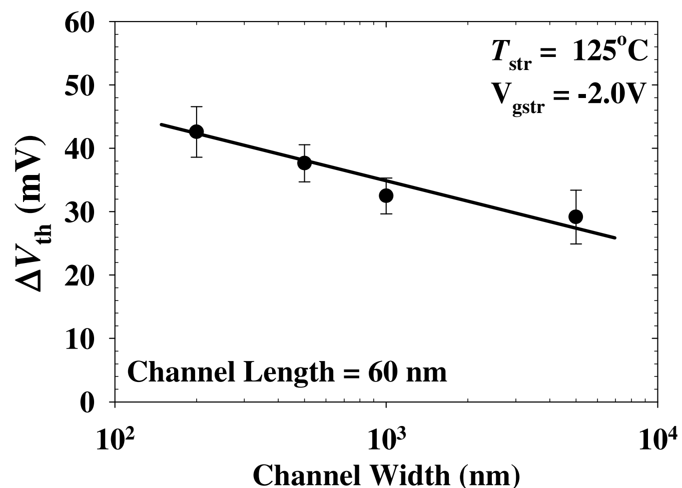

(b)

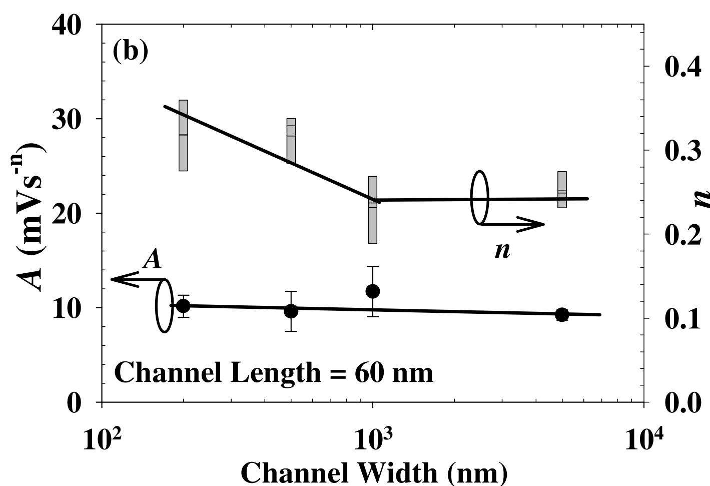

(c)

Figure 4.8: *(a) Typical NBTI degradation ΔV_{th} as a function of stress time t for p-MOSFETs with short channel length of 60 nm, and with wide and narrow channel width of 5000 nm and 200 nm, respectively; (b) ΔV_{th} as a function of device channel width; (b) the extracted pre-factor A and power-law factor n as a function of device channel width. The samples size is 4 and the lines are for guiding the eyes only.*

ATTENTION: The Singapore Copyright Act applies to the use of this document. Nanyang Technological University Library

However, it has to be pointed out that this section only shows a preliminary study on geometry dependence of NBTI. As discussed above, the effect of strain/stress and possible 2-D or 3-D hydrogen diffusion are two possible reasons that could explain the experimental results, i.e., increase in ΔV_{th} of short channel devices and increase in ΔV_{th} of narrow width devices (with short channel length), respectively. Both of them have some limitations. Firstly, only qualitative explanations are provided here and there are no strong quantitative correlations between the theory and experimental results, especially for the relatively-unchanged n for short channel device and relatively-unchanged A for narrow width device. Moreover, measurement used here is not free of delay yet, and it certainly has some impact on the experimental results obtained although the trend predicted here should be correct. Furthermore, the variation of experimental results, especially for the devices with short channel length, as shown in Fig. 4.7, is relatively big, and the sample size used her is also quite limited. Therefore, further studies are required to reveal the true mechanism of geometry dependence of NBTI.

4.5 Summary

In summary, an analytical reaction-diffusion (R-D) model has been proposed to describe the NBTI process in a wide time scale covering the three regimes of reaction, transition and diffusion. A power-law factor of ~1 is experimentally observed for nitrided gate oxide, which shows clear evidence of the existence of the reaction-limited regime for NBTI, and the nitrogen effect on NBTI has been examined, which indeed is going to be further illustrated with more details in the next chapter. The analytical R-D model has also been extended to become a more general model

ATTENTION: The Singapore Copyright Act applies to the use of this document. Nanyang Technological University Library

that also describes the cases of other possible H-related diffusing species, such as the positively-charged hydrogen ion H^+ and the hydrogen molecule H_2. Lastly, based on the analytical geometry-dependent R-D model, the geometry dependence of NBTI has been investigated. The experimental results for the devices with smaller dimensions are explained by the effect of strain and possible 2-D or 3-D hydrogen diffusion with R-D model.

ATTENTION: The Singapore Copyright Act applies to the use of this document. Nanyang Technological University Library

CHAPTER 5 NITROGEN-WORSEN NBTI IN P-MOSFETS

In this chapter, nitrogen-worsen negative bias temperature instability (NBTI) is systematically studied. Nitrided gate oxides with different interfacial nitrogen concentrations are prepared by different nitridation processes, and all NBTI experimental data can be well described by an analytical reaction-dispersive-diffusion (R-DD) model in the diffusion-limited regime. NBTI results for the nitrided gate oxide further confirm that both the interfacial nitrogen concentration and nitrogen depth profile play important roles in the nitrogen-worsen NBTI. In addition, the influence of hydrogen dispersive diffusion on NBTI is also examined, and the NBTI experiments further verify that the analytical R-DD model can well explain NBTI degradation including its dependence on the stress time, the stress temperature and the interfacial nitrogen concentration, and its power-law behaviors as well. Furthermore, first-principles calculation is carried out to examine the effects of nitrogen either as the reaction site at the interface or as adjacent atoms near the interface in terms of the reaction energy. Lower reaction energies due to the incorporation of nitrogen imply that nitrogen is a more effective hydrogen-originated hole trapping center than oxygen, and hence worsens NBTI. It is also found that trapping at vacancy defect has the strongest dependence on the effect of nitrogen as the adjacent atoms. Lastly, the role of nitrogen in NBTI is investigated in terms of its influence on electro-negativity and atomic charge distribution of nitrogen, oxygen and silicon atoms at the interface.

ATTENTION: The Singapore Copyright Act applies to the use of this document. Nanyang Technological University Library

5.1 Introduction

The mechanism of NBTI degradation can be well described by the classical reaction-diffusion (R-D) model [61, 68], which has been reviewed in section 2.4, Chapter 2 and also extensively studied and expanded in Chapter 4. In our previous work as shown in section 4.2, Chapter 4, the experimental results confirm linear time-dependence of N_{it} in the reaction-limited regime and also show a clear transition regime between the reaction-limited and diffusion-limited regimes. However, a correct treatment should also include the dispersive nature of the diffusion/drift process in amorphous material [138-140], i.e. the diffusion constant D_H ought to be replaced by a time-dependent expression of $D_{H0}(\nu t)^{\beta-1}$, where $\beta = kT/E_0$ is the dispersion parameter ($0 \leq \beta \leq 1$), E_0 is the characteristic energy scale, and ν is the characteristic frequency. Moreover, it has been intensively reported that incorporation of nitrogen into gate oxide (i.e. nitrided oxide or oxynitride) worsens NBTI degradation [34-38, 71, 94, 107-109, 111, 140, 212], and NBTI degradation is also strongly dependent on the nitrogen depth profile [74, 108]. However, the impact of nitrogen in the reaction-limited regime has not been reported yet.

In this chapter, an in-depth investigation and theoretical study of NBTI in pure and nitrided gate oxides have been conducted for a better understanding on the nitrogen-worsen NBTI phenomenon [219]. An analytical NBTI model is developed here by taking into account the dispersive nature of diffusion, and it also covers all the three regimes of reaction, transition and diffusion. The influence of hydrogen dispersive diffusion in nitrided gate oxides on NBTI is also examined and the NBTI experiments verify that the analytical reaction-dispersive-diffusion (R-DD) model can well describe NBTI degradation, including its dependence on the stress time, the

ATTENTION: The Singapore Copyright Act applies to the use of this document. Nanyang Technological University Library

stress temperature and the interfacial nitrogen concentration, and its power-law behaviors as well [220]. To further understand the origin of the nitrogen-worsen NBTI, atomic modeling of NBTI for both pure and nitrided gate oxides is also carried out by using first-principles calculations, in terms of the influence of nitrogen on the reaction energy, electro-negativity and atomic charge distribution of nitrogen, oxygen and silicon atoms at the interface. With the analytical R-D model and NBTI atomic modeling, we hope to give a clearer picture of nitrogen-worsen NBTI.

5.2 Effect of Nitrided Oxide on NBTI

5.2.1 Experimental

The devices used in this work are fabricated with a standard CMOS process. The major process conditions for nitrided gate oxide samples are summarized in Table 5.1 and described as follows: the nitrided gate oxides are grown by rapid thermal oxidation and followed by either in-situ rapid thermal nitridation (RTO) in NO gas ambient (denoted as "RTNO") with an interfacial nitrogen concentration of 3.7 at. % or decoupled plasma nitridation (denoted as "DPNO") with interfacial nitrogen concentrations of 3.0, 8.0, and 15.0 at. %. The gate oxide thickness is about 18 Å. The device channel width/length is 20/0.15 µm, and the nominal voltage (V_{dd}) is -1.5 V. To minimize unwanted measurement-induced recovery, single-point saturation current measurement method [182] is used to extract threshold voltage shift (ΔV_{th}), and direct-current current-voltage (DCIV) measurement [36, 179-181] is also conducted to determine interface trap generation ΔN_{it}.

ATTENTION: The Singapore Copyright Act applies to the use of this document. Nanyang Technological University Library

Sample No.	Oxidation	Nitridation	N (at. %)	Anneal	Final EOT (Å)
1 RTNO	RTO	NO	3.7	N2/O2 1050°C	18.01
2 DPNO		DPN	3.0		18.83
3 DPNO		DPN	8.0		17.84
4 DPNO		DPN	15.0		17.83

Table 5.1: *Major process conditions for the nitrided gate oxide samples.*

5.2.2 Results and Discussion

According to the R-D model [61, 68, 132, 133], regardless of the exact diffusing species, a very common observation on NBTI degradation is that the interface trap (N_{it}) or positive oxide charge (N_{ot}) generation exhibits a power-law dependence on the stress time and hence the net threshold voltage shift ΔV_{th} can be expressed as:

$$\Delta V_{th} = \frac{q\left(N_{it} + N_{ot}\right)}{C_{ox}} = At^n \qquad (5.1)$$

where q is the unit electronic charge, C_{ox} is the oxide capacitance, A is the pre-factor and n is the power-law factor. NBTI degradation (i.e. ΔV_{th} as a function of the stress time) for different nitrided oxides at V_{gstr} = -2.2 V and T_{str} = 125 or 25 °C are shown in Fig. 5.1. As can be seen from the figure, NBTI in RTNO sample with an interfacial nitrogen concentration of (denoted as "N =") 3.7 at. % is much higher than that in DPNO sample with N = 3.0 at. %. This implies that with a similar interfacial nitrogen concentration, DPNO has a better NBTI immunity than RTNO, which confirms that nitrogen depth profile plays an important role in NBTI. Moreover, the results in Fig. 5.1 also show that among DPNO samples, NBTI degradation gets worse as the nitrogen concentration increases, which indicates the enhancement effect of the nitrogen at the interface.

ATTENTION: The Singapore Copyright Act applies to the use of this document. Nanyang Technological University Library

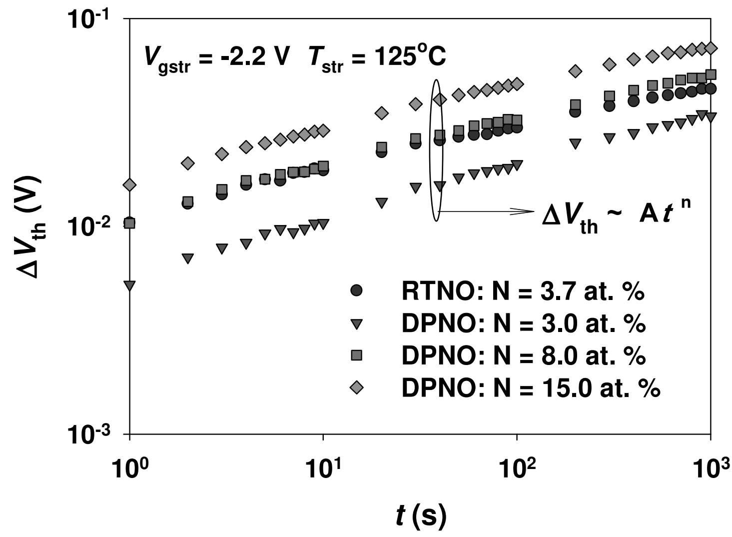

(a)

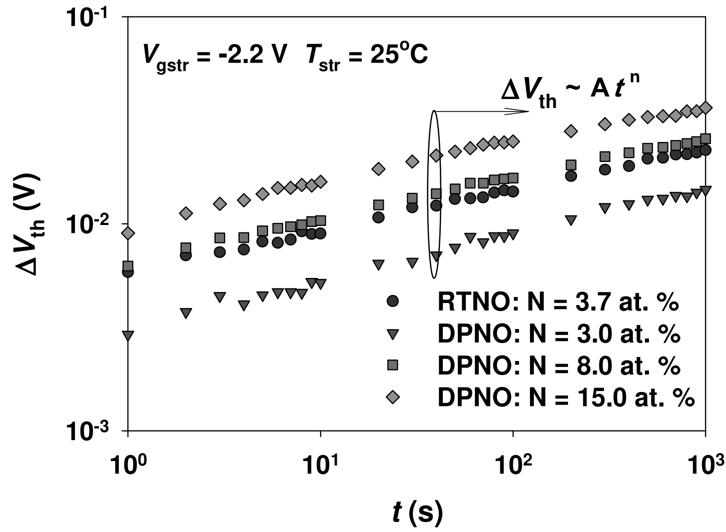

(b)

Figure 5.1: *Threshold voltage shift* ΔV_{th} *as a function of stress time* t *in the diffusion-limited regime for nitrided gate oxides at the stress condition: (a)* V_{gstr} = -2.2 V *and* T_{str} = 125 °C *and (b)* V_{gstr} = -2.2 V *and* T_{str} = 25 °C.

ATTENTION: The Singapore Copyright Act applies to the use of this document. Nanyang Technological University Library

Sample No.	N at. %	T_{str} = 25°C	T_{str} = 75°C	T_{str} = 125°C	E_a (eV)
1 RTNO	3.7	0.0059	0.0085	0.0117	0.0697
2 DPNO	3.0	0.0031	0.0046	0.0058	0.0644
3 DPNO	8.0	0.0066	0.0089	0.0116	0.0574
4 DPNO	15.0	0.0102	0.0140	0.0178	0.0569

Table 5.2: *Summary of the extracted A values for all test samples at V_{gstr} = -2.2 V and T_{str} = 25, 75 and 125 °C. The activation energy E_a obtained from Fig. 5.2 is included.*

Sample No.	N at. %	T_{str} = 25°C	T_{str} = 75°C	T_{str} = 125°C	E_0 (eV)
1 RTNO	3.7	0.1973	0.2045	0.2046	0.295
2 DPNO	3.0	0.2278	0.2404	0.2639	0.060
3 DPNO	8.0	0.1990	0.2163	0.2263	0.079
4 DPNO	15.0	0.1889	0.2001	0.2113	0.096

Table 5.3: *Summary of the extracted n value for all test samples at V_{gstr} = -2.2 V and T_{str} = 25, 75 and 125 °C. The characteristic energy scale E_0 obtained from Fig. 5.5 is included.*

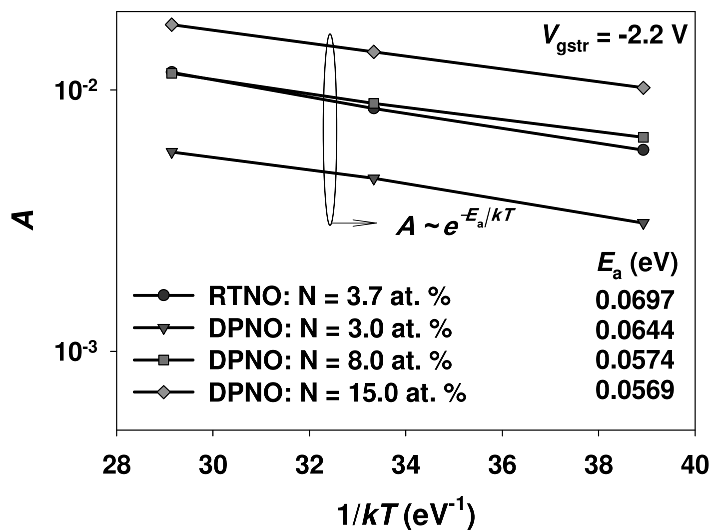

Figure 5.2: *Arrhenius plots of the pre-factor A for different nitrided gate oxide samples. The activation energies (E_a) obtained from the Arrhenius plots are also summarized in Table 5.1. The NBTI stress is carried out at V_{gstr} = -2.2 V for 1000s.*

ATTENTION: The Singapore Copyright Act applies to the use of this document. Nanyang Technological University Library

The extracted *A* and *n* values for all the samples are summarized in Tables 5.2 and 5.3, respectively. In an ideal case, Arrhenius plot of *A* as a function of $1/kT$ can be constructed to extract the activation energy (E_a). As shown in Fig. 5.2, E_a for all the samples are in the range of 0.056 ~ 0.070 eV. E_a of RTNO sample with N = 3.7 at. % is larger than that of DPNO samples, while for DPNO samples, E_a decreases with increasing nitrogen concentration. In other words, as compared with DPNO samples, RTNO sample exhibits a stronger temperature dependence of NBTI, and the temperature dependence for DPNO samples is weaker for higher interfacial nitrogen concentration. However, Table 5.3 shows that *n* values for different samples are not constant and they seem to follow a general trend for all the samples, i.e., *n* slightly increases with temperature. According to previous studies [138-140], this strongly suggests that a dispersive diffusion should be involved in the NBTI process.

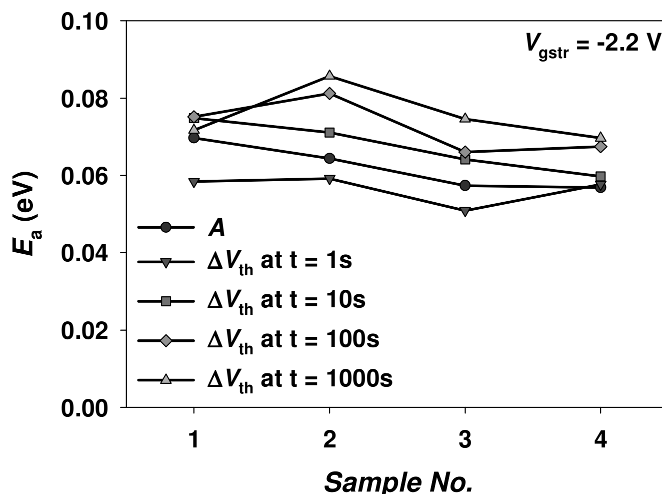

Figure 5.3: *E_a extracted from Arrhenius plots of A and ΔV_{th} for stress time t = 1, 10, 100, and 1000 s for different samples: sample 1 is RTNO sample with N concentration of 3.7 at. %, and samples 2, 3 and 4 are DPNO samples with N concentration of 3.0, 8.0 and 15.0 at. %, respectively. The NBTI stress is carried out at V_{gstr} = -2.2 V.*

ATTENTION: The Singapore Copyright Act applies to the use of this document. Nanyang Technological University Library

Sample No.	**N at. %**	***t* = 1s**	***t* = 10s**	***t* = 100s**	***t* = 1000s**
1 RTNO	3.7	0.0584	0.0748	0.0752	0.0717
2 DPNO	3.0	0.0592	0.0711	0.0812	0.0857
3 DPNO	8.0	0.0509	0.0641	0.0661	0.0746
4 DPNO	15.0	0.0577	0.0598	0.0675	0.0697

Table 5.4: *Summary of E_a (in eV) obtained from the Arrhenius plots of ΔV_{th} for stress time t = 1, 10, 100, and 1000s. The NBTI stress is carried out at V_{gstr} = -2.2 V.*

To further confirm this, several other Arrhenius plots of ΔV_{th} at stress time t = 1, 10, 100, 1000 s are also constructed to extract E_{a}, and the results are summarized in Table 5.4 and plotted in Fig. 5.3. As can be clearly seen in the figure, E_{a} is not constant for each sample. In addition, there is no consistent trend for all the four nitrided oxide samples, which also strongly indicates a non-Arrhenius behavior of NBTI. Therefore, we should take the dispersive nature of hydrogen diffusion into account in order to build a more reliable NBTI model.

5.3 Physical Modeling of NBTI

5.3.1 Analytical Reaction-Dispersive-Diffusion Model for NBTI

Based on the analytical R-D model discussed in section 4.2, Chapter 4, within the framework of standard R-D model [61, 68], by incorporating the dispersive nature of hydrogen-related diffusing species, i.e. $D_{\mathrm{H}} = D_{\mathrm{H0}}(\nu t)^{\beta-1}$, we can solve the basic set of the reaction equation (Eq. (4.1)), the diffusion/drift equation (Eq. (4.2)) and the conservation equation (Eq. (4.4)), with the same approach as the analytical R-D model, and thus interface trap generation N_{it} is obtained as shown in Eq. (5.2):

ATTENTION: The Singapore Copyright Act applies to the use of this document. Nanyang Technological University Library

$$N_{it}(t) = \frac{2A_0 t}{\left(1+\sqrt{1+4A_0 B_0 t^{\frac{4-\beta}{2}}}\right)} = \frac{2k_F N_O t}{\left(1+\sqrt{1+4k_F N_O \frac{k_R}{\frac{1}{2}\sqrt{D_{H0}\nu^{\beta-1}}} t^{\frac{4-\beta}{2}}}\right)} \quad (5.2)$$

where $A_0 = k_F N_O$ and $B_0 = 2k_R \big/ \left(D_{H0}\nu^{\beta-1}\right)^{\frac{1}{2}}$.

From Eq. (5.2), two distinguished regimes can be observed for the N_{it} generation:

1). the reaction-limited regime (when $4A_0B_0t^{(4-\beta)/2} << 1$), in which

$$N_{it}(t) = A_0 t = k_F N_O t \quad (5.3)$$

and 2) the diffusion-limited regime (when $4A_0B_0t^{(4-\beta)/2} >> 1$), in which

$$N_{it}(t) = \sqrt{\frac{A_0}{B_0}} t^{\frac{\beta}{4}} = \sqrt{\frac{k_F N_O}{2k_R}} \left(D_{H0}\nu^{\beta-1}\right)^{\frac{1}{4}} t^{\frac{\beta}{4}} \quad (5.4)$$

In the reaction-limited regime, Eq. (4.7) clearly shows that N_{it} generation increases linearly with time, which is also suggested by Alam, *et al.* [132, 133], while in the diffusion-limited regime, Eq. (5.4) gives the power-law time-dependence with an exponent factor n of $\beta/4$ for dispersive diffusion, being consistent with the previous studies [138-140]. For the ideal case of non-dispersive diffusion (i.e., β = 1), the power-law factor n becomes 1/4. As discussed previously in Chapter 4, the analytical R-D model is quite preliminary, which was developed at the early stage of my work and corresponds to the ideal case of non-dispersive diffusion. With more evidence from the experimental results, as discussed in section 5.2, the dispersive nature of hydrogen should be taken into account, and regardless of oxide or nitrided oxide, the dispersive diffusion is believed to govern the time kinetics of NBTI.

ATTENTION: The Singapore Copyright Act applies to the use of this document. Nanyang Technological University Library

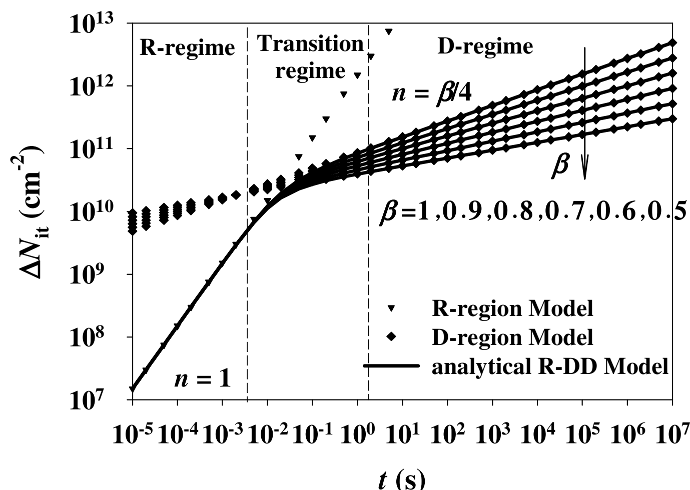

Figure 5.4: *Interface trap generation ΔN_{it} as a function of NBTI stress time. ΔN_{it} is calculated with the reaction-limited regime (R-regime) model (i.e. Eq. (5.3)), diffusion-limited regime (D-regime) model (i.e. Eq. (5.4)), and analytical R-DD model (i.e. Eq. (5.2)), respectively. n is the power-law factor, β ($0<\beta\leq 1$) is the dispersion parameter, and ν is the characteristic frequency.*

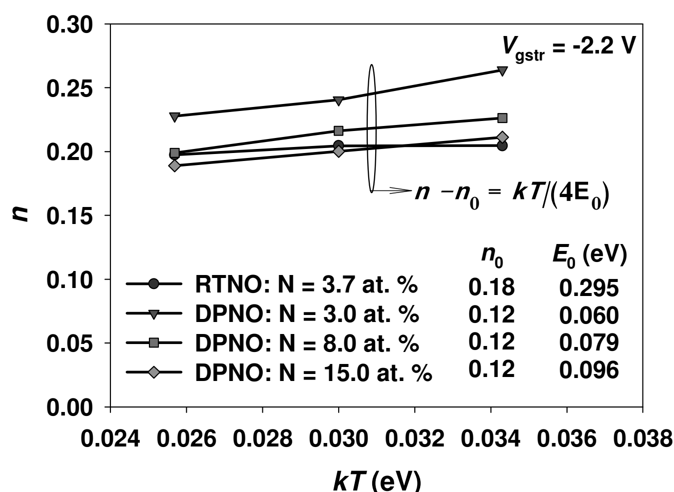

Figure 5.5: *Linear plot of power-law factor n as a function of kT to extract the characteristic energy scale E_0 for different nitrided gate oxides samples.*

ATTENTION: The Singapore Copyright Act applies to the use of this document. Nanyang Technological University Library

With Eq. (5.2), simulated data with different β values can be obtained and the results are shown in Fig. 5.4. As can be seen from the figure, Eq. (5.2) can accurately describe both the reaction-limited and diffusion-limited regimes. From the definition of the dispersion parameter β, one can get the n factor:

$$n = \frac{\beta}{4} \sim \frac{kT}{4E_0} \tag{5.5}$$

From the experimentally-extracted n factors as summarized in Table 5.3 and also shown in Fig. 5.5, the characteristic energy scale E_0 can be obtained with Eq. (5.5) for all the nitrided oxide samples with a compensation of n by subtracting a constant n_0,. The E_0 result is summarized in Table 5.3 and also plotted in Fig. 5.5. Note that n_0 could be an indicator of the measurement effect on NBTI. In an ideal case, with no measurement delay (which is practically not achievable), n_0 should be 0. E_0 for the RTNO sample with N = 3.7 at. % is much higher than those for DPNO samples, which indicates that the n factor of the DPNO samples has stronger temperature dependence than that of the RTNO sample.

On the other hand, for DPNO samples, E_0 increases gradually with increasing interfacial nitrogen concentration. Moreover, n_0 values for DPNO samples with different interfacial nitrogen concentrations are quite comparable, with a same value of ~0.12, which is about 0.06 lower than that of RTNO sample. The results further confirm that, not only the interfacial nitrogen concentration plays a role in nitrogen-worsen NBTI, but also the nitrogen depth profile in nitrided gate oxide has a significant impact on NBTI.

To further confirm this, we have used the activation energy concept by removing the non-Arrhenius part from the right side of Eq. (5.4) to make it Arrhenius; in other

ATTENTION: The Singapore Copyright Act applies to the use of this document. Nanyang Technological University Library

words, instead of using A and ΔV_{th}, we would use $A/v^{(\beta-1)/4}$ and $\Delta V_{th}/\{v^{(\beta-1)/4}\tilde{t}^{\beta/4}\}$ to extract the activation energy E_a again with the previous results in Fig. 5.1 and Table 5.2. The new E_a values are summarized in Table 5.5 and also shown in Fig 5.6. The E_a values extracted with either $A/v^{(\beta-1)/4}$ and $\Delta V_{th}/\{v^{(\beta-1)/4}\tilde{t}^{\beta/4}\}$ for different stress time are quite consistent for each sample. The E_a value of the RTNO sample is higher than those of the DPNO samples, but there is no significant difference in the E_a values among the DPNO samples with different interfacial nitrogen concentrations. This suggests that E_a might be more related to the nitrogen profile rather than the interfacial nitrogen concentration. However, E_a obtained here, with the dispersive nature of hydrogen diffusion taken into account, is quite difficult to establish a direct relationship with the bond-breaking of Si-H at the interface, hydrogen hopping, NBTI reaction and hydrogen diffusion, since the dispersive hydrogen diffusion would have made the NBTI process more complicated. Moreover, regarding the comparison of the extracted values for E_a, since the dispersive hydrogen diffusion plays an important role in NBTI and also complicates the NBTI process, E_a extracted in section 5.2.2 and previously may not be so meaningful, although it still gives some clues as discussed above. Another minor reason is that, even if the activation energy is still valid for NBTI, i.e., assuming the ideal case of non-dispersive process, many factors can still affect the extracted values, such as devices specification, sample preparation, test methodology, etc., and thus the comparison may not be meaningful at all, unless all the conditions for two samples are identical, as discussed above for DPNO samples. On the other hand, as shown in Fig. 5.1 (a) and (b), we can observe larger NBTI degradation for the DPNO sample with higher interfacial nitrogen concentration, which can be mainly due to the increase in the initial density (N_0) of the trivalent Si-H bonds at the interface and the increase in the diffusion constant (D_{H0}) as well.

ATTENTION: The Singapore Copyright Act applies to the use of this document. Nanyang Technological University Library

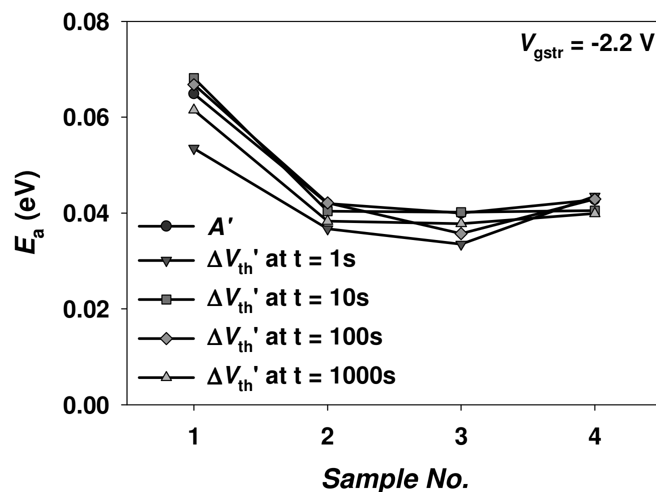

Figure 5.6: *The activation energy E_a extracted from the Arrhenius plots using either $A'(= A/v^{(\beta-1)/4})$ or $\Delta V_{th}'(= \Delta V_{th}/[\, v^{(\beta-1)/4} t^{\beta/4}])$. The NBTI stress is carried out at V_{gstr} = -2.2 V for 1000 seconds.*

Sample No.	N at. %	*A'*	*t* = 1s	*t* = 10s	*t* = 100s	*t* = 1000s
1 RTNO	3.7	0.0649	0.0535	0.0682	0.0668	0.0615
2 DPNO	3.0	0.0420	0.0367	0.0404	0.0421	0.0383
3 DPNO	8.0	0.0400	0.0335	0.0402	0.0357	0.0378
4 DPNO	15.0	0.0428	0.0435	0.0405	0.0429	0.0399

Table 5.5: *Summary of activation energies E_a (eV) obtained from Arrhenius plots of $A'(= A/v^{(\beta-1)/4})$ or $\Delta V_{th}'(= \Delta V_{th}/[\, v^{(\beta-1)/4} t^{\beta/4}])$ at V_{gstr} = -2.2 V for various stress time t.*

5.3.2 Influence of Dispersive Hydrogen Diffusion in Nitrides Gate Oxide on NBTI

To further examine the influence of dispersive hydrogen diffusion in the nitrided gate oxide on NBTI by using the analytical R-DD model, the experiments are carried out at different stress temperatures (T_{str}) in a wider range of 25-225°C. Figure 5.7

ATTENTION: The Singapore Copyright Act applies to the use of this document. Nanyang Technological University Library

shows the measured and simulated interface trap generation ΔN_{it} as a function of stress time under the stress condition of V_{gstr} = -2.2 V and T_{str} = 25 °C for the DPNO samples. As discussed previously in section 4.2, Chapter 4, the analytical R-D model can reasonably-well describe the NBTI results at T_{str} = 125 °C for the DPNO samples with a constant power-law factor of 1/4. However, as shown in Fig. 5.7, at lower T_{str} = 25 °C, especially for the DPNO sample with higher interfacial nitrogen concentration of 15.0 at. %, the analytical R-D model can no longer well match the measured NBTI results in the diffusion-limited regime. Instead, by taking the dispersive hydrogen diffusion into account, the analytical R-DD model can well describe the NBTI results in all three regimes, namely, the reaction-limited, transition and diffusion-limited regimes at any stress conditions.

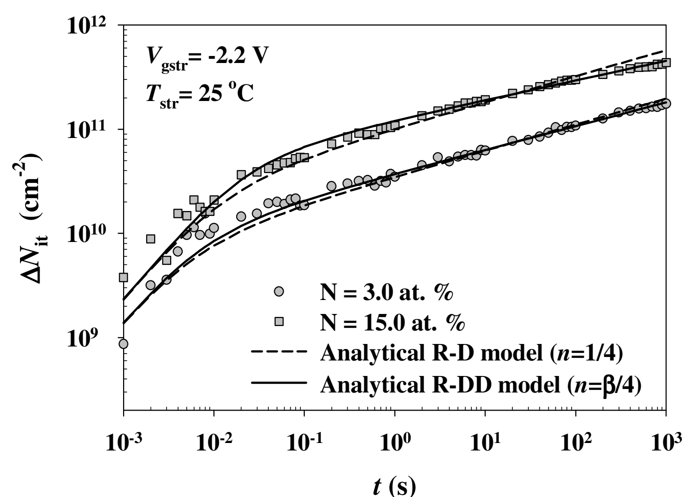

Figure 5.7: *Simulations to the experimental result of the stress time dependence of interface trap generation* ΔN_{it}*. The NBTI stress was carried out at the voltage* V_{gstr} = *-2.2V and the temperature* T_{str} = *25°C. The simulation was carried out with either the analytical R-D model [9] or the analytical R-DD model (i.e., Eq.(1)).*

ATTENTION: The Singapore Copyright Act applies to the use of this document. Nanyang Technological University Library

This is further verified in Fig. 5.8. As can be seen in the figure, rather than a constant of 1/4, the power-law factor n is linearly dependent on the stress temperature T_{str} and the measured n values can be well predicted by the trends calculated with the analytical R-DD model for the DPNO samples with different interfacial nitrogen concentrations in a much wider range of stress temperature.

Besides, the n value is found to be lower for a higher interfacial nitrogen concentration, which suggests a stronger hydrogen dispersive diffusion in nitrided gate oxides with higher nitrogen concentration. According to the analytical R-DD model, the n factor depends on the characteristic energy scale E_0, which is actually due to the dependence of E_0 on the interfacial nitrogen concentration. As can be seen in Fig. 5.9, E_0 increases as the interfacial nitrogen concentration increases, and a lower n value is resulted for a higher nitrogen concentration. This indicates that the hydrogen dispersive diffusion is enhanced by the interfacial nitrogen in terms of the increase of E_0.

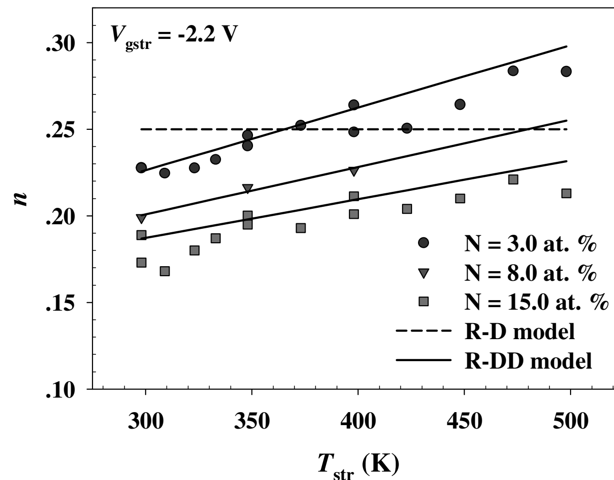

Figure 5.8: *Dependence of the power-law factor n on the stress temperature* T_{str}.

ATTENTION: The Singapore Copyright Act applies to the use of this document. Nanyang Technological University Library

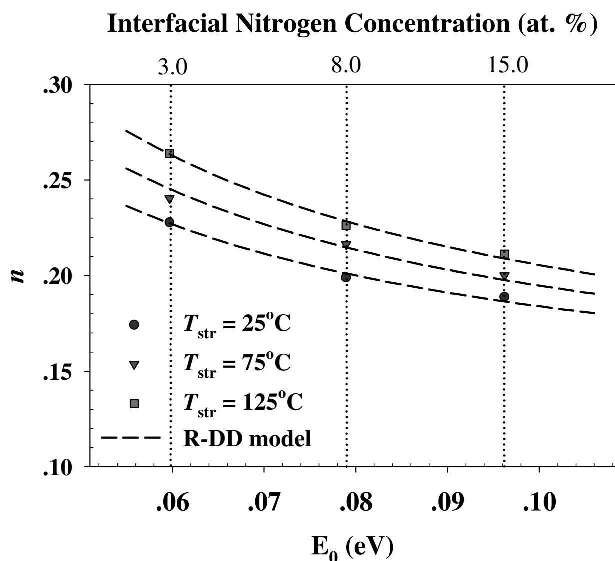

Figure 5.9: *Influence of the interfacial nitrogen concentration on the power-law factor n in terms of the dependence of n on the characteristic energy scale* E_0.

It can be concluded from Eq. (5.4) that the dispersive diffusion can lead to a non-Arrhenius behavior in the Arrhenius plot of the pre-factor A versus $1/kT$ due to the temperature dependence of dispersion parameter β. This is confirmed by the NBTI experiment, as shown in Fig. 5.10. As can be seen in this figure, a higher interfacial nitrogen concentration causes a more significant non-Arrhenius behavior, which is due to the dependence of E_0 on the nitrogen concentration. Fig. 5.10 also shows that the A value is higher for a higher interfacial nitrogen concentration, indicating that NBTI degradation is worsen by more nitrogen content in nitrided gate oxide. The early work by Zhang *et al.* [221] shows that ΔV_{th} increases for a lower measurement temperature for a fixed number of defects. Based on this, the non-Arrhenius behavior in Fig. 5.10 would be much worse when eliminating the effect of ΔV_{th} increase for a lower measurement temperature, because ΔV_{th} and thus A is expected to be higher under higher temperature stress (i.e. lower $1/kT$) when measured at room temperature.

ATTENTION: The Singapore Copyright Act applies to the use of this document. Nanyang Technological University Library

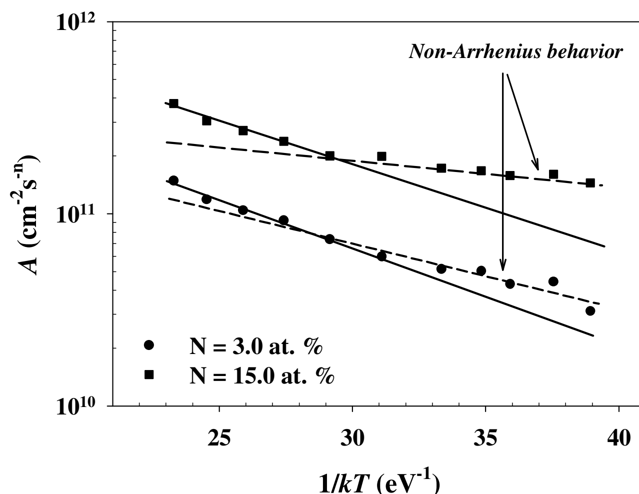

Figure 5.10: *Arrhenius plots of pre-factor A. The lines are for guiding the eyes only.*

5.4 Atomic Modeling of NBTI

To further understand the origin of nitrogen-worsen NBTI, atomic modeling of NBTI for both pure and nitrided gate oxide (i.e. SiO_2 and SiO_xN_y) is carried out via first-principles calculation. First-principles calculation has been performed using a linear combination of hybrid gradient-corrected density functional theory method with Becke's exchange function [222] and the Lee-Yang-Parr correction function [223] for all electronic structure calculations. The electronic structure is expanded using a mixed Gaussian basis set with split-valence-type and polarization functions on all atoms and the dangling bonds at exposed surface of the clusters are saturated with hydrogen atoms. Indeed, with first-principles calculation, Tan *et al.* [36, 110, 212, 213, 218] have already done many works to examine the effect of nitrogen acting either as the reaction site or as adjacent atoms at the interface on NBTI, and thus in this section, only some highlights of the nitrogen effect on NBTI in terms of the reaction energy,

ATTENTION: The Singapore Copyright Act applies to the use of this document. Nanyang Technological University Library

electro-negativity and atomic charge distribution of nitrogen, oxygen and silicon atoms at the interface, are given, mainly to further explain the nitrogen-worsen NBTI phenomenon that has been observed experimentally and analyzed with the analytical R-DD model in previous sections 5.2 and 5.3, respectively. More details on atomic modeling of nitrogen-worsen NBTI can be found in our published work [219].

5.4.1 Atomic Modeling of Nitrogen Effect on NBTI

As NBTI degradation could be mainly attributed to a two-stage process that consists of a hydrogen-originated hole-trapping electrochemical reaction [61, 68] at the interface and subsequent hydrogen diffusion, the reaction energy (E_R) of this electrochemical reaction can be used to examine the effect of nitrogen on NBTI. More specifically, the hydrogen-originated hole-trapping reaction for pure and nitrided oxide, i.e., the overall NBTI reactions, can be described as follows [212, 213]:

At the Si/SiO_2 interface:

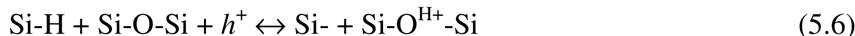

$$\text{Si-H} + \text{Si-O-Si} + h^+ \leftrightarrow \text{Si-} + \text{Si-O}^{H+}\text{-Si} \quad (5.6)$$

At the Si/SiO_xN_y interface:

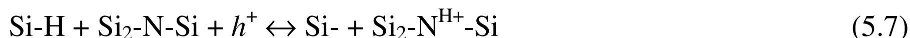

$$\text{Si-H} + \text{Si}_2\text{-N-Si} + h^+ \leftrightarrow \text{Si-} + \text{Si}_2\text{-N}^{H+}\text{-Si} \quad (5.7)$$

where Si-H is the hydrogen-terminated trivalent Si bond, Si-O-Si and Si_2-N-Si stand for the bridging oxygen and nitrogen at the interface, respectively, h^+ is the positively-charged hole in the inversion layer, Si- is the positively-charged silicon dangling bond that acts as an interface trap, Si-O^{H+}-Si and Si_2-N^{H+}-Si are the

ATTENTION: The Singapore Copyright Act applies to the use of this document. Nanyang Technological University Library

positively-charged oxide traps where the hydrogen-related species might diffuse away from the interface. The interface traps (Si-) are generated from the dissociation of hydrogen-terminated trivalent Si bonds (Si-H) by interaction with cold holes (h^+) in the inversion layer at the interface during the NBTI stress.

On the other hand, for the hydrogen ion trapping reaction as in the previous studies [36, 110, 218], from first-principles calculation, the reaction energy E_R is obtained to be -8.51eV or -9.54eV for the pure oxide or nitrided oxide, respectively. The negative sign of E_R indicates that the trapping process is exothermic and a more negative E_R indicates that the NBTI reaction will occur more readily. Therefore, the likelihood of the hydrogen ion to be trapped at the nitrided oxide interface is much higher than that at the pure oxide interface. In other words, the nitrogen atom is a more effective hydrogen trapping center as compared to the oxygen atom. Although the nitrogen effect as discussed above is mainly based on the hydrogen ion trapping reaction, which could be quite different from the overall NBTI reactions as shown in Eq. (5.6) or (5.7), the hydrogen ion trapping could be treated as the part of the overall NBTI reactions. Moreover, the overall NBTI reactions as shown in Eq. (5.6) or (5.7) do not specify the hydrogen-related diffusing species (H^0, H^+, or H_2). Therefore, based on the similar nature of hydrogen species, it may still lead to a general conclusion that the reaction energy of the hydrogen-originated hole-trapping reaction at the nitrided oxide interface is lower than that at the pure oxide interface.

Indeed, when the oxygen or nitrogen acts as the hydrogen-originated hole trapping center, the reaction energy E_R of the overall NBTI reactions as shown in Eq. (5.6) or Eq. (5.7), can be obtained with first-principles calculation to be 8.84eV or 7.81eV, respectively [212]. A lower E_R for nitrogen acting the reaction site, i.e., Eq.

ATTENTION: The Singapore Copyright Act applies to the use of this document. Nanyang Technological University Library

(5.7), indicates that nitrogen is a more effective hole trapping center than oxygen. As a result, NBTI for nitrided oxide is expected to be worse than that for pure oxide. Moreover, at the actual nitrided oxide interface, oxygen and nitrogen co-exist as the reaction sites, i.e., both NBTI reactions as shown in Eqs. (5.6) and (5.7) occur upon NBTI stress. This implies that the actual NBTI reaction energy E_R for the nitrided oxide is between 8.84eV and 7.81eV. More specifically, E_R for a lower nitrogen concentration at the interface is higher and approaching to 8.84eV if the nitrogen is zero, whereas a higher nitrogen concentration leads to a lower E_R value that becomes 7.81eV when all the oxygen bridging atoms at the interface are replaced by nitrogen. Therefore, it can be used to well explain why NBTI degradation is much worse for DPNO sample with higher interfacial nitrogen concentration. A higher interfacial nitrogen concentration means more nitrogen as the bridging atoms, which results with lower E_R for the overall NBTI reaction at the interface, and thus more NBTI degradation is expected for a higher interfacial nitrogen concentration.

Moreover, instead of acting as the reaction site at the interface, the nitrogen may also replace the oxygen in the gate oxide. Since NBTI reaction is believed to occur mainly at the interface, only adjacent nitrogen near the interface is considered. More specifically, by taking the Si-O-Si system in the NBTI reaction as shown in Eq. (5.6) for example, one of the two Si atoms in the simplified Si-O-Si system is in the oxide and thus terminated by three adjacent oxygen atoms, i.e. Si-O-Si-O_3 (assuming that Si at the right-hand side is in the gate oxide). When nitrogen is incorporated, it may replace the adjacent oxygen atoms. The nitrogen may replace one, two or three adjacent oxygen atoms, and thus Si-O-Si-O_3 will become Si-O-Si-NO_2, Si-O-Si-N_2O or Si-O-Si-N_3, respectively. Similarly, first-principles calculation can be carried out for these modified NBTI reactions with nitrogen as the replacement of adjacent

ATTENTION: The Singapore Copyright Act applies to the use of this document. Nanyang Technological University Library

oxygen atoms near the interface, and the reaction energy E_R can be obtained. Here, for simplicity and comparison purpose as well, relative reaction energy ΔE_R is introduced here, and the relative reaction energy ΔE_R is defined as $\Delta E_R = E_R - E_{R,0}$, where $E_{R,0}$ is the reference reaction energy for the pure oxide, i.e. 8.84eV for the reaction as shown in Eq. (5.6). Therefore, the effect of adjacent nitrogen atoms in terms of the relative reaction energy ΔE_R for either oxygen or nitrogen as the trapping center can be examined with first-principle calculation and the results are shown in Fig. 5.11. Figure 5.11 also shows the effect of vacancy defect as the trapping center on the NBTI reaction energy and the effect of adjacent nitrogen atoms for vacancy defect as the trapping center as well. When the vacancy defect (denoted as "Si-V-Si") at the interface acts as the trapping center, the overall NBTI reaction is as follows:

$$\text{Si-H} + \text{Si-V-Si} + h^+ \leftrightarrow \text{Si-} + \text{Si-V}^{\text{H+}}\text{-Si} \quad (5.8)$$

As can be seen from Fig. 5.11, regardless of the type of the trapping center at the interface, ΔE_R decreases as the number of adjacent nitrogen atoms increases. The negative ΔE_R indicates that the NBTI reaction at the nitrided oxide interface occurs more readily than that at the pure oxide interface. Moreover, the lower ΔE_R due to the incorporation of nitrogen as the adjacent atoms near the interface further confirms that the nitrogen worsens NBTI for all cases. In other words, more nitrogen, either as the reaction site at the interface or by replacing the adjacent oxygen near the interface, leads to lower reaction energy and thus higher NBTI degradation. One possible explanation is given as follows. As compared with the oxygen atom, the nitrogen atom acts as a more effective trapping center, and thus with the existence of nitrogen trapping center at the interface or the adjacent nitrogen atoms near the interface, the reaction site or the cluster becomes more effective to trap positive charges such as

ATTENTION: The Singapore Copyright Act applies to the use of this document. Nanyang Technological University Library

holes or hydrogen ions. Therefore, the reaction becomes easier and thus ΔE_R is lower with more adjacent nitrogen atoms. Similarly, with the same number of adjacent nitrogen atoms, ΔE_R for nitrogen as the trapping center should be also lower than that for oxygen as the trapping center. Nevertheless, as can be seen in Fig. 5.11, although nitrogen is a more effective trapping center than oxygen, they follow a similar dependence on the effect of adjacent nitrogen, whereas hole trapping at the vacancy defect has the strongest dependence on the effect of adjacent nitrogen.

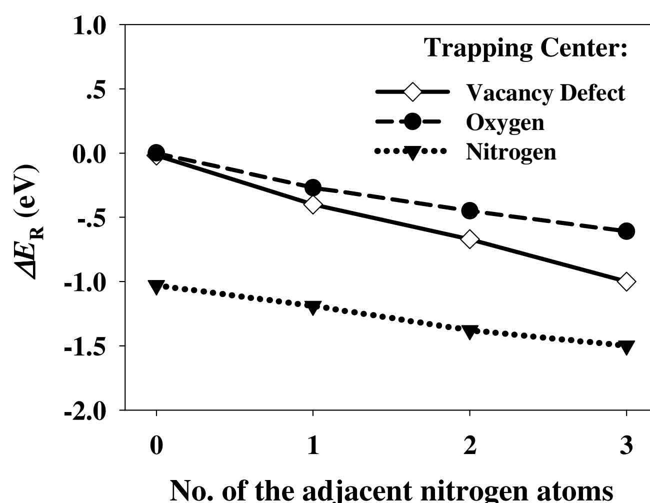

Figure 5.11: *Relative reaction energy ΔE_R as a function of the number of adjacent nitrogen atoms for three possible types of trapping centers at the interface, namely, vacancy defect, oxygen and nitrogen.*

5.4.2 Nitrogen Effect on Atomic Charge Distribution

To provide further evidence of the nitrogen effect on NBTI, atomic charge distribution of nitrogen, oxygen and silicon atoms at the interface is also obtained with first-principles calculation by using three different approaches: Mulliken atomic

ATTENTION: The Singapore Copyright Act applies to the use of this document. Nanyang Technological University Library

charge analysis [224], Chirlian-Francll interface cluster model [225], and natural population analysis [226].

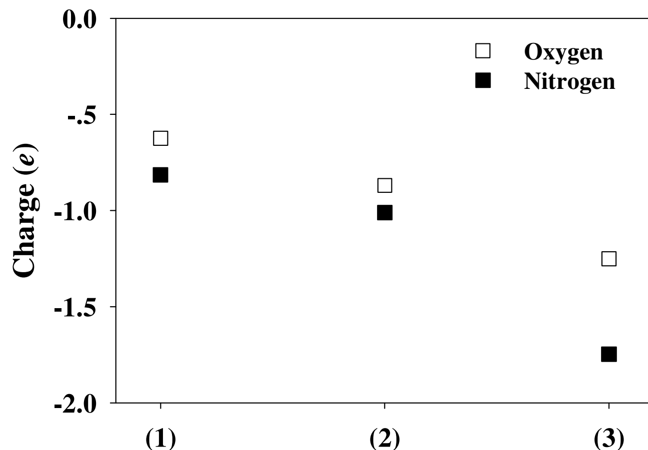

Figure 5.12: *Comparison of the atomic charge for the bridging oxygen or nitrogen atom in Si-O-Si or Si_2-N-Si system, respectively, by using three different approaches: (1) Mulliken atomic charge analysis [224], (2) Chirlian-Francll interface cluster model [225], and (3) natural population analysis [226].*

Due to dipole effect, all three methods assign bridging oxygen or nitrogen atom with a negative charge and Si atoms with positive charges. As a result, the bridging oxygen or nitrogen atom would become an effective trapping center for the positive charges such as holes and hydrogen ions. As can be seen from the Fig. 5.12, although the magnitude of the negative charge assigned to the bridging oxygen or nitrogen atom differs for different methods, all three approaches consistently give the same trend that nitrogen acting as the bridging atom has a larger negative atomic charge than oxygen, which in turn confirms that nitrogen is a more effective hydrogen-originated hole-trapping center than oxygen.

ATTENTION: The Singapore Copyright Act applies to the use of this document. Nanyang Technological University Library

Moreover, as the number of adjacent nitrogen atoms increases, localized structures at the interface are expected to become stronger negative centers and thus become even more effective localized trapping sites for holes or positive ions. Therefore, the atomic charge distribution of nitrogen, oxygen and silicon atoms at the interface can help explain the results of worse NBTI degradation with incorporation of nitrogen as the adjacent atoms near the interface.

5.5 Summary

In summary, nitrogen-worsen NBTI has been systematically studied by experimental investigations, physical modeling and atomic modeling. NBTI for the nitrided gate oxide is well described by an analytical reaction-dispersive-diffusion (R-DD) model in diffusion-limited regime, and it is found that both the interfacial nitrogen concentration and the nitrogen profile in the nitrided oxides play important roles in the nitrogen-worsen NBTI. The influence of dispersive hydrogen diffusion in nitrided gate oxides on NBTI has been examined and the NBTI experiments verify that the R-DD model can well explain NBTI degradation including its dependence on the stress time, stress temperature and interfacial nitrogen concentration, and its power-law behaviors as well. Lastly, first-principles calculation is carried out to examine the effects of nitrogen acting as either the reaction site or the adjacent atoms at the interface, in terms of the NBTI reaction energy, electro-negativity and atomic charge distribution of nitrogen, oxygen and silicon atoms at the interface.

ATTENTION: The Singapore Copyright Act applies to the use of this document. Nanyang Technological University Library

CHAPTER 6 IMPACT OF PROCESS TECHNOLOGIES ON NBTI

In this chapter, NBTI degradation in *p*-MOSFETs is thoroughly investigated and the impact of advanced process technologies on NBTI is examined. Stress proximity technique can improve NBTI significantly while laser spike annealing is found to worsen NBTI. Moreover, characterization of NBTI in high-performance devices with ultrathin gate dielectrics is carried out. In particular, the impact of post-nitridation annealing on NBTI is investigated. It is observed that NBTI in the high-performance devices can be quite pronounced even at or slightly above the operating voltage and thus NBTI in *p*-MOSFETs with ultrathin gate dielectrics would become one of the most critical device reliability challenges for further down-scaling.

6.1 Introduction

For advanced technology nodes, CMOS scaling has been mainly driven by stress-induced mobility enhancement techniques. In other words, stress engineering and material innovations have replaced geometric scaling as the main contributors to continuous improvement in CMOS devices. For *n*-MOSFETs, stress memorization technique (SMT) [203, 204] has been widely integrated with the tensile stressed nitride liner [198, 199, 205, 206, 227, 228] in order to boost electron mobility, whereas for *p*-MOSFETs, localized compressive strain along the channel direction can be induced by various techniques, such as compressive stressed nitride liner [198, 199,

ATTENTION: The Singapore Copyright Act applies to the use of this document. Nanyang Technological University Library

205, 206], embedded SiGe in source/drain region [227, 228], and stress proximity technique (SPT) [198, 199] as well. Moreover, laser annealing (LA) or laser-spike annealing (LSA) [200-202] has been extensively studied and thus integrated into the process, mainly to activate source/drain dopant more effectively, minimize dopant out-diffusion and thus enhance device performance. On the other hand, in order to meet stringent electrical specifications, process innovation and optimization have become very critical and necessary, especially for further development of the high-performance devices with ultrathin gate dielectrics.

For sub-90nm technology nodes, NBTI in *p*-MOSFETs with ultrathin nitrided oxide as the gate dielectrics has become one major device reliability issue and starts to limit the lifetime of CMOS device [31]. Various kinds of new process techniques, as mentioned above, have been incorporated into the generic wafer-manufacturing process flow in order to boost device performance. However, their impact on NBTI has not been well understood yet. Therefore, it is of great interest to examine the impact of these new process techniques on NBTI. In this chapter, the characterization of NBTI in 65nm or 45nm *p*-MOSFEFs with various new process technologies is carried out, and the impact of these process technologies on NBTI in both lower-power and high-performance *p*-MOSFETs is examined.

6.2 Impact of Stress Proximity Technique on NBTI

In order to boost device performance, stress engineering, such as stress memorization technique (SMT) [203, 204] and dual stress liner (DSL) [198, 199, 205, 206] and NiSi salicidation [229, 230], is widely explored. Stress proximity technique

ATTENTION: The Singapore Copyright Act applies to the use of this document. Nanyang Technological University Library

(SPT) [198, 199] is another effective performance-enhancement technique particularly for *p*-MOSFETs. SPT is inserted after salicidation by removing the off-set spacer 2 in order to maximize the stress proximity effect and thus enhance the strain transfer into the channel during subsequent deposition of the compressive nitride stress liner.

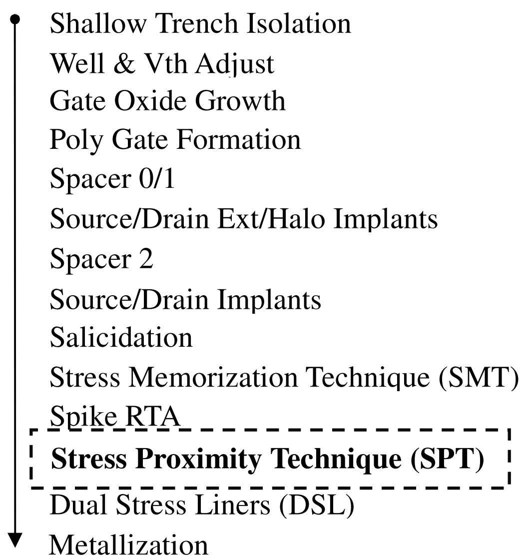

Figure 6.1: *Schematic diagram of CMOS fabrication process flow with SPT.*

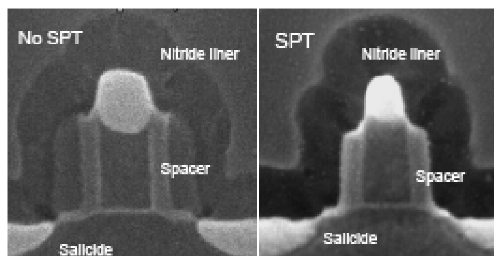

Figure 6.2: *SEM cross sections of devices with and without SPT. After [198].*

A schematic diagram of CMOS process flow with SPT is shown in Fig. 6.1, and SEM cross sections of devices with and without SPT are shown in Fig. 6.2. As can be seen in Fig. 6.2, SEM cross section clearly shows that, for the device with SPT, only the L-shaped spacer 1 remains after the removal of spacer 2, and thus the stress

ATTENTION: The Singapore Copyright Act applies to the use of this document. Nanyang Technological University Library

proximity effect can be largely enhanced during subsequent nitride stressor deposition, which in turn improve the device performance significantly.

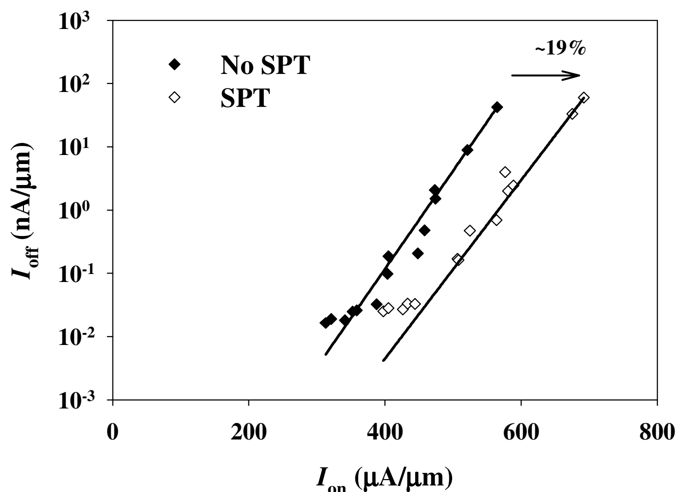

Figure 6.3: *Comparison of device performance between p-MOSFETs with and without SPT. About 19% I_{on} improvement is achieved by SPT process.*

Figure 6.3 clearly shows that SPT can improve the electrical performance of *p*-MOSFETs by as much as 19%, which agrees quite well with the previous report [198]. However, no study has been reported on NBTI in *p*-MOSFETs that are fabricated with the SPT process, although the impact of SPT on NBTI is critical to the process qualification and optimization. In this section, the impact of SPT on NBTI is investigated, and the impact is correlated to the change in stress profile in the device induced by SPT, based on the first-principles calculation of NBTI reactions and the simulation of stress in the MOSFETs. In particular, the simulation of stress change in the device is used to examine the impact of SPT-induced stress on NBTI. Since it is difficult to accurately measure the actual stress in the device, the simulation provides a simple and effective way to investigate the change in stress induced by SPT. The

ATTENTION: The Singapore Copyright Act applies to the use of this document. Nanyang Technological University Library

simulation shows a significant reduction in stress along the vertical direction at interface, which is believed to be responsible for the improvement of NBTI by SPT.

6.2.1 Experimental

The *p*-MOSFETs used here were fabricated by 65 nm low-power process either with or without SPT. The nitrided gate oxide thickness for both samples with and without SPT is the same, about 17.5 Å, since the additional spacer removal for SPT process is carried out after the growth of gate oxide and poly-Si gate and there is no extra thermal process as well. The channel width is 2 µm and the channel length is 60 nm. The nominal operating voltage (V_{dd}) is -1.2 V. For the NBTI stress conditions, the stress temperature (T_{str}) is in the range of 25~125 °C and the gate stress voltage (V_{gstr}) is from -1.6 V to -3.0 V, and the default stress condition corresponds to T_{str} = 125 °C and V_{gstr} = -2.3 V. To minimize the recovery during NBTI characterization, the single-point saturation drain current (I_{dsat}) measurement [182] is used to extract the threshold voltage shift (ΔV_{th}). Moreover, the conventional *I-V* measurement method and 1st on-the-fly (OTF) measurement method [40, 152] in a short time range are also conducted to re-confirm the trend observed by using the single-point I_{dsat} method.

6.2.2 Impact of SPT on NBTI: Experimental Results

The improvement of NBTI by SPT can be clearly seen from Fig. 6.4 through the comparison between the samples with and without SPT. Figure 6.4(a) shows the comparison of the dependence of threshold voltage shift (ΔV_{th}) on stress time (t) in the

ATTENTION: The Singapore Copyright Act applies to the use of this document. Nanyang Technological University Library

diffusion-limited regime, which is commonly observed and well explained by the R-D model [10]-[15]. Both samples show power-law time dependence of ΔV_{th}, but NBTI in the sample with SPT is much lower than that without SPT for a given stress time. Figure 6.4(b) shows the comparison of the stress-temperature (T_{str}) dependence of ΔV_{th}. ΔV_{th} of the sample with SPT is significantly smaller than that without SPT at any stress temperatures. As can be seen in Fig.6.4(b) also, relative NBTI improvement by SPT, defined as $(\Delta V_{th,NoSPT} - \Delta V_{th,SPT})/\Delta V_{th,NoSPT} \times 100\%$, where $\Delta V_{th\ NoSPT}$ and $\Delta V_{th,SPT}$ are the threshold voltage shifts of the samples without and with SPT under the same condition, respectively, is larger at a higher stress temperature. Figure 6.4(c) shows the comparison of the stress-voltage (V_{gstr}) dependence of ΔV_{th}. As can be seen in the figure, ΔV_{th} is reduced by SPT regardless of stress voltage, and the relative NBTI improvement by SPT is more significant at lower stress voltage. Larger relative NBTI improvement by SPT at lower gate voltage implies that improvement of NBTI by SPT at the nominal operating voltage (V_{dd}) is even more significant than that at gate stress voltage of -2.3 V. In other words, SPT would give a much lower NBTI-induced ΔV_{th} at V_{dd} and thus yield a much longer device lifetime.

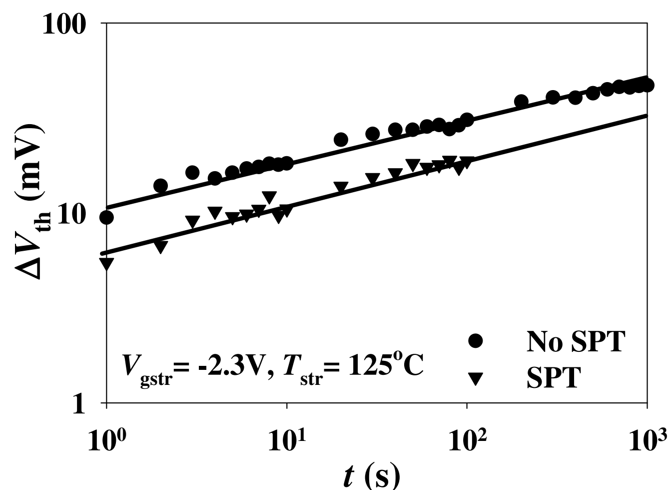

(a)

ATTENTION: The Singapore Copyright Act applies to the use of this document. Nanyang Technological University Library

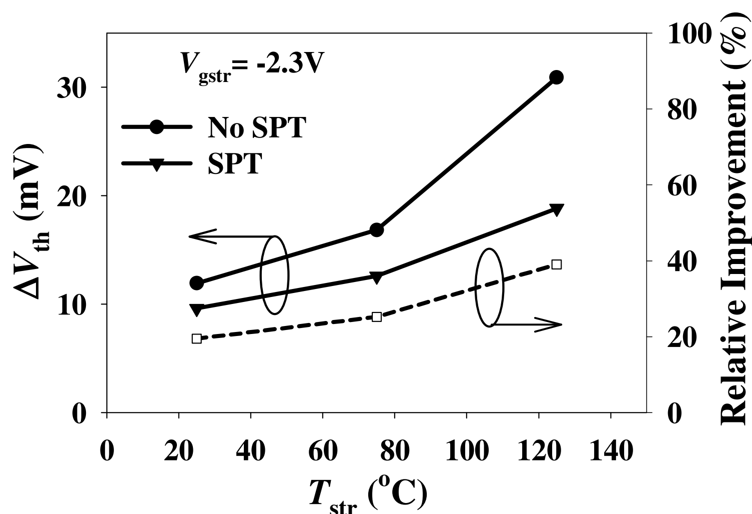

(b)

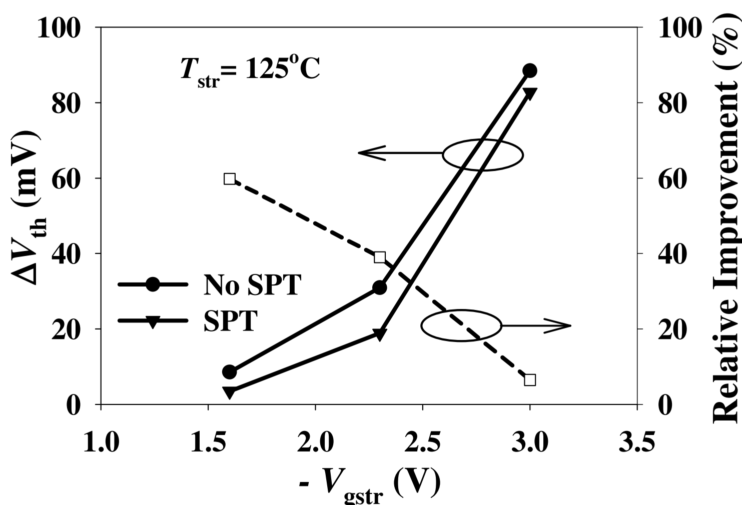

(c)

Figure 6.4: *Comparison of NBTI degradation between the samples with and without SPT. (a) The threshold voltage shift (ΔV_{th}) is measured as a funtion of stress time (t) at gate stress voltage (V_{gstr}) of -2.3 V and stress temperature (T_{str}) of 125 °C; (b) ΔV_{th} is measured as a funtion of T_{str} at V_{gstr} = -2.3 V for stress time of 100 s; and (c) ΔV_{th} is measured as a funtion of V_{gstr} at T_{str} = 125 °C for stress time of 100 s. The relative NBTI improvement by SPT is shown in (b) and (c). The lines are for guiding eyes only.*

ATTENTION: The Singapore Copyright Act applies to the use of this document. Nanyang Technological University Library

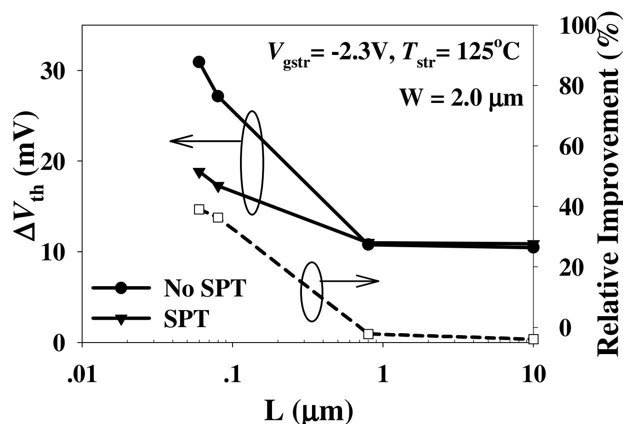

Figure 6.5: *Comparison of NBTI degradation between the samples with and without SPT and the relative NBTI improvement by SPT as a function of channel length. The stress voltage is -2.3 V, stress temperature is 125 °C, and stress time is 100 s.*

Moreover, Figure 6.5 shows the influence of SPT on the channel-length dependence of NBTI-induced ΔV_{th}. As can be clearly seen in the figure, although NBTI degradation is more siginifcant for shorter channel length, the relative NBTI improvement by SPT is larger for shorter channel length.

6.2.3 Impact of Interfacial Strain on NBTI: First-principles Calculation

The improvement of NBTI by SPT could be related to changes of stress in the MOSFETs induced by SPT. SPT is believed to enhance the transfer of compressive strain into the channel, which boosts hole mobility and thus improves device performance [198]. However, how strain affects NBTI is not clear yet, and hence in this section, first-principles calculation is carried out to examine the effect of strain on NBTI. Since the change in bond angle in the atomic structure could be a good indicator of strain, the bond angle is changed in a certain range (±40°) from the one

ATTENTION: The Singapore Copyright Act applies to the use of this document. Nanyang Technological University Library

obtained at the equilibrium stage to simulate the strain in the atomic structure, and subsequently the geometry of the atomic structure is optimized for all other degrees of freedom, e.g., at equilibrium, the bond angles ∠Si-Si-H and ∠Si-Si-Si in the Si_3-Si-H structure are obtained to be 108° and 110.86°, respectively. With strain, the bond angles ∠Si-Si-H and ∠Si-Si-Si are varied in the ranges of (108° ± 40°) and (110.86° ± 40°), where positive sign indicates tensile strain along channel direction and negative sign indicates compressive strain. Based on the R-D model [68, 132, 133, 211, 219], NBTI degradation can be well explained by cold-hole assisted dissociation of hydrogen-terminated trivalent silicon bonds (Si-H) at the interface, the effect of strain on the Si-H dissociation process is examined first in terms of the change in Si-H bonding energy (ΔE_B). Figure 6.6(a) shows ΔE_B as a function of the change in bond angle of ∠Si-Si-H or ∠Si-Si-Si in the Si_3-Si-H structure. As shown in the figure, under either compressive or tensile strain, the Si-H bonding-energy (E_B) decreases with the strain. This means that the Si-H bond becomes weaker when the strain is higher. In other words, the strain is favorable to the Si-H dissociation.

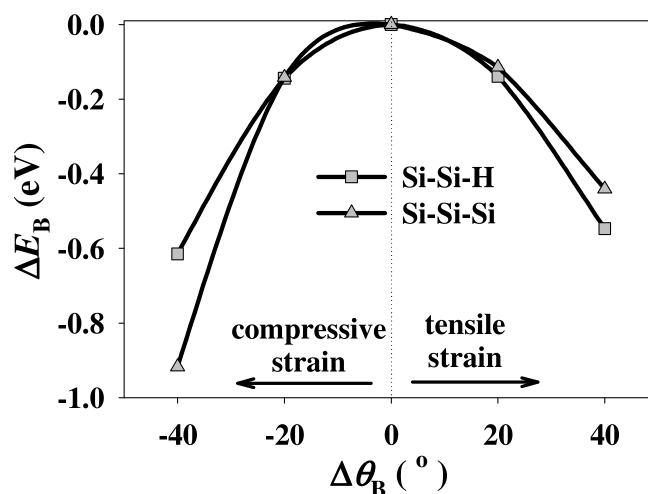

(a)

ATTENTION: The Singapore Copyright Act applies to the use of this document. Nanyang Technological University Library

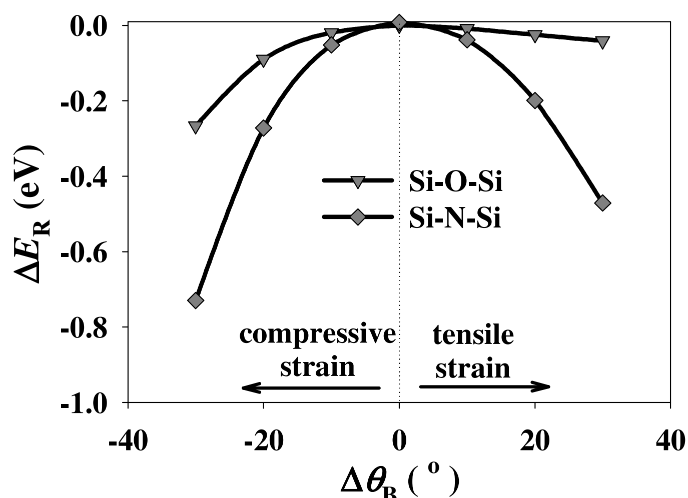

(b)

Figure 6.6: *(a) Change in Si-H bonding-energy (ΔE_B) as a function of change in bond angle ($\Delta\theta_B$); and (b) change in NBTI reaction energy (ΔE_R) as a function of $\Delta\theta_B$. The values of Si-H bonding-energy and NBTI reaction energy corresponding to the bond angle in equilibrium (i.e., $\Delta\theta_B = 0$) are taken as references. In (a), the bond angle is either ∠Si-Si-H or ∠Si-Si-Si in the Si_3-Si-H structure at interface; and in (b) the bond angle is ∠Si-O-Si and ∠Si-N-Si for pure oxide and nitrided oxide, respectively.*

On the other hand, the effect of strain on the NBTI reaction energy (E_R) is also investigated. Similarly, the bond angle ∠Si-O-Si or ∠Si-N-Si at pure or nitrided gate oxide interface, respectively, is changed in a certain range (±30°) to simulate the strain effect. The hydrogen-originated NBTI reaction is examined by using first-principles calculation and the change in NBTI reaction energy (ΔE_R) as a function of the change in bond angle ($\Delta\theta_B$) for both pure oxide and nitrided oxide is obtained and shown in Fig. 6.6(b). As shown in the figure, the reaction energy decreases as the change in bond angle becomes larger, indicating that the NBTI reaction is worsen by either

ATTENTION: The Singapore Copyright Act applies to the use of this document. Nanyang Technological University Library

compressive or tensile strain. Moreover, Fig. 6.6(b) clearly shows that the impact of strain on NBTI degradation is more severe in nitrided oxide than that in pure oxide, which raises another critical issue that the nitrogen-worsen NBTI effect will become more pronounced when the stress/strain at nitrided oxide interface increases. It is clear from the above discussions that the strain worsens NBTI degradation in terms of the reductions in both Si-H bonding-energy and NBTI reaction energy.

6.2.4 Impact of SPT on Stress Transfer: Process Simulation

To understand the improvement of NBTI by SPT, it is necessary to know the change in SPT-induced stress in the MOSFETs. A simulation of the stress profile in the MOSFET with SPT is done with TCAD process simulator. The simulated process flow is briefly described as follows. Process simulation starts with the initialization of mesh and mask drawing for the *p*-channel devices, followed by well definition and V_{th} adjustment implantation. The subsequent step is gate stack growth, which mainly consists of ultra-thin gate oxide growth and poly-Si gate definition. The thickness of nitrided gate oxide is about 12Å and the channel length is 50nm. After the gate stack growth, spacer 1 is deposited, followed by extension/halo implant in source/drain (S/D) region, and then spacer 2 is deposited, followed by S/D implant. A subsequent spike annealing is carried out, mainly for S/D dopant activation. SPT process is inserted by removing the spacer 2, and lastly DSL process is used, which in particular for *p*-MOSFETs corresponds to the deposition of 3.0 GPa compressive stressed nitrided liner. One-dimensional simulation results including the device structure, dopant profile and stress distribution are obtained for devices with and without SPT.

ATTENTION: The Singapore Copyright Act applies to the use of this document. Nanyang Technological University Library

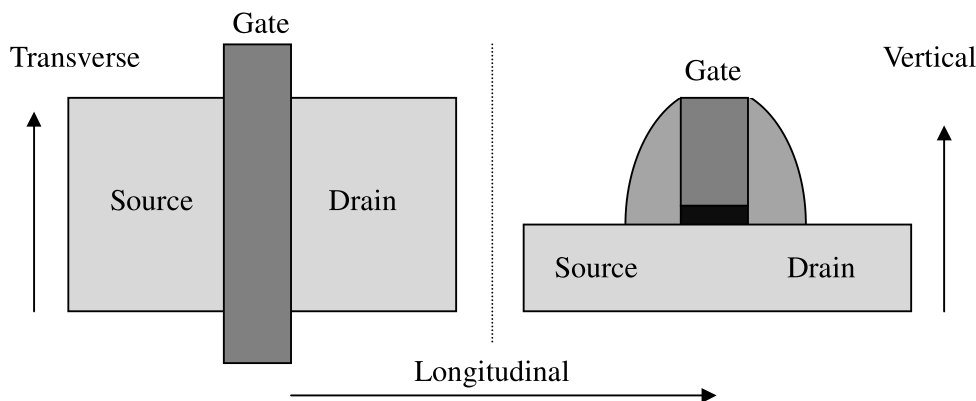

Figure 6.7: *Definitions of the directions for device simulation.*

Definitions of the directions for the device simulation are shown in Fig. 6.7: the channel direction is defined as the longitudinal direction, the lateral poly-Si gate direction is defined as the transverse direction, and the out-of-plane gate direction is defined as the vertical direction. Moreover, for device performance, based on the piezoresistance effect [231, 232], a compressive strain along the longitudinal channel direction in the channel region is highly desired to boost hole mobility and thus is most critical for *p*-MOSFETs; besides, a tensile strain along the transverse direction has less impact on improving device performance for *p*-MOSFETs but may still be quite important, and a tensile strain along the vertical direction nearly has no effect on the performance improvement for *p*-MOSFETs.

Stress distributions in *p*-MOSFETs with and without SPT can be obtained from TCAD process simulation, and the results are shown in Fig. 6.8. From Fig. 6.8, the main observations on stress distributions in *p*-MOSFETs with and without SPT, particularly in the regions of gate oxide interface and the channel, are highlighted as follows. Along the longitudinal (X) direction, i.e., the channel direction, a deep encroachment of compressive stress into the poly-Si gate at the position slightly above

ATTENTION: The Singapore Copyright Act applies to the use of this document. Nanyang Technological University Library

the gate oxide interface can be observed for *p*-MOSFETs with SPT, and it clearly indicates that the stress transfer from the compressive liner is more effective with SPT than without SPT. Along the transverse (Y) direction, a small compressive stress is resulted for the SPT sample near the gate oxide interface and in the channel region as well, whereas a small tensile stress is observed for the sample without SPT. Nevertheless, stresses along the transverse direction are quite insignificant for both samples. Along the vertical (Z) direction, large tensile stresses are induced in the critical regions for both samples with and without SPT. Moreover, a small compressive stress is observed in the S/D extension area for the SPT sample, which indicates a smaller tensile stress near that region than that without SPT. In short, SPT largely enhances the transfer of compressive stress along the longitudinal channel direction, which is mostly desired to boost hole mobility, and thus leads to an improvement in device performance. However, the stress distributions in Fig. 6.8 can only provide a qualitative comparison between the samples with and without SPT. Therefore, further investigations on the stress profiles at the critical regions for both samples must be conducted and the results ought to be compared quantitatively.

Positions	at the interface		in the oxide		in the channel	
(x = 0)	SPT	No SPT	SPT	No SPT	SPT	No SPT
Longitudinal stress (MPa)	-473	-408	-182	-134	-462	-407
Transverse stress (MPa)	-21.4	24.5	-1.26	36.7	-22.3	22.7
Vertical stress (MPa)	397	496	403	499	383	488

Table 6.1: *A summary of the extracted stress values at the location (x = 0) for devices with and without SPT along the longitudinal, transverse and vertical directions, at three different positions: at the interface, in the oxide and in the channel.*

ATTENTION: The Singapore Copyright Act applies to the use of this document. Nanyang Technological University Library

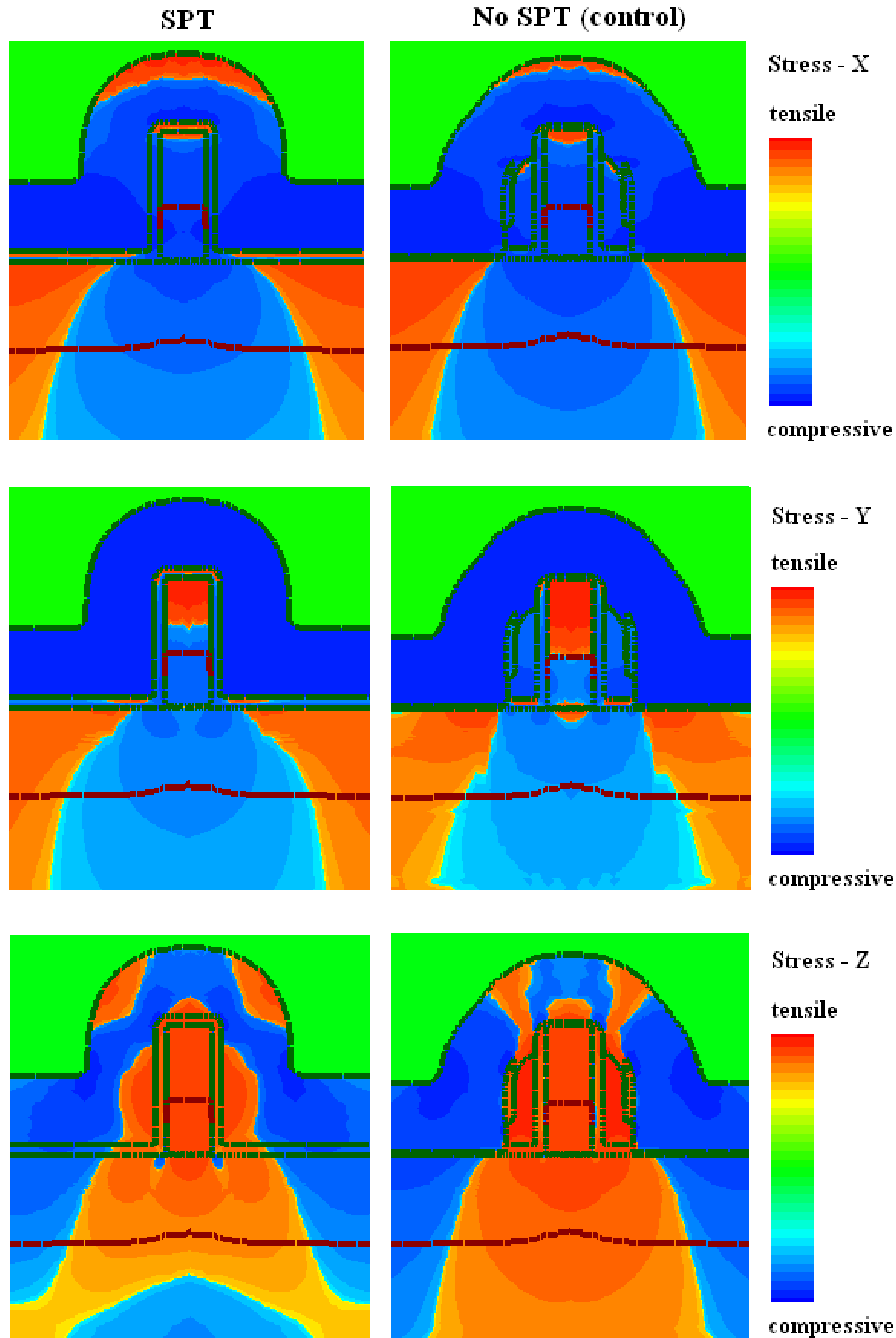

Figure 6.8: *Stress distributions in p-MOSFETs with and without SPT along the longitudinal (X), transverse (Y) and vertical (Z) directions. The dimension of each device stress map is about 0.4µm x 0.4µm, and the channel length is 50nm.*

ATTENTION: The Singapore Copyright Act applies to the use of this document. Nanyang Technological University Library

The simulated stress profiles (i.e., stress as a function of distance *x* in the channel direction) in *p*-MOSFETs with and without SPT at the interface along the longitudinal direction (i.e., the channel direction), transverse direction (i.e., the lateral direction) and vertical direction (i.e., the out-of-plane direction), are plotted in Fig. 6.9. As can be seen in the figure, compressive stress along the longitudinal direction is enhanced by SPT, the small tensile stress along the transverse direction is changed to a small compressive stress by SPT, and the tensile stress along the vertical direction is largely reduced by SPT. In fact, the stress profiles at different positions, i.e., at the interface, in the oxide and in the channel, can also be extracted, and the critical stress values for devices with and without SPT at $x = 0$ are summarized in Table 6.1. Moreover, stress profiles in *p*-MOSFETs with and without SPT as a function of distance *x* for the three different positions: at the interface, in the oxide and in the channel, can also be extracted. Figure 6.10 shows the results along the longitudinal direction as an example. Indeed, the stress profiles along different directions at different positions can be well represented by the critical stress values in Table 6.1.

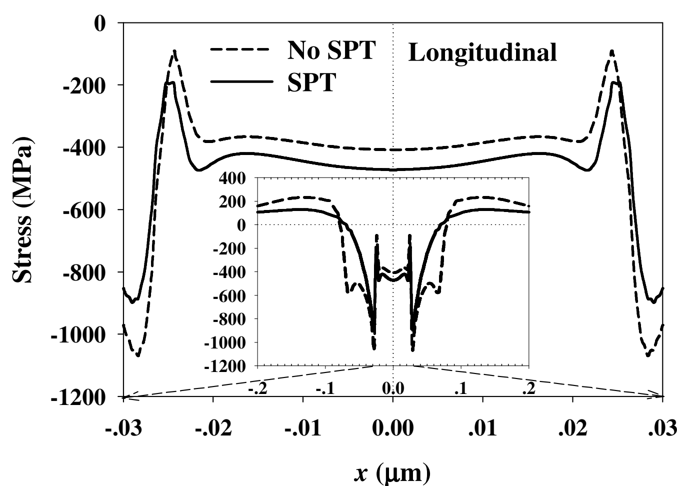

(a)

ATTENTION: The Singapore Copyright Act applies to the use of this document. Nanyang Technological University Library

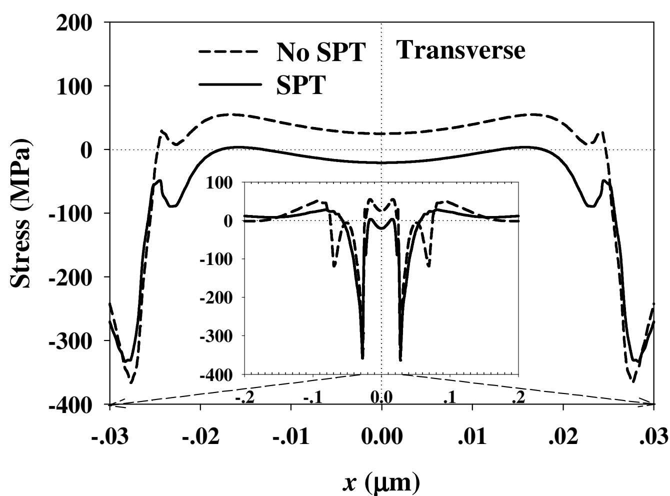

(b)

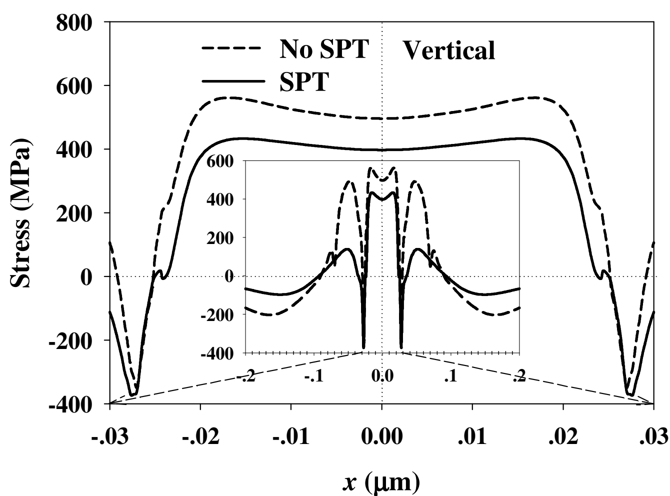

(c)

Figure 6.9: *Simulated stress profiles in p-MOSFETs with and without SPT at the interface along the longitudinal (a), transverse (b), and vertical (c) directions as a function of distance x in the channel direction. The results are directly extracted from the device stress maps in Fig. 6.8.*

ATTENTION: The Singapore Copyright Act applies to the use of this document. Nanyang Technological University Library

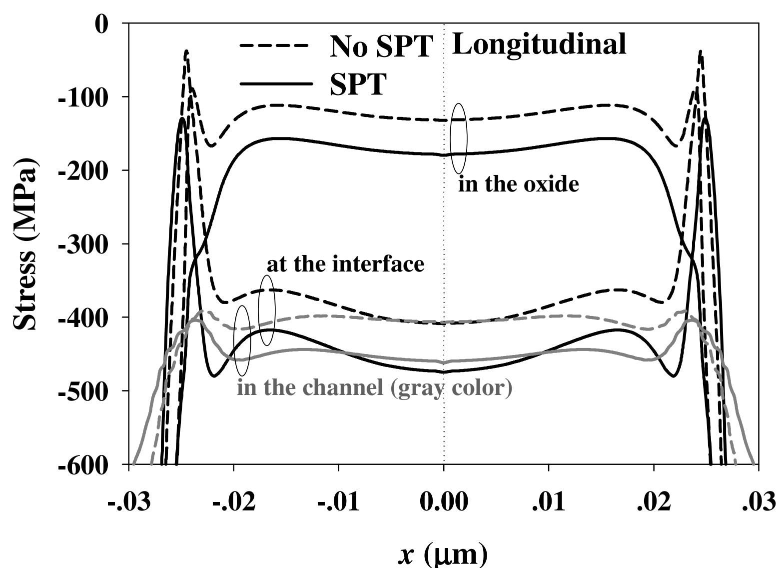

Figure 6.10: *Simulated stress profiles in p-MOSFETs with and without SPT along the longitudinal direction as a function of distance x for the three different positions: at the interface, in the oxide (denoted by the gray color lines), and in the channel.*

As discussed previously, for improvement of device performance, based on the piezoresistance effect [231, 232], compressive strain along the longitudinal direction in the channel region is most desired to boost hole mobility and thus is most critical for *p*-MOSFETs. It is very clear from Fig. 6.10 that compressive stress in the channel is significantly enhanced by SPT. More specifically, as given in Table 6.1, with the deposition of the same compressive stressed nitride liner, SPT process can more effectively transfer compressive stress of about 462 MPa along the longitudinal direction in the channel, which is about 14% larger than that of about 407 MPa without SPT. Therefore, SPT-induced enhancement in the transfer of compressive stress leads to higher strain in the channel, and thus boosts hole mobility and improves device performance.

ATTENTION: The Singapore Copyright Act applies to the use of this document. Nanyang Technological University Library

6.2.5 Improvement of NBTI by SPT

Although compressive stress along the longitudinal direction is significantly enhanced by SPT, tensile stress along the vertical direction is largely reduced by SPT. The large reduction in tensile stress along the vertical direction is believed to be responsible for the improvement of NBTI by SPT, as discussed below. As can be seen in Table 6.1, the reduction in tensile stress along the vertical direction is larger than the increase in the compressive stress along the longitudinal direction by SPT for all the positions (i.e., at the interface, in the oxide or in the channel).

Moreover, the longitudinal stress direction is less favorable for strain-induced bond angle changes. Assuming a rigid Si_3-Si-Si system near the interface, the bond angle ∠Si-Si-Si can be calculated to be 109.47°, while in the Si_3-Si-H system, the bond angles ∠Si-Si-H and ∠Si-Si-Si are obtained to be 108° and 110.86°, respectively. Indeed, bond angle change in the rigid system due to mechanical stress/strain can be calculated mathematically. When stress/strain is applied to the system, the bond angle ∠Si-Si-Si would change accordingly. Therefore, an indicator of the overall bond angle change should be specified, and it is defined as the sum of all possible bond angle changes in magnitude. Moreover, when stress/strain is applied along different directions, which could be longitudinal or vertical, the bond angle changes are also quite different. As shown in Fig. 6.11, with the same amount of strain, the change in the bond angle ∠Si-Si-Si (or ∠Si-Si-H) is found to be larger when the strain is along the vertical direction than that along the longitudinal channel direction. In other words, strain along the vertical direction has a more significant impact on bond distortion.

ATTENTION: The Singapore Copyright Act applies to the use of this document. Nanyang Technological University Library

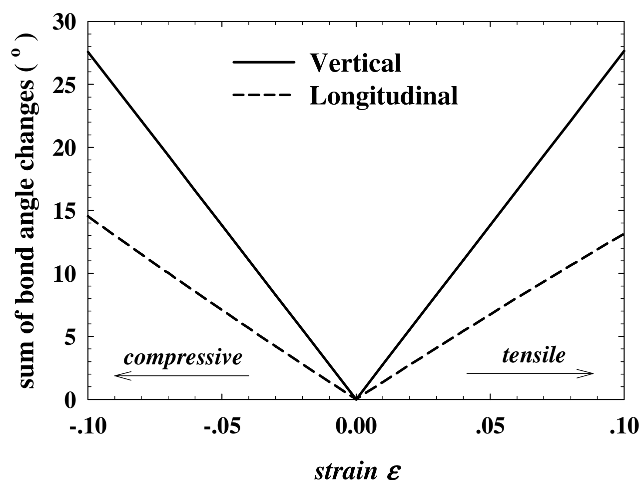

Figure 6.11: *Sum of the bond angle changes in magnitude as a function of the strain induced in either vertical or longitudinal direction. Poisson's ratio used in the calculation is 0.28 for both directions.*

As can be seen in Table 6.1, it shows that, for the sample with SPT, at the interface, the tensile stress along the vertical direction is obtained to be 397 MPa in magnitude, which is much smaller than that of 496 MPa for the sample without SPT. Therefore, although SPT induces more compressive stress along the longitudinal channel direction, which boosts hole mobility and hence improves device performance, a large reduction in tress along the vertical direction is also achieved by SPT, and it in turn leads to a decrease in the overall bond distortion. According to Figs. 6.6, less bond distortion means a higher bonding-energy (i.e., a stronger Si-H bond) and a higher NBTI reaction energy as well, and hence smaller NBTI degradation is expected for the devices with SPT. In addition, one may also think that stress along the vertical direction is more relevant to NBTI reaction as the electric field is along the vertical direction during NBTI stress, and thus reduction in the strain along the vertical direction is responsible for the NBTI improvement by SPT.

ATTENTION: The Singapore Copyright Act applies to the use of this document. Nanyang Technological University Library

The dependence of NBTI degradation on stress temperature, stress voltage and channel length, as shown in Fig. 6.4(b), Fig. 6.4(c) and Fig. 6.5, respectively, can be further discussed based on the impact of stress/strain on NBTI. The dependence of NBTI on stress temperature could be due to the enhanced NBTI reaction at a higher temperature or the direct or indirect impact of SPT-induced strain on the hydrogen dispersive diffusion process in the oxide, and a better improvement by SPT at a higher temperature could be attributed to the enhanced reduction in the vertical stress by SPT at a higher temperature. The simulation of stress at different temperatures was carried out and the result is summarized in Table 6.2. For both the samples with and without SPT, as the temperature increases, the vertical and longitudinal stresses become less tensile and less compressive, respectively, while the transverse stress remains small. When the temperature increases from 25°C to 125°C, the reduction in vertical tensile stress is 8.06% for the sample without SPT, while it is 9.07% for the sample with SPT. The reduction in vertical stress by SPT is 19.96% at 25°C and 20.83% at 125°C. Therefore, the enhanced reduction in vertical stress at a higher temperature could be one of the reasons for the better improvement by SPT at a higher temperature. Regarding the stress-voltage dependence, it is believed that the external stress voltage could also enhance the distortion of Si-H bonds at interface and thus enhance the NBTI reaction also. Although the absolute improvement of NBTI by SPT does not have a strong dependence on the magnitude of stress voltage, the relative improvement by SPT could decrease with the magnitude of stress voltage, which is basically due to the fact that the NBTI-induced ΔV_{th} for the sample without SPT is higher at a higher stress voltage. In other words, the relative NBTI improvement by SPT should be more significant at a lower voltage, as shown in Fig. 6.4(c). The explanation of the improvement of NBTI by SPT based on the impact of stress/strain

ATTENTION: The Singapore Copyright Act applies to the use of this document. Nanyang Technological University Library

on NBTI could be further supported by the influence of SPT on the channel-length dependence of NBTI. As shown in Fig. 6.5, no improvement by SPT is observed for the channel length longer than 0.8 μm, and the relative NBTI improvement by SPT is more significant for a shorter channel length. The most possible reason for this channel-length dependence is that the reduction in vertical tensile stress by SPT is more significant for a shorter channel length.

Positions	T = 25°C		T = 75°C		T = 125°C	
(x = 0)	SPT	No SPT	SPT	No SPT	SPT	No SPT
Longitudinal stress (MPa)	-473	-408	-448	-381	-423	-355
Transverse stress (MPa)	-21.4	24.5	-19.4	26.5	-17.4	28.4
Vertical stress (MPa)	397	496	379	476	361	456

Table 6.2: *A summary of the extracted stress values at the interface for devices with and without SPT along the longitudinal, transverse and vertical directions, at three different temperatures.*

From above discussion, SPT is found to reduce NBTI degradation in *p*-MOSFETs quite significantly, and the effect of stress/strain on NBTI is used to explain the improvement of NBTI by SPT in terms of first-principles calculation and process simulation. It is understandable that SPT can enhance the transfer of stress during subsequent deposition of compressive stressed nitride liner by removing spacer 2, since the resulting spacer is thinner, i.e., the distance between nitride liner and channel is shorter. However, how it reduces the vertical tensile stress is still not so clear. It might be qualitatively explained as follows. As can be seen in Fig. 6.2, SEM cross sections clearly show that: the device with SPT has a thinner L-shaped spacer and thus has a sharp corner when contacting with the nitride liner (i.e., with an L-shaped interface), while the device without SPT has a thicker spacer, which contacts with

ATTENTION: The Singapore Copyright Act applies to the use of this document. Nanyang Technological University Library

nitride liner through a smoother surface of spacer 2. For the device with SPT, a shorter distance between channel and nitride liner (due to thinner spacer) mainly contributes to the enhanced longitudinal compressive stress, while the L-shaped interface between spacer and nitride liner might lead to a reduced vertical tensile stress, since compressive stress at the corner of L-shaped spacer (which is near the edge of channel region) can be transferred more effectively in all directions and thus partially compensate tensile stress along the vertical direction. Further process simulation at different temperature, as shown in Table 6.2, also predicts the same trend that SPT would reduce vertical tensile stress but increase longitudinal compressive stress, although it is not directly proven by stress measurement since it is difficult to determine experimentally the exact distribution of stress/strain profile in real device, especially when the device is small, which is also why we use process simulation here to simulate stress profile.

Furthermore, the effect of strain/stress, in terms of the results by experimental investigation, first-principles calculation and process simulation, as discussed above, can be used to explain the improvement of NBTI by SPT. However, it should be carefully accessed when the strain is used to explain NBTI. For SPT process, the stress/strain is induced after the oxide growth and thus it has very negligible impact on the gate oxide. If the strain is introduced before the oxide growth, the strain in channel might cause structural difference in the Si substrate and thus have an impact on the gate oxide growth. As a result, the effect of strain is more complicated and the ultrathin gate oxide becomes another important factor that affects the behavior of NBTI degradation.

ATTENTION: The Singapore Copyright Act applies to the use of this document. Nanyang Technological University Library

6.3 Impact of Laser Spike Annealing on NBTI

In advanced technology nodes, besides stress engineering, novel junction profile engineering techniques, such as laser annealing (LA) or laser spike annealing (LSA) [200-202], are also widely adapted to further boost device performance. LA is hotter than the conventional rapid thermal annealing (RTA) or spike annealing (SA), and thus can be carried out in an ultra-short time, typically in the micro/nano-second range, mainly to minimize dopant out-diffusion and form an ultra-shallow doping profile. LA can increase dopant activation and effectively remove implantation defects as well. However, due to process integration and manufacturability issues, LA is normally implemented together with the conventional spike-RTA. In this study, LA is inserted after spike annealing, which is denoted as "laser spike annealing (LSA)" process.

6.3.1 Experimental

The devices used in this study are fabricated by 45nm low-power process with either conventional spike-RTA or LSA. The nitrided gate oxide thickness is about 18 Å, and the nominal voltage (V_{dd}) is -1.1 V. The channel width is 2 μm and the channel length is 48 nm. In the following discussion, the control sample that implements spike-RTA process is denoted as "Spike", while the sample fabricated with LSA process is denoted as "LSA". For the NBTI stress conditions, the stress temperature (T_{str}) is in the range of 25~125 °C and the gate stress voltage (V_{gstr}) is in between -1.6 V to -3.0 V, and the default stress condition corresponds to T_{str} = 125 °C and V_{gstr} = -2.3 V. For NBTI measurement, the conventional current-voltage (I-V) sweep method is used here to measure the drain current degradation and threshold voltage shift

ATTENTION: The Singapore Copyright Act applies to the use of this document. Nanyang Technological University Library

(ΔV_{th}). Moreover, to minimize measurement-induced recovery during NBTI characterization, the technique of single-point saturation drain current (I_{dsat}) measurement [182] is used to extract the threshold voltage shift (ΔV_{th}) and the device lifetime is also extrapolated for different V_{gstr} at T_{str} = 125 °C.

6.3.2 Results & Discussion

As can be seen in Fig. 6.12, LSA can improve the electrical performance of *p*-MOSFETs by as much as 5%. In this section, the impact of LSA on NBTI and the device lifetime are to be investigated. Figure 6.13 clearly shows that the electrical performance of *p*-MOSFETs is largely degraded in terms of typical *I*-*V* characteristics of the device, such as I_{dsat}, I_{dlin}, and G_m, when NBTI stress is applied.

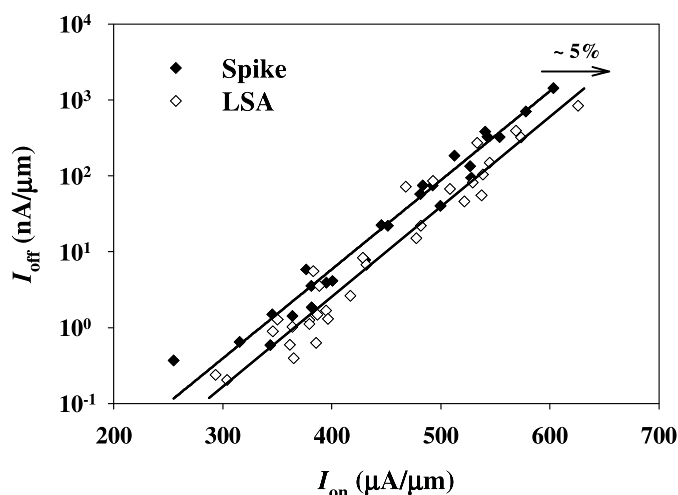

Figure 6.12: *Electrical performance comparisons of p-MOSFETs with laser spike annealing (denoted as "LSA") and spike-RTA process (denoted as "Spike"). About 5% I_{on} improvement is achieved by LSA.*

ATTENTION: The Singapore Copyright Act applies to the use of this document. Nanyang Technological University Library

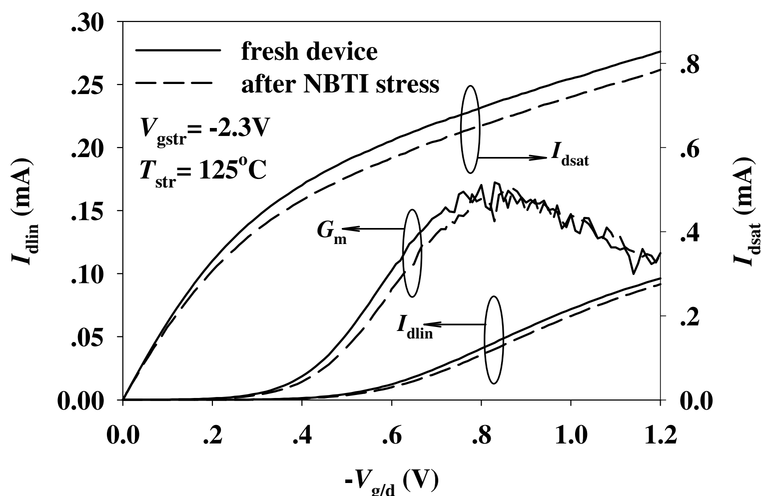

Figure 6.13: *Typical I_d-V_g and I_d-V_d sweep curves for p-MOSFETs with LSA process, before and after the NBTI stress of 1000 s.*

Moreover, the comparison of NBTI degradation, in terms of threshold voltage shift (ΔV_{th}) and NBTI-induced drain current decrease (both ΔI_{dsat} and ΔI_{dlin}), between the samples with spike-RTA and LSA are shown in Fig. 6.14. Figure 6.14(a) shows ΔV_{th} as a function of stress time and it is quite clear that LSA yields a much higher ΔV_{th} than the conventional spike-RTA process. The same conclusion also holds for NBTI-induced drain current degradation (both ΔI_{dsat} and ΔI_{dlin}), as shown in Fig. 6.14(b). Indeed, LSA-worsen NBTI could be mainly due to more damages induced by the subsequent laser annealing process at/near the substrate/oxide interface or even in the gate oxide, and the additional damages would either increase the initial defect density of Si-H bonds at the interface or form more oxide trap centers that favor hole trapping and hydrogen diffusion as well. As a result, upon NBTI stress, the reaction occurs more readily, and thus interface trap generation and/or hole trapping will be enhanced, which in turn lead to LSA-worsen NBTI.

ATTENTION: The Singapore Copyright Act applies to the use of this document. Nanyang Technological University Library

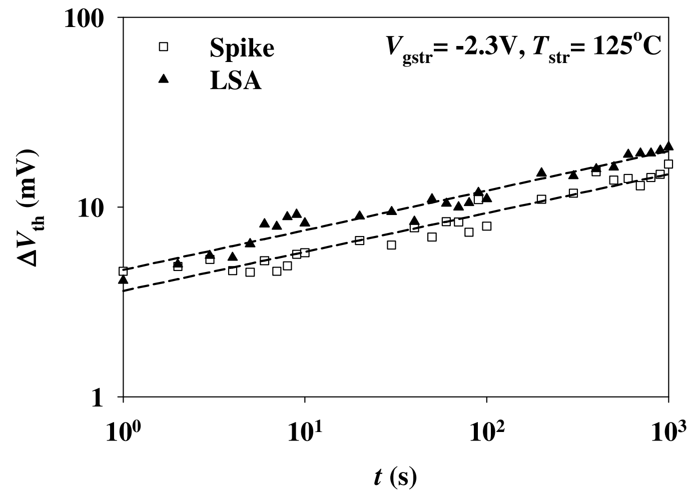

(a)

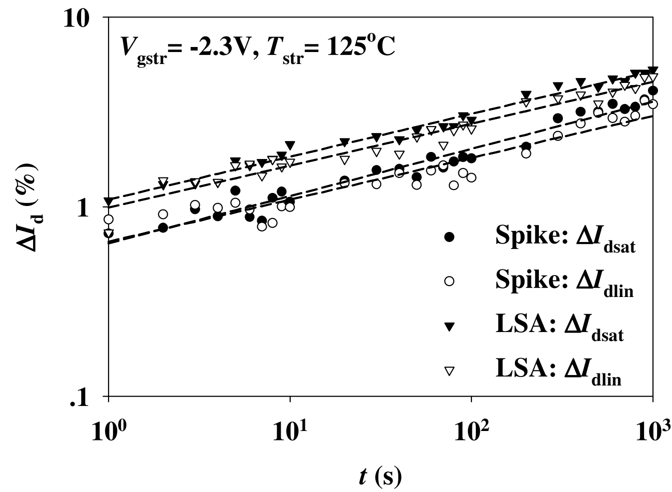

(b)

Figure 6.14: *Comparison of NBTI degradation between the samples with spike-RTA and LSA process. The threshold voltage shift* (ΔV_{th}) *(a), the shift in saturation drain current* (ΔI_{dsat}) *and the shift in linear drain current* (ΔI_{dlin}) *(b) are measured as a funtion of stress time (t) at gate stress voltage* (V_{gstr}) *of -2.3 V and stress temperature* (T_{str}) *of 125 °C.*

ATTENTION: The Singapore Copyright Act applies to the use of this document. Nanyang Technological University Library

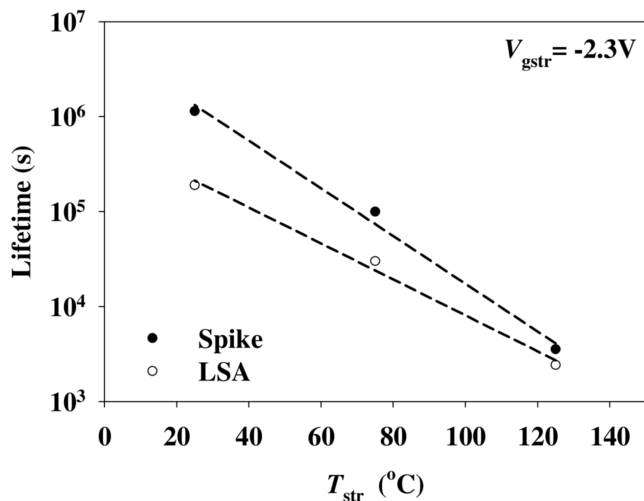

(a)

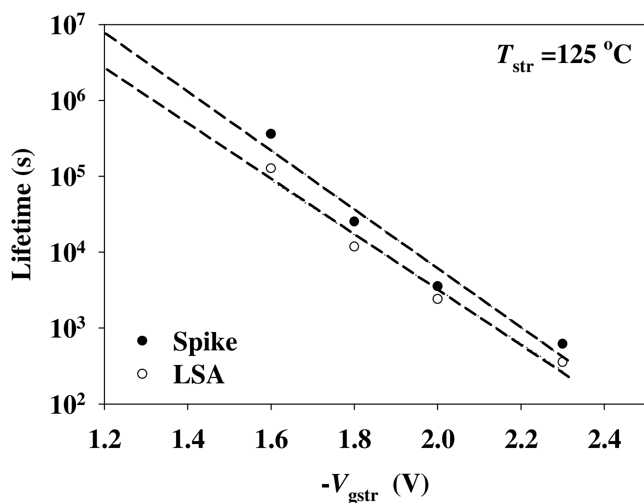

(b)

Figure 6.15: *The extrapolated device lifetime for both the samples with spike-RTA and LSA process.*

Moreover, device lifetimes for both samples with spike-RTA and LSA processes can be obtained and the results are shown in Fig. 6.15. Here the device failure

ATTENTION: The Singapore Copyright Act applies to the use of this document. Nanyang Technological University Library

criterion is based on ΔV_{th} criterion: if V_{th} of a device in magnitude increases by 5% of V_{dd}, i.e. 60 mV, the device is considered as "failed". It is further confirmed that the device lifetime for the sample with LSA process is much lower than that with spike-RTA process, either at V_{gstr} = -2.0V for different T_{str}, as shown in Figure 6.15(a), or at T_{str} = 125 °C for different V_{gstr}, as shown in Fig. 6.15(b). However, from the results shown in Fig. 6.15, the device lifetime for either sample with spike-RTA or LSA is much shorter than the target of equivalent 5-year DC lifetime. Therefore, further process optimization on spike-RTA and LSA is required.

6.4 Characterization of NBTI in High-performance p-MOEFETs with Ultrathin Gate Dielectrics

As discussed in previous sections, impact of various process technologies on NBTI in 65nm- or 45nm-node low-power devices could be quite significant. It shows that NBTI degradation in *p*-MOSFETs has become a most critical device reliability issue for advanced technology nodes. In fact, NBTI degradation is much more severe in high-performance devices, because the gate dielectric is more aggressively down-scaled for high-performance devices so as to achieve a much higher drive current, which in turn leads to higher leakage and more power consumption as well. Therefore, a high-quality ultra-thin gate dielectric is quite critical for achieving the goals of high performance, low leakage and good device reliability as well. In this section, characterization of NBTI in high-performance *p*-MOSFETs with ultrathin gate nitrided oxide is carried out, and NBTI degradation is observed to be quite significant even at or slightly above the operating voltage.

ATTENTION: The Singapore Copyright Act applies to the use of this document. Nanyang Technological University Library

6.4.1 Experimental

The *p*-MOSFETs used here are fabricated by a 65 nm high-performance process. The nitrided gate oxide is grown by rapid thermal oxidation (RTO), followed by de-coupled plasma nitridation (DPN). After that, the sample is annealed in N_2 at 1000°C and then subjected to O_2 anneal at 1100°C. The thickness of nitrided gate oxide is about 11.5 Å. The channel width and length are 2 μm and 60 nm, respectively. The nominal voltage (V_{dd}) is -1.1 V. To minimize measurement-induced recovery during NBTI characterization, the technique of single-point saturation drain current (I_{dsat}) measurement [182] is used to extract the threshold voltage shift (ΔV_{th}). The stress temperature (T_{str}) is in the range of 25~125 °C and the gate stress bias (V_{gstr}) is in the range of -1.21 V to -2.0 V. Moreover, the conventional *I-V* sweep method and the 1st on-the-fly (OTF) measurement method [40, 152] in a short time range are conducted to re-confirm the trend that is observed with the single-point I_{dsat} method.

6.4.2 Results and Discussion

Typical NBTI degradation (ΔV_{th}) in high-performance *p*-MOSFETs at different T_{str} and V_{gstr} are shown in Fig. 6.16. Fig. 6.16(a) clearly shows that at V_{gstr} = -1.5 V, higher T_{str} yields higher NBTI degradation, while Fig. 6.16(b) shows that ΔV_{th} is larger for larger V_{gstr} (in magnitude) at T_{str} = 125 °C. Moreover, as shown in Fig. 6.16(b) also, NBTI degradation at low V_{gstr} of -1.21 V, i.e., 1.1*V_{dd}, is observed to be quite significant. This clearly indicates that NBTI in high-performance devices with ultra-thin nitrided gate oxides of less than 12Å is quite severe.

ATTENTION: The Singapore Copyright Act applies to the use of this document. Nanyang Technological University Library

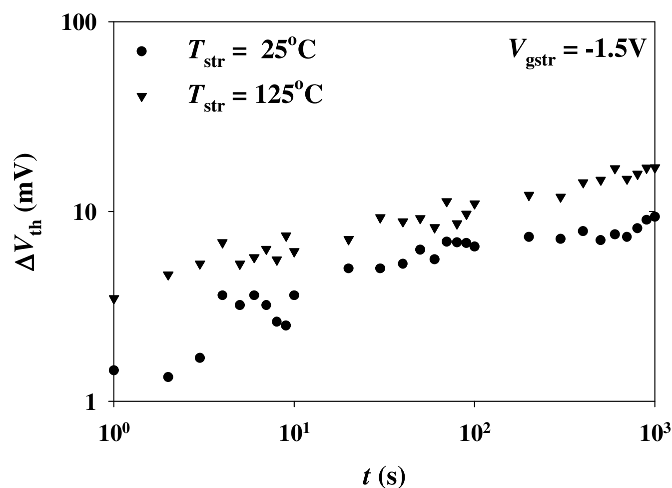

(a)

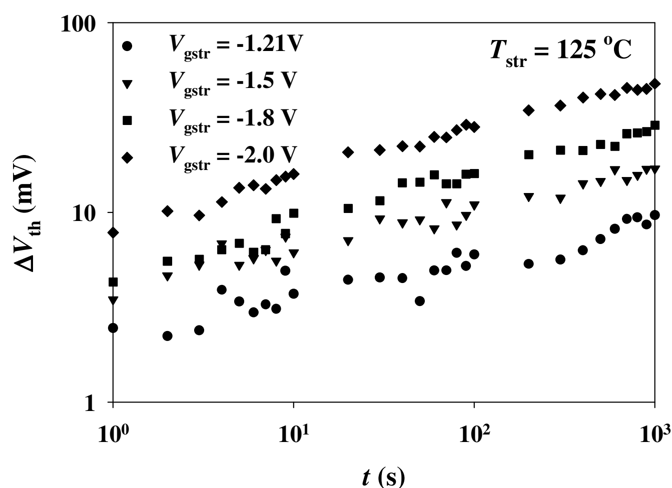

(b)

Figure 6.16: *NBTI degradation in high-preformance p-MOSFETs with ultra-thin nitrided gate oxide. The threshold voltage shift (ΔV_{th}) are measured as a funtion of stress time (t): (a) at gate stress voltage V_{gstr} = -1.5V for different stress temperatures T_{str}; and (b) at T_{str} = 125 °C for different V_{gstr}.*

ATTENTION: The Singapore Copyright Act applies to the use of this document. Nanyang Technological University Library

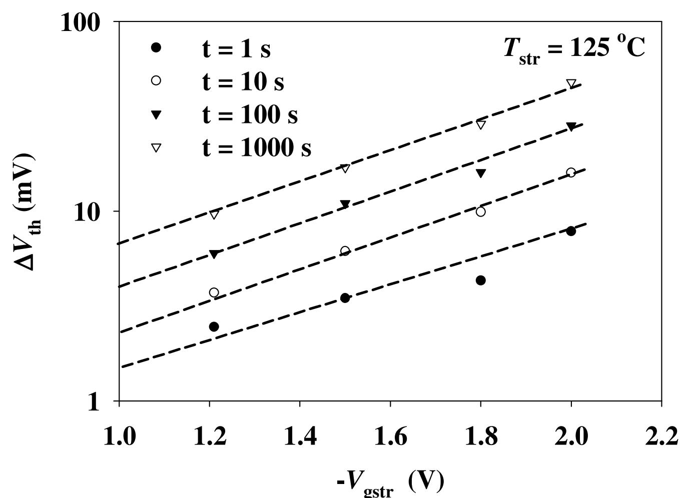

Figure 6.17: *The threshold voltage shift (ΔV_{th}) in high-performance p-MOSFETs as a funtion of V_{gstr} at T_{str} = 125 °C for stress time of 1, 10, 100, 1000s.*

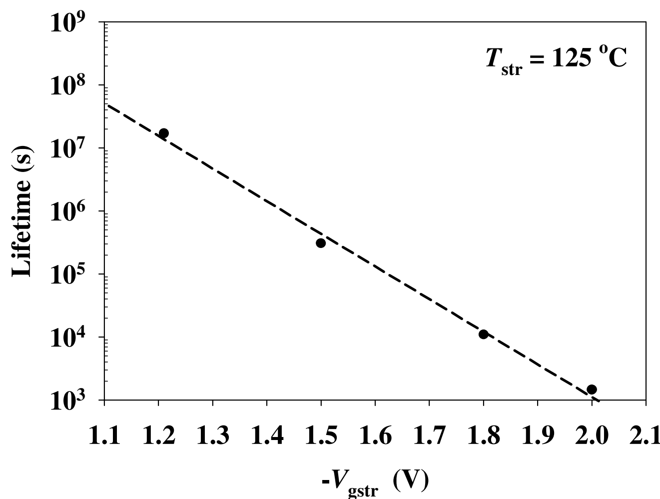

Figure 6.18: *The extrapolated device lifetime of high-performance p-MOSFETs at T_{str} = 125 °C and different V_{gstr}. The lines are for guiding the eyes only.*

Moreover, Fig. 6.17 shows the plot of ΔV_{th} as a function of V_{gstr} at T_{str} = 125 °C for stress time of 1, 10, 100, 1000 s. As can be seen in the figure, regardless of the stress time, NBTI-induced ΔV_{th} follows the same trend, and ΔV_{th} at operating voltage

ATTENTION: The Singapore Copyright Act applies to the use of this document. Nanyang Technological University Library

can be estimated from the plot, which is in the range of 1 to 10 mV at T_{str} = 125 °C, depending on the stress time. As the time goes on, NBTI degradation is expected to be quite significant even at operating voltage. Furthermore, Fig. 6.17 shows the extrapolated device lifetime of high-performance *p*-MOSFETs at T_{str} = 125 °C for different V_{gstr}, where the lifetime is extracted, based on ΔV_{th} at 5% of V_{dd}, i.e. 55mV. From the results shown in Fig. 6.17, the device lifetime of high-performance *p*-MOSFETs is less than 5×10^7 s (equivalent to ~1.6 years), which is lower than the target of equivalent 5-year DC lifetime. Therefore, further process optimization is needed to pass NBTI qualification for high-performance *p*-MOSFETs with ultra-thin nitrided gate oxide.

6.5 Summary

In summary, the impact of various process technologies on NBTI in *p*-MOSFETs has been examined. SPT can improve NBTI quite significantly. Strain effect on NBTI is examined with first-principles calculation, which shows that a larger strain leads to higher NBTI degradation. Process simulation shows that although the compressive stress along the channel direction is enhanced by SPT, the vertical tensile stress is greatly reduced by SPT, and it is believed to be responsible for NBTI improvement by SPT. On the other hand, LSA worsens NBTI degradation, and it might be mainly due to the damage induced by the high temperature laser annealing process at the interface or in the gate oxide. Moreover, NBTI degradation in high-performance devices with ultrathin gate oxides has been observed to be quite significant even at or slightly above the operating voltage.

ATTENTION: The Singapore Copyright Act applies to the use of this document. Nanyang Technological University Library

CHAPTER 7 CONCLUSION AND RECOMMENDATIONS

This thesis has presented research work on the characterization and modeling of negative bias temperature instability (NBTI) in *p*-MOSFET. This work has covered a systematical study on NBTI degradation in *p*-MOSFETS with ultra-thin nitrided gate oxides and thus further enhanced the understanding of NBTI mechanism, in terms of experimental investigations, physical modeling and atomic modeling as well. In this chapter, the overall work presented in this thesis is briefly summarized, and some suggestions are also given for future work.

7.1 Conclusion

7.1.1 Characterization of NBTI and NBTI Recovery

NBTI in *p*-MOSFETs is significantly underestimated by using the conventional characterization techniques due to severe NBTI recovery during the measurements. Therefore, a simple NBTI characterization technique of measuring single-point saturation drain current has been proposed to minimize unwanted NBTI recovery during measurement. This method is accurate as proven by a carefully-designed experiment. With this method, the measurement time can be reduced and thus a closer-to-real threshold voltage shift is obtained, which in turn yields a more reliable

ATTENTION: The Singapore Copyright Act applies to the use of this document. Nanyang Technological University Library

power-law factor. Obviously, accurate information of these parameters is very critical for the understanding of NBTI mechanism and depicts a more realistic NBTI picture.

Since NBTI in *p*-MOSFETs has become one of the key device reliability challenges for advanced CMOS technology nodes, NBTI in-line test becomes quite crucial and necessary. NBTI in-line test has been developed here to monitor NBTI degradation in device during development. With in-line test, we can directly examine the impact of new process technologies on NBTI during development, rather than wait until the device is done but found to fail in the NBTI off-line qualification test. Moreover, if well benchmarked, NBTI in-line test could become an alternative tool for process qualification and the results from NBTI in-line test could also be used for the purpose of process optimization.

NBTI gets recovered immediately when the stress is removed. As a result, the electrical measurement always tends to underestimate NBTI degradation due to its unavoidable measurement time. This measurement-induced additional NBTI recovery must be taken into account because it directly affects the time frame, especially during NBTI recovery. In our work, highly-reproducible NBTI recovery phenomenon is observed, and hence by using different measurement time intervals for the characterization of NBTI recovery, the critical measurement time can be extracted. Thereafter, within the modulated time frame, a combined empirical model for NBTI recovery has been proposed to describe the entire process of NBTI recovery in a wide time range, and the effect of measurement time delay on NBTI has also been examined.

ATTENTION: The Singapore Copyright Act applies to the use of this document. Nanyang Technological University Library

7.1.2 Modeling and Geometry Dependence of NBTI

A compressive study on the modeling of NBTI has been given in this work. An analytical reaction-diffusion (R-D) model within the framework of standard R-D model has been proposed. This model can well describe the NBTI process in a wide time scale covering the three regimes of reaction, transition and diffusion. A power-law factor of ~1 is experimentally observed for the nitrided gate oxides, which shows clear evidence of the existence of the reaction-limited regime for NBTI. The analytical R-D model can also be used to examine the nitrogen effect on NBTI. Moreover, the analytical R-D model has been extended to include the cases of other possible hydrogen diffusing species, such as the hydrogen ion H^+ and hydrogen molecule H_2.

Besides, an analytical geometry-dependent R-D model has been established for two- or three-dimensional hydrogen diffusion, and the geometry dependence of NBTI has been extensively studied. It is experimentally observed that NBTI increases when the channel-length or channel-width decreases. The increase of NBTI with decreasing channel-length can be attributed to the enhancement of the NBTI reaction due to the increase of stress/strain in device as a result of channel-length reduction, which is proven by process simulation. Stress effect on the NBTI reaction is examined by first-principles calculation. It is found that NBTI degradation is worsen by strain, in terms of the NBTI reaction energy E_R and the bond breaking of Si-H bonds at the interface. Therefore, the increase of NBTI with decreasing channel-length can be mainly attributed to the enhancement of the NBTI reaction by the increase of stress as a result of channel-length reduction. On the other hand, the increase of NBTI with decreasing channel-width is explained in terms of the evolution of hydrogen diffusion

ATTENTION: The Singapore Copyright Act applies to the use of this document. Nanyang Technological University Library

towards a two- or three-dimensional diffusion with channel-width reduction.

7.1.3 Nitrogen Effects on NBTI and Modeling of Nitrogen-worsen NBTI

Nitrogen-worsen NBTI in *p*-MOSFETs has been systematically studied by using experimental investigations, physical modeling and atomic modeling. The nitrided gate oxide samples are prepared by different nitridation processes and the experimental results show that both interfacial nitrogen concentration and nitrogen depth profile play important roles in the nitrogen-worsen NBTI, which indeed can be well described by an analytical reaction-dispersive-diffusion (R-DD) model in the diffusion-limited regime. The R-DD model is mainly based on our previous analytical R-D model by incorporating dispersive nature of hydrogen diffusion in NBTI process. In addition, the influence of dispersive hydrogen diffusion on NBTI has been examined, and the NBTI experiments further verify that the R-DD model can well explain NBTI degradation including its dependence on stress time, stress temperature and interfacial nitrogen concentration, and power-law behaviors as well. Furthermore, first-principles calculation has been carried out to examine the effects of nitrogen either as the reaction site at the interface or as adjacent atoms near the interface, in terms of the reaction energy of NBTI reaction. Lower reaction energies due to the incorporation of nitrogen suggest that nitrogen is a more effective hydrogen-originated hole-trapping center than oxygen, and hence worsens NBTI. Nevertheless, it has been found that the trapping at vacancy defect has the strongest dependence on the effect of nitrogen as adjacent atoms. Lastly, the role of nitrogen in NBTI is investigated, in terms of its influence on the electro-negativity and atomic charge distribution of nitrogen, oxygen and silicon atoms at the interface.

ATTENTION: The Singapore Copyright Act applies to the use of this document. Nanyang Technological University Library

7.1.4 Impacts of Advanced Process Technologies on NBTI

NBTI in 65nm or 45nm node *p*-MOSFETs with ultrathin gate dielectrics is investigated, and in particular, the impacts of process technologies on NBTI have been examined. Stress proximity technique (SPT) is found to improve NBTI quite significantly. The effect of strain on NBTI is examined with first-principles calculation, which shows that larger strain leads to higher NBTI degradation. Process simulation shows that although compressive stress along the channel direction is enhanced by SPT, vertical tensile stress is greatly reduced by SPT, which is believed to be responsible for the improvement of NBTI. On the other hand, LSA worsens NBTI, which might be mainly due to the damage induced by high-temperature laser annealing process at the interface or in the oxide. Moreover, NBTI in high-performance devices with ultrathin nitrided gate oxides has been examined. It is found that NBTI can be quite pronounced even at or slightly above the operating voltage, which in turn makes NBTI one of the most critical device reliability challenges for further down-scaling of gate dielectrics.

7.2 Recommendations

7.2.1 Physical Modeling of NBTI Recovery and Dynamic NBTI

As reviewed in Chapter 2, NBTI recovery phenomenon was widely observed and reported [40, 77, 79, 152, 167-170]. In Chapter 3, some experimental investigations of

ATTENTION: The Singapore Copyright Act applies to the use of this document. Nanyang Technological University Library

NBTI recovery was carried out, and measurement effect on NBTI and NBTI recovery was also examined. Although various NBTI models have been proposed and in our work the reaction-diffusion model has been solved analytically so as to describe the NBTI process in a wider time scale for nitrided gate oxides, very few physical models for NBTI recovery have been developed.

Regardless of the physical models, NBTI recovery is believed to associate closely with either re-passivation of interface trap or hole de-trapping of oxide traps, or both. Indeed, within these NBTI models, NBTI recovery could be addressed accordingly and hence these physical models can be validated by comparing the results between analytical prediction and experimental observation in both NBTI and NBTI recovery phases. Moreover, the model for NBTI recovery can benefit a lot in real application. Together with NBTI model, it can be used to predict more accurate device lifetime due to dynamic NBTI stress, since, in real application, the device is operating under AC condition.

7.2.2 Identification of Hydrogen-related Diffusion Species

NBTI is mainly attributed to the generation of interface trap (N_{it}) and/or oxide trapped charge (N_{ot}) in devices under NBTI stress. The interface trap is generated from the dissociation of hydrogen-terminated trivalent Si-H bonds at the interface with the interaction of hole in the inversion layer under NBTI stress. The released hydrogen species diffuses away from the interface, and it initially favors interface trap generation but starts to limit the further generation as time goes on. Based on the reaction-diffusion model [61, 68, 132-134, 211], which is also extensively studied in

ATTENTION: The Singapore Copyright Act applies to the use of this document. Nanyang Technological University Library

our work, particularly in Chapter 4, or other N_{it}-based models as reviewed in Chapter 2, the nature of hydrogen species could affect the behaviors of NBTI greatly, in terms of its time-dependence, temperature-dependence and stress-voltage-dependence. On the other hand, hole trapping in oxide trap might also be affected by hydrogen diffusion. Therefore, an identification of the hydrogen-related diffusing species, which could be the neutral atomic hydrogen (H^o), hydrogen ion or proton (H^+), molecular hydrogen (H_2), or even as a part of the hydroxyl group (OH), hydronium (H_3O^+) and hydroxide ions (OH^-), would help further understand the underlying NBTI mechanism.

7.2.3 NBTI for High-K Gate Dielectrics

In order to further boost device performance and reduce the leakage as well, the high-k/metal-gate scheme has been implemented, first by Intel in 45nm-node manufacturing process and followed by worldwide other leading semiconductor companies in 32nm technology node and beyond. Indeed, both NBTI and PBTI have become most critical reliability issues for HfO_2-based high-k dielectrics [91, 233-236]. A lot of research work in this area has been carried out in recent years, but much still has to be further studied about the land lying under the ice, so as to reveal the underlying BTI mechanism in high-k dielectrics, in terms of experimental instigations, physical modeling and atomic modeling. Moreover, dynamic BTI degradation in high-k dielectrics and the impact of NBTI, PBTI and their interaction on digital and analog integrated circuits (ICs) can also be systematically studied.

ATTENTION: The Singapore Copyright Act applies to the use of this document. Nanyang Technological University Library

List of Publications

Journals:

1. **J. B. Yang**, T. P. Chen, S. S. Tan and L. Chan, "Analytical reaction-diffusion model and the modeling of nitrogen-enhanced negative bias temperature instability", *Appl. Phys. Lett.*, 88, 172109 (2006).
2. **J. B. Yang**, T. P. Chen, S. S. Tan and L. Chan, "A simple negative bias temperature instability characterization methodology to minimize the immediate recovery effect during measurement", *Jpn. J. Appl. Phys.*, Vol. 45, No. 8A, pp. 6137-6140, (2006).
3. **J. B. Yang**, T. P. Chen, S. S. Tan, C. M. Ng and L. Chan, "Modeling and characterization of nitrogen-enhanced negative bias temperature instability in *p*-channel MOSFETs," *J. Electrochem. Soc.*, 154 (12), G255-G261 (2007).
4. **J. B. Yang**, T. P. Chen, S. S. Tan, C. M. Ng, and L. Chan, "Influence of hydrogen dispersive diffusion in nitrided gate oxide on negative bias temperature instability", *Appl. Phys. Lett.*, 93, 013501 (2008).
5. **J. B. Yang**, T. P. Chen, Y. Gong, S. S. Tan, C. M. Ng, and L. Chan, "Improvement of negative bias temperature instability by stress proximity technique", *IEEE Trans. Electron Devices*, 57, No. 1, p. 238-243 (2010).
6. **J. B. Yang**, T. P. Chen, Y. Gong, S. S. Tan, C. M. Ng, and L. Chan, "Geometry dependence of negative bias temperature instability in *p*-channel MOSFETs", submitted to *J. Appl. Phys.*.
7. **J. B. Yang**, T. P. Chen, S. S. Tan, C. M. Ng, and L. Chan, "Characterization of negative bias temperature instability recovery within the modulated measurement time frame", submitted to *J. Phys. D: Appl. Phys.*.

ATTENTION: The Singapore Copyright Act applies to the use of this document. Nanyang Technological University Library

8. **J. B. Yang**, T. P. Chen, S. S. Tan, C. M. Ng and L. Chan, "An analytical reaction-dispersive-diffusion model and the influence of nitridation process on negative bias temperature instability", submitted to *Jpn. J. Appl. Phys.*.

Conferences:

1. **J. B. Yang**, T. P. Chen, S. S. Tan and L. Chan, "A novel empirical model for NBTI recovery with the modulated measurement time frame", 13th IEEE International Symposium on the Physical and Failure Analysis of Integrated Circuits (IPFA 2006), 3 to 7 July 2006, Meritus Mandarin, Singapore.
2. **J. B. Yang**, T. P. Chen, S. S. Tan, C. M. Ng and L. Chan, "Modeling and characterization of negative bias temperature instability in p-channel MOSFETs", invited talk, Ninth International Symposium on Silicon Nitride, Silicon Dioxide Thin Insulating Films and Emerging Dielectrics, 211th Meeting of The Electrochemical Society, May 6-11, 2007, Chicago, USA.

ATTENTION: The Singapore Copyright Act applies to the use of this document. Nanyang Technological University Library

BIBLIOGRAPHY

[1] W. Shockley, "The theory of p-n junctions in semiconductors and p-n junction transistors," *Bell Syst. Tech. J.,* vol. 28, pp. 435-439, 1949.

[2] J. Bardeen and W. Brattain, "The transistor, a semi-conductor triode," *Physical Review,* vol. 74, pp. 230-231, 1948.

[3] J. E. Lilienfeld, "Method and apparatus for controlling electric currents," *US Patent 1745175,* 1930.

[4] J. E. Lilienfeld, "Device for controlling electric current," *US Patent 1900018,* 1933.

[5] O. Heil, "Improvements in or relating to electrical amplifiers and other control arrangements and devices," *GB Patent 439457,* 1934.

[6] D. Kahang and M. M. Atalla, "Silicon-silicon dioxide field induced surface devices," *IRE Solid-State Device Res. Conf.,* 1960.

[7] F. Wanlass and C. T. Sah, "Nanowatt logic using field-effect metal-oxide-semiconductor triodes," *IEEE Int. Solid-State Circuits Conf.,* pp. 32-33, 1963.

[8] J. S. Kilby, "Invention of the integrated circuits," *IEEE Transaction on Electron Devices,* vol. 23, pp. 648-654, 1976.

[9] G. E. Moore, "Cramming more components onto integrated circuits," *Electronics Magazine,* vol. 38, 1965.

[10] G. E. Moore, "Progress in digital integrated circuit," *IEDM Tech. Dig.,* pp.

ATTENTION: The Singapore Copyright Act applies to the use of this document. Nanyang Technological University Library

11-13, 1975.

[11] C. Hu, "Future CMOS scaling and reliability," *Proceedings of the IEEE,* vol. 81, pp. 682-689, 1993.

[12] Y. Taur, D. A. Buchanan, W. Chen, D. J. Frank, K. E. Ismail, S. H. Lo, G. A. Sai-Halasz, R. G. Viswanathan, H. C. Wann, S. J. Wind, and H. S. Wong, "CMOS scaling into the nanometer regime," *Proceedings of the IEEE,* vol. 85, pp. 486-504, 1997.

[13] S. Asai and Y. Wada, "Technology challenges for integration near and below 0.1 micrometers," *Proceedings of the IEEE,* vol. 85, pp. 505-520, 1997.

[14] M. M. Atalla, "Semiconductor devices having dielectric coatings," *U.S. Patent 3206670,* 1965.

[15] *The International Technology Roadmap for Semiconductors (ITRS), International Semiconductor Association (ISA),* 2007.

[16] P. Olivo, T. N. Nguyen, and B. Ricco, "High-field-induced degradation in ultra-thin SiO2 films," *IEEE Transactions on Electron Devices,* vol. 35, pp. 2259-2267, 1988.

[17] D. J. Dimaria and E. Cartier, "Mechanism for stress-induced leakage currents in thin silicon dioxide films," *Journal of Applied Physics* vol. 78, pp. 3883-3894, 1995.

[18] M. Depas, T. Nigam, and M. M. Heyns, "Soft breakdown of ultra-thin gate oxide layers," *IEEE Transactions on Electron Devices,* vol. 43, pp. 1499-1504, 1996.

ATTENTION: The Singapore Copyright Act applies to the use of this document. Nanyang Technological University Library

[19] D. J. DiMaria and J. H. Stathis, "Ultimate limit for defect generation in ultra-thin silicon dioxide," *Applied Physics Letters* vol. 71, pp. 3230-3232, 1997.

[20] E. Vincent, S. Bruyere, C. Papadas, and P. Mortini, "Dielectric reliability in deep-submicron technologies: From thin to ultrathin oxides," *Microelectronics Reliability,* vol. 37, pp. 1499-1506, 1997.

[21] J. H. Stathis and D. J. DiMaria, "Reliability projection for ultra-thin oxides at low voltage," in *Technical Digest - International Electron Devices Meeting*, San Francisco, CA, USA, 1998, pp. 167-170.

[22] R. Rodriguez, E. Miranda, R. Pau, J. Sune, M. Nafria, and X. Aymerich, "Monitoring the degradation that causes the breakdown of ultrathin (<5 nm) SiO2 gate oxides," *IEEE Electron Device Letters,* vol. 21, pp. 251-253, 2000.

[23] R. Degraeve, B. Kaczer, and G. Groeseneken, "Reliability: A possible showstopper for oxide thickness scaling?," *Semiconductor Science and Technology,* vol. 15, pp. 436-444, 2000.

[24] K. Okada, "Gate oxide lifetime limited by `B-mode' stress induced leakage current and the scaling limit of silicon dioxides in the direct tunnelling regime," *Semiconductor Science and Technology,* vol. 15, pp. 478-484, 2000.

[25] L. Pantisano and K. P. Cheung, "Stress-induced leakage current (SILC) and oxide breakdown: Are they from the same oxide traps?," *IEEE Transactions on Device and Materials Reliability,* vol. 1, pp. 109-112, 2001.

[26] C. Duvvury, D. J. Redwine, and H. J. Stiegler, "Leakage current degradation in

ATTENTION: The Singapore Copyright Act applies to the use of this document. Nanyang Technological University Library

N-MOSFET's due to hot-electron stress," *Electron device letters,* vol. 9, pp. 579-581, 1988.

[27] Y. Leblebici and S.-M. Kang, "Modeling of nMOS transistors for simulation of hot-carrier-induced device and circuit degradation," *IEEE Transactions on Computer-Aided Design of Integrated Circuits and Systems,* vol. 11, pp. 235-246, 1992.

[28] S. E. Rauch Iii, F. J. Guarin, and G. LaRosa, "Impact of E-E scattering to the hot carrier degradation of deep submicron NMOSFET's," *IEEE Electron Device Letters,* vol. 19, pp. 463-465, 1998.

[29] S. H. Renn, C. Raynaud, J. L. Pelloie, and F. Balestra, "A thorough investigation of the degradation induced by hot-carrier injection in deep submicron N- and P-channel partially and fully depleted unibond and SIMOX MOSFET's," *IEEE Transactions on Electron Devices,* vol. 45, pp. 2146-2152, 1998.

[30] C. Lin, S. Biesemans, L. K. Han, K. Houlihan, T. Schiml, K. Schruefer, C. Wann, J. Chen, and R. Mahnkopf, "Hot carrier reliability for 0.13µm CMOS technology with dual gate oxide thickness," in *Technical Digest - International Electron Devices Meeting*, San Francisco, CA, 2000, pp. 135-137.

[31] N. Kimizuka, T. Yamamoto, T. Mogami, K. Yamaguchi, K. Imai, and T. Horiuchi, "Impact of Bias Temperature Instability for Direct Tunneling Ultrathin Gate Oxide on MOSFET Scaling," in *Proceedings of Symposium on VLSI Technology*, 1999, pp. 73-74.

ATTENTION: The Singapore Copyright Act applies to the use of this document. Nanyang Technological University Library

[32] A. T. Krishnan, V. Reddy, S. Chakravarthi, J. Rodriguez, S. John, and S. Krishnan, "NBTI Impact on Transistor & Circuit: Models, Mechanisms & Scaling Effects," in *Technical Digest - International Electron Devices Meeting*, Washington, DC, 2003, pp. 349-352.

[33] D. K. Schroder and J. A. Babcock, "Negative bias temperature instability: Road to cross in deep submicron silicon semiconductor manufacturing," *Journal of Applied Physics,* vol. 94, pp. 1-18, 2003.

[34] N. Kimizuka, K. Yamaguchi, K. Imai, T. Iizuka, C. T. Liu, R. C. Keller, and T. Horiuchi, "NBTI enhancement by nitrogen incorporation into ultrathin gate oxide for 0.10-μm gate CMOS generation," in *Digest of Technical Papers - Symposium on VLSI Technology*, Honolulu, HI, USA, 2000, pp. 92-93.

[35] Y. Mitani, M. Nagamine, H. Satake, and A. Toriumi, "NBTI mechanism in ultra-thin gate dielectric - Nitrogen-originated mechanism in SiON," in *Technical Digest - International Electron Devices Meeting*, San Francisco, CA, 2002, pp. 509-512.

[36] S. S. Tan, T. P. Chen, J. M. Soon, K. P. Loh, C. H. Ang, and L. Chan, "Nitrogen-enhanced negative bias temperature instability: An insight by experiment and first-principle calculations," *Applied Physics Letters* vol. 82, pp. 1881-1883, 2003.

[37] S. Tsujikawa, T. Mine, K. Watanabe, Y. Shimamoto, R. Tsuchiya, K. Ohnishi, T. Onai, J. Yugami, and S. Kimura, "Negative bias temperature instability of pMOSFETs with ultra-thin SiON gate dielectrics," in *Annual Proceedings -*

ATTENTION: The Singapore Copyright Act applies to the use of this document. Nanyang Technological University Library

Reliability Physics (Symposium), Dallas, TX, 2003, pp. 183-188.

[38] S. Mahapatra, M. A. Alam, P. B. Kumar, T. R. Dalei, and D. Saha, "Mechanism of negative bias temperature instability in CMOS devices: Degradation, recovery and impact of nitrogen," in *Technical Digest - International Electron Devices Meeting, IEDM*, San Francisco, CA, 2004, pp. 105-108.

[39] M. Ershov, S. Saxena, H. Karbasi, S. Winters, S. Minehane, J. Babcock, R. Lindley, P. Clifton, M. Redford, and A. Shibkov, "Dynamic recovery of negative bias temperature instability in p-type metal-oxide-semiconductor field-effect transistors," *Applied Physics Letters* vol. 83, pp. 1647-1649, 2003.

[40] S. Rangan, N. Mielke, and E. C. C. Yeh, "Universal Recovery Behavior of Negative Bias Temperature Instability," in *Technical Digest - International Electron Devices Meeting*, Washington, DC, 2003, pp. 341-344.

[41] S. Chakravarthi, A. T. Krishnan, V. Reddy, C. F. Machala, and S. Krishnan, "A comprehensive framework for predictive modeling of negative bias temperature instability," in *Annual Proceedings - Reliability Physics (Symposium)*, Phoenix, AZ., 2004, pp. 273-282.

[42] M. L. Green, E. P. Gusev, R. Degraeve, and E. L. Garfunkel, "Ultrathin (<4 nm) SiO2 and Si-O-N gate dielectric layers for silicon microelectronics: Understanding the processing, structure, and physical and electrical limits," *Appl. Phys. Rev.,* vol. 90, pp. 2057-2121, 2001.

[43] F. H. P. M. Habraken and A. E. T. Kuiper, "Silicon nitride and oxynitride

ATTENTION: The Singapore Copyright Act applies to the use of this document. Nanyang Technological University Library

films," *Mater. Sci. Eng.,* vol. R12, pp. 123-175, 1994.

[44] L. K. Han, D. Wristers, J. Yan, M. Bath, and D. L. Kwang, "Highly suppressed boron penetration in NO-nitrided SiO2 for p+-polysilicon gated MOS device applications," *IEEE Elec. Dev. Lett.,* vol. 16, pp. 319-321, 1995.

[45] K. S. Chang-Liao and H. C. Lai, "Correlation between nitrogen concentration profile and infrared spectroscopy in silicon dioxide," *Appl. Phys. Lett.,* vol. 72, pp. 2280-2282, 1998.

[46] Y. H. Ha, S. Kim, S. Y. Lee, J. H. Kim, D. H. Baek, H. K. Kim, and D. W. Moona, "Relaxation of the Si lattice strain in the Si(001)-SiO2 interface by annealing in N2O," *Appl. Phys. Lett.,* vol. 74, pp. 3510-3512, 1999.

[47] S. L. Zhang, J. T. Wang, W. Kaplan, and M. Ostling, "Silicon nitride films deposited from SiH2Cl2---NH3 by low pressure chemical vapor deposition: kinetics, thermodynamics, composition and structure," *Thin Solid Films* vol. 213, pp. 182-191, 1992.

[48] D. Wang, T. P. Ma, J. W. Golz, B. L. Halpern, and J. J. Schmitt, "High-quality MNS capacitors prepared by jet vapor deposition at room temperature," *IEEE Elec. Dev. Lett.,* vol. 13, pp. 482-484, 1992.

[49] H. Goto, K. Shibahara, and S. Yokoyama, "Atomic layer controlled deposition of silicon nitride with self-limiting mechanism," *Appl. Phys. Lett.,* vol. 68, pp. 3257-3259, 1996.

[50] H. Kobayashi, T. Mizokuro, Y. Nakato, K. Yoneda, and Y. Todokoro, "Nitridation of silicon oxide layers by nitrogen plasma generated by low

ATTENTION: The Singapore Copyright Act applies to the use of this document. Nanyang Technological University Library

energy electron impact," *Appl. Phys. Lett.,* vol. 71, pp. 1978-1980, 1997.

[51] G. Lucovsky, A. Banerjee, B. Hinds, B. Claflin, K. Koh, and H. Yang, "Minimization of sub-oxide transition regions at Si-SiO2 interfaces by 900°C rapid thermal annealing," *Microelectron. Eng.,* vol. 36, pp. 207-210, 1997.

[52] B. E. Deal, "Standardized terminology for oxide charges associated with thermally oxidized silicon," *Electron Devices, IEEE Transactions on,* vol. 27, pp. 606 - 608, 1980.

[53] T. Yaur and T. H. Ning, *Fundamentals of Modern VLSI Devices*: Cambridge University Express, 1998.

[54] Y. Miura and Y. Matukura, "Investigation of silicon-silicon dioxide interface using MOS structure," *Jpn. J. Appl. Phys.,* vol. 5, p. 180, 1966.

[55] A. Goetzberger and H. E. Nigh, "Surface charge after annealing of Al-SiO2-Si structures under bias," *Proc. IEEE.,* vol. 54, p. 1454, 1966.

[56] B. E. Deal, M. Sklar, A. S. Grove, and E. H. Snow, "Characteristics of the Surface-State Charge (Qss) of Thermally Oxidized Silicon," *Journal of the Electrochemical Society* vol. 114, pp. 266-274, 1967.

[57] A. Goetzberger, A. D. Lopez, and R. J. Strain, "On the formation of surface states during stress aging of thermal Si-SiO2 interfaces," *Journal of the Electrochemical Society* vol. 120, pp. 90-96, 1973.

[58] B. E. Deal, "The Current Understanding of Charges in the Thermally Oxidized Silicon Structure," *Journal of the Electrochemical Society* vol. 121, pp. 198C-205C, 1974.

ATTENTION: The Singapore Copyright Act applies to the use of this document. Nanyang Technological University Library

[59] A. Goetzberger, V. Heine, and E. H. Nicollian, "Surface states in silicon from charges in the oxide coating," *Applied Physics Letters* vol. 12, pp. 95-97, 1968.

[60] D. J. Breed, "A new model for the negative voltage instability in MOS devices," *Applied Physics Letters* vol. 26, pp. 116-118, 1975.

[61] K. O. Jeppson and C. M. Svensson, "Negative bias stress of MOS devices at high electric fields and degradation of MNOS devices," *Journal of Applied Physics* vol. 48, pp. 2004-2014, 1977.

[62] N. Shiono, O. Nakajima, and C. Hashimoto, "Kinetics of changes in Nf and Dit at the Si-SiO2 interface under long-term positive as well as negative bias-temperature aging," *Journal of the Electrochemical Society* vol. 130, pp. 138-143, 1983.

[63] G. Haller, M. Knoll, D. Braunig, F. Wulf, and W. R. Fahrner, "Bias-temperature stress on metal-oxide-semiconductor structures as compared to ionizing irradiation and tunnel injection," *J. Appl. Phys.,* vol. 56, pp. 1844-1850, 1984.

[64] C. E. Blat, E. H. Nicollian, and a. E. H. Poindexter, "Mechanism of negative-bias-temperature instability," *Journal of Applied Physics* vol. 69, pp. 1712-1720, 1991.

[65] C. R. Helms and E. H. Poindexter, "The silicon-silicon-dioxide system: its microstructure and imperfections," *Rep. Prog. Phys.,* vol. 57, pp. 791-854, 1994.

ATTENTION: The Singapore Copyright Act applies to the use of this document. Nanyang Technological University Library

[66] S. Ogawa, M. Shimaya, and N. Shiono, "Interface-trap generation at ultrathin SiO2 (4-6 nm)-Si interface during negative-bias temperature aging," *J. Appl. Phys.,* vol. 77, pp. 1137-1148, 1995.

[67] T. Yamamoto, K. Uwasawa, and T. Mogami, "Bias temperature instability in scaled p+ polysilicon gate p-MOSFET," *IEEE Trans. Electron. Devives,* vol. 46, pp. 921-926, 1999.

[68] S. Ogawa and N. Shiono, "Generalized diffusion-reaction model for the low-field charge-buildup instability at the Si-SiO2 interface," *Physical Review B,* vol. 51, pp. 4218-4230, 1995.

[69] C. H. Liu, M. T. Lee, C. Y. Lin, J. Chen, K. Schruefer, J. Brighten, N. Rovedo, T. B. Hook, M. V. Khare, S. F. Huang, C. Wann, T. C. Chen, and T. H. Ning, "Mechanism and process dependence of negative bias temperature instability (NBTI) for pMOSFETs with ultrathin gate dielectrics," in *Technical Digest - International Electron Devices Meeting*, Washington, DC, 2001, pp. 861-864.

[70] E. Morifuji, T. Kumamori, M. Muta, K. Suzuki, I. De, A. Shibkov, S. Saxena, T. Enda, N. Aoki, W. Asano, H. Otani, M. Nishigori, K. Miyamoto, F. Matsuoka, T. Noguchi, and M. Kakumu, "New considerations for highly reliable PMOSFETs in 100 nm generation and beyond," in *IEEE Symposium on VLSI Circuits, Digest of Technical Papers*, Kyoto, 2001, pp. 117-118.

[71] C. H. Ang, C. M. Lek, S. S. Tan, B. J. Cho, T. Chen, W. Lin, and J. G. Zhen, "Negative bias temperature instability on plasma-nitrided silicon dioxide film," *Japanese Journal of Applied Physics, Part 2: Letters,* vol. 41, 2002.

ATTENTION: The Singapore Copyright Act applies to the use of this document. Nanyang Technological University Library

[72] S. Inaba, T. Shimizu, S. Mori, K. Sekine, K. Saki, H. Suto, H. Fukui, M. Nagamine, M. Fujiwara, T. Yamamoto, M. Takayanagi, I. Mizushima, K. Okano, S. Matsuda, H. Oyamatsu, Y. Tsunashima, S. Yamada, Y. Toyoshima, and H. Ishiuchi, "Device performance of sub-50 nm CMOS with ultra-thin plasma nitrided gate dielectrics," in *Technical Digest - International Electron Devices Meeting*, San Francisco, CA, 2002, pp. 651-654.

[73] C. H. Liu, M. T. Lee, C. Y. Lin, J. Chen, Y. T. Loh, F. T. Liou, K. Schruefer, A. A. Katsetos, Z. Yang, N. Rovedo, T. B. Hook, C. Wann, and T. C. Chen, "Mechanism of threshold voltage shift (Δ Vth) caused by negative bias temperature instability (NBTI) in deep submicron pMOSFETs," *Japanese Journal of Applied Physics, Part 1: Regular Papers and Short Notes and Review Papers,* vol. 41, pp. 2423-2425, 2002.

[74] S. S. Tan, T. P. Chen, C. H. Ang, Y. L. Tan, and L. Chan, "Influence of nitrogen proximity from the Si/SiO2 interface on negative bias temperature instability," *Japanese Journal of Applied Physics, Part 2: Letters,* vol. 41, 2002.

[75] G. Chen, K. Y. Chuah, M. F. Li, D. S. H. Chan, C. H. Ang, J. Z. Zheng, Y. Jin, and D. L. Kwong, "Dynamic NBTI of PMOS transistors and its impact on device lifetime," in *Annual Proceedings - Reliability Physics (Symposium)*, Dallas, TX, 2003, pp. 196-202.

[76] M. F. Li, G. Chen, C. Shen, X. P. Wang, H. Y. Yu, Y. C. Yeo, and D. L. Kwong, "Dynamic bias-temperature instability in ultrathin SiO2 and HfO2 metal-oxide-semiconductor field effect transistors and its impact on device

ATTENTION: The Singapore Copyright Act applies to the use of this document. Nanyang Technological University Library

lifetime," *Japanese Journal of Applied Physics, Part 1: Regular Papers and Short Notes and Review Papers,* vol. 43, pp. 7807-7814, 2004.

[77] S. S. Tan, T. P. Chen, C. H. Ang, and L. Chan, "A new waveform-dependent lifetime model for dynamic NBTI in PMOS transistor," in *Annual Proceedings - Reliability Physics (Symposium)*, 2004, pp. 35-39.

[78] N. K. Jha, P. S. Reddy, D. K. Sharma, and V. R. Rao, "NBTI degradation and its impact for analog circuit reliability," *IEEE Transactions on Electron Devices,* vol. 52, pp. 2609-2615, 2005.

[79] S. S. Tan, T. P. Chen, and L. Chan, "Dynamic NBTI lifetime model for inverter-like waveform," *Microelectronics Reliability,* vol. 45, pp. 1115-1118, 2005.

[80] T. Yang, M. F. Li, C. Shen, C. H. Ang, C. Zhu, Y. C. Yeo, G. Samudra, S. C. Rustagi, M. B. Yu, and D. L. Kwong, "Fast and slow dynamic NBTI components in p-MOSFET with SiON dielectric and their impact on device life-time and circuit application," in *Digest of Technical Papers - Symposium on VLSI Technology*, Kyoto, 2005, pp. 92-93.

[81] Y. Chen, J. Zhou, S. Tedja, F. Hui, and A. S. Oates, "Stress-induced MOSFET mismatch for analog circuits," in *International Integrated Reliability Workshop Final Report*, Lake Tahoe, CA, 2001, pp. 41-43.

[82] S. E. Rauch Iii, "The statistics of NBTI-induced VT and β mismatch shifts in pMOSFETs," *IEEE Transactions on Device and Materials Reliability,* vol. 2, pp. 89-93, 2002.

ATTENTION: The Singapore Copyright Act applies to the use of this document. Nanyang Technological University Library

[83] Y. Nishida, H. Sayama, K. Ohta, H. Oda, M. Katayama, Y. Inoue, H. Morimoto, and M. Inuishi, "SoC CMOS technology for NBTI/HCI immune I/O and analog circuits implementing surface and buried channel structures," in *Technical Digest - International Electron Devices Meeting*, Washington, DC, 2001, pp. 869-872.

[84] H. S. Momose, T. Ohguro, K. Kojima, S. I. Nakamura, and Y. Toyoshima, "1.5-nm gate oxide CMOS on (110) surface-oriented Si substrate," *IEEE Transactions on Electron Devices,* vol. 50, pp. 1001-1008, 2003.

[85] A. Bravaix, D. Goguenheim, N. Revil, and E. Vincent, "Hot-carrier damage in AC-stressed deep submicrometer CMOS technologies," in *International Integrated Reliability Workshop Final Report*, Lake Tahoe, CA, USA, 1999, pp. 61-65.

[86] B. C. Paul, K. Kang, H. Kufluoglu, M. A. Alam, and K. Roy, "Impact of NBTI on the temporal performance degradation of digital circuits," *IEEE Electron Device Letters,* vol. 26, pp. 560-562, 2005.

[87] K. Kang, H. Kufluoglu, M. A. Alam, and K. Roy, "Efficient transistor-level sizing technique under temporal performance degradation due to NBTI," in *IEEE International Conference on Computer Design, ICCD 2006*, San Jose, CA, 2006, pp. 216-221.

[88] R. Kuroda, K. Watanabe, A. Teramoto, M. Mifuji, T. Yamaha, S. Sugawa, and T. Ohmi, "Accurate circuit performance prediction model and lifetime prediction method of NBT stressed devices for highly reliable ULSI circuits,"

ATTENTION: The Singapore Copyright Act applies to the use of this document. Nanyang Technological University Library

in *2006 IEEE International Conference on Integrated Circuit Design and Technology, ICICDT'06*, Padova, 2006.

[89] A. G. Ravesz, "The Role of Hydrogen in SiO2 Films on Silicon," *J Electrochem Soc,* vol. 126, pp. 122-130, 1979.

[90] J. Krauser, F. Wulf, M. A. Briere, J. Steiger, and D. Bra 藹 unig, "Study of hydrogen incorporation in MOS-structures after various process steps using nuclear reaction analysis (NRA)," *Microelectronic Engineering* vol. 22, pp. 65-68, 1993.

[91] K. Onishi, R. Choi, C. S. Kang, H. J. Cho, Y. H. Kim, R. E. Nieh, J. Han, S. A. Krishnan, M. S. Akbar, and J. C. Lee, "Bias-temperature instabilities of polysilicon gate HfO2 MOSFETs," *IEEE Transactions on Electron Devices,* vol. 50, pp. 1517-1524, 2003.

[92] H. H. Tseng, M. E. Ramo?n, L. Hebert, P. J. Tobin, D. Triyoso, J. M. Grant, Z. X. Jiang, D. Roan, S. B. Samavedam, D. C. Gilmer, S. Kalpat, C. Hobbs, W. J. Taylor, O. Adetutu, and B. E. White, "ALD HfO2 using Heavy Water (D2O) for Improved MOSFET Stability," in *Technical Digest - International Electron Devices Meeting*, Washington, DC, 2003, pp. 83-86.

[93] H. H. Tseng, M. E. Ramon, L. Hebert, P. J. Tobin, D. Triyoso, S. Kalpat, J. M. Grant, Z. X. Jiang, D. C. Gilmer, D. Menke, W. J. Taylor, O. Adetutu, and B. E. White, "Threshold voltage instability and plasma induced damage of PolySi/HfO 2 devices - Positive impact of deuterium incorporation," in *2004 International Conference on Integrated Circuit Design and Technology,*

ATTENTION: The Singapore Copyright Act applies to the use of this document. Nanyang Technological University Library

ICICDT, Austin, TX, 2004, pp. 255-259.

[94] T. B. Hook, R. Bolam, W. Clark, J. Burnham, N. Rovedo, and L. Schutz, "Negative bias temperature instability on three oxide thicknesses (1.4/2.2/5.2 nm) with nitridation variations and deuteration," *Microelectronics Reliability,* vol. 45, pp. 47-56, 2005.

[95] S. M. Cho, J. H. Lee, M. Chang, M. S. Jo, H. S. Hwang, J. K. Lee, and S. B. Hwang, "High pressure deuterium annealing effect on nano-scale CMOS devices with different channel width," in *2006 IEEE Nanotechnology Materials and Devices Conference, NMDC*, Gyeongju, 2006, pp. 98-99.

[96] Y. Mitani and H. Satake, "Re-examination of deuterium effect on negative bias temperature instability in ultra-thin gate oxides," in *2006 IEEE International Conference on Integrated Circuit Design and Technology, ICICDT'06*, Padova, 2006.

[97] T. M. Pan, "Channel length dependence of negative bias temperature instability on pMOSFETs with either B- or BF2 -implanted source/drain," *Journal of the Electrochemical Society* vol. 153, 2006.

[98] X. Han and Y. Hao, "NBTI effect of ultra deep-submicron devices," *Pan Tao Ti Hsueh Pao/Chinese Journal of Semiconductors,* vol. 24, pp. 626-630, 2003.

[99] M. Makabe, T. Kubota, and T. Kitano, "Bias-Temperature degradation of pMOSFETs: Mechanism and suppression," *Annual Proceedings - Reliability Physics (Symposium),* pp. 205-209, 10 April 2000 through 13 April 2000 2000.

[100] T. B. Hook, E. Adler, F. Guarin, J. Lukaitis, N. Rovedo, and K. Schruefer,

ATTENTION: The Singapore Copyright Act applies to the use of this document. Nanyang Technological University Library

"The effects of fluorine on parametrics and reliability in a 0.18-um 3.5/6.8 nm dual gate oxide CMOS technology," *IEEE Transactions on Electron Devices,* vol. 48, pp. 1346-1353, 2001.

[101] G. Innertsberger, R. Jurk, J. Felsner, R. Kakoschke, B. Yuwono, T. Schlo?sser, W. Krautschneider, and A. Gschwandtner, "The influence of fluorine on various mos devices," *Materials Research Society Symposium - Proceedings,* vol. 567, pp. 589-595, 1999.

[102] D. Y. Lee, T. Y. Huang, H. C. Lin, W. J. Chiang, G. W. Huang, and T. Wang, "Effects of Process and Gate Doping Species on Negative-Bias-Temperature Instability of p-Channel MOSFETs," *Journal of the Electrochemical Society* vol. 151, 2004.

[103] T. Sasaki, F. Ootsuka, H. Ozaki, T. Hoshi, M. Tomikawa, M. Yasuhira, and T. Arikado, "Effect of boron and fluorine incorporation in SiON gate insulator with optimized nitrogen profile," *Japanese Journal of Applied Physics, Part 1: Regular Papers and Short Notes and Review Papers,* vol. 43, pp. 1837-1842, 2004.

[104] D. M. Fleetwood, X. J. Zhou, L. Tsetseris, S. T. Pantelides, and R. D. Schrimpf, "Hydrogen model for negative bias temperature instabilities in MOS gate dielectrics," in *Proceedings - Electrochemical Society*, Quebec, 2005, pp. 267-278.

[105] T. B. Hook, J. S. Burnham, and R. J. Bolam, "Nitrided gate oxides for 3.3-V logic application: reliability and device design considerations," *IBM Journal of*

ATTENTION: The Singapore Copyright Act applies to the use of this document. Nanyang Technological University Library

Research and Development, vol. 43, pp. 393-406, 1999.

[106] P. Chaparala, J. Shibley, and P. Lim, "Threshold voltage drift in PMOSFETs due to NBTI and HCI," in *International Integrated Reliability Workshop Final Report*, Lake Tahoe, CA, USA, 2000, pp. 95-97.

[107] M. Houssa, C. Parthasarathy, N. Espreux, J. L. Autran, and N. Revil, "Impact of Nitrogen on Negative Bias Temperature Instability in p-Channel MOSFETs," *Electrochemical and Solid-State Letters,* vol. 6, 2003.

[108] T. Sasaki, K. Kuwazawa, K. Tanaka, J. Kato, and D. L. Kwong, "Engineering of nitrogen profile in an ultrathin gate insulator to improve transistor performance and NBTI," *IEEE Electron Device Letters,* vol. 24, pp. 150-152, 2003.

[109] S. S. Tan, T. P. Chen, C. H. Ang, and L. Chan, "Relationship between interfacial nitrogen concentration and activation energies of fixed-charge trapping and interface state generation under bias-temperature stress condition," *Applied Physics Letters* vol. 82, pp. 269-271, 2003.

[110] S. S. Tan, T. P. Chen, J. M. Soon, K. P. Loh, C. H. Ang, W. Y. Teo, and L. Chan, "Linear relationship between H+-trapping reaction energy and defect generation: Insight into nitrogen-enhanced negative bias temperature instability," *Applied Physics Letters* vol. 83, pp. 530-532, 2003.

[111] Y. Mitani, "Influence of nitrogen in ultra-thin SiON on negative bias temperature instability under AC stress," in *Technical Digest - International Electron Devices Meeting, IEDM*, San Francisco, CA, 2004, pp. 117-120.

ATTENTION: The Singapore Copyright Act applies to the use of this document. Nanyang Technological University Library

[112] A. T. Krishnan, V. Reddy, and S. Krishnan, "Impact of charging damage on negative bias temperature instability," in *Technical Digest - International Electron Devices Meeting*, Washington, DC, 2001, pp. 865-868.

[113] A. Suzuki, K. Tabuchi, H. Kimura, T. Hasegawa, S. Kadomura, K. Kakamu, H. Kudo, M. Kawano, A. Tsukune, and M. Yamada, "A strategy using a copper/low-k BEOL process to prevent negative-bias temperature instability (NBTI) in p-MOSFETs with ultra-thin gate oxide," in *IEEE Symposium on VLSI Circuits, Digest of Technical Papers*, Honolulu, HI, 2002, pp. 216-217.

[114] D. Y. Lee, H. C. Lin, M. F. Wang, M. Y. Tsai, T. Y. Huang, and T. Wang, "Enhanced negative-bias-temperature instability of p-channel metal-oxide-semiconductor transistors due to plasma charging damage," *Japanese Journal of Applied Physics, Part 1: Regular Papers and Short Notes and Review Papers,* vol. 41, pp. 2419-2422, 2002.

[115] S. C. Song, S. Filipiak, A. Perera, M. Turner, F. Huang, S. G. H. Anderson, L. Kang, B. Min, D. Menke, S. Tukunang, and S. Venkatesan, "Avoiding plasma induced damage to gate oxide with conductive top film (CTF) on PECVD contact etch stop layer," in *IEEE Symposium on VLSI Circuits, Digest of Technical Papers*, Honolulu, HI, 2002, pp. 72-73.

[116] V. S. Chang, L. A. Ragnarsson, H. Y. Yu, M. Aoulaiche, T. Conard, K. M. Yin, T. Schram, J. W. Maes, S. De Gendt, and S. Biesemans, "Effects of Al2O3 dielectric cap and nitridation on device performance, scalability, and reliability for advanced high-κ/metal gate pMOSFET applications," *IEEE Transactions*

ATTENTION: The Singapore Copyright Act applies to the use of this document. Nanyang Technological University Library

on Electron Devices, vol. 54, pp. 2738-2749, 2007.

[117] S. S. Chung, D. C. Huang, Y. J. Tsai, C. S. Lai, C. H. Tsai, P. W. Liu, Y. H. Lin, C. T. Tsai, G. H. Ma, S. C. Chien, and S. W. Sun, "New observations on the uniaxial and biaxial strain-induced hot carrier and NBTI reliabilities for 65nm node CMOS devices and beyond," in *Technical Digest - International Electron Devices Meeting, IEDM*, San Francisco, CA, 2006.

[118] C. Y. Lu, H. C. Lin, Y. F. Chang, and T. Y. Huang, "Device characteristics and aggravated negative bias temperature instability in p-channel metal-oxide-semiconductor field-effect transistors with uniaxial compressive strain," *Japanese Journal of Applied Physics, Part 1: Regular Papers and Short Notes and Review Papers,* vol. 45, pp. 3064-3069, 2006.

[119] G. Thareja, L. Jack, A. V. Y. Thean, V. Vartanian, and B. Y. Nguyen, "NBTI reliability of strained SOI MOSFETs," in *Conference Proceedings from the International Symposium for Testing and Failure Analysis*, Austin, TX, 2006, pp. 423-425.

[120] S. S. Chung, D. K. Lo, J. J. Yang, and T. C. Lin, "Localization of NBTI-induced oxide damage in direct tunneling regime gate oxide pMOSFET using a novel low gate-leakage gated-diode (L2-GD) method," in *Technical Digest - International Electron Devices Meeting*, San Francisco, CA, 2002, pp. 513-516.

[121] S. J. Chen, T. C. Lin, D. K. Lo, J. J. Yang, S. S. Chung, T. Y. Kao, R. Y. Shiue, C. J. Wang, and Y. K. Peng, "An improved interface characterization technique

ATTENTION: The Singapore Copyright Act applies to the use of this document. Nanyang Technological University Library

for a full-range profiling of oxide damage in ultra-thin gate oxide CMOS devices," in *Annual Proceedings - Reliability Physics (Symposium)*, Dallas, TX, 2003, pp. 203-207.

[122] D. S. Ang, G. A. Du, and S. Wang, "Mechanism of bias-temperature instability: Results from positive gate stress," in *Proceedings of the International Symposium on the Physical and Failure Analysis of Integrated Circuits, IPFA*, Bangalore, 2007, pp. 96-99.

[123] K. Onishi, C. S. Kang, R. Choi, H. J. Cho, S. Gopalan, R. Nieh, E. Dharmarajan, and J. C. Lee, "Reliability characteristics, including NBTI, of polysilicon gate HfO2 MOSFET's," in *Technical Digest - International Electron Devices Meeting*, Washington, DC, 2001, pp. 659-662.

[124] M. Haussa, M. Aoulaiche, S. Van Elshocht, S. De Gendt, G. Groeseneken, and M. M. Heyns, "Negative bias temperature instabilities in HfSiON/TaN-based pMOSFETs," in *Technical Digest - International Electron Devices Meeting, IEDM*, San Francisco, CA, 2004, pp. 121-124.

[125] M. Houssa, S. De Gendt, G. Groeseneken, and M. M. Heyns, "Negative bias temperature instabilities in SiO2/HfO 2-based hole channel FETs," *Journal of the Electrochemical Society* vol. 151, 2004.

[126] S. Zafar, B. H. Lee, and J. Stathis, "Evaluation of NBTI in HfO2 Gate-Dielectric Stacks With Tungsten Gates," *IEEE Electron Device Letters,* vol. 25, pp. 153-155, 2004.

[127] S. Zafar, B. H. Lee, J. Stathis, A. Callegari, and T. Ning, "A model for negative

ATTENTION: The Singapore Copyright Act applies to the use of this document. Nanyang Technological University Library

bias temperature instability (NBTI) in oxide and high-k pFETs," in *Digest of Technical Papers - Symposium on VLSI Technology*, Honolulu, HI, 2004, pp. 208-209.

[128] X. Garros, G. Reimbold, D. Duret, C. Leroux, B. Guillaumot, O. Louveau, C. Hobbs, and F. Martin, "Interface states in HFO2 stacks with metal gate: Nature, passivation, generation," in *IEEE International Reliability Physics Symposium Proceedings*, San Jose, CA, 2005, pp. 55-60.

[129] S. Kalpat, H. H. Tseng, M. Ramon, M. Moosa, D. Tekleab, P. J. Tobin, D. C. Gilmer, R. I. Hegde, C. Capasso, C. Tracy, and B. E. White Jr, "BTI characteristics and mechanisms of metal gated HfO2 films with enhanced Interface/Bulk Process Treatments," *IEEE Transactions on Device and Materials Reliability,* vol. 5, pp. 26-34, 2005.

[130] N. Wu, Q. Zhang, C. Zhu, C. Shen, M. F. Li, D. S. H. Chan, and N. Balasubramanian, "BTI and charge trapping in germanium p- And n-MOSFETs with CVD HfO 2 gate dielectric," in *Technical Digest - International Electron Devices Meeting, IEDM*, Washington, DC, MD, 2005, pp. 555-558.

[131] J. Ushio, T. Maruizumi, and K. Kushida-Abdelghafar, "Interface structures generated by negative-bias temperature instability in Si/SiO2 and Si/SiOxNy interfaces," *Applied Physics Letters* vol. 81, p. 1818, 2002.

[132] M. A. Alam, "A Critical Examination of the Mechanics of Dynamic NBTI for PMOSFETs," in *Technical Digest - International Electron Devices Meeting*,

ATTENTION: The Singapore Copyright Act applies to the use of this document. Nanyang Technological University Library

Washington, DC, 2003, pp. 345-348.

[133] M. A. Alam and S. Mahapatra, "A comprehensive model of PMOS NBTI degradation," *Microelectronics Reliability,* vol. 45, pp. 71-81, 2005.

[134] M. A. Alam, H. Kufluoglu, D. Varghese, and S. Mahapatra, "A comprehensive model for PMOS NBTI degradation: Recent progress," *Microelectronics Reliability,* vol. 47, pp. 853-862, 2007.

[135] S. Zafar, J. Stathis, A. Callegari, and T. Ning, "A statistical mechanics model for NBTI in oxides," in *Meeting Abstracts*, Los Angeles, CA, 2005, p. 1446.

[136] S. Zafar, "Statistical mechanics based model for negative bias temperature instability induced degradation," *Journal of Applied Physics* vol. 97, pp. 1-9, 2005.

[137] J. H. Stathis and S. Zafar, "The negative bias temperature instability in MOS devices: A review," *Microelectronics Reliability,* vol. 46, pp. 270-286, 2006.

[138] B. Kaczer, V. Arkhipov, R. Degraeve, N. Collaert, G. Groeseneken, and M. Goodwin, "Disorder-controlled-kinetics model for negative bias temperature instability and its experimental verification," in *IEEE International Reliability Physics Symposium Proceedings*, San Jose, CA, 2005, pp. 381-387.

[139] B. Kaczer, V. Arkhipov, R. Degraeve, N. Collaert, G. Groeseneken, and M. Goodwin, "Temperature dependence of the negative bias temperature instability in the framework of dispersive transport," *Applied Physics Letters* vol. 86, pp. 1-3, 2005.

[140] B. Kaczer, V. Arkhipov, M. Jurczak, and G. Groeseneken, "Negative bias

ATTENTION: The Singapore Copyright Act applies to the use of this document. Nanyang Technological University Library

temperature instability (NBTI) in SiO2 and SiON gate dielectrics understood through disorder-controlled kinetics," *Microelectronic Engineering* vol. 80, pp. 122-125, 22 June 2005 through 24 June 2005 2005.

[141] V. I. Arkhipov and A. I. Rudenko, "Diffusion of nonquilibrium carriers in disordered materials," *SOV PHYS SEMICOND,* vol. V 16, pp. 530-531, 1982.

[142] V. I. Arkhipov and A. I. Rudenko, "Drift and diffusion in materials with traps - 2. Non-equilibrium transport regime," *Philosophical Magazine B: Physics of Condensed Matter; Electronic, Optical and Magnetic Properties,* vol. 45, pp. 189-207, 1982.

[143] T. Grasser, W. Gos, and B. Kaczer, "Dispersive transport and negative bias temperature instability: Boundary conditions, initial conditions, and transport models," *IEEE Transactions on Device and Materials Reliability,* vol. 8, pp. 79-96, 2008.

[144] V. Huard, M. Denais, F. Perrier, N. Revil, C. Parthasarathy, A. Bravaix, and E. Vincent, "A thorough investigation of MOSFETs NBTI degradation," *Microelectronics Reliability,* vol. 45, pp. 83-98, 2005.

[145] V. Huard, M. Denais, and C. Parthasarathy, "NBTI degradation: From physical mechanisms to modelling," *Microelectronics Reliability,* vol. 46, pp. 1-23, 2006.

[146] V. Huard, C. Parthasarathy, N. Rallet, C. Guerin, M. Mammase, D. Barge, and C. Ouvrard, "New characterization and modeling approach for NBTI degradation from transistor to product level," in *Technical Digest -*

ATTENTION: The Singapore Copyright Act applies to the use of this document. Nanyang Technological University Library

International Electron Devices Meeting, IEDM, Washington, DC, 2007, pp. 797-800.

[147] R. A. B. Devine, J. L. Autran, W. L. Warren, K. L. Vanheusdan, and J. C. Rostaing, "Interfacial hardness enhancement in deuterium annealed 0.25 渭m channel metal oxide semiconductor transistors," *Applied Physics Letters* vol. 70, pp. 2999-3001, 1997.

[148] A. Stesmans, "Dissociation kinetics of hydrogen-passivated Pb defects at the (111)Si/SiO2 interface," *Physical Review B - Condensed Matter and Materials Physics,* vol. 61, pp. 8393-8403, 2000.

[149] A. Haggag, W. McMahon, K. Hess, K. Cheng, J. Lee, and J. Lyding, "High-performance chip reliability from short-time-tests Statistical models for optical interconnect and HCl/TDDB/NBTI deep-submicron transistor failures," in *Annual Proceedings - Reliability Physics (Symposium)*, Orlando, FL, 2001, pp. 271-279.

[150] V. Huard, C. R. Parthasarathy, C. Guerin, and M. Denais, "Physical modeling of negative bias temperature instabilities for predictive extrapolation," in *IEEE International Reliability Physics Symposium Proceedings*, San Jose, CA, 2006, pp. 733-734.

[151] M. Denais, A. Bravaix, V. Huard, C. Parthasarathy, C. Guerin, G. Ribes, F. Perrier, M. Mairy, and D. Roy, "Paradigm shift for NBTI characterization in ultra-scaled CMOS technologies," in *IEEE International Reliability Physics Symposium Proceedings*, San Jose, CA, 2006, pp. 735-736.

ATTENTION: The Singapore Copyright Act applies to the use of this document. Nanyang Technological University Library

[152] C. R. Parthasarathy, M. Denais, V. Huard, G. Ribes, E. Vincent, and A. Bravaix, "New insights into recovery characteristics post NBTI stress," in *IEEE International Reliability Physics Symposium Proceedings*, San Jose, CA, 2006, pp. 471-477.

[153] C. R. Parthasarathy, M. Denais, V. Huard, G. Ribes, E. Vincent, and A. Bravaix, "New insights into recovery characteristics during PMOS NBTI and CHC degradation," *IEEE Transactions on Device and Materials Reliability,* vol. 7, pp. 130-137, 2007.

[154] T. Yang, C. Shen, M. F. Li, C. H. Ang, C. X. Zhu, Y. C. Yeo, G. Samudra, and D. L. Kwong, "Interface trap passivation effect in NBTI measurement for p-MOSFET with SiON gate dielectric," *IEEE Electron Device Letters,* vol. 26, pp. 758-760, 2005.

[155] T. Yang, C. Shen, M. F. Li, C. H. Ang, C. X. Zhu, Y. C. Yeo, G. Samudra, S. C. Rustagi, M. B. Yu, and D. L. Kwong, "Fast DNBTI components in p-MOSFET with SiON dielectric," *IEEE Electron Device Letters,* vol. 26, pp. 826-828, 2005.

[156] Y. Nissan-Cohen, J. Shappir, and D. Frohman-Bentchkowsky, "Dynamic model of trapping-detrapping in SiO2," *Journal of Applied Physics* vol. 58, pp. 2252-2261, 1985.

[157] A. Kerber, E. Cartier, L. Pantisano, M. Rosmeulen, R. Degraeve, T. Kauerauf, G. Groeseneken, H. E. Maes, and U. Schwalke, "Characterization of the VT-instability in SiO2 / HfO2 gate dielectrics," in *Annual Proceedings -*

ATTENTION: The Singapore Copyright Act applies to the use of this document. Nanyang Technological University Library

Reliability Physics (Symposium), Dallas, TX, 2003, pp. 41-45.

[158] C. Shen, M. F. Li, X. P. Wang, H. Y. Yu, Y. P. Feng, A. T. L. Lim, Y. C. Yeo, D. S. H. Chan, and D. L. Kwong, "Negative U traps in HfO2 gate dielectrics and frequency dependence of dynamic BTI in MOSFETs," in *Technical Digest - International Electron Devices Meeting, IEDM*, San Francisco, CA, 2004, pp. 733-736.

[159] M. F. Li, C. Shen, T. Yang, G. Chen, and D. Huang, "The physical origins of fast and slow components in NBTI degradation for p-MOS transistors with SiON gate dielectric," in *ECS Transactions*, Chicago, IL, 2007, pp. 167-183.

[160] D. S. Ang and K. L. Pey, "Evidence for two distinct positive trapped charge components in NBTI stressed p-MOSFETs employing ultrathin CVD silicon nitride gate dielectric," *IEEE Electron Device Letters,* vol. 25, pp. 637-639, 2004.

[161] D. S. Ang, S. Wang, and C. H. Ling, "Evidence of two distinct degradation mechanisms from temperature dependence of negative bias stressing of the ultrathin gate p-MOSFET," *IEEE Electron Device Letters,* vol. 26, pp. 906-908, 2005.

[162] D. S. Ang and S. Wang, "Recovery of the NBTI-stressed ultrathin gate p-MOSFET: The role of deep-level hole traps," *IEEE Electron Device Letters,* vol. 27, pp. 914-916, 2006.

[163] D. S. Ang, S. Wang, G. A. Du, and Y. Z. Hu, "A consistent deep-level hole trapping model for negative bias temperature instability," *IEEE Transactions*

ATTENTION: The Singapore Copyright Act applies to the use of this document. Nanyang Technological University Library

on Device and Materials Reliability, vol. 8, pp. 22-34, 2008.

[164] D. S. Ang and S. Wang, "New observations on the damage relaxation mechanisms in p-MOSFETs under dynamic NBTI stressing," in *IEEE International Reliability Physics Symposium Proceedings*, San Jose, CA, 2005, pp. 706-707.

[165] D. S. Ang, "Observation of suppressed interface state relaxation under positive gate biasing of the ultrathin oxynitride gate p-MOSFET subjected to negative-bias temperature stressing," *IEEE Electron Device Letters,* vol. 27, pp. 412-415, 2006.

[166] D. S. Ang and S. Wang, "Insight into the suppressed recovery of NBTI-stressed ultrathin oxynitride gate pMOSFET," *IEEE Electron Device Letters,* vol. 27, pp. 755-758, 2006.

[167] H. Usui, M. Kanno, and T. Morikawa, "Time and voltage dependence of degradation and recovery under pulsed negative bias temperature stress," in *Annual Proceedings - Reliability Physics (Symposium)*, Dallas, TX, 2003, pp. 610-611.

[168] S. Aota, S. Fujii, Z. W. Jin, Y. Ito, K. Utsumi, E. Morifuji, S. Yamada, F. Matsuoka, and T. Noguchi, "A new method for precise evaluation of dynamic recovery of negative bias temperature instability," in *IEEE International Conference on Microelectronic Test Structures*, Leuven, 2005, pp. 197-199.

[169] C. T. Chan, H. C. Ma, C. J. Tang, and T. Wang, "Investigation of post-NBTI stress recovery in pMOSFETs by direct measurement of single oxide charge

ATTENTION: The Singapore Copyright Act applies to the use of this document. Nanyang Technological University Library

De-trapping," in *Digest of Technical Papers - Symposium on VLSI Technology*, Kyoto, 2005, pp. 90-91.

[170] C. Schlunder, W. Heinrigs, W. Gustin, and H. Reisinger, "On the impact of the NBTI recovery phenomenon on lifetime prediction of modern p-MOSFETs," in *IEEE International Integrated Reliability Workshop Final Report*, South Lake Tahoe, CA, 2006, pp. 1-4.

[171] A. S. Grove and D. J. Fitzgerald, "Surface effects on p-n junctions: Characteristics of surface space-charge regions under non-equilibrium conditions," *Solid State Electronics,* vol. 9, pp. 783-806, 1966.

[172] J. S. Brugler and P. G. A. Jespers, "Charge pumping in MOS devices," *Electron Devices, IEEE Transactions on,* vol. 16, pp. 297 - 302, 1969.

[173] G. Groeseneken, H. E. Maes, N. Beltran, and R. F. De Keersmaecker, "A reliable approach to charge-pumping measurements in MOS transistors," *IEEE Transactions on Electron Devices,* vol. ED-31, pp. 42-53, 1984.

[174] P. Heremans, J. Witters, G. Groeseneken, and H. E. Maes, "Analysis of the charge pumping technique and its application for the evaluation of MOSFET degradation," *IEEE Transactions on Electron Devices,* vol. 36, pp. 1318-1335, 1989.

[175] N. C. Das and V. Nathan, "Hot carrier degradation in MOSFETs: A charge pumping study," *Semiconductor Science and Technology,* vol. 8, pp. 549-554, 1993.

[176] S. Mahapatra, C. D. Parikh, and J. Vasi, "New technique to profile hot-carrier

ATTENTION: The Singapore Copyright Act applies to the use of this document. Nanyang Technological University Library

induced interface state generation in nMOSFETs using charge pumping," in *Proceedings of SPIE - The International Society for Optical Engineering*, Delhi, India, 1998, pp. 1030-1033.

[177] S. Mahapatra, C. D. Parikh, and J. Vasi, "A new "multifrequency" charge pumping technique to profile hot-carrier-induced interface-state density in nmosfets," *IEEE Transactions on Electron Devices,* vol. 46, pp. 960-967, 1999.

[178] S. Mahapatra, C. D. Parikh, J. Vasi, V. Ramgopal Rao, and C. R. Viswanathan, "Direct charge pumping technique for spatial profiling of hot-carrier induced interface and oxide traps in MOSFETs," *Solid-State Electronics,* vol. 43, pp. 915-922, 1999.

[179] A. Neugroschel, C.-T. Sah, K. M. Han, M. S. Carroll, T. Nishida, J. T. Kavalieros, and Y. Lu, "Direct-current measurements of oxide and interface traps on oxidized silicon," *IEEE Transactions on Electron Devices,* vol. 42, pp. 1657-1662, 1995.

[180] B. B. Jie, M. F. Li, C. L. Lou, W. K. Chim, D. S. H. Chan, and K. F. Lo, "Investigation of interface traps in LDD pMOST's by the DCIV method," *IEEE Electron Device Letters,* vol. 18, pp. 583-585, 1997.

[181] J. Cai, "Monitoring interface traps by DCIV method," *IEEE Electron Device Letters,* vol. 20, pp. 60-63, 1999.

[182] J. B. Yang, T. P. Chen, S. S. Tan, and L. Chan, "A simple negative bias temperature instability characterization methodology to minimize the

ATTENTION: The Singapore Copyright Act applies to the use of this document. Nanyang Technological University Library

immediate recovery effect during measurement," *Japanese Journal of Applied Physics, Part 1: Regular Papers and Short Notes and Review Papers,* vol. 45, pp. 6137-6140, 2006.

[183] M. Denais, A. Bravaix, V. Huard, C. Parthasarathy, M. Bidaud, G. Ribes, D. Barge, L. Vishnubhotla, B. Tavel, Y. Rey-Tauriac, F. Perrier, N. Revil, F. Arnaud, and P. Stolk, "New hole trapping characterization during NBTI in 65NM node technology with distinct nitridation processing," in *IEEE International Integrated Reliability Workshop Final Report*, S. Lake Tahoe, CA, 2004, pp. 121-124.

[184] M. Denais, A. Bravaix, V. Huard, C. Parthasarathy, G. Ribes, F. Perrier, Y. Rey-Tauriac, and N. Revil, "On-the-fly characterization of NBTI in ultra-thin gate oxide PMOSFET's," in *Technical Digest - International Electron Devices Meeting, IEDM*, San Francisco, CA, 2004, pp. 109-112.

[185] M. Denais, V. Huard, C. Parthasarathy, G. Ribes, F. Perrier, N. Revil, and A. Bravaix, "Interface trap generation and hole trapping under NBTI and PBTI in advanced CMOS technology with a 2-nm gate oxide," *IEEE Transactions on Device and Materials Reliability,* vol. 4, pp. 715-722, 2004.

[186] M. Denais, V. Huard, C. Parthasarathy, G. Ribes, F. Perrier, N. Revil, and A. Bravaix, "New methodologies of NBTI characterization eliminating recovery effects," in *ESSCIRC 2004 - Proceedings of the 34th European Solid-State Device Research Conference*, Leuven, 2004, pp. 265-268.

[187] G. A. Du, D. S. Ang, Y. Z. Hu, S. Wang, and C. M. Ng, "Physical framework

ATTENTION: The Singapore Copyright Act applies to the use of this document. Nanyang Technological University Library

for NBTI: Insight from ultra-fast switching measurement of NBTI recovery," in *IEEE International Reliability Physics Symposium Proceedings*, Phoenix, AZ, 2008, pp. 735-736.

[188] Y. Z. Hu, D. S. Ang, and G. A. Du, "An improved methodology for monitoring NBTI induced threshold voltage shift of scaled," in *IEEE International Reliability Physics Symposium Proceedings*, Phoenix, AZ, 2008, pp. 743-744.

[189] W. J. Liu, Z. Y. Liu, D. Huang, C. C. Liao, L. F. Zhang, Z. H. Gan, W. Wong, C. Shen, and M. F. Li, "On-the-fly interface trap measurement and its impact on the understanding of NBTI mechanism for p-MOSFETs with SiON gate dielectric," in *Technical Digest - International Electron Devices Meeting, IEDM*, Washington, DC, 2007, pp. 813-816.

[190] M. Ershov, R. Lindley, S. Saxena, A. Shibkov, S. Minehane, J. Babcock, S. Winters, H. Karbasi, T. Yamashita, P. Clifton, and M. Redford, "Transient effects and characterization methodology of negative bias temperature instability in pMOS transistors," in *Annual Proceedings - Reliability Physics (Symposium)*, Dallas, TX, 2003, pp. 606-607.

[191] P. J. McWhorter and P. S. Winokur, "Simple technique for separating the effects of interface traps and trapped-oxide charge in metal-oxide-semiconductor transistors," *Applied Physics Letters* vol. 48, pp. 133-135, 1986.

[192] T. Matsuoka, S. Taguchi, Q. D. M. Khosru, K. Taniguchi, and C. Hamaguchi, "Degradation of inversion layer electron mobility due to interface traps in

ATTENTION: The Singapore Copyright Act applies to the use of this document. Nanyang Technological University Library

metal-oxide-semiconductor transistors," *Journal of Applied Physics* vol. 78, pp. 3252-3257, 1995.

[193] N. Arora, "MOSFET Models for VLSI Circuit Simulation," 1993, p. 542.

[194] H. Aono, E. Murakami, K. Okuyama, A. Nishida, M. Minami, Y. Ooji, and K. Kubota, "Modeling of NBTI saturation effect and its impact on electric field dependence of the lifetime," *Microelectronics Reliability,* vol. 45, pp. 1109-1114, 2005.

[195] C. L. Chen, Y. M. Lin, C. J. Wang, and K. Wu, "A new finding on NBTI lifetime model and an investigation on NBTI degradation characteristic for 1.2nm ultra thin oxide," in *IEEE International Reliability Physics Symposium Proceedings*, San Jose, CA, 2005, pp. 704-705.

[196] P. B. Kumar, R. Sharma, P. R. Nair, D. R. Nair, S. Kamohara, S. Mahapatra, and J. Vasi, "Mechanism of drain disturb in SONOS flash EEPROMs," in *IEEE International Reliability Physics Symposium Proceedings*, San Jose, CA, 2005, pp. 186-190.

[197] J. F. Zhang, Z. Jo, M. H. Chang, B. Kaczer, and G. Groeseneken, "Real Vth instability of pMOSFETs under practical operation conditions," in *Technical Digest - International Electron Devices Meeting, IEDM*, Washington, DC, 2007, pp. 817-820.

[198] X. Chen, S. Fang, W. Gao, T. Dyer, Y. W. Teh, S. S. Tan, Y. Ko, C. Baiocco, A. Ajmera, J. Park, J. Kim, R. Stierstorfer, D. Chidambarrao, Z. Luo, N. Nivo, P. Nguyen, J. Yuan, S. Panda, O. Kwon, N. Edleman, T. Tjoa, J. Widodo, M.

ATTENTION: The Singapore Copyright Act applies to the use of this document. Nanyang Technological University Library

Belyansky, M. Sherony, R. Amos, H. Ng, M. Hierlemann, D. Coolbough, A. Steegen, I. Yang, J. Sudijono, T. Schiml, J. H. Ku, and C. Davis, "Stress proximity technique for performance improvement with dual stress liner at 45nm technology and beyond," in *Digest of Technical Papers - Symposium on VLSI Technology*, 2006, pp. 60-61.

[199] J. Yuan, S. S. Tan, Y. M. Lee, J. Kim, R. Lindsay, V. Sardesai, T. Hook, R. Amos, Z. Luo, W. Lee, S. Fang, T. Dyer, N. Rovedo, R. Stierstorfer, Z. Yang, J. Li, K. Barton, H. Ng, J. Sudijono, J. Ku, M. Hierlemann, and T. Schiml, "A 45nm low cost low power platform by using integrated dual-stress-liner technology," in *Digest of Technical Papers - Symposium on VLSI Technology*, 2006, pp. 100-101.

[200] S. Talwar, D. Markle, and M. Thompson, "Junction scaling using lasers for thermal annealing," *Solid State Technology,* vol. 46, pp. 83-84+86+88, 2003.

[201] S. K. H. Fung, H. T. Huang, S. M. Cheng, K. L. Cheng, S. W. Wang, Y. P. Wang, Y. Y. Yao, C. M. Chu, S. J. Yang, W. J. Liang, Y. K. Leung, C. C. Wu, C. Y. Lin, S. J. Chang, S. Y. Wu, C. F. Nieh, C. C. Chen, T. L. Lee, Y. Jin, S. C. Chen, L. T. Lin, Y. H. Chiu, H. J. Tao, C. Y. Fu, S. M. Jang, K. F. Yu, C. H. Wang, T. C. Ong, Y. C. See, C. H. Diaz, M. S. Liang, and Y. C. Sun, "65nm CMOS high speed, general purpose and low power transistor technology for high volume foundry application," in *Digest of Technical Papers - Symposium on VLSI Technology*, Honolulu, HI, 2004, pp. 92-93.

[202] A. Shima, Y. Wang, S. Talwar, and A. Hiraiwa, "Ultra-shallow junction

ATTENTION: The Singapore Copyright Act applies to the use of this document. Nanyang Technological University Library

formation by non-melt laser spike annealing for 50-nm gate CMOS," in *Digest of Technical Papers - Symposium on VLSI Technology*, Honolulu, HI, 2004, pp. 174-175.

[203] C. H. Chen, T. L. Lee, T. H. Hou, C. L. Chen, C. C. Chen, J. W. Hsu, K. L. Cheng, Y. H. Chiu, H. J. Tao, Y. Jin, C. H. Diaz, S. C. Chen, and M. S. Liang, "Stress memorization technique (SMT) by selectively strained-nitride capping for sub-65nm high-performance strained-Si device application," in *Digest of Technical Papers - Symposium on VLSI Technology*, 2004, pp. 56-57.

[204] C. Ortolland, P. Morin, C. Chaton, E. Mastromatteo, C. Populaire, S. Orain, F. Leverd, P. Stolk, F. Boeuf, and F. Arnaud, "Stress memorization technique (SMT) optimization for 45nm CMOS," in *Digest of Technical Papers - Symposium on VLSI Technology*, 2006, pp. 78-79.

[205] H. S. Yang, R. Malik, S. Narasimha, Y. Li, R. Divakaruni, P. Agnello, S. Allen, A. Antreasyan, J. C. Arnold, K. Bandy, M. Belyansky, A. Bonnoit, G. Bronner, V. Chen, X. Chen, Z. Chen, D. Chidambarrao, A. Chou, W. Clark, S. W. Crowder, B. Engel, H. Harifuchi, S. F. Huang, R. Jagannathan, F. F. Jamin, Y. Kohyama, H. Kuroda, C. W. Lai, H. K. Lee, W. H. Lee, E. H. Lim, W. Lai, A. Mallikarjunan, K. Matsumoto, A. McKnight, J. Nayak, H. Y. Ng, S. Panda, R. Rengarajan, M. Steigerwalt, S. Subbanna, K. Subramanian, J. Sudijono, G. Sudo, S. P. Sun, B. Tessier, Y. Toyoshima, P. Tran, R. Wise, R. Wong, I. Y. Yang, C. H. Wann, L. T. Su, M. Horstmann, T. Feudel, A. Wei, K. Frohberg, G. Burbach, M. Gerhardt, M. Lenski, R. Stephan, K. Wieczorek, M. Schaller, H.

ATTENTION: The Singapore Copyright Act applies to the use of this document. Nanyang Technological University Library

Salz, J. Hohage, H. Ruelke, J. Klais, P. Huebler, S. Luning, R. Van Bentum, G. Grasshoff, C. Schwan, E. Ehrichs, S. Goad, J. Buller, S. Krishnan, D. Greenlaw, M. Raab, and N. Kepler, "Dual stress liner for high performance sub-45nm gate length SOI CMOS manufacturing," in *Technical Digest - International Electron Devices Meeting, IEDM*, 2004, pp. 1075-1077.

[206] M. Shima, K. Okabe, A. Yamaguchi, T. Sakoda, K. Kawamura, S. Pidin, M. Okuno, T. Owada, K. Sugimoto, J. Ogura, H. Kokura, H. Morioka, T. Watanabe, T. Isome, K. Okoshi, T. Mori, Y. Hayami, H. Minakata, A. Hatada, Y. Shimamune, A. Katakami, H. Ota, T. Sakuma, T. Miyashita, K. Hosaka, H. Fukutome, N. Tamura, T. Aoyama, K. Sukegawa, M. Nakaishi, S. Fukuyama, S. Nakai, M. Kojima, S. Sato, M. Miyajima, K. Hashimoto, and T. Sugii, "High-performance low operation power transistor for 45nm node universal applications," in *Digest of Technical Papers - Symposium on VLSI Technology*, 2006, pp. 156-157.

[207] J. B. Yang, T. P. Chen, S. S. Tan, and L. Chan, "A novel empirical model for NBTI recovery with the modulated measurement time frame," in *Proceedings of the International Symposium on the Physical and Failure Analysis of Integrated Circuits, IPFA*, 2006, pp. 33-36.

[208] B. Kaczer, T. Grasser, P. J. Roussel, J. Martin-Martinez, R. O'Connor, B. J. O'Sullivan, and G. Groeseneken, "Ubiquitous relaxation in BTI stressing-new evaluation and insights," in *IEEE International Reliability Physics Symposium Proceedings*, Phoenix, AZ, 2008, pp. 20-27.

ATTENTION: The Singapore Copyright Act applies to the use of this document. Nanyang Technological University Library

[209] T. Grasser, W. Gus, V. Sverdlov, and B. Kaczer, "The universality of NBTI relaxation and its implications for modeling and characterization," in *Annual Proceedings - Reliability Physics (Symposium)*, Phoenix, AZ, 2007, pp. 268-280.

[210] H. Reisinger, O. Blank, W. Heinrigs, A. Muhlhoff, W. Gustin, and C. Schlunder, "Analysis of NBTI degradation- and recovery-behavior based on ultra fast VT -measurements," in *IEEE International Reliability Physics Symposium Proceedings*, San Jose, CA, 2006, pp. 448-453.

[211] J. B. Yang, T. P. Chen, S. S. Tan, and L. Chan, "Analytical reaction-diffusion model and the modeling of nitrogen-enhanced negative bias temperature instability," *Applied Physics Letters* vol. 88, 2006.

[212] S. S. Tan, T. P. Chen, C. H. Ang, and L. Chan, "Mechanism of nitrogen-enhanced negative bias temperature instability in pMOSFET," *Microelectronics Reliability,* vol. 45, pp. 19-30, 2005.

[213] S. S. Tan, T. P. Chen, C. H. Ang, and L. Chan, "Atomic modeling of nitrogen neighboring effect on negative bias temperature instability of pMOSFETs," *IEEE Electron Device Letters,* vol. 25, pp. 504-506, 2004.

[214] J. L. Regolini, D. Benoit, and P. Morin, "Passivation issues in active pixel CMOS image sensors," *Microelectronics Reliability,* vol. 47, pp. 739-742, 2007.

[215] D. Benoit, J. Regolini, and P. Morin, "Hydrogen desorption and diffusion in PECVD silicon nitride. Application to passivation of CMOS active pixel

ATTENTION: The Singapore Copyright Act applies to the use of this document. Nanyang Technological University Library

sensors," *Microelectronic Engineering,* vol. 84, pp. 2169-2172, 2007/10//.

[216] H. Kufluoglu and M. A. Alam, "Theory of interface-trap-induced NBTI degradation for reduced cross section MOSFETs," *IEEE Transactions on Electron Devices,* vol. 53, pp. 1120-1130, 2006.

[217] H. S. Rhee, H. Lee, T. Ueno, D. S. Shin, S. H. Lee, Y. Kim, A. Samoilov, P. O. Hansson, M. Kim, H. S. Kim, and N. I. Lee, "Negative bias temperature instability of carrier-transport enhanced pMOSFET with performance boosters," in *Technical Digest - International Electron Devices Meeting, IEDM*, Washington, DC, MD, 2005, pp. 692-695.

[218] J. M. Soon, K. P. Loh, S. S. Tan, T. P. Chen, W. Y. Teo, and L. Chan, "Study of negative-bias temperature-instability-induced defects using first-principle approach," *Applied Physics Letters* vol. 83, pp. 3063-3065, 2003.

[219] J. B. Yang, T. P. Chen, S. S. Tan, C. M. Ng, and L. Chan, "Modeling and characterization of nitrogen-enhanced negative-bias temperature instability in p-channel MOSFETs," *Journal of the Electrochemical Society* vol. 154, 2007.

[220] J. B. Yang, T. P. Chen, S. S. Tan, C. M. Ng, and L. Chan, "Influence of hydrogen dispersive diffusion in nitrided gate oxide on negative bias temperature instability," *Applied Physics Letters* vol. 93, 2008.

[221] J. F. Zhang, M. H. Chang, and G. Groeseneken, "Effects of Measurement Temperature on NBTI," *IEEE Electron Device Letters,* vol. 28, pp. 298-300, 2007.

[222] A. D. Becke, "A new mixing of Hartree-Fock and local density-functional

ATTENTION: The Singapore Copyright Act applies to the use of this document. Nanyang Technological University Library

theories," *The Journal of Chemical Physics,* vol. 98, pp. 1372-1377, 1993.

[223] C. Lee, W. Yang, and R. G. Parr, "Development of the Colle-Salvetti correlation-energy formula into a functional of the electron density," *Physical Review B* vol. 37, pp. 785-789, 1988.

[224] R. S. Mulliken, "Criteria for the construction of good self-consistent-field molecular orbital wave functions, and the significance of LCAO-MO population analysis," *The Journal of Chemical Physics,* vol. 36, pp. 3428-3439, 1962.

[225] L. E. Chirlain and M. M. Francl, "Atomic Charges Derived from Electrostatic Potentials: A Detailed Study," *J. Comp. Chem.,* vol. 8, p. 894, 1987.

[226] A. E. Reed, R. B. Weinstock, and F. Weinhold, "Natural population analysis," *The Journal of Chemical Physics,* vol. 83, pp. 735-746, 1985.

[227] T. Ghani, M. Armstrong, C. Auth, M. Bost, P. Charvat, G. Glass, T. Hoffmann, K. Johnson, C. Kenyon, J. Klaus, B. McIntyre, K. Mistry, A. Murthy, J. Sandford, M. Silberstein, S. Sivakumar, P. Smith, K. Zawadzki, S. Thompson, and M. Bohr, "A 90nm High Volume Manufacturing Logic Technology Featuring Novel 45nm Gate Length Strained Silicon CMOS Transistors," in *Technical Digest - International Electron Devices Meeting*, Washington, DC, 2003, pp. 978-980.

[228] Q. Ouyang, M. Yang, J. Holt, S. Panda, H. Chen, H. Utomo, M. Fischetti, N. Rovedo, J. Li, N. Klymko, H. Wildman, T. Kanarsky, G. Costrini, D. M. Fried, A. Bryant, J. A. Ott, M. Ieong, and C. Y. Sung, "Investigation of CMOS

ATTENTION: The Singapore Copyright Act applies to the use of this document. Nanyang Technological University Library

devices with embedded SiGe source/drain on hybrid orientation substrates," in *Digest of Technical Papers - Symposium on VLSI Technology*, Kyoto, 2005, pp. 28-29.

[229] F. Deng, R. A. Johnson, P. M. Asbeck, S. S. Lau, W. B. Dubbelday, T. Hsiao, and J. Woo, "Salicidation process using NiSi and its device application," *Journal of Applied Physics* vol. 81, pp. 8047-8051, 1997.

[230] P. S. Lee, K. L. Pey, D. Mangelinck, J. Ding, A. T. S. Wee, and L. Chan, "Improved NiSi salicide process using presilicide N2+ implant for MOSFETs," *IEEE Electron Device Letters,* vol. 21, pp. 566-568, 2000.

[231] C. S. Smith, "Piezoresistance effect in germanium and silicon," *Physical Review,* vol. 94, pp. 42-49, 1954.

[232] C. H. Ge, C. C. Lin, C. H. Ko, C. C. Huang, Y. C. Huang, B. W. Chan, B. C. Perng, C. C. Sheu, P. Y. Tsai, L. G. Yao, C. L. Wu, T. L. Lee, C. J. Chen, C. T. Wang, S. C. Lin, Y. C. Yeo, and C. Hu, "Process-Strained Si (PSS) CMOS Technology Featuring 3D Strain Engineering," in *Technical Digest - International Electron Devices Meeting*, Washington, DC, 2003, pp. 73-76.

[233] S. J. Doh, H. S. Jung, Y. S. Kim, H. J. Lim, J. P. Kim, J. H. Lee, N. I. Lee, H. K. Kang, K. P. Suh, S. G. Park, S. B. Kang, G. H. Choi, Y. S. Chung, H. S. Baik, H. S. Chang, M. H. Cho, D. W. Moon, H. B. Park, M. Cho, and C. S. Hwang, "Improvement of NBTI and Electrical Characteristics by Ozone Pre-treatment and PBTI issues in HfAIO(N) High-k Gate Dielectrics," in *Technical Digest - International Electron Devices Meeting*, Washington, DC,

ATTENTION: The Singapore Copyright Act applies to the use of this document. Nanyang Technological University Library

2003, pp. 943-946.

[234] C. Choi, C. S. Kang, C. Y. Kang, R. Choi, H. J. Cho, Y. H. Kim, S. J. Rhee, M. Akbar, and J. C. Lee, "The effects of nitrogen and silicon profile on high-K MOSFET performance and bias temperature instability," in *Digest of Technical Papers - Symposium on VLSI Technology*, Honolulu, HI, 2004, pp. 214-215.

[235] K. Torii, K. Shiraishi, S. Miyazaki, K. Yamabe, M. Boero, T. Chikyow, K. Yamada, H. Kitajima, and T. Arikado, "Physical model of BTI, TDDB and SILC in HfO2-based high-k gate dielectrics," in *Technical Digest - International Electron Devices Meeting, IEDM*, San Francisco, CA, 2004, pp. 129-132.

[236] S. Zafar, A. Kumar, E. Gusev, and E. Cartier, "Threshold voltage instabilities in high-k gate dielectric stacks," *IEEE Transactions on Device and Materials Reliability,* vol. 5, pp. 45-64, 2005.